

# UC Davis

## UC Davis Electronic Theses and Dissertations

### Title

Air Quality Implications of Energy Decarbonization and Using Biogas in California

### Permalink

<https://escholarship.org/uc/item/0w9919bp>

### Author

Li, Yin

### Publication Date

2021

Peer reviewed|Thesis/dissertation

Air Quality Implications of Energy Decarbonization and Using Biogas in California

By

YIN LI  
DISSERTATION

Submitted in partial satisfaction of the requirements for the degree of

DOCTOR OF PHILOSOPHY

in

Civil and Environmental Engineering

in the

OFFICE OF GRADUATE STUDIES

of the

UNIVERSITY OF CALIFORNIA

DAVIS

Approved:

---

Michael J. Kleeman, Chair

---

Thomas M. Young

---

Peter G. Green

Committee in Charge

2021

This page is left blank intentionally

## Acknowledgements

For the past seven years of my Ph.D. study, I have received a great amount of support and assistance from many people whom I would like to take the chance to sincerely thank.

I would first like to thank my advisor, Professor Michael Kleeman, without whom there wouldn't even be a chance for me to pursue Ph.D. study. Professor Kleeman has helped me so much with the lab, field, and modeling work. From his engineering thoughts and broad spectrum of skills I always get inspired and learn a lot. Professor Kleeman encourages me to think independently and critically, from which I benefit not only in professional work but also for the rest of my life!

I would like to give my most grateful thanks to the Biogas group. We have been together for almost 7 years and the group has taught me every level of professional work from experimental techniques to journal article writing. I would like to thank our PIs: Dr. Thomas Young, Dr. Peter Green, Dr. Norman Kado, Dr. Bryan Jenkins, Dr. Ruihong Zhang, and Dr. Chris Vogel for all the generous guidance and encouragement that lead and support me along the way. I would like to thank my colleagues Chris Alaimo, Luann Wong, Minji Kim, Joshua Peppers, Jian Xue, Chao Wan, and Katherine Chin for all the hard work, inspiring ideas and warm greetings they brought to the group. I enjoyed working with you all and was fortunate to learn from the group's expertise.

I would like to give my heartfelt thanks to the supervisors and team of testing Cell 7 at the Haagen-Smit Laboratory during the early spring of 2017 when we were at El Monte. Special thanks are due to Tin Truong, Aiko Matsunaga, Hyun-Ji Lee, Bruce Frodin, Henry Toutoundjian, Manuel Cruz, Thomas Valencia, Wayne McMahon, Mang Zhang, Richard Ling and the dedicated staff in the Organic Analysis Section and Aerosol Analysis and Methods Evaluation Section. I deeply cherish the experience and memory of working with you all for the two months. It was busy, challenging and incredible.

I would like to thank California Air Resources Board (CARB), California Energy Commission (CEC) and Environmental Protection Agency (US EPA) for kindly sponsoring the research work in this thesis. I would also like to thank all the biogas/RNG producers who collaborated with this study, as well as

Xiguang Chen and Helee LLC for their in-kind support through the provision of the membrane separation unit used to upgrade biogas to RNG. Thanks also due to Martin Shafer from the University of Wisconsin laboratory for all the ROS analyses.

I would like to thank my friends and collages Xin Yu, Anikender Kumar, Yiting Li, Wei Xue, Chao Wan, Youyou Zhang, Yuru Wang, Tongbi Tu, Mengmeng Fang and so many more! It has been such a memorable part of life that we shared, talked, get inspired and supported by each other. I would also like to thank a very special friend, Jiarui, who found me stray in the darkness and kept encouraging me with sharp remarks, sympathetic patience and adorable humor.

I would like to thank my cousin Shaocheng Wang and his wife Dos Xie who picked me up at LAX and set me up for the years of Ph.D. studies from that first landing in the states. I would like to thank my parents for supporting me unconditionally, materially and mentally, till where I am and where I will be.

## Abstract

California Assembly Bill 32 (AB32) sets the goal to reduce greenhouse gas (GHG) emissions to a level 80% below 1990 levels by 2050. This deep decarbonization target requires major technology advancement and energy structure transition to a renewable and sustainable future. The environmental aspects of such a transition should be evaluated carefully before major investments in infrastructure are made. Biogas is a promising renewable energy resource in California that shares many similarities with natural gas but with the advantage of being carbon neutral since it generates energy from organic waste. However, biogas contains trace levels of numerous chemical compounds that depend on the feedstock and production process. The air quality implications of using biogas in different situations should be examined carefully before widespread adoption across California.

The second chapter of this thesis characterizes the chemical and biological composition of raw biogas produced at five facilities using different feedstocks. The toxicity of combusted biogas is tested under fresh and photo-chemically aged conditions. Results find no strong evidence of potential occupational health risk from the five California biogas sites. Results also show no obvious differences between the toxicity of different biogas combustion exhaust after atmospheric dilution and aging. The third chapter of this thesis examines the emissions from the combustion of upgraded biogas that has CO<sub>2</sub> removed and CH<sub>4</sub> concentrated to be qualified as renewable natural gas (RNG). A light-duty cargo van was tested with CNG and two RNG blends on a chassis dynamometer to compare the toxicity of the resulting exhaust. CNG vehicle engine exhaust showed a higher or similar level of various toxicity responses, and photochemical reactions did not seem to alter the observed trend. These preliminary results suggest that utilizing biogas for direct heat and electricity generation or as vehicle fuel after upgrading could be useful strategies to reduce carbon intensity without negatively impacting air quality or public health.

The fourth chapter of this thesis extends the scope by modeling air pollutant emissions from all California socio-economic sectors under different energy scenarios in the year 2050. To study the air quality

implications of some key resources and technologies in the decarbonization transition, a total of six different scenarios were analyzed for various particulate and gaseous pollutant emissions. These scenarios include: 1) a business-as-usual future reference scenario "BAU", 2) a partial GHG reduction scenario that constrains only through 2030 with 40% reduction "CAP30", 3) a climate-friendly 80% GHG reduction scenario featuring deep penetration of advanced technologies and renewable energies "GHGAi", a same 80% GHG reduction scenario with the deployment of biomass carbon capture and sequestration technology "CCS", and two variation scenarios on GHGAi that examine the effect of using more natural gas in built environment "NGB" and power generation "NGT". Results show that major air quality benefits are expected from the GHGAi scenario, which includes aggressive decarbonization of electricity supply, electrification of most end-use appliances, improvement of appliances efficiency, and deployment of low-carbon transportation fuels and technologies. Bio-CCS technology holds promise as a shortcut to GHG mitigation and the utilization of natural gas bridges the transition from traditional to renewable energy systems, but neither of these technologies appear to be optimal from a future air quality management perspective. Adoption of biogas as an energy source plays a small but constructive role in the overall transition of California's energy system towards a low carbon future.

Chapter 2 is published as:

*Yin Li, Christopher P. Alaimo, Minji Kim, Norman Y. Kado, Joshua Peppers, Jian Xue, Chao Wan, Peter G. Green, Ruihong Zhang, Bryan M. Jenkins, Christoph F. A. Vogel, Stefan Wuertz, Thomas M. Young, and Michael J. Kleeman. (2019) Composition and toxicity of biogas produced from different feedstocks in California. Environmental science & technology, 53(19), pp.11569-11579.*

Chapter 3 is published as:

*Yin Li, Jian Xue, Joshua Peppers, Norman Y. Kado, Christoph F.A. Vogel, Christopher P. Alaimo, Peter G. Green, Ruihong Zhang, Bryan M. Jenkins, Minji Kim, Thomas M. Young, and Michael J. Kleeman. (2021) Chemical and Toxicological Properties of Emissions from a Light-Duty Compressed Natural Gas Vehicle Fueled with Renewable Natural Gas. Environmental Science & Technology, 55(5), pp.2820-2830.*

Chapter 4 is submitted and currently under review:

*Yin Li, Christopher Yang, Yiting Li, Anikender Kumar, and Michael J. Kleeman. (2021) Future Emissions of Particles and Gases that Cause Regional Air Pollution in California under Different Greenhouse Gas Mitigation Strategies. Atmospheric Environment.*

## Table of Contents

<b>Acknowledgements .....</b>	<b>iii</b>
<b>Abstract.....</b>	<b>v</b>
<b>Chapter 1 – Introduction.....</b>	<b>1</b>
<b>Chapter 2 – Biogas composition and direct use for electricity generation.....</b>	<b>4</b>
<b>2.1 Background.....</b>	<b>4</b>
<b>2.2 Methods .....</b>	<b>5</b>
2.2.1 Biogas sources.....	5
2.2.2 Chemical analysis.....	6
2.2.3 Biological analysis .....	8
2.2.4 Toxicological analysis.....	8
<b>2.3 Results and discussion.....</b>	<b>10</b>
2.3.1 Biogas composition .....	10
2.3.2 Biogas engine combustion exhaust.....	19
<b>2.4 Implications .....</b>	<b>20</b>
<b>2.5 Appendix.....</b>	<b>24</b>
<b>Chapter 3 – Biomethane as a vehicle fuel.....</b>	<b>34</b>
<b>3.1 Background.....</b>	<b>34</b>
<b>3.2 Methods .....</b>	<b>35</b>
3.2.1 RNG sample collection and analysis .....	35
3.2.2 Vehicle exhaust collection and chemical analysis.....	36
3.2.3 Vehicle exhaust toxicological analysis.....	38
3.2.4 Photochemical aging of exhaust .....	40
<b>3.3 Results and discussion.....</b>	<b>41</b>
3.3.1 Fuel composition .....	41
3.3.2 Exhaust composition .....	41
3.3.3 Atmospheric aging of exhaust .....	46
3.3.4 Exhaust toxicity.....	47
<b>3.4 Implications .....</b>	<b>51</b>
<b>3.5 Appendix.....</b>	<b>53</b>
<b>Chapter 4 – Future Emissions of Particles and Gases under Different Greenhouse Gas Mitigation Strategies.....</b>	<b>73</b>
<b>4.1 Background.....</b>	<b>73</b>
<b>4.2 Methods .....</b>	<b>75</b>
4.2.1 The CA-TIMES model and future scenarios .....	75
4.2.2 The updated CA-REMARQUE model .....	77
4.2.3 Air Quality Model .....	78

4.2.4 Health Impact Model.....	79
<b>4.3 Results and discussion.....</b>	<b>79</b>
4.3.1 Energy system transition and GHG emission.....	79
4.3.2 Particulate and gaseous pollutant emissions from different future scenarios .....	81
4.3.3 Particulate and gaseous pollutant emissions from different socio-economic sectors .....	84
4.3.4 Airborne Particulate Matter Concentrations .....	91
4.3.5 Public Health Benefits.....	93
<b>4.4 Implications .....</b>	<b>94</b>
<b>4.5 Appendix.....</b>	<b>96</b>
<b><i>Chapter 5 – Conclusions.....</i></b>	<b><i>126</i></b>
<b><i>References.....</i></b>	<b><i>129</i></b>

TABLE 2-1 SUMMARY OF BIOGAS PRODUCTION SITES CHARACTERIZED IN THIS STUDY.....	6
FIGURE 2-1 MAJOR COMPONENT CONCENTRATIONS BY VOLUME IN DRY BIOGAS STREAMS .....	11
FIGURE 2-2 TOTAL SULFUR-CONTAINING COMPOUND CONCENTRATION (PPM <sub>v</sub> ) AND SPECIATION IN DIFFERENT BIOGAS STREAMS.....	13
FIGURE 2-3 TOTAL HALOCARBON CONCENTRATION (PPM <sub>v</sub> ) AND SPECIATION IN DIFFERENT BIOGAS STREAMS .....	14
FIGURE 2-4 TOTAL BTEX CONCENTRATION (PPM <sub>v</sub> ) AND SPECIATION IN DIFFERENT BIOGAS STREAMS.....	15
FIGURE 2-5 TOTAL SILOXANE CONCENTRATION (PPMV) AND SPECIATION IN DIFFERENT BIOGAS STREAMS .....	16
TABLE 2-2 CONCENTRATION OF ARSENIC (As), ANTIMONY (Sb), LEAD (Pb), COPPER (Cu) AND ALUMINUM (Al) IN DIFFERENT BIOGAS STREAMS (MG · M <sup>-3</sup> ).....	17
TABLE 2-3 RESULTS OF BIOLOGICAL ANALYSIS (CULTIVATION AND qPCR).....	18
FIGURE 2-6 BIOASSAY RESULTS OF ON-SITE BIOGAS ENGINE/TURBINE EXHAUST AGED UNDER DARK AND LIGHT CONDITIONS.....	20
TABLE 2-4 CONCENTRATION OF TOTAL S-CONTAINING COMPOUNDS IN BIOGAS AND BIOMETHANE STREAMS AND EMISSION FACTORS OF SO <sub>2</sub> FROM BURNING THESE GAS STREAMS .....	21
TABLE 2-5 CONCENTRATION OF SELECTED COMPOUNDS IN DILUTED AND ATMOSPHERICALLY AGED ENGINE EXHAUST, THEIR EMISSION FACTORS FROM BURNING IN BIOGAS ENGINES, AND CORRESPONDING EMISSION FACTORS FOR NATURAL GAS ENGINES .....	22
TABLE S. 2-1 TEDLAR BAG SAMPLE ANALYSIS SPECIFICATIONS .....	25
TABLE S. 2-2 TARGET COMPOUNDS IN TEDLAR SAMPLE BAG ANALYSIS .....	26
TABLE S. 2-3 SORBENT TUBES SAMPLING AND ANALYSIS SPECIFICATIONS .....	27
TABLE S. 2-4 TARGET COMPOUNDS AND THEIR LOQS IN XAD-2 SORBENT TUBE ANALYSIS.....	28
TABLE S. 2-5 TARGET COMPOUNDS AND THEIR LOQS IN CHARCOAL SORBENT TUBE ANALYSIS.....	29
TABLE S. 2-6 TARGET COMPOUNDS AND THEIR LOQS IN SILICA SORBENT TUBE ANALYSIS .....	30
TABLE S. 2-7 CONCENTRATION RANGE OF SELECTED HALOCARBONS (MG · M <sup>-3</sup> ) MEASURED AT DIFFERENT LANDFILL SITES AND PERMISSIBLE OCCUPATIONAL EXPOSURE LEVELS BY CAL/OSHA AND OEHHA .....	30
TABLE S. 2-8 AVERAGE CONCENTRATION OF BTEX (BENZENE, TOLUENE, ETHYLBENZENE AND XYLENES) MEASURED IN DIFFERENT BIOGAS STREAMS (MG · M <sup>-3</sup> ) AND PERMISSIBLE OCCUPATIONAL EXPOSURE LEVELS BY CAL/OSHA AND OEHHA .....	31
TABLE S. 2-9 CONCENTRATION OF SILOXANES IN DIFFERENT BIOGAS STREAMS (MG · M <sup>-3</sup> ).....	31
TABLE S. 2-10 CONCENTRATION OF METALS IN DIFFERENT BIOGAS STREAMS .....	32
FIGURE S. 2-1 MAP LOCATIONS OF THE BIOGAS FACILITIES STUDIED.....	33
FIGURE S. 2-2 CONCENTRATION (PPMV) OF CARBONYLS IN DIFFERENT BIOGAS STREAMS.....	33
TABLE 3-1. COMPOSITION OF DIFFERENT FUELS USED IN THIS STUDY. ....	36
FIGURE 3-1 (A)-(X). EMISSION FACTORS (MG·MILE <sup>-1</sup> ) OF DIFFERENT POLLUTANTS FOR THE AVERAGED COLD-START UC CYCLE AS WELL AS DIFFERENT PHASES OF THE CYCLE. ....	44
ERROR BAR REPRESENTS STANDARD DEVIATION OF TUNNEL BACKGROUND MEASUREMENT. ....	44
FIGURE 3-2 UC CYCLE-AVERAGED EMISSION FACTOR OF ULTRAFINE PARTICLE (PM <sub>0.1</sub> ) (A) MASS (µG·MILE <sup>-1</sup> ) AND (B) NUMBER (µG·MILE <sup>-1</sup> ) FROM THE TESTED VEHICLE RUNNING ON DIFFERENT FUELS.....	46
FIGURE 3-3 CONCENTRATION (PPB) OF SELECTED COMPOUNDS MEASURED FROM CHAMBER AFTER 3H OF AGING UNDER EITHER DARK OR LIGHT CONDITION .....	47
FIGURE 3-4 TOXICITY OF VEHICLE EXHAUST RUNNING ON DIFFERENT FUELS. ....	48
FIGURE 3-5 SUMMARY OF ELASTIC NET REGRESSION RESULTS ON THE LINEAR COEFFICIENTS BETWEEN CHEMICAL FEATURES AND TOXICITY RESPONSES.....	49
FIGURE 3-6 ABUNDANCE OF SELECTED CHEMICAL COMPOUNDS THAT HAD NON-ZERO COEFFICIENT ASSOCIATED WITH TOXICITY RESPONSES. .....	50
FIGURE 3-7 MUTAGENIC SCORE CALCULATED BASED ON GAS PHASE CONCENTRATION MEASURED BY PTR-MS AND AMES TEST CONSENSUS SCORE GIVEN BY THE VEGA-QSAR MODEL .....	51
TABLE S.3- 1 EXPERIMENTALLY DETERMINED LIMIT OF DETECTION (LOD) FOR DIFFERENT COMPOUNDS MEASURED BY FTIR .....	62
TABLE S.3- 2 EXPERIMENTALLY DETERMINED LIMIT OF DETECTION (LOD) FOR DIFFERENT COMPOUNDS MEASURED BY PTR-MS.....	62
TABLE S.3- 3 CONCENTRATION (%) OF MAJOR COMPOUNDS MEASURED IN DIFFERENT FUELS. ....	63
TABLE S.3- 4 CONCENTRATION (PPBV) OF DIFFERENT SULFUR-CONTAINING COMPOUNDS MEASURED IN DIFFERENT FUELS. LIMIT OF QUANTIFICATIONS (LOQs), AVERAGE VALUES AS WELL AS STANDARD DEVIATIONS FROM 3 MEASUREMENTS ARE REPORTED. NOTE THAT VALUES BELOW LOQs ARE POSSIBLE BECAUSE RNG1 AND RNG2 ARE BLENDS FROM CNG AND DIFFERENT BIOMETHANE SOURCES WHICH CAN EACH HAVE MEASURED VALUES ABOVE OR BELOW LOQs.....	64
TABLE S.3- 5 CONCENTRATION (PPBV) OF DIFFERENT HYDROCARBONS MEASURED IN DIFFERENT FUELS. ....	65

TABLE S.3- 6 PM MASS ( $\mu\text{G}/\text{FILTER}$ ) COLLECTED FOR DIFFERENT TOXICITY ASSAYS. ....	66
TABLE S.3- 7 ABUNDANCE (IN PEAK AREA) OF COMPOUNDS DETECTED WITH XAD + GC/MS ANALYSIS FROM DIFFERENT EXHAUST SAMPLES. ....	66
FIGURE S.3- 1 SPEED TRACE FROM THE CALIFORNIA UNIFIED CYCLE <sup>111</sup> . ....	68
FIGURE S.3- 2 FUEL ECONOMY AND EMISSION FACTORS OF DIFFERENT POLLUTANTS FOR THE AVERAGED COLD-START UC CYCLE AS WELL AS DIFFERENT PHASES OF THE CYCLE. ERROR BARS DEFINE THE RANGE (MIN AND MAX VALUES) SET BY THE DUPLICATE TESTS. ....	68
FIGURE S.3- 3 (A)-(F). TIME SERIES OF CONCENTRATION OF DIFFERENT POLLUTANTS (PPM) MEASURED BY FTIR IN THE FIRST 150 SECONDS OF THE COLD-START UC CYCLE. ....	69
THE RANGE FOR EACH FUEL IS OUTLINED BY THE DUPLICATE MEASUREMENTS FROM TWO COLD-START UC CYCLE TESTS. ....	69
FIGURE S.3- 4 TIME SERIES OF PARTICLE MASS CONCENTRATION ( $\mu\text{G}\cdot\text{M}^{-3}$ ) AND NUMBER CONCENTRATION ( $\#\cdot\text{CM}^{-3}$ ) MEASURED FROM THE CVS DILUTION TUNNEL. ....	70
SHOWING THE TRACE OF RNG2 AS AN EXAMPLE. ....	70
FIGURE S.3- 5 DISTRIBUTION OF (A) ULTRAFINE PARTICLE MASS EMISSION FACTOR ( $\text{MG}\cdot\text{MILE}^{-1}$ ) AND (B) ULTRAFINE PARTICLE NUMBER EMISSION FACTOR ( $\#\cdot\text{MILE}^{-1}$ ) FROM THE TESTED VEHICLE RUNNING ON DIFFERENT FUELS. THE RANGE FOR EACH FUEL (SHADED AREA) IS OUTLINED BY THE DUPLICATE MEASUREMENTS FROM TWO COLD-START UC CYCLE TESTS. ....	71
FIGURE S.3- 6 TYPICAL CONCENTRATION PROFILES (PPB) DURING ATMOSPHERIC AGING. (A) CONCENTRATION OF XYLENE DURING DARK AGING; (B) CONCENTRATION OF XYLENE DURING LIGHT AGING; (C) CONCENTRATION OF ETHENONE DURING DARK AGING; (D) CONCENTRATION OF ETHENONE DURING LIGHT AGING. ....	72
FIGURE 4-1. CALIFORNIA ENERGY SYSTEM TRANSITION AS REPRESENTED BY THE PERCENTAGE OF DIFFERENT TYPES OF PRIMARY ENERGY IN 2010 AND 2050 SCENARIOS. ....	80
FIGURE 4-2. TOTAL GREENHOUSE GAS EMISSION (M TON CO <sub>2</sub> -EQ) FROM DIFFERENT ECONOMIC SECTORS MODELED BY CA-TIMES IN 2010 AND 2050 DIFFERENT SCENARIOS. ....	81
FIGURE 4-3. POLLUTANT EMISSION CHANGE (%) IN DIFFERENT SCENARIOS RELATIVE TO THEIR REFERENCE SCENARIO. ....	83
(A) ULTRAFINE PARTICULATE MATTER EMISSIONS FROM DIFFERENT SECTORS UNDER DIFFERENT SCENARIOS. ....	83
(B) ULTRAFINE, FINE, AND COARSE PARTICULATE MATTER EMISSIONS FROM THE BAU SCENARIO. ....	83
FIGURE 4-5. PM <sub>0.1</sub> EMISSION ( $\mu\text{G}\cdot\text{M}^{-2}\cdot\text{MIN}^{-1}$ ) FROM RESIDENTIAL AND COMMERCIAL SECTOR. ....	86
(A) PM <sub>0.1</sub> EMISSION ( $\mu\text{G}\cdot\text{M}^{-2}\cdot\text{MIN}^{-1}$ ) FROM RESIDENTIAL AND COMMERCIAL SECTOR IN THE BAU SCENARIO, AND (B-F) CHANGES IN PM <sub>0.1</sub> EMISSIONS ( $\mu\text{G}\cdot\text{M}^{-2}\cdot\text{MIN}^{-1}$ ) RELATIVE TO THE INDICATED REFERENCE SCENARIO. ....	86
FIGURE 4-6. PM <sub>0.1</sub> EMISSION ( $\mu\text{G}\cdot\text{M}^{-2}\cdot\text{MIN}^{-1}$ ) FROM ELECTRICITY GENERATION. ....	88
(A) PM <sub>0.1</sub> EMISSIONS ( $\mu\text{G}\cdot\text{M}^{-2}\cdot\text{MIN}^{-1}$ ) FROM ELECTRICITY GENERATION IN THE BAU SCENARIO, AND (B-F) CHANGES IN PM <sub>0.1</sub> EMISSIONS ( $\mu\text{G}\cdot\text{M}^{-2}\cdot\text{MIN}^{-1}$ ) RELATIVE TO THE INDICATED REFERENCE SCENARIO. ....	88
FIGURE 4-7. PM <sub>2.5</sub> EMISSION ( $\mu\text{G}\cdot\text{M}^{-2}\cdot\text{MIN}^{-1}$ ) FROM ELECTRICITY GENERATION, CCS-BAU. ....	89
FIGURE 4-8. PROJECTION OF PM <sub>2.5</sub> CONCENTRATION IN 2050. ....	92
(A) LONG-TERM PM <sub>2.5</sub> CONCENTRATIONS PREDICTED UNDER THE BAU EMISSIONS INVENTORY, AND (B-F) CHANGE IN LONG-TERM PM <sub>2.5</sub> CONCENTRATIONS ASSOCIATED WITH CHANGING ENERGY PORTFOLIOS RELATIVE TO THE INDICATED REFERENCE SCENARIO IN THE PANEL TITLE. ALL UNITS $\mu\text{G}\cdot\text{M}^{-3}$ . ....	92
FIGURE 4-9. AVOIDED MORTALITY DUE TO IMPROVED AIR QUALITY ASSOCIATED WITH CHANGING ENERGY PORTFOLIOS RELATIVE TO THE BAU SCENARIO. SIZE OF POPULATION IN 2050 IS ESTIMATED TO BE 45 MILLION. PUBLIC HEALTH BENEFITS ESTIMATION ASSUMES A PRESENT-DAY VALUE OF A STATISTICAL LIFE EQUIVALENT TO USD7.6M. ALL CALCULATIONS PERFORMED WITH BENMAP-CE. ....	93
TABLE S.4- 1 POLICIES REPRESENTED IN THE BAU SCENARIO. A MORE DETAILED DESCRIPTION OF THE ASSUMPTIONS ASSOCIATED WITH EACH OF THE POLICIES ARE PRESENTED IN APPENDIX D. OF YANG ET AL., 2014 <sup>127</sup> . ....	98
TABLE S.4- 2 EMISSION INVENTORY CODE (EIC) CROSS-REFERENCE TABLE BETWEEN EMFAC VEHICLE CLASS AND TECHNOLOGY AND CA- TIMES VEHICLE TYPES. ....	98
FIGURE S.4- 1 PRIMARY ENERGY CONSUMPTION (PJ) FROM 2010 TO 2050 IN DIFFERENT CA-TIMES SCENARIOS. ....	99
FIGURE S.4- 2 GHG EMISSION (M TON CO <sub>2</sub> -EQ) FROM DIFFERENT ECONOMIC SECTORS OVER THE YEARS IN DIFFERENT CA-TIMES SCENARIOS. ....	100
FIGURE S.4- 3 (A-C). ULTRAFINE (PM <sub>0.1</sub> ), FINE (PM <sub>2.5</sub> ) AND COARSE (PM <sub>10</sub> ) PARTICULATE MATTER EMISSION RATES FROM DIFFERENT SCENARIOS. ....	101
FIGURE S.4- 4 ENERGY DEMAND (PJ) FROM ON-ROAD VEHICLES IN YEAR 2050. ....	102
FIGURE S.4- 5 ENERGY DEMAND (PJ) FROM OFF-ROAD EQUIPMENT AND RAILROADS IN YEAR 2050. (DSL=DIESEL, GSL=GASOLINE, ETH=ETHANOL, NGA=NATURAL GAS, BDL=BIODIESEL, ELC=ELECTRICITY) ....	102
FIGURE S.4- 6 ENERGY DEMAND (PJ) FROM AIRCRAFTS IN YEAR 2050. ....	102

FIGURE S.4- 7 ENERGY DEMAND (PJ) FROM MARINE VESSELS IN YEAR 2050. (RFO=RESIDUAL FUEL OIL, BRFO=BIO-DERIVED RESIDUAL FUEL OIL, DSL=DIESEL, BDL=BIODIESEL, GSL=GASOLINE, ETH=ETHANOL).....	103
FIGURE S.4- 8 ENERGY DEMAND (PJ) FROM RESIDENTIAL (RSD) AND COMMERCIAL (COM) BUILDINGS IN YEAR 2050. (ELC=ELECTRICITY, NGA=NATURAL GAS).....	103
FIGURE S.4- 9 ELECTRICITY GENERATION (PJ) FROM DIFFERENT RESOURCES IN YEAR 2050. ....	103
FIGURE S.4- 10 ENERGY DEMAND FROM PETROLEUM REFINING PROCESSES (PJ) IN YEAR 2050. (OIL=CRUDE OIL, NGA=NATURAL GAS) .....	104
FIGURE S.4- 11 ENERGY OUTPUT FROM BIOREFINERIES (PJ) IN YEAR 2050. (ETH=ETHANOL, BRFO=BIO-DERIVED RESIDUAL FUEL OIL, BDL=BIODIESEL, BGSL=BIO-GASOLINE, BJF=BIO-DERIVED JET FUEL, BAVG=BIO-DERIVED AVIATION GASOLINE) .....	104
FIGURE S.4- 12 HYDROGEN PRODUCTION (PJ) FROM DIFFERENT PROCESSES IN YEAR 2050. ....	104
FIGURE S.4- 13 POLLUTANT EMISSION CHANGE (%) IN DIFFERENT SCENARIOS NGB AND NGT RELATIVE TO THE BAU SCENARIO. STACKED COLORED BARS REPRESENT CONTRIBUTIONS FROM DIFFERENT SOCIO-ECONOMIC SECTORS .....	105
FIGURE S.4- 14 PM <sub>2.5</sub> EMISSIONS (UG·M <sup>-2</sup> ·MIN <sup>-1</sup> ) FROM RESIDENTIAL AND COMMERCIAL SECTOR.....	106
FIGURE S.4- 15 PM <sub>2.5</sub> EMISSIONS (UG·M <sup>-2</sup> ·MIN <sup>-1</sup> ) FROM ELECTRICITY GENERATION. ....	107
FIGURE S.4- 16 PM <sub>2.5</sub> EMISSIONS (UG·M <sup>-2</sup> ·MIN <sup>-1</sup> ) FROM MARINE VESSELS AND AIRCRAFTS. ....	108
FIGURE S.4- 17 PM <sub>2.5</sub> EMISSIONS (UG·M <sup>-2</sup> ·MIN <sup>-1</sup> ) FROM OFF-ROAD EQUIPMENT AND RAILROAD. ....	109
FIGURE S.4- 18 PM <sub>2.5</sub> EMISSIONS (UG·M <sup>-2</sup> ·MIN <sup>-1</sup> ) FROM ON-ROAD VEHICLE TAILPIPE. ....	110
FIGURE S.4- 19 PM <sub>2.5</sub> EMISSIONS (UG·M <sup>-2</sup> ·MIN <sup>-1</sup> ) FROM ON-ROAD VEHICLE TIRE AND BREAK WEAR. ....	111
FIGURE S.4- 20 PM <sub>2.5</sub> EMISSIONS (UG·M <sup>-2</sup> ·MIN <sup>-1</sup> ) FROM FUEL SUPPLY PROCESSES. ....	112
FIGURE S.4- 21 PM <sub>2.5</sub> EMISSIONS (UG·M <sup>-2</sup> ·MIN <sup>-1</sup> ) FROM OTHER PROCESSES. (INCLUDING (A) INDUSTRIAL AND AGRICULTURAL EMISSIONS, AND (B) DUST EMISSIONS) THAT ARE NOT VARYING WITH SCENARIOS. ....	113
FIGURE S.4- 22 PM <sub>0.1</sub> EMISSIONS (UG·M <sup>-2</sup> ·MIN <sup>-1</sup> ) FROM MARINE VESSELS AND AIRCRAFTS. ....	114
FIGURE S.4- 23 PM <sub>0.1</sub> EMISSIONS (UG·M <sup>-2</sup> ·MIN <sup>-1</sup> ) FROM OFF-ROAD EQUIPMENT AND RAILROAD. ....	115
FIGURE S.4- 24 PM <sub>0.1</sub> EMISSIONS (UG·M <sup>-2</sup> ·MIN <sup>-1</sup> ) FROM ON-ROAD VEHICLE TAILPIPE. ....	116
FIGURE S.4- 25 PM <sub>0.1</sub> EMISSIONS (UG·M <sup>-2</sup> ·MIN <sup>-1</sup> ) FROM ON-ROAD VEHICLE TIRE AND BREAK WEAR. ....	117
FIGURE S.4- 26 PM <sub>0.1</sub> EMISSIONS (UG·M <sup>-2</sup> ·MIN <sup>-1</sup> ) FROM FUEL SUPPLY PROCESSES. ....	118
FIGURE S.4- 27 PM <sub>0.1</sub> EMISSIONS (UG·M <sup>-2</sup> ·MIN <sup>-1</sup> ) FROM OTHER PROCESSES. (INCLUDING (A) INDUSTRIAL AND AGRICULTURAL EMISSIONS, AND (B) DUST EMISSIONS) THAT ARE NOT VARYING WITH SCENARIOS. ....	119
FIGURE S.4- 28 NO <sub>x</sub> EMISSIONS (PPB·M·MIN <sup>-1</sup> ) FROM RESIDENTIAL AND COMMERCIAL BUILDINGS.....	120
FIGURE S.4- 29 NO <sub>x</sub> EMISSIONS (PPB·M·MIN <sup>-1</sup> ) FROM ELECTRICITY GENERATION. ....	121
FIGURE S.4- 30 NO <sub>x</sub> EMISSIONS (PPB·M·MIN <sup>-1</sup> ) FROM MARINE VESSELS AND AIRCRAFTS. ....	122
FIGURE S.4- 31 NO <sub>x</sub> EMISSIONS (PPB·M·MIN <sup>-1</sup> ) FROM OFF-ROAD EQUIPMENT AND RAILROAD. ....	123
FIGURE S.4- 32 NO <sub>x</sub> EMISSIONS (PPB·M·MIN <sup>-1</sup> ) FROM ON-ROAD VEHICLE TAILPIPE. ....	124
FIGURE S.4- 33 NO <sub>x</sub> EMISSIONS (PPB·M·MIN <sup>-1</sup> ) FROM FUEL SUPPLY PROCESSES. ....	125

# Chapter 1 – Introduction

Air quality (AQ) management relies on a fundamental understanding of the pollution problem and careful evaluation of potential control strategies that can then be carried out over the long time periods required for new technologies to be adopted. The AQ management cycle repeats when new scientific research suggests that changes to air pollution regulations are needed in order to protect public health. California has led the world in AQ management of the past 70 years. Some of the major accomplishments over this time span include the development of chemical mechanisms to understand the composition of smog and the origin of smog-forming components, the development of technology to reduce refinery and fueling station gasoline evaporation, controlling tailpipe NO<sub>x</sub> emission, and promoting cleaner fuels and technologies such as natural gas, methanol and electric vehicles. In recent years, California has taken a leading position at the intersection of AQ research and future climate mitigation. New challenges will need to be overcome as California seeks the optimal future sustainable development pathway to reduce greenhouse gas (GHG) emissions and achieve improved AQ that benefits all segments of society.

California's Global Warming Solutions Act of 2006 (California state law Assembly Bill 32), sets the goal to reduce GHG emissions to 2000 levels by 2010, to 1990 levels by 2020, and to a level 80% below 1990 levels by 2050. The passage of Senate Bill (SB) 32 in 2016 further requires GHG emissions to be reduced to 40% below 1990 levels by 2030. Moreover, SB100 passed in late 2018 requires that 100% of all retail sales of electricity come from a combination of renewable energy and carbon-zero resources by the year 2045. None of these laws prescribe the exact technology mixture that should be used to achieve the indicated emissions reductions. Numerous alternatives exist that each have different costs and environmental impacts. Most importantly in the context of this research, the air quality aspects of California's energy transition should be examined to fully understand the total societal benefits provided by each potential source of low carbon energy. Previous studies have shown that the monetary value of air

quality benefits and disbenefits as public health outcomes is comparable to the investment needed to adopt different energy decarbonization pathways<sup>1,2</sup>.

Numerous AQ research questions arise in the analysis of low carbon fuels as some resources and technologies appear to be promising for climate change mitigation, but their air quality implications are not well understood. One example is the potential benefits or disbenefits of biogas adoption. Produced from anaerobic digestion of a variety of types of organic waste, biogas contains mainly methane and carbon dioxide. It can be burnt directly for heat and electricity or upgraded by removing CO<sub>2</sub> to produce a fuel that can substitute for natural gas in vehicle engines or home appliances. Harnessing biogas as an energy source prevents the release of methane that would otherwise be emitted from poor waste management practices. Biogas utilization also offsets the carbon emission that would otherwise be added to the atmosphere through fossil fuel combustion. California has the largest potential for biogas production among the U.S. states. The energy potentially from biogas is equivalent to 5% of current natural gas consumption in the electric power sector or 56% of natural gas consumption in the transportation sector<sup>3,4</sup>. Despite all the potential climate benefits, widespread adoption of biogas should be approached cautiously due to potential air quality impacts. Biogas contains trace levels of complicated chemical compounds that vary depending on the feedstock (food waste, farm waste, municipal waste, energy crop...) and production process (digester design, temperature, clean-up procedure...). Some of these trace chemicals are known to be toxic, and they may likewise yield toxic products during the digestion, combustion, and photochemical reaction processes. The potential air quality impacts of biogas must be carefully compared to fossil natural gas before this new energy source is endorsed and supported by government agencies with incentives.

A second example of important research questions at the intersection of climate change and air quality arises from efforts to develop carbon capture and sequestration (CCS) technology where carbon dioxide emissions from a stationary source are separated from the flue gas stream, pressurized, and transported to geological reservoirs. Despite the controversy on the actual carbon capture efficiency not being able to offset the energy penalty of running the apparatus, CCS is considered an essential strategy to meet the decarbonization goal in some of the world's major economies. Theoretical studies predict that CCS

technology paired with fossil energy plants reduces carbon intensity and CCS technology paired with biomass-based powerplants strips carbon out of the atmosphere, generating "negative" carbon emission. The detailed AQ aspects of CCS technology have received very little study in peer-reviewed literature, leaving many unanswered questions about this approach to climate mitigation.

This thesis aims to fill some of the research gaps at the intersection of AQ and future energy system transition. Chapters 2 and 3 evaluate the AQ implications of using biogas for electricity generation and as vehicle fuel. Chemical composition is analyzed in unburnt biogas, combusted biogas exhaust, and photochemically aged biogas combustion exhaust. Toxicity analysis is performed with combustion exhaust to assess the potential public health impact of widespread biogas utilization. Chapter 4 broadens the scope and studies air pollutant emission from the future energy system with modeling work. Six scenarios are created to represent different future situations which include "business-as-usual", partial decarbonization, deep decarbonization, deep decarbonization with the help of CCS, and deep decarbonization with loosened natural gas limitations in power generation or built environment. Emission inventory containing various particulate and gaseous pollutants is generated with 4km resolution, and the AQ implications from the future scenarios are discussed based on the modeled result of state-wide pollutant concentration in the year 2050.

## **Chapter 2 – Biogas composition and direct use for electricity generation**

### **2.1 Background**

Biogas is a renewable fuel produced from the anaerobic digestion of organic feed stocks including municipal waste, farm waste, food waste and energy crops. Raw biogas typically consists of methane (50-75%), carbon dioxide (25-50%) and smaller amounts of nitrogen (2-8%). Trace levels of hydrogen sulfide, ammonia, hydrogen and various volatile organic compounds are also present in biogas depending on the feedstock<sup>5</sup>. Life cycle assessment studies have shown that deploying biogas technologies can effectively reduce greenhouse gas (GHG) emissions and therefore reduce the climate impact of energy consumption<sup>6-8</sup>. Biogas production and utilization practices also help diversify energy systems while simultaneously promoting sustainable waste management practices<sup>5,9</sup>. California is promoting biogas utilization by mandating the low carbon fuels, offering grants to develop biogas production facilities, and providing assistance in accessing pipeline infrastructure<sup>3,10,11</sup>.

There are many environmental factors to consider when developing biogas energy sources including the potential for air quality impacts. California is home to 7 of the 10 most polluted cities in the United States<sup>12</sup> and so the widespread utilization of any new fuel must be carefully analyzed for effects on air quality and human health. The concentrations of minor chemical and biological components in biogas differ from those found in other fuels. Some of these components have the potential to be toxic to human health and the environment, to form toxic substances during the combustion process, or to form toxic substances after photochemical aging in the atmosphere.

The California Air Resources Board (CARB) and the Office of Environmental Health Hazard Assessment (OEHHA) compiled a list of twelve trace components potentially present in biogas at levels significantly above traditional fossil natural gas including carcinogens (arsenic, p-dichlorobenzene, ethylbenzene, n-nitroso-di-n-propylamine, vinyl chloride) and non-carcinogens (antimony, copper, hydrogen sulfide, lead, methacrolein, mercaptans, toluene). A limited dataset of measurements is available

to characterize levels of these biogas components in California. Measurements of landfill biogas composition have been made over many decades around the world to identify sources of odor, to reduce ground level volatile organic compound (VOC) contamination, and to optimally recover biogas as an energy source<sup>13</sup>. Trace components identified in landfill biogas include halocarbons, aromatic hydrocarbons and siloxanes<sup>14-19</sup>. Animal waste has significant biogas potential in California but often contains sulfur compounds that must be removed prior to use<sup>20,21</sup>. Food waste is a relatively new feedstock that has only been analyzed for biogas plant performance<sup>22,23</sup>. Previous studies have tested biogas or simulated biogas burning in engines or turbines, focusing on engine/turbine performance, NOx and small hydrocarbon emissions<sup>24-29</sup>, but these studies did not examine trace chemical compounds in the engine combustion exhaust that could pose environmental and human health concerns.

Here we report the composition and toxicity of biogas produced and directly used for electricity production at five different facilities in California. Samples at each site were collected over three separate days spanning a range of environmental conditions. Comprehensive measurements were performed for 273 different features including major biogas chemical components, a variety of different organic and inorganic trace components, trace elements, and microorganisms. Concentrations were compared to previously reported measurements and to the regulatory limits specified by OEHHA and the California Division of Occupational Safety and Health (Cal/OSHA). A standard biomarker assay was used to evaluate the oxidative capacity of biogas combustion exhaust and the associated short-term inflammatory response. A carcinogen screening mutagenicity bioassay was used to evaluate the probability that biogas combustion exhaust will damage DNA, leading to increased cancer risk over longer time periods. These comprehensive measurements help to understand the potential air quality impacts of widespread biogas production and combustion for electricity generation across California.

## **2.2 Methods**

### **2.2.1 Biogas sources**

A total of eighteen sets of samples were collected from five biogas facilities: 1) dairy waste biogas produced by a flushed manure collection and covered lagoon system, 2) dairy waste biogas produced by a scraped manure collection and digester system, 3) food waste biogas, 4) food waste biogas mixed with nearby landfill gas, 5a) biogas produced by the core portion of a regional landfill, and 5b) biogas produced from perimeter of the same regional landfill. The biogas production and utilization technologies used at each site are summarized in Table 2-1. A map showing the locations of all biogas facilities studied is present in Figure S. 2-1. All of the facilities generate electricity on-site using engines or turbines tuned to operate on biogas.

Table 2-1 Summary of biogas production sites characterized in this study

<b>Biogas Streams</b>	<b>Type of feedstock</b>	<b>Biogas Production technology</b>	<b>Gas end use</b>
1	Dairy farm cow manure (flushed). 1200 cows total. Surface water.	Covered lagoon Lower Mesophilic (20-30°C) Retention time 100 days	Fuel for internal combustion engine to generate electricity
2	Dairy farm cow manure (scraped). 1200 cows total. Ground water.	Single continuously stirred digester Mesophilic (35-40°C) Retention time 50 days	Fuel for internal combustion engine to generate electricity
3	Food waste 25 tons per day	Three-stage digester Thermophilic (50-55°C) Retention time 21 days	(a) Fuel for internal combustion engine to generate electricity (b) Upgrade to biomethane using membrane system
4	Varying amount of food waste, animal bedding and waste, municipal organic waste Landfill	Three-stage digester Thermophilic (50-55°C) Retention time 21 days 15 acres since early 1970s	Fuel for micro gas turbines to generate electricity
5	Landfill (core part)	Residential and commercial waste since 1967 (1,084 acres)	Fuel for gas turbines to generate electricity
6	Landfill (perimeter)	Residential and commercial waste since 1967 (1,084 acres)	Flared

### 2.2.2 Chemical analysis

Biogas is a complex matrix containing hundreds of trace chemical compounds that cover a broad range of functional groups with different volatility. Multiple sampling and analysis techniques are

employed to measure the full range of compound classes. Common sampling methods include collecting high volatility compounds in Tedlar (polyvinyl fluoride) bags or in metal canisters, enriching lower volatility compounds onto solid sorbent tubes, and stripping polar compounds using liquid sorbents in glass impingers. The widely used analysis procedures include compound separation using gas or liquid chromatography optionally coupled with a desorption unit followed by detectors that may be compound-specific or general mass spectrometers. Detection limits are typically tens to hundreds of parts per billion by volume for different compounds<sup>13,14,16-18,30-32</sup>.

The current study employed sampling and analysis techniques following the practices summarized above as published by the EPA (TO-15<sup>32</sup>, 8081b<sup>33</sup>, 8270d<sup>34</sup>, 8082a<sup>35</sup>, 29<sup>36</sup>) and ASTM (D1945<sup>37</sup>, D6228<sup>38</sup>) standard laboratory methods. Tedlar® sample bags were collected under positive system pressure or using a “Vac-U-Chamber” (SKC-West, Inc.) vacuum sampling apparatus if biogas pressure was negative. Each Tedlar bag sample analysis included a pure nitrogen system blank and calibration standards. Tedlar sample bags were directly connected to the instruments summarized in Table S. 2-1 and analyzed for the 119 compounds listed in Table S. 2-2. Semi-volatile and/or reactive chemical compounds were collected on three different types of sorbent tubes: XAD-2 sorbent tubes, coconut charcoal sorbent tubes and DNPH-treated silica gel tubes. Flow through each sorbent tube was controlled at 1.0 L · min<sup>-1</sup> using a calibrated variable area flow meter with built-in stainless steel valve followed by a downstream Teflon diaphragm pump (R202-FP-RA1, Air Dimensions Inc.). All sorbent tubes were sealed until just prior to sampling, and immediately capped at the conclusion of sampling. Each sample analysis run included a system blank, two sample blanks, and calibration standards. A multi-point calibration curve generated from the calibration standard was used to quantify the target compounds. Table S. 2-3 lists collection times, extraction methods and analysis methods for each sorbent tube. A comprehensive list of target chemical compounds in each sampling/analysis pathway is presented in Table S. 2-4 - Table S. 2-6 (102+33+13=148 compounds total). Biogas samples for metals analysis were collected using three serial glass impingers that each contained 20 mL of 5% nitric acid and 10% hydrogen peroxide in double deionized (18.2 MOhm\*cm) water. Liquid solutions from each of the impingers were transferred into separate capped vials and then analyzed with

inductively coupled plasma mass spectrometry (Agilent 7500i ICP-MS, operated with a Glass Expansion AR50 MicroMist nebulizer).

### 2.2.3 Biological analysis

Samples for biological analysis were collected on two 47 mm polycarbonate filters (0.4  $\mu\text{m}$  pore-size) to support analysis for cultivable microorganisms and corrosion inducing bacteria DNA. Sample flow rates ranged from 1-5  $\text{L} \cdot \text{min}^{-1}$  over times ranging from 2-4 hours. Condensate transported along with biogas was also collected. Individual filters were placed in 50 ml Falcon tubes containing 15 ml phosphate buffered saline (PBS). Filters were eluted in PBS by vortexing the Falcon tube for 5s followed by manual shaking for 2 min in a biosafety cabinet. Cultivable aerobic and anaerobic bacteria in eluates and condensates were enumerated by propagation in different growth media using the most probable number (MPN) tests<sup>39,40</sup>. Positive samples in the MPN tests were further characterized using DNA sequencing by conducting polymerase chain reaction (PCR) targeting 16S rRNA<sup>41</sup>. This allowed simultaneous identification of different bacteria species in each sample. Nucleic acids in eluates and condensates were extracted using the FAST DNA® SPIN KIT for Soil (MP Biomedicals, Irvine, CA) following the manufacturer's protocol. Five qPCR assays targeting total bacteria and corrosion inducing bacteria including sulfate reducing bacteria (SRB), iron oxidizing bacteria (IOB) and acid producing bacteria (APB) were selected from the literature<sup>42-46</sup>.

### 2.2.4 Toxicological analysis

Samples of biogas combustion exhaust were collected from five different electricity generators summarized in Table 2-1 after dilution with pre-cleaned background air. A 5.5  $\text{m}^3$  Teflon photochemical reaction chamber (0.051 mm NORTON FEP fluoropolymer film) installed in a 24-foot mobile trailer was used to simulate atmospheric aging of diluted exhaust under both light (daytime  $\text{UV}=50 \text{ W m}^{-2}$ ) and dark (nighttime) conditions at each test facility. The reaction chamber was flushed three times before each test with air that was pre-cleaned using granulated activated carbon to remove background gases followed by a

High Efficiency Particulate Arrestance (HEPA) filter to remove background particles. Dark aging tests started by filling the reaction chamber to 50% capacity with clean air, followed by injecting combustion exhaust through a 1/2-inch diameter insulated stainless steel transfer line at a flow rate of  $26 \text{ L} \cdot \text{min}^{-1}$  ( $50\sim 55^\circ\text{C}$ ) for 255 seconds. The reaction chamber was then filled to 100% capacity with clean air within 90 seconds, yielding a well-mixed system at a dilution ratio of approximately 50:1. The diluted exhaust was aged in the chamber for 3 hours before collection onto 47 mm Teflon filters (Zefluor,  $2 \mu\text{m}$  pore size) at  $20 \text{ L} \cdot \text{min}^{-1}$  for 3.5 hours. Light aging tests followed the same experimental protocol with the exception that 100 liters of VOC surrogate gas ( $1.125 \pm 0.022$  ppmv m-xylene and  $3.29 \pm 0.07$  ppmv n-hexane in air, Scott Marrin, Inc.) was injected into the chamber immediately after the combustion exhaust, creating a final VOC concentration of 90 ppbv. Hydroxyl radical concentrations during the light aging tests were calculated to be  $5\text{-}6 \times 10^6$  molecules  $\text{cm}^{-3}$  based on the decay rate of the m-xylene and final ozone concentrations at the end of the 3 hour experiment were measured to be 110~125 ppb.

The expression of in-vitro pro-inflammatory markers was measured in human U937 macrophage cells (American Tissue Culture Collection, Manassas, VA). Macrophages are the first line of defense in human lungs, and substances in engine exhaust sample may interact with the macrophage cells through the Toll-Like Receptors (TLR), Aryl hydrocarbon Receptor (AhR) and the NF-KappaB protein complex to induce inflammatory responses. Biomarkers checked in this study include Cytochrome P450 monooxygenase (CYP1A1: marker for polycyclic aromatic hydrocarbons), Interleukin 8 (IL-8: marker for inflammation), and Cyclooxygenase (COX-2: a key enzyme for production of prostaglandins mediating pain and inflammation). After a 6-hr treatment of exhaust filter extract, mRNA was isolated from U937 macrophage cells and reverse-transcribed into cDNA for quantitative expression analysis using qPCR. Results were normalized to housekeeping gene  $\beta$ -Actin expression and expressed as fold increase of mRNA in treated cells relative to untreated cells<sup>47</sup>. The mutagenicity bioassay was carried out via a micro-suspension modification of the *Salmonella*/microsome Ames assay<sup>48,49</sup> that is ten times more sensitive than the standard plate incorporation test. Frame-shift mutations of *Salmonella typhimurium* tester strain TA98 were observed. TA98 requires exogenous histidine (His<sup>-</sup>) for growth, however substances in exhaust

samples could cause deletion or addition of nucleotides in the DNA sequence of TA98 histidine gene (frame-shift), resulting in TA98's ability to manufacture histidine ( $\text{His}^+$ ). The resultant colonies are referred to as "Revertants" as the DNA sequence is changed back to its original correct form. Liver homogenate (S9) from male Aroclor-induced Sprague Dawley rats (Mol Tox, Boone, NC) was added to the assay to provide metabolic activation of the sample.

## 2.3 Results and discussion

### 2.3.1 Biogas composition

Concentrations of major biogas components (methane, carbon dioxide, nitrogen and oxygen) are shown in Figure 2-1. Methane ( $\text{CH}_4$ ) content of the different biogas streams varied from 49.5% to 70.5% with the exception of perimeter landfill biogas (biogas 6) which contained only 35.4% methane due to high levels of air intrusion into the gas extraction system. Biogas produced from flushed dairy waste using a covered lagoon (biogas 1) had the highest measured methane concentration. In contrast, biogas produced from scraped dairy waste in an anaerobic digester (biogas 2) had a much lower methane concentration of 51.3%. Similar trends were reported by Saber et al. who measured the average methane concentration in a covered lagoon dairy biogas facility in the western US to be 67.6%, while the methane concentration in a complete mixed dairy biogas digester in the western US was only 60.5%<sup>50</sup>. In addition, the biogas 2 facility adds iron chloride to digester slurry. Iron chloride is known to inhibit anaerobic digestion processes, resulting in lower biogas methane content<sup>51</sup>. Core landfill biogas had an average methane concentration of 49.5%, which fell into the range reported by previous studies conducted in US and Europe<sup>14,15,17</sup>. The carbon dioxide content in the biogas ranged from 20.2% in lagoon dairy biogas (biogas 1) to 46.9% in food waste/landfill biogas (biogas 4). Concentrations of  $\text{CH}_4$  and  $\text{CO}_2$  observed in this study fall in the range commonly reported for biogas. Another important GHG formed during the life cycle of organic waste management is nitrous oxide ( $\text{N}_2\text{O}$ ).  $\text{N}_2\text{O}$  is known to account for more than 20% of the total global warming

potential (100-yr scale) associated with GHGs emissions from organic waste storage practices<sup>52,53</sup>, but N<sub>2</sub>O is unlikely to form in the anaerobic digestion process that produces biogas<sup>54</sup>.

Small amounts of nitrogen (N<sub>2</sub>, < 8%) and oxygen (O<sub>2</sub>, <0.5%) were measured in biogas streams one through four. Air is commonly injected into the anaerobic digestion process at a rate of 2-6% to inhibit the formation of hydrogen sulfide<sup>55</sup>. The rate of anaerobic methane production does not decrease and may even increase when a small amount of oxygen is introduced, while the rate of hydrogen sulfide production is strongly reduced<sup>56</sup>. Higher concentrations of air are entrained into the landfill biogas by blowers that create negative pressure in porous collection pipes leading to air intrusion through the soil into the biogas stream. Air intrusion rates were higher at the perimeter of the landfill because less biogas was produced in this region, requiring more air intrusion to supply the extracted gas volume.

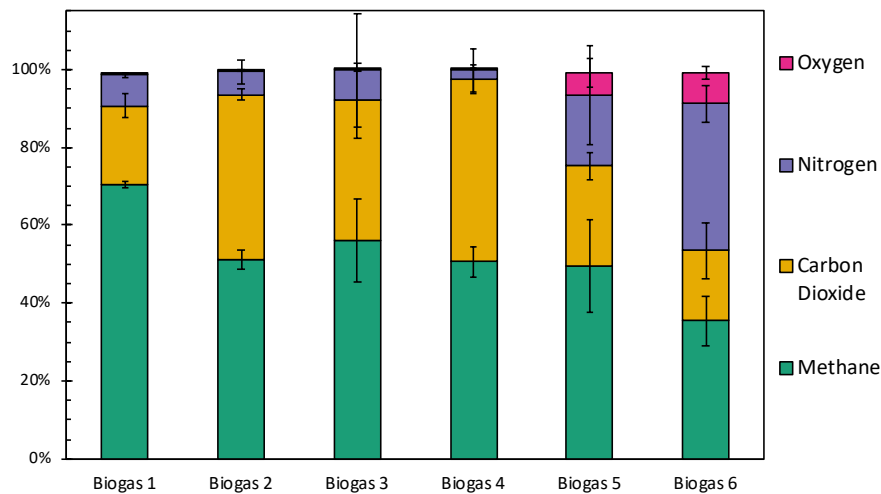


Figure 2-1 Major component concentrations by volume in dry biogas streams

### *Sulfur-containing compounds*

Figure 2-2 shows concentration of sulfur-containing compounds and their speciation. The amount of total sulfur-containing compounds varied significantly between different biogas facilities, reflecting the impact of both feedstock composition and primary sulfur control methods. The dairy biogas facility with covered lagoon (biogas 1) had the lowest total sulfur concentration composed mostly of sulfur dioxide with very little hydrogen sulfide. In contrast, the dairy biogas facility with the digester (biogas 2) had the second

highest total sulfur, nearly half of which (by volume) was hydrogen sulfide. Both of these dairy facilities used simple air injection to reduce H<sub>2</sub>S production, and the digester dairy facility also added iron chloride to the digester to further control H<sub>2</sub>S. This suggests that the covered lagoon dairy achieved optimum operating conditions for anaerobic digestion and biological desulfurization, with an effective combination of hydraulic retention time, lagoon temperature, pH, and air injection rates. Different feedstock at the two dairy facilities may also contribute to different biogas sulfur content. A dairy biogas study in the eastern US found that differences in water sulfur concentration explained differences in biogas sulfur concentration from some facilities<sup>21</sup>. In the current study, biogas facility 1 used lagoon water to flush the dairy stalls with periodic dilution using surface water sources. Biogas facility 2 did not have access to surface water sources and so used ground water exclusively. Landfills with active blower systems inevitably have air intrusion in the biogas which helps reduce sulfur content. The fraction of sulfur dioxide in perimeter landfill biogas stream is higher than that in core landfill biogas stream, indicating a more oxidized environment in the perimeter part compared to the core. Biogas 4 included contributions from a nearby landfill which produced a sulfur profile similar to that of the core landfill. Biogas 3 had the highest concentration of total sulfur-containing compounds. Levels of H<sub>2</sub>S (77.7ppm) and mercaptans (42.8ppm) in biogas 3 both exceeded OEHHA risk management trigger levels (22ppm for H<sub>2</sub>S and 12ppm for mercaptans), but were still well below the lower action level (216ppm for H<sub>2</sub>S and 120ppm for mercaptans)<sup>9</sup>. This suggests that no health risk concerns have been identified but routine monitoring of biogas sulfur content is advisable. Overall, the total sulfur concentrations measured in the current study fell into the lower end of the range reported in previous studies<sup>21,50</sup>.

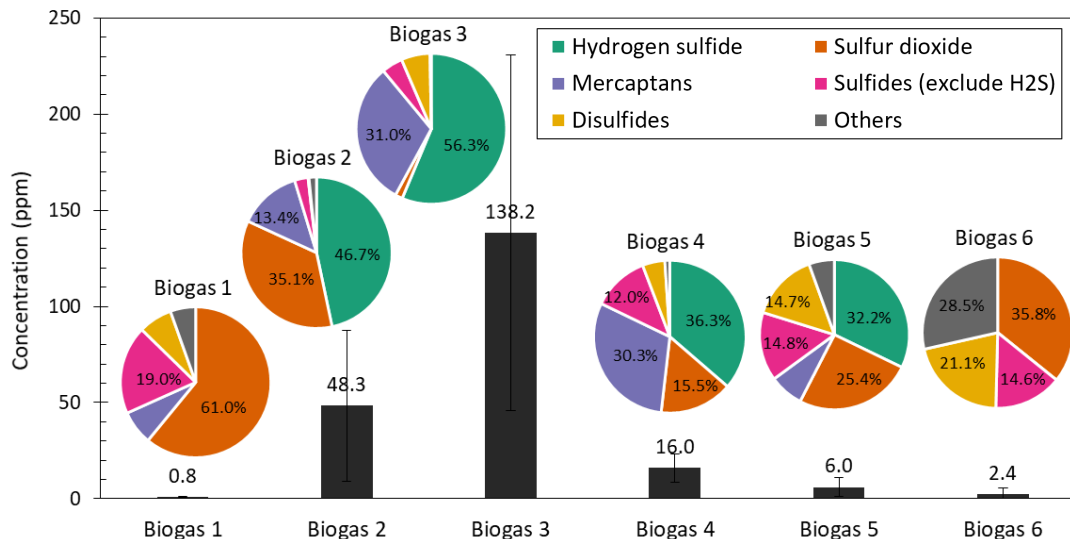


Figure 2-2 Total sulfur-containing compound concentration (ppm<sub>v</sub>) and speciation in different biogas streams

### **Halocarbons**

Figure 2-3 shows that the two landfill biogas streams (5&6) had the highest total halocarbon concentrations, while the dairy waste and food waste biogas facilities (1-3) produced biogas with lower total halocarbon concentrations. Biogas 4 had intermediate halocarbon concentrations because it was a mixture and food waste biogas and landfill gas. These trends reflect the halocarbon content of different feedstocks. Dairy biogas produced from the digester (biogas 2) had more chlorinated compounds than biogas produced from the covered lagoon (biogas 1) possibly due to the addition of iron chloride to the slurry, providing an additional source of chlorine. Chlorofluorocarbons (CFCs) commonly used as refrigerants were present in landfill biogas. Larger chloroalkenes (trichloroethene and tetrachloroethene) commonly used as degreasers were also detected in landfill biogas, along with smaller chloroalkenes that are likely breakdown products of the anaerobic digestion process<sup>57</sup>. Biogas 2 (dairy digester) unexpectedly contained chloroethene, suggesting that there were some cleaning processes involved in the operation of this digester. Table S. 2-7 compares selected halocarbon species with available data from previous studies on landfill biogas, together with the Cal/OSHA permissible exposure levels (PELs) and OEHHA risk management trigger levels (if available). Levels of halocarbons fall in the wide concentration range reported

by previous landfill studies and are well below the PELs, indicating negligible occupational health concern. Studies have shown that halocarbons form corrosive products during combustion in engines, resulting in earlier failure of engine parts. However, total halocarbon concentration found in biogas from all different streams in this study are safely below the level that might cause early engine parts corrosion<sup>14</sup>.

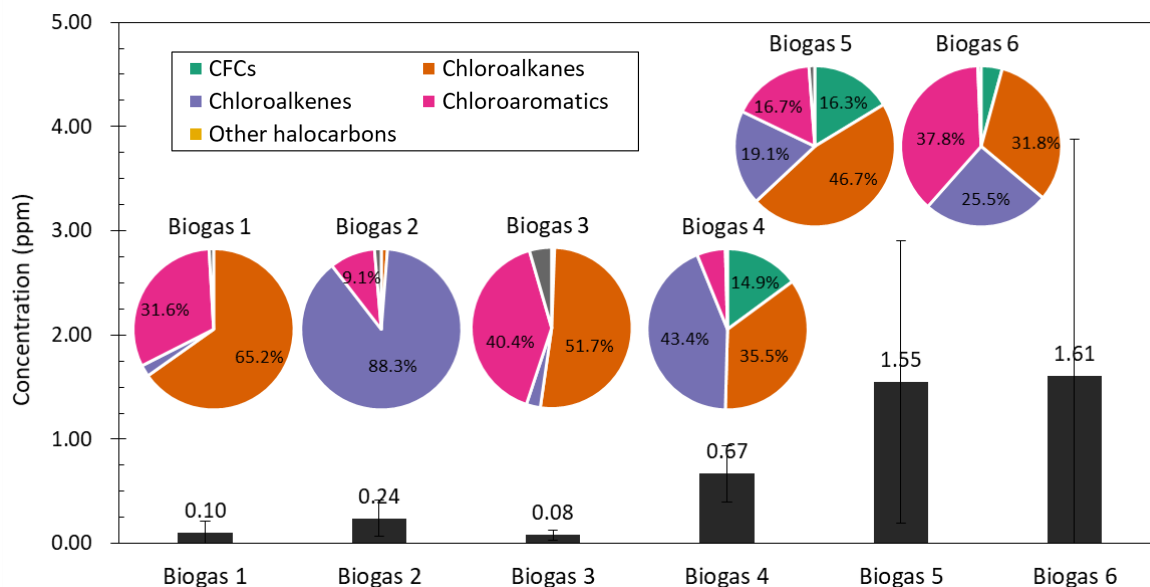


Figure 2-3 Total halocarbon concentration (ppm<sub>v</sub>) and speciation in different biogas streams

## BTEX

Benzene, toluene ethylbenzene and xylene (BTEX) compounds are regulated as “hazardous air pollutants” by the US EPA. Benzene is a known human carcinogen, while toluene, ethylbenzene and xylenes are harmful to the human nervous system and can cause eye and throat irritation during high level exposure. Consumer products such as paints, rubber, adhesives, cosmetics and pharmaceuticals are major sources of BTEX<sup>58</sup>. Figure 2-4 shows that landfill biogas had much higher BTEX than food waste and dairy waste biogas because municipal solid waste contains many consumer products. Biogas 4 had intermediate BTEX concentrations because it is a mixture of food waste and landfill biogas. Table S. 2-8 lists average concentration of BTEX in each biogas stream, together with the PELs given by Cal/OSHA and risk management trigger levels by OEHHA. All of the biogas averaged BTEX compound concentrations were

below the 8-h averaged PEL. Concentrations of benzene in landfill biogas were just below the PEL, indicating that routine monitoring of BTEX concentrations is advisable at landfills.

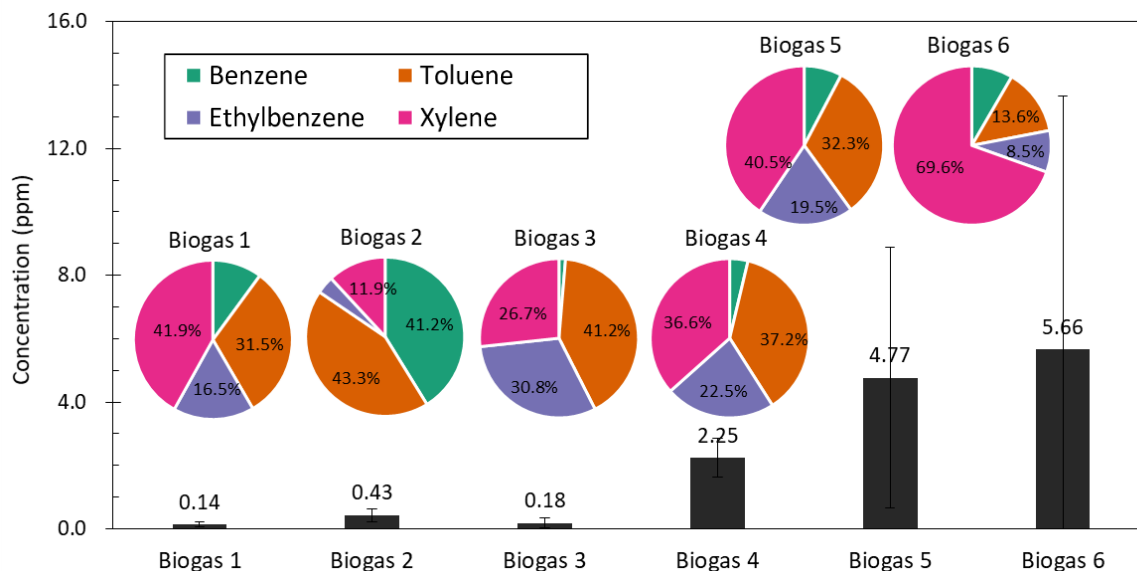


Figure 2-4 Total BTEX concentration (ppm) and speciation in different biogas streams

### *Siloxanes*

Figure 2-5 presents siloxane concentrations from different biogas streams. Biogas 4, 5 and 6 had high total siloxanes because of the many siloxane-containing compounds in the landfill feedstock including personal care products, fabric softeners, and surface treatment formulas. Notably, although biogas 4 was a mixture of food waste biogas and landfill biogas, it contained even more siloxanes than the pure landfill biogas streams (5 & 6). This indicated that the landfill site which contributed to biogas 4 had received more siloxane-containing products compared to the landfill site producing biogas 5&6. Biogas 1, 2 and 3 had low siloxane concentrations made up mostly by D4 (decamethyltetrasiloxane) and D5 (dodecamethylpentasiloxane) species. Table S. 2-9 lists concentration of each siloxane species in the top three high-siloxane biogas streams (biogas 4, 5 and 6), together with measured values from previous landfill studies. Siloxane concentrations in landfill gas are variable but L2 (hexamethyldisiloxane), D4 and D5 are consistently found to be the most abundant species. Although siloxanes are not considered to be directly

toxic to the environment or human health, siloxane combustion forms silica (SiO<sub>2</sub>) nanoparticles (Dp<100nm). Silica nanoparticles can degrade engine performance and increase CO emission by abrading engine parts, depressing spark plug functionality, and deactivating emission control system<sup>17,18,59</sup>. Engine manufacturers typically set siloxanes concentration limits ranging from 10 to 28 mg · m<sup>-3</sup><sup>60</sup>. All of the biogas streams measured in the current study met this requirement<sup>60</sup>. Nanoparticles are also known to be toxic due to their large surface-to-volume ratio and ability to translocate in the human body, but the exact short- and long-term effects of Si-based nanoparticles are not yet completely understood<sup>61</sup>.

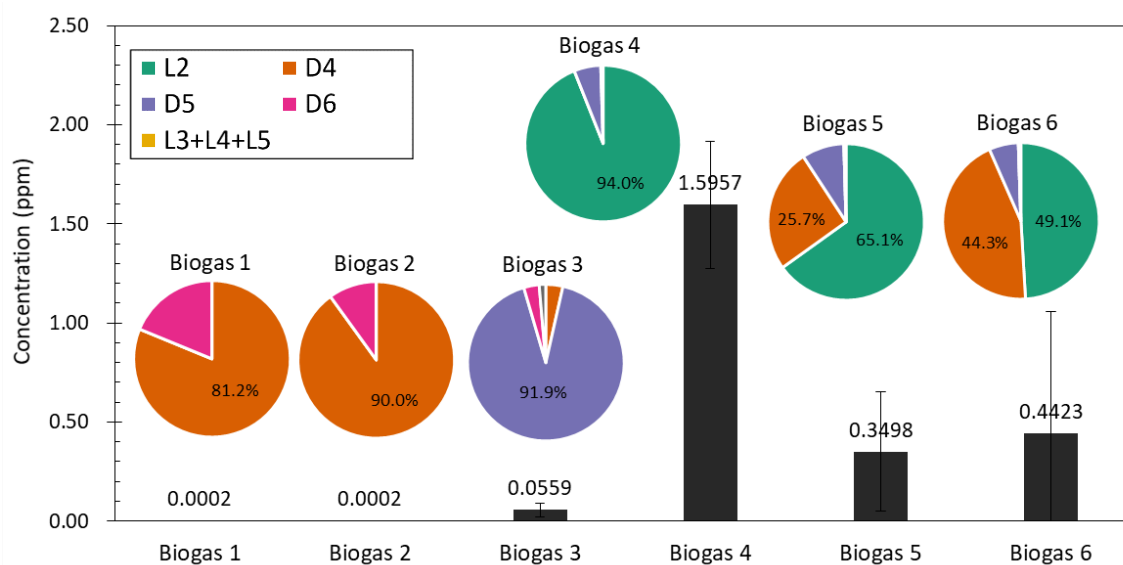


Figure 2-5 Total siloxane concentration (ppmv) and speciation in different biogas streams L2 (Hexamethyldisiloxane), L3 (Hexamethylcyclotrisiloxane), L4 (Decamethyltetrasiloxane), L5 (Dodecamethylpentasiloxane), D4 (Octamethylcyclotetrasiloxane), D5 (Decamethylcyclopentasiloxane), D6 (Dodecamethylcyclohexasiloxane)

### Metals

A total of 24 different elements were analyzed in the biogas streams with all measured values reported in

Table S. 2-10. Concentrations of arsenic (As), antimony (Sb), lead (Pb), copper (Cu) and aluminum (Al) are summarized in Table 2-2. Concentrations of antimony, lead, copper and aluminum in biogas fall well below the Cal/OSHA PELs and OEHHA risk management trigger levels. Arsenic concentrations in some landfill biogas samples slightly exceeded the Cal/OSHA 8-h PEL, but the average concentrations were below the PELs as well as the risk management trigger level, indicating negligible potential health risks. Possible sources of arsenic in biogas include semiconductor electronic devices deposited into landfills or pesticides / herbicides that make it into the organic waste stream.

Table 2-2 Concentration of arsenic (As), antimony (Sb), lead (Pb), copper (Cu) and aluminum (Al) in different biogas streams ( $\mu\text{g} \cdot \text{m}^{-3}$ ).

Element	As	Sb	Pb	Cu	Al
LOD	0.005	0.005	0.1	0.005	0.2
Biogas 1	0.315± 0.432	0.259± 0.184	1.7± 2.4	0.000± 0.000	0.0± 0.0
Biogas 2	0.012± 0.018	0.006± 0.009	7.4± 10.5	0.000± 0.000	0.0± 0.0
Biogas 3	0.230± 0.380	0.310± 0.170	0.0± 0.0	0.005± 0.008	0.0± 0.0
Biogas 4	1.600± 1.400	1.600± 1.800	0.1± 0.3	0.000± 0.000	2.2± 5.0
Biogas 5	8.500± 3.400	12.500± 12.500	0.8± 0.8	0.000± 0.000	0.0± 0.0
Biogas 6	4.200± 2.300	1.300± 2.000	0.7± 1.1	0.200± 0.340	5.6± 9.6
<b>Cal/OSHA</b> 8h average PEL <sup>67</sup>	10	500	50	100	5000
<b>OEHHA</b> trigger level <sup>67</sup>	19	600	75	60	-

Results expressed in (average value ± 1 standard deviation).  
Concentrations below LOD (limit of detection) are denoted as 0±0.

### ***Bacteria***

Table 2-3 summarizes the biological entities measured in the biogas samples. Cultivable (spore-forming) bacteria were detected two times in three samples (biogas 1-dairy), one time in three samples (biogas 2-dairy) and six times in eleven samples (biogas 3-food waste). Cultivable biologicals were less commonly found in landfill biogas streams (two out of seven samples for biogas 4, and one out of six samples for biogas 5 & 6). Basic Logical Assignment Search Tool (BLAST) database analysis determined that cultivable biologicals were closely related to *Bacillus* spp. or *Paenibacillus* spp. which are gram-positive, spore-forming bacteria found in a variety of environments including soil, water, and rhizosphere.

Approximately 10 to 100 MPN per m<sup>3</sup> were measured in the current study, which is comparable to results from previous studies reporting cultivable bacteria concentrations in biogas<sup>62,63</sup>.

Total bacteria concentrations assessed by qPCR were below sample limits of detection (SLODs) in most biogas streams except for the landfills. Sulfate reducing bacteria (SRB) target genes were not detected in any samples, consistent with the results from previous studies on dairy and landfill biogas<sup>40,62</sup>. Iron oxidizing bacteria (IOB) were found only once in most biogas streams except for biogas 4 (twice in seven samples). DNA sequencing of qPCR amplicons revealed that IOB were closely related to *Gallionella capsiferriformans* and *Leptothrix* spp.. Acid producing bacteria (APB) target gene (*buk*) was detected in biogas 1, 3 and 4. One-way ANOVA analysis showed that the mean values of IOB and APB were not statistically different from their SLODs ( $p > 0.05$ ). Therefore, IOB and APB will not likely reduce the service life of biogas facilities characterized in the current study.

Table 2-3 Results of biological analysis (cultivation and qPCR)

Parameter <sup>a</sup>	Biogas 1	Biogas 2	Biogas 3	Biogas 4	Biogas 5	Biogas 6
Cultivation analysis (MPN • m <sup>-3</sup> ) <sup>b</sup>						
Live aerobic bacteria	34 ± 7 (2/3)	<SLOD (0/3)	<SLOD (0/4)	87 ± 39 (2/7)	<SLOD (0/3)	<SLOD (0/3)
Live anaerobic bacteria	<SLOD (0/3)	<SLOD (0/3)	<SLOD (0/4)	<SLOD (0/7)	<SLOD (0/3)	<SLOD (0/3)
Live aerobic spore bacteria	<SLOD (0/3)	22 ± 10 (1/3)	32 ± 14 (2/4)	32 ± 13 (2/7)	<SLOD (0/3)	29 ± 19 (1/3)
Live anaerobic spore bacteria	<SLOD (0/3)	<SLOD (0/3)	<SLOD (0/4)	<SLOD (0/7)	<SLOD (0/3)	<SLOD (0/3)
qPCR analysis (gene copies • m <sup>-3</sup> )						
Total bacteria	<SLOD (0/3)	<SLOD (0/3)	<SLOD (0/4)	<SLOD (0/7)	3600 ± 2300 (1/3)	4300 ± 4000 (1/3)
Sulfate reducing bacteria (SRB)	<SLOD (0/3)	<SLOD (0/3)	<SLOD (0/4)	<SLOD (0/7)	<SLOD (0/3)	<SLOD (0/3)
Iron oxidizing bacteria (IOB)	450 ± 440 (1/3)	29 ± 23 (1/3)	190 ± 190 (1/4)	170 ± 100 (2/7)	430 ± 550 (1/3)	23 ± 24 (1/3)
Acid producing bacteria (APB)	180 ± 180 (1/3)	<SLOD (0/3)	160 ± 100 (2/4)	800 ± 560 (2/7)	<SLOD (0/3)	<SLOD (0/3)

(a) Results shown are means ± standard errors. Data below sample limits of detection (SLODs) were assumed to be the half of the SLODs for mean calculation. The median SLODs of cultivation tests were 23 MPN per m<sup>3</sup>. The median SLODs of qPCR were 3200, 22, 140, 13, and 16 gene copies per m<sup>3</sup> for total bacteria, SRB, IOB and APB,

respectively. The number of detects out of total samples tested is shown in parenthesis. Condensate water data were combined with raw biogas data if applicable.  
(b) MPN, most probable number

### 2.3.2 Biogas engine combustion exhaust

Figure 2-6 (a-d) shows bioassay results measured from particulate matter collected on filters for on-site biogas engine/turbine exhaust aged under dark and light conditions. Panels (a)-(c) present levels of biomarker expression (CYP1A1, IL-8 and COX-2, respectively) in U937 human macrophages after a 6-hr treatment with biogas engine exhaust extract. Results are expressed as fold increase above blank levels. Overall, the biomarker responses from biogas electricity generators at sites 1-5 were similar under dark conditions. Photochemical aging did not appear to strongly influence these results, with the exception that biogas 2 engine exhaust induced notably greater expression of the monooxygenase enzyme CYP1A1 and pro-inflammatory signaling protein IL-8 under light conditions. These samples likely contained polycyclic aromatic hydrocarbons which could be metabolized into carcinogens by CYP1A1 and materials that could lead to inflammatory responses when inhaled.

Figure 2-6 (d) shows the result of the mutagenic bioassay (*Salmonella*/microsome Ames assay) under dark and light conditions. The number of TA98 revertants from a field blank sample (clean air and surrogate VOC gases aged in the photochemical reaction chamber) was subtracted from the biogas test results. No activity over spontaneous background was observed for biogas 2 dark, biogas 4 light, and biogas 5 both dark and light conditions. Exhaust from biogas 1 showed higher mutagenicity concentrations than other biogas streams. Photochemical aging did not strongly affect the mutagenicity of the exhaust, suggesting that photochemical reactions will likely not change the genotoxic properties of particulate matter exhaust from biogas engines.

Overall, engine exhaust from dairy biogas (biogas 1 and 2) showed slightly higher bioassay activity than exhaust from other biogas sources, especially after aging under simulated UV light. A previous study indicated that particulate matter from dairy farms can induce pro-inflammatory responses with toxic and immunogenic substances such as histamine, endotoxins, different antigens and microorganisms<sup>47</sup>. The

observed higher activities in dairy biogas combustion exhaust may actually be driven by dairy farm background air drawn into the engines during the combustion process, rather than the combustion products of biogas itself. Moreover, a previous study by Xue, et al. showed that ultrafine particle emission from biogas-fueled engines are influenced more strongly by the engine and combustion technology than by the fuel composition<sup>64</sup>. The relationships between the properties of the fuel, the properties of the gas-phase combustion exhaust, the properties of the PM in the combustion exhaust, and the toxicity of the PM are not fully understood in the current study, but the current results suggest that the toxicity of the dairy biogas combustion exhaust merits further investigation.

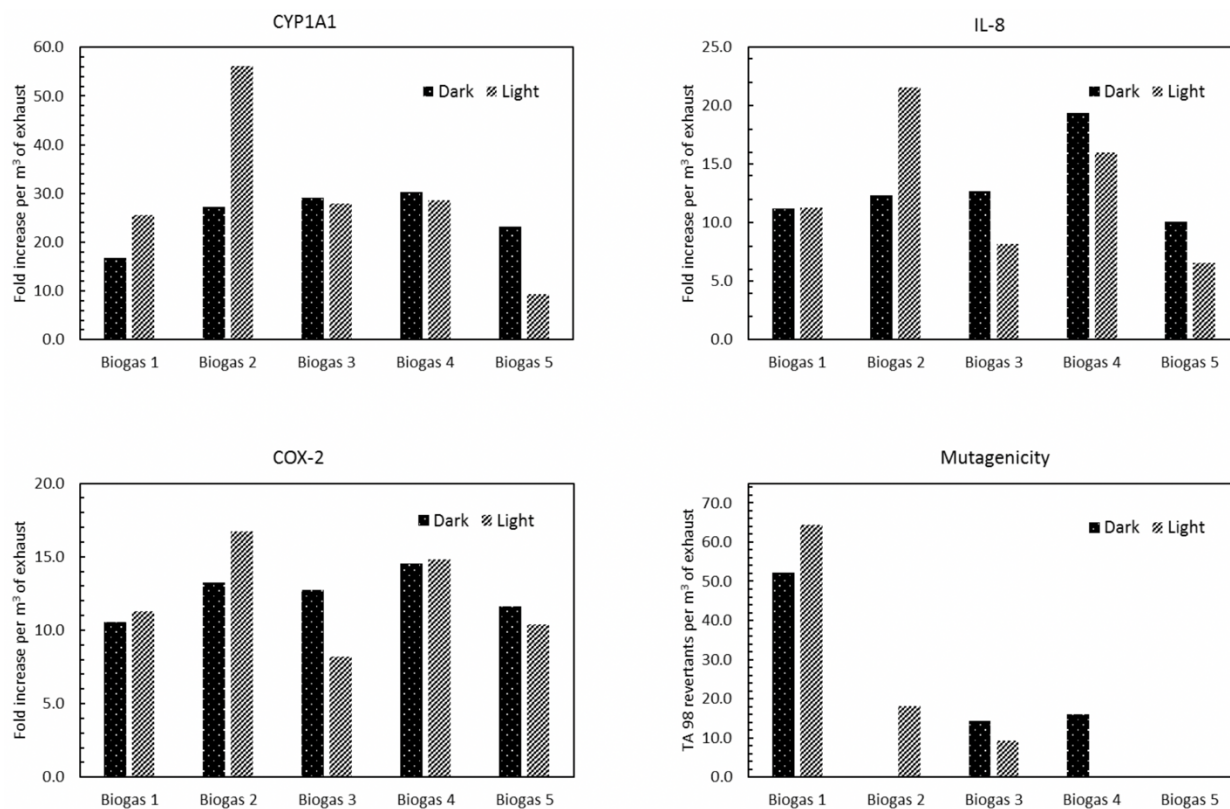


Figure 2-6 Bioassay results of on-site biogas engine/turbine exhaust aged under dark and light conditions (a) fold increase of CYP1A1 per m<sup>3</sup> of engine exhaust, (b) fold increase of IL-8 per m<sup>3</sup> of engine exhaust, (c) fold increase of COX-2 per m<sup>3</sup> of engine exhaust, and (d) number of TA98 net revertants per m<sup>3</sup> of engine exhaust

## 2.4 Implications

Calculated emission factors (EFs) of SO<sub>2</sub> and selected organic compounds are summarized in Table 2-4 and Table 2-5 to support future predictions of the aerosol formation potential of biogas burning in engines. SO<sub>2</sub> EFs ( $\frac{\text{g-SO}_2 \text{ (or mg-SO}_2\text{)}}{\text{m}^3\text{-biogas}}$  or  $\frac{\text{lb-SO}_2}{10^6 \text{ Btu energy}}$ ) were estimated for each biogas stream, assuming that all the S-containing compounds in the fuel are converted to SO<sub>2</sub> under stoichiometric combustion conditions. Calculations were carried out for both raw biogas and for upgraded biogas (biomethane) as summarized in Table 2-4. SO<sub>2</sub> EFs range from 1.71 x 10<sup>-4</sup> lb MMBtu<sup>-1</sup> to 3.5 x 10<sup>-2</sup> lb MMBtu<sup>-1</sup> in raw biogas due to variability in fuel sulfur and methane content. SO<sub>2</sub> EFs for biomethane range from 1.06 to 4.07 x 10<sup>-4</sup> lb MMBtu<sup>-1</sup> because the pre-cleaning steps for the upgrading process remove sulfur from the fuel<sup>65</sup>. For reference, the SO<sub>2</sub> EF from natural gas fired stationary reciprocating engines<sup>66</sup> is 5.88 x 10<sup>-4</sup> lb MMBtu<sup>-1</sup> which is comparable to the biomethane EFs calculated in the current study.

Table 2-4 Concentration of total S-containing compounds in biogas and biomethane streams and emission factors of SO<sub>2</sub> from burning these gas streams

	Biogas			Biomethane		
	Total S in fuel <sup>a</sup> (ppm)	EF - SO <sub>2</sub> (g m <sup>-3</sup> -biogas)	EF - SO <sub>2</sub> (lb/MMBtu)	Total S in fuel <sup>a</sup> (ppm)	EF - SO <sub>2</sub> (mg m <sup>-3</sup> -biomethane)	EF - SO <sub>2</sub> (lb/MMBtu)
Biogas 1	0.81±0.29	0.002±0.001	(1.71±0.74)E-04	/	/	/
Biogas 2	48.28±39.33	0.117±0.095	(1.52±0.99)E-02	0.648±0.197	1.56±0.48	(1.06±0.32)E-04
Biogas 3	138.19±92.51	0.334±0.223	(3.50±2.32)E-02	1.706±0.697	4.12±1.68	(2.71±1.12)E-04
Biogas 4	15.95±7.50	0.039±0.018	(4.18±1.88)E-03	2.583±1.296	6.23±3.13	(4.07±2.08)E-04
Biogas 5	6.00±4.96	0.014±0.012	(1.81±1.25)E-03	/	/	/

<sup>a</sup>Concentration results expressed as (average value ± 1 standard deviation).

Concentrations of different semi-volatile organic compounds, PAHs and extended hydrocarbons in the engine exhaust were measured after injection into the photochemical reaction chamber and aging under dark or light conditions. Note that concentrations were diluted by a factor of ~50 to represent true atmospheric conditions which resulted in low measured values close to method detection limits. Concentrations vary from site to site due to this issue and so median results across all locations are shown rather than results for individual locations. Table 2-5 summarizes concentrations of various organic

compounds in exhaust as well as the calculated EFs. Median values are reported along with minimum and maximum values in the parentheses. EFs for 4-stroke lean-burn natural gas fired reciprocating engines<sup>66</sup> are listed in the last column of Table 2-5 as a reference point. EFs of various organic compounds from biogas-fired engines are generally comparable or lower than EFs from natural gas-fired engines.

Table 2-5 Concentration of selected compounds in diluted and atmospherically aged engine exhaust, their emission factors from burning in biogas engines, and corresponding emission factors for natural gas engines

Compounds	Concentration <sup>a</sup> (ppb)	EF <sup>a</sup> (mg m <sup>-3</sup> -biogas)	EF <sup>a</sup> (lb MMBtu <sup>-1</sup> )	natural gas engines <sup>66</sup> EF (lb MMBtu <sup>-1</sup> )
1,3-Dichlorobenzene	0.003 (0-0.014)	0.007 (0-0.034)	0.78 (0-3.53) E-06	/
1,4-Dichlorobenzene	0.003 (0-0.015)	0.007 (0-0.364)	0.07 (0-3.78) E-05	/
Benzyl Alcohol	0.008 (0-0.053)	0.014 (0-0.095)	1.50 (0-9.89) E-06	/
m,p-Cresol	0.011 (0-0.028)	0.020 (0-0.051)	2.08 (0-5.29) E-06	/
2,4-Dichlorophenol	0.009 (0-0.015)	0.025 (0-0.040)	2.55 (0-4.14) E-06	/
Naphthalene	0.035 (0-0.075)	0.075 (0-0.160)	0.78 (0-1.66) E-05	7.44E-05
2-Methylnaphthalene	0.005 (0-0.015)	0.012 (0-0.035)	1.24 (0-3.68) E-06	3.32E-05
1-Methylnaphthalene	0.010 (0-0.033)	0.024 (0-0.078)	2.47 (0-8.07) E-06	/
Dimethyl phthalate	0.004 (0-0.011)	0.014 (0-0.034)	1.44 (0-3.58) E-06	/
2,4-Dinitrotoluene	0.052 (0-0.139)	0.158 (0-0.423)	1.65 (0-4.40) E-05	/
Diethyl phthalate	0.012 (0-0.037)	0.044 (0-0.136)	0.46 (0-1.42) E-05	/
Phenanthrene	0.002 (0-0.007)	0.005 (0-0.020)	0.55 (0-2.05) E-06	1.04E-05
Di-n-butyl phthalate	0.002 (0-0.006)	0.007 (0-0.028)	0.76 (0-2.92) E-06	/
Bis(2-ethylhexyl) phthalate	0.003 (0-0.011)	0.020 (0-0.074)	2.04 (0-7.66) E-06	/
(1-Methylethyl) benzene	0.011 (0-0.090)	0.021 (0-0.181)	0.22 (0-1.89) E-05	/
1,2,4-Trimethylbenzene	0.009 (0-0.064)	0.019 (0-0.128)	0.20 (0-1.33) E-05	1.43E-05
1,3,5-Trimethylbenzene	0.035 (0-0.242)	0.071 (0-0.487)	0.74 (0-5.06) E-05	3.38E-05
Decane	0.020 (0-0.346)	0.047 (0-0.822)	0.49 (0-8.55) E-05	/
Tetradecane	0.013 (0-0.048)	0.044 (0-0.157)	0.45 (0-1.64) E-05	/
Hexadecane	0.017 (0-0.048)	0.064 (0-0.183)	0.67 (0-1.91) E-05	/
Octadecane	0.013 (0-0.021)	0.053 (0-0.091)	5.53 (0-9.46) E-06	/
Eicosane	0.015 (0-0.024)	0.073 (0-0.115)	0.76 (0-1.20) E-05	/

<sup>a</sup> Median value across all biogas streams. Values inside parentheses are minimum and maximum

The current study characterizes the range of trace composition profiles for California biogas produced from different feedstocks. These trace component characteristics play a central role in determining what upgrading steps are required to enable biogas energy recovery<sup>65</sup> and what routine

monitoring protocols are needed to protect pipeline infrastructure and public health. Quantifying the broad array of trace contaminants in biogas is challenging for two reasons. First, the composition of biogas varies with feedstock, weather condition, digester operating parameters, etc. Second, different laboratories employ different sampling and analysis techniques that can lead to different detection limits. Characterizing the distribution of concentrations for each contaminant requires repeated measurements across multiple seasons using identical methods followed by statistical analysis. The biogas industry should agree on a set of sampling and analysis protocols to facilitate inter-comparison of results from different laboratories.

No strong evidence of potential occupational health risk was detected at any of the five California biogas sites. This study also found no obvious differences between the toxicity of different biogas combustion exhaust streams after atmospheric dilution and aging. Future studies should continue to characterize the variability of the trace chemical composition of biogas combustion exhaust to enable a more detailed statistical analysis of potential public health impacts of large biogas energy recovery facilities.

## 2.5 Appendix

Table S. 2-1 Tedlar bag sample analysis specifications

Table S. 2-2 Target compounds in Tedlar sample bag analysis

Table S. 2-3 Sorbent tubes sampling and analysis specifications

Table S. 2-4 Target compounds in XAD-2 sorbent tube analysis

Table S. 2-5 Target compounds in charcoal sorbent tube analysis

Table S. 2-6 Target compounds in silica sorbent tube analysis

Table S. 2-7 Concentration range of selected halocarbons ( $\text{mg} \cdot \text{m}^{-3}$ ) measured at different landfill sites and permissible occupational exposure levels by Cal/OSHA and OEHHA

Table S. 2-8 Average concentration of BTEX measured in different biogas streams ( $\text{mg} \cdot \text{m}^{-3}$ ) and permissible occupational exposure levels by Cal/OSHA and OEHHA

Table S. 2-9 Concentration of siloxanes in different biogas streams ( $\text{mg} \cdot \text{m}^{-3}$ )

Table S. 2-10 Concentration of metals in different biogas streams ( $\mu\text{g} \cdot \text{m}^{-3}$ )

Figure S. 2-1 Map locations of the biogas facilities studied

Figure S. 2-2 Concentration (ppmv) of carbonyls in different biogas streams

Table S. 2-1 Tedlar bag sample analysis specifications

Compounds targeted	Analysis method	
Major compounds (carbon dioxide, methane, nitrogen, oxygen, etc...)	Agilent 6850 gas chromatograph + thermal conductivity detector	Sample loop: 250µl, split ratio 20:1 Inlet temperature and pressure: 270°C, 16psi Column: Agilent J&W CP-Sil5 CB for formaldehyde 60mx0.32mmx8.00µm Column flow rate: 2.4ml/min Total helium flow rate: 53.7ml/min Temperature program: -20°C for 5min, ramp to 150°C at 10°C/min, hold at 150°C for 2min, ramp to 280°C at 150°C/min, and hold for 2min Detector temperature and flow: 250°C, reference flow 20ml/min, make-up flow 4.6ml/min
Hydrogen sulfide	Agilent 6850 gas chromatograph + flame photometric detector	Sample loop: 0.1ml or 1ml, split-less Inlet temperature and pressure: 50°C, 10.4psi Column flow rate: 2.4ml/min Total helium flow rate: 53.3ml/min Column: Agilent J&W HP1 30mx0.32mmx5.00µm Temperature program: 35°C for 3min, ramp to 260°C at 50°C/min, hold at 260°C for 4min Detector temperature and flow: 250°C, H <sub>2</sub> flow 50ml/min, air flow 60ml/min, make-up flow (N <sub>2</sub> ) 57.6ml/min
Volatile organic compounds, volatile sulfur compounds (exclude H <sub>2</sub> S), volatile halocarbons	Markes Unity 2 gas sampling/thermal desorption system + Agilent 6890/5973N Gas chromatograph – Mass spectrometer	Sulfur trap: Markes U-T6SUL-2S, hold at 25°C Sample flow: 50ml/min for 2.0min Desorption: 300°C for 3.0min Transfer line: 140°C Column: Agilent J&W DB-VRX column 60 m x 0.25 mm x 1.40 µm Temperature program: 45°C for 3min, ramp to 190°C at 10°C/min, ramp to 250°C at 20°C/min, hold at 250°C for 8min

Table S. 2-2 Target compounds in Tedlar sample bag analysis

Major compounds	Volatile sulfur compounds	Volatile halocarbons		Volatile organic compounds
Nitrogen/Carbon Monoxide	Sulfur Dioxide	Dichlorodifluoromethane	1,1,2,3,4,4-hexachloro-1,3-	1,3-Butadiene
Oxygen/Argon	Carbonyl sulfide	1,2-dichloro-1,1,2,2-tetrafluoroethane	Butadiene	Benzene
Methane	Carbon disulfide	1,1,2-trichloro-1,2,2-trifluoroethane	Chlorobenzene	Toluene
Carbon Dioxide	Methyl mercaptan	Trichlorofluoromethane	1,2-dichlorobenzene	Ethylbenzene
Ammonia	Ethyl mercaptan	Dichloromethane	1,3-dichlorobenzene	m,p-Xylene
Hydrogen	Isopropyl mercaptan	Chloroform	1,4-Dichlorobenzene	o-Xylene
Ethane	n-Propyl mercaptan	Carbon Tetrachloride	1,2,3-Trichlorobenzene	Styrene
Ethene	t-Butyl mercaptan	Chloroethane	1,2,4-trichlorobenzene	Isopropylbenzene
Ethyne	Dimethyl sulfide	1,1-dichloroethane	2-Chlorotoluene	4-Ethyltoluene
Propane	Methyl Ethyl sulfide	1,2-Dichloroethane	4-Chlorotoluene	n-Propylbenzene
Propene	Diethyl sulfide	1,1,1-trichloroethane	Bromomethane	1,3,5-trimethylbenzene
Propadiene	Di-tert-butyl sulfide	1,1,2-trichloroethane	dibromomethane	tert-butylbenzene
Propyne	Dimethyl Disulfide	1,1,1,2-tetrachloroethane	Bromoform	1,2,4-Trimethylbenzene
i-Butane	Diethyl Disulfide	1,1,2,2-tetrachloroethane	bromochloromethane	s-Butylbenzene
n-Butane	Methyl Ethyl Disulfide	Chloroethene	bromodichloromethane	p-Isopropyltoluene
1-Butene	Methyl i-Propyl Disulfide	1,1-dichloroethene	dibromochloromethane	n-butylbenzene
i-Butene	Methyl n-Propyl Disulfide	cis-1,2-Dichloroethene	1,2-dibromoethane	Naphthalene
trans-2-Butene	Methyl t-Butyl Disulfide	Trans-1,2-dichloroethene	Bromochloroethane	Pyridine
cis-2-Butene	Ethyl i-Propyl Disulfide	Trichloroethene	1,2-dibromo-3-	Nitrobenzene
1,3-Butadiene	Ethyl n-Propyl Disulfide	Tetrachloroethene	chloropropane	
Isoprene	Ethyl t-Butyl Disulfide	1,2-dichloropropane	bromobenzene	
i-Pentane	Di-i-Propyl Disulfide	2,2-dichloropropane		
n-Pentane	i-Propyl n-Propyl Disulfide	1,2,3-trichloropropane		
neo-Pentane	Di-n-Propyl Disulfide	3-chloropropene		
Pentenes	i-Propyl t-Butyl Disulfide	1,1-dichloropropene		
	n-Propyl t-Butyl Disulfide	cis-1,3-dichloropropene		
	Di-t-Butyl Disulfide	trans-1,3-dichloropropene		

Table S. 2-3 Sorbent tubes sampling and analysis specifications

Sampling media	Compounds targeted	Sampling duration	Extraction method	Analysis method	
Charcoal tube	Extended hydrocarbons, Siloxanes	60min at 1 L min <sup>-1</sup>	1ml ethyl acetate Sonicate 30min	Agilent 7890 gas chromatograph + Agilent 7200 quadrupole time-of-flight mass spectrometer	Injection volume: 1.0µl Injection temperature: 250°C Column: Agilent J&W HP5-MS UI 30mx0.25mmx0.25µm Column flow: Helium 0.8ml/min Temperature program: 35°C for 3min, 30°C to 325°C at 4°C/min, hold at 325°C for 3min
XAD-2 tube	Semi-volatile organic compounds, Polycyclic aromatic hydrocarbons, Polychlorinated biphenyls, Semi-volatile sulfur compounds, Pesticides	60min at 1 L min <sup>-1</sup>	1ml ethyl acetate Sonicate 30min	Agilent 7890 gas chromatograph + Agilent 7200 quadrupole time-of-flight mass spectrometer	Injection volume: 1.0µl Injection temperature: 250°C Column: Agilent J&W HP5-MS UI 30mx0.25mmx0.25µm Column flow: Helium 0.8ml/min Temperature program: 35°C for 3min, 30°C to 325°C at 4°C/min, hold at 325°C for 3min
Silica tube with dinitrophenylhydrazine (DNPH) coating	Carbonyls	1min at 1 L min <sup>-1</sup>	1ml acetonitrile Sonicate 30min	Agilent 1200 liquid chromatograph + Agilent 6530 quadrupole time-of-flight mass spectrometer	Injection volume: 10µl Column: Restek Ultra C <sub>18</sub> 5µm 250x4.6mm Gradient program: 40% A (deionized water with 1mM ammonium acetate) and 60% B (acetonitrile/H <sub>2</sub> O, 95/5 v/v, with 1mM ammonium acetate) for 7min, linear increase to 100% B at 20min, hold at 100% B for 0.5min

Table S. 2-4 Target compounds and their LOQs in XAD-2 sorbent tube analysis

Semi-volatile sulfur-containing compounds	LOQ (ppbv)	Semi-volatile organic compounds and PAHs	LOQ (ppbv)	Semi-volatile organic compounds and PAHs	LOQ (ppbv)	Pesticides	LOQ (ppbv)
Dimethyl Trisulfide	0.007	2,4-dichlorophenol	0.057	4-chlorophenyl phenyl ether	0.009	a-BHC	0.006
Diethyl Trisulfide	0.007	4-Chloroaniline	0.029	4-Nitroaniline	0.135	b-BHC	0.013
Di-t-Butyl Trisulfide	0.007	4-chloro-3-methylphenol	0.003	Diphenylamine	0.011	g-BHC	0.013
Thiophene	10	2-methylnaphthalene	0.013	Azobenzene	0.020	d-BHC	0.006
C1-Thiophenes	10	1-methylnaphthalene	0.003	4-Bromophenyl phenyl ether	0.007	Heptachlor	0.005
C2-Thiophenes	0.017	Hexachlorocyclopentadiene	0.014	Hexachlorobenzene	0.007	Aldrin	0.001
C3-Thiophenes	0.007	2,4,6-trichlorophenol	1.890	Pentachlorophenol	1.401	Heptachlor epoxide	0.002
Benzothiophene	0.007	2,4,5-trichlorophenol	0.472	Phenanthrene	0.021	g-Chlordane	0.001
C1-Benzothiophenes	0.063	2-chloronaphthalene	0.006	Anthracene	0.052	Endosulfan I	0.005
C2-Benzothiophenes	0.006	2-Nitroaniline	0.068	Carbazole	0.056	a-Chlordane	0.002
Thiophane	10	1,4-dinitrobenzene	0.222	Di-n-butyl phthalate	0.013	Dieldrin	0.010
Thiophenol	10	Dimethyl phthalate	0.048	Fluoranthene	0.005	4,4'-DDE	0.006
<b>Semi-volatile organic compounds and PAHs</b>	<b>LOQ (ppbv)</b>	1,3-dinitrobenzene	0.222	Pyrene	0.002	Endrin	0.010
N-nitrosodimethylamine	1.259	2,6-dinitrotoluene	0.102	Benzyl butyl phthalate	0.060	Endosulfan II	0.009
Phenol	5.000	Acenaphthylene	0.002	Bis(2-ethylhexyl)adipate	0.025	4,4'-DDD	0.006
2-Chlorophenol	0.007	1,2-Dinitrobenzene	0.555	Benzo(a)anthracene	0.008	Endrin aldehyde	0.024
2-methylphenol	0.017	3-Nitroaniline	0.068	Chrysene	0.008	Endosulfan sulfate	0.002
bis(2-chloroisopropyl)ether	0.055	Acenaphthene	0.006	Bis(2-ethylhexyl)phthalate	0.048	4,4'-DDT	0.005
N-Nitroso-di-n-propylamine	0.029	4-nitrophenol	0.671	Di-n-octyl phthalate	0.048	Endrin ketone	0.010
3-methylphenol	0.017	Dibenzofuran	0.011	Benzo(b)fluoranthene	0.037	Methoxychlor	0.011
4-methylphenol	0.003	2,4-dinitrotoluene	0.102	Benzo(k)fluoranthene	0.037		
Isophorone	0.027	2,3,4,6-Tetrachlorophenol	0.402	Benzo(a)pyrene	0.037		
2-nitrophenol	0.013	2,3,5,6-Tetrachlorophenol	1.609	Indeno(1,2, 3-cd)pyrene	0.135		
2,4-dimethylphenol	0.031	Diethyl Phthalate	0.084	Dibenzo(a, h)anthracene	0.134		

Bis(2-chloroethoxy)methane	0.011	Fluorene	0.022	Benzo[g,h,i]perylene	0.068		
----------------------------	-------	----------	-------	----------------------	-------	--	--

Table S. 2-5 Target compounds and their LOQs in charcoal sorbent tube analysis

Organic silicon compounds	LOQ (ppbv)	Extended hydrocarbons	LOQ (ppbv)	Extended hydrocarbons	LOQ (ppbv)
1,1,3,3-Tetramethyldisiloxane	5	Cyclopentane	1.875	Nonanes	0.029
Pentamethyldisiloxane	5	Methylcyclopentane	1.875	Decanes	0.003
Hexamethyldisilane	5	Cyclohexane	1.875	Undecanes	0.012
Hexamethyldisiloxane	5	Methylcyclohexane	1.870	Dodecanes	0.002
Octamethyltrisiloxane	0.04	C3 Benzenes	0.008	Tridecanes	0.002
Octamethylcyclotetrasiloxane	0.03	C1 Naphthalenes	0.007	Tetradecanes	0.009
Decamethyltetrasiloxane	0.03	C2 Naphthalenes	0.012	Pentadecanes	0.009
Decamethylcyclopentasiloxane	0.03	Hexanes	1.875	Hexadecanes	0.002
Dodecamethylpentasiloxane	0.02	Heptanes	1.901	Heptadecanes	0.002
Dodecamethylcyclohexasiloxane	0.04	2,2,4-Trimethylpentane	1.870	Octadecanes	0.004
		Octanes	1.870	Nonadecanes	0.004
				Eicosanes+	0.003

Table S. 2-6 Target compounds and their LOQs in silica sorbent tube analysis

Carbonyl compounds	LOQ (ppbv)	Carbonyl compounds	LOQ (ppbv)
Formaldehyde	0.006	Methacrolein (Isobutenal)	0.053
Acetaldehyde	0.001	Butyraldehyde (Butanal)	0.003
Acrolein (2-propenal)	0.003	Benzaldehyde	0.002
Propionaldehyde	0.003	Valeraldehyde (Pentanal)	0.002
Crotonaldehyde	0.053	p-Tolualdehyde	0.002
2-Butanone (MEK)	0.026	Hexanaldehyde (Hexanal)	0.000

Table S. 2-7 Concentration range of selected halocarbons ( $\text{mg} \cdot \text{m}^{-3}$ ) measured at different landfill sites and permissible occupational exposure levels by Cal/OSHA and OEHHA

	Landfill biogas (5&6) in this study	Eklund et al. (1998) <sup>15</sup>	Allen et al. (1997) <sup>14</sup>	Cal/OSAH PELs <sup>68</sup>	OEHHA <sup>9</sup>
<b>Total Halocarbons</b>	9.90-15.65	-	246-1239	-	-
Dichlorodifluoromethane	ND*-1.68	6.28	<0.5-231	4950	-
Trichlorofluoromethane	ND-0.21	-	<0.5-74	5600	-
Chloroethene	ND-0.24	-	<0.1-87	-	0.84
1,2-Dichloroethene	ND-1.99	-	1-182	790	-
Trichloroethene	ND-0.48	-	<0.1-152	135	-
Tetrachloroethene	ND-1.10	-	<0.1-255	170	-
Chlorobenzene	ND-0.74	5.29	-	46	-
Dichlorobenzene	ND-3.99	24.35	-	60	5.7

\*ND means not detected

Table S. 2-8 Average concentration of BTEX (Benzene, Toluene, Ethylbenzene and Xylenes) measured in different biogas streams ( $\text{mg} \cdot \text{m}^{-3}$ ) and permissible occupational exposure levels by Cal/OSHA and OEHHA

	<b>Benzene</b>	<b>Toluene</b>	<b>Ethylbenzene</b>	<b>Xylene</b>
Biogas 1	0.04	0.15	0.10	0.27
Biogas 2	0.56	0.73	0.06	0.20
Biogas 3	0.22	0.37	0.27	0.09
Biogas 4	0.27	3.15	2.20	3.55
Biogas 5	1.76	5.46	3.95	8.06
Biogas 6	3.04	5.79	4.16	9.63
<b>Cal/OSHA PELs<sup>68</sup></b>	<b>3.19</b>	<b>37</b>	<b>22</b>	<b>435</b>
<b>OEHHA<sup>9</sup></b>	<b>-</b>	<b>904</b>	<b>26</b>	<b>-</b>

Table S. 2-9 Concentration of siloxanes in different biogas streams ( $\text{mg} \cdot \text{m}^{-3}$ )

	L2	D3	L3	D4	L4	D5	L5	D6
Biogas 4	9.996	-	0.049	0.001	0.008	1.258	0.002	0.031
Biogas 5	2.253	-	0.086	0.000	0.050	0.000	0.001	0.002
Biogas 6	2.858	-	0.004	0.125	0.000	0.018	ND	ND
(Urban et al., 2009) <sup>69</sup>	3.1-5.0	0.5-0.84	-	10.6-15	<0.1	3.0-3.3	-	-
(Rasi, 2009) <sup>59</sup>	0.03-0.63	<0.1	<0.01	<0.67	ND	<0.3	-	-
(Schweigkofler and Niessner, 2001) <sup>70</sup>	0.7-0.9	0.4-0.44	-	4.8-5.1	-	0.6-0.65	-	-
(Schweigkofler and Niessner, 1999) <sup>18</sup>	1.04-1.31	0.01	0.03-0.05	7.97-8.84	<0.01	0.5-1.09	-	ND
	0.38-0.77	0.31-0.45	0.04	4.24-5.03	<0.01	0.4-0.53	-	ND

Table S. 2-10 Concentration of metals in different biogas streams  
 Results expressed in (average value  $\pm$  1 standard deviation).  
 Concentrations below limit of detection (LOD) are denoted as 0 $\pm$ 0. All values in unit  $\mu\text{g} \cdot \text{m}^{-3}$

Element	LOD	Biogas 1	Biogas 2	Biogas 3	Biogas 4	Biogas 5	Biogas 6
Be	0.005	0 $\pm$ 0	0 $\pm$ 0	0.009 $\pm$ 0.009	0 $\pm$ 0	0.013 $\pm$ 0.004	0 $\pm$ 0
Cr	0.005	0.926 $\pm$ 1.31	0.061 $\pm$ 0.028	0.21 $\pm$ 0.24	0.34 $\pm$ 0.76	0 $\pm$ 0	0.19 $\pm$ 0.14
Mn	0.005	0 $\pm$ 0	0.067 $\pm$ 0.047	0.005 $\pm$ 0.008	0.48 $\pm$ 0.95	0 $\pm$ 0	0.24 $\pm$ 0.26
Co	0.005	0.00617 $\pm$ 0.00873	0.006 $\pm$ 0.008	0.018 $\pm$ 0.013	0.062 $\pm$ 0.14	0 $\pm$ 0	0.003 $\pm$ 0.005
Ni	0.02	0.272 $\pm$ 0.384	0.12 $\pm$ 0.15	0.074 $\pm$ 0.13	0 $\pm$ 0	0 $\pm$ 0	0 $\pm$ 0
Zn	0.2	0 $\pm$ 0	7.8 $\pm$ 8.7	0.56 $\pm$ 0.96	0.14 $\pm$ 0.3	0 $\pm$ 0	0.56 $\pm$ 0.96
Se	0.2	0.648 $\pm$ 0.458	0.21 $\pm$ 0.30	0.14 $\pm$ 0.24	0.45 $\pm$ 0.65	0.15 $\pm$ 0.15	0.20 $\pm$ 0.35
Sr	0.01	0 $\pm$ 0	0.005 $\pm$ 0.008	0 $\pm$ 0	0 $\pm$ 0	0.1 $\pm$ 0.1	0.009 $\pm$ 0.016
Mo	0.005	0.0988 $\pm$ 0.114	14.1 $\pm$ 20.4	0.009 $\pm$ 0.009	0 $\pm$ 0	0 $\pm$ 0	0 $\pm$ 0
Cd	0.005	0.204 $\pm$ 0.249	0 $\pm$ 0	0.005 $\pm$ 0.008	0.003 $\pm$ 0.007	0 $\pm$ 0	0 $\pm$ 0
Ba	0.02	0.0247 $\pm$ 0.0349	0 $\pm$ 0	0 $\pm$ 0	1.6 $\pm$ 2.2	1.5 $\pm$ 1.5	0 $\pm$ 0
Hg	0.005	0 $\pm$ 0	0 $\pm$ 0	0 $\pm$ 0	0.006 $\pm$ 0.014	0.008 $\pm$ 0.008	0 $\pm$ 0
Tl	0.005	0.00617 $\pm$ 0.00873	0.011 $\pm$ 0.016	0.014 $\pm$ 0.015	0 $\pm$ 0	0 $\pm$ 0	0.003 $\pm$ 0.005
Cu	0.005	0 $\pm$ 0	0.006 $\pm$ 0.008	0.005 $\pm$ 0.008	0 $\pm$ 0	0 $\pm$ 0	0.20 $\pm$ 0.34
As	0.005	0.315 $\pm$ 0.432	0.022 $\pm$ 0.021	0.23 $\pm$ 0.38	1.6 $\pm$ 1.4	8.5 $\pm$ 3.4	4.2 $\pm$ 2.3
Sb	0.005	0.259 $\pm$ 0.184	0.028 $\pm$ 0.028	0.31 $\pm$ 0.17	1.6 $\pm$ 1.8	12.5 $\pm$ 12.5	1.3 $\pm$ 2.0
Pb	0.1	1.73 $\pm$ 2.44	0 $\pm$ 0	0 $\pm$ 0	0.14 $\pm$ 0.31	0.8 $\pm$ 0.8	0.65 $\pm$ 1.1
Na	2	0 $\pm$ 0	0 $\pm$ 0	0 $\pm$ 0	0 $\pm$ 0	0 $\pm$ 0	0 $\pm$ 0
Mg	0.2	0 $\pm$ 0	0.56 $\pm$ 0.79	3.0 $\pm$ 4.9	0 $\pm$ 0	6.2 $\pm$ 6.2	0 $\pm$ 0
Al	0.2	0 $\pm$ 0	0 $\pm$ 0	0 $\pm$ 0	2.2 $\pm$ 5.	0 $\pm$ 0	5.6 $\pm$ 9.6
K	1	0 $\pm$ 0	0 $\pm$ 0	1.02 $\pm$ 1.76	0 $\pm$ 0	0 $\pm$ 0	0 $\pm$ 0
Ca	1	0 $\pm$ 0	92.6 $\pm$ 89.7	8.3 $\pm$ 14.4	1.2 $\pm$ 2.6	54 $\pm$ 52	14.5 $\pm$ 23.7
Fe	1	1.91 $\pm$ 2.71	0 $\pm$ 0	4.4 $\pm$ 7.6	9.6 $\pm$ 21	0 $\pm$ 0	0 $\pm$ 0
Sn	0.02	0 $\pm$ 0	0 $\pm$ 0	0.88 $\pm$ 0.19	0.05 $\pm$ 0.11	0.55 $\pm$ 0.05	0.40 $\pm$ 0.56

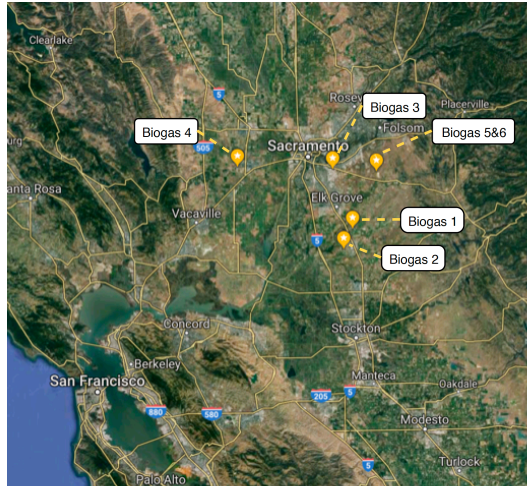


Figure S. 2-1 Map locations of the biogas facilities studied  
 Map from Google Maps: <https://goo.gl/maps/ogpi5QAiX4n2qhXk6>

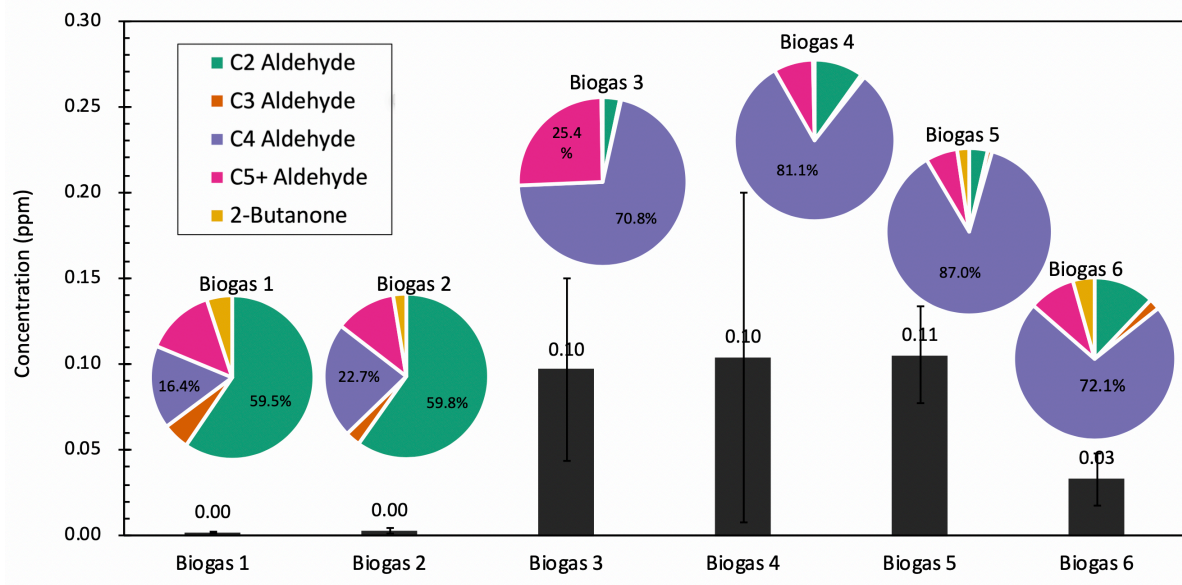


Figure S. 2-2 Concentration (ppmv) of carbonyls in different biogas streams.  
 Error bars represent 1 standard deviation of total carbonyl concentration. Chemical species quantified include acetaldehyde (C2), propionaldehyde, acrolein (C3), butyraldehyde, methacrolein (C4), (iso)valeraldehyde, hexanaldehyde, benzaldehyde, 2,5-Dimethylbenzaldehyde (C5+), and 2-butanone.

## Chapter 3 – Biomethane as a vehicle fuel

### 3.1 Background

Biogas produced from anaerobic digestion of organic waste is a useful renewable fuel that has lower lifecycle greenhouse gas (GHG) emissions than fossil fuels<sup>6,8</sup>. Raw biogas is typically only used for heat and power generation at the local production site because it has low methane (CH<sub>4</sub>) content (50%-75%) and high carbon dioxide (CO<sub>2</sub>) share (25%-50%). Upgraded biogas that removes CO<sub>2</sub> and other trace chemicals (hydrogen sulfide, halocarbons, siloxanes, etc.) can be used as a replacement fuel for traditional fossil natural gas in most applications. In California, biogas that has been upgraded to more than 89% methane<sup>4</sup> can be used as a transportation fuel commonly referred to as renewable natural gas (RNG) that can help reduce “well-to-wheels” GHG emissions by more than 50%<sup>71</sup> compared to fossil compressed natural gas (CNG).

A careful analysis of potential environmental and human health impacts should be conducted before widespread adoption of any new fuel, including RNG. Subramanian et al.<sup>72</sup> compared RNG and CNG vehicle emissions, finding slightly lower fuel economy and higher emissions of carbon monoxide (CO), hydrocarbons (HCs), and oxides of nitrogen (NO<sub>x</sub>) emissions from a RNG vehicle. Lim et al.<sup>73</sup> found that total hydrocarbons (THCs) in vehicle exhaust increase with increasing fuel CH<sub>4</sub> content, while exhaust polycyclic aromatic hydrocarbons (PAHs) and NO<sub>x</sub> increase with increasing concentration of higher hydrocarbons (ethane, propane, etc.) in the fuel. The relationship between fuel and exhaust composition has also been studied by modifying CNG composition<sup>74-78</sup>. Exhaust HCs were found to be correlated with fuel composition, and exhaust NO<sub>x</sub>, CO and PM were related to the technology used in the vehicle engine and exhaust control system. A few previous studies also measured CNG vehicle exhaust toxicity with bacterial mutagenicity tests and concluded that PM-induced toxicity

response can be attributed to lubricating oil emissions and nitro-PAHs in the exhaust<sup>79-82</sup>. No previous study has examined exhaust toxicity from RNG fueled vehicles.

In this study, exhaust emissions from a light-duty cargo van operating on commercial CNG and two RNG blends was analyzed for regulated compounds (CO<sub>2</sub>, CO, NO<sub>x</sub>, N<sub>2</sub>O, CH<sub>4</sub>, HCs), particulate matter (PM), and a variety of unregulated compounds (alcohols, aldehydes, ketone, organic acids, aromatics, etc.). Exhaust was photochemically aged in a smog chamber to understand how chemical properties would evolve in the atmosphere. Exhaust toxicity was characterized with three different bioassays, and the pollutant contributions to toxicity were evaluated with elastic net regression combined with predictions from a mutagenicity model (VEGA-QSAR). Results from this study help inform scientists and regulators about the potential air quality and public health impacts of widespread adoption of RNG as a transportation fuel.

## **3.2 Methods**

### **3.2.1 RNG sample collection and analysis**

RNG was collected from three different biogas facilities (two food waste digesters and one dairy waste digester) using a mobile membrane separation unit (model HL-X1, Helee Inc., Hayward, CA) as described in previous studies<sup>65,83</sup>. RNG was compressed to 3600 psi in 61 L cylinders (CNG Cylinders International, Oxnard, CA) using a natural gas compressor designed for refueling CNG vehicles (PHILL Compressor, BRC Fuel Maker Corporation; Cherasco, Italy). Each cylinder required ~10 hours to fill using the small compressor, and 2-3 cylinders were filled at each site depending on the availability of RNG. The collected gas therefore represents the average composition of RNG over 2-3 days.

The fuel cylinder in the test vehicle maintained a minimum gas pressure of 1000 psi during normal operation. This resulted in fuel blending when the tank was refilled (~1/3 old fuel and ~2/3 new fuel).

Note that fuel blending would frequently occur in real-world practice when vehicles switch between different CNG and RNG fueling stations depending on location. Table 3-1 lists the chemical compositions of the three different gaseous fuel blends tested in the current study. The first was commercial CNG from a commercial filling station (3528 E Foothill Blvd, Pasadena, CA 91107). The second, named RNG1, was a mixture of 27.8% CNG and 72.2% RNG from a food waste digester. The third, named RNG2, was a mixture of 7.7% CNG, 33.5% RNG from dairy waste, 34.4% RNG from a food waste digester, and 24.4% RNG from a second food digester. Table S.3- 3 through Table S.3- 5 in the supplementary material list concentrations of all the measured pollutants.

Table 3-1. Composition of different fuels used in this study.

Concentration of methane, ethane, propane, carbon dioxide, nitrogen and oxygen are reported in percentage (with 1 standard deviation). Concentration of different hydrocarbons and sulfur-containing compounds are reported in ppm by volume (with 1 standard deviation). Fuel higher heating value and stoichiometric air-fuel ratio are calculated based on the measured major compounds (%) listed in this table.

<b>Compound</b>	<b>unit</b>	<b>CNG</b>	<b>RNG 1</b>	<b>RNG 2</b>
Methane	%	91.2% ± 0.8%	93.5% ± 1.3%	93.3% ± 0.6%
Ethane	%	5.41% ± 0.18%	1.50% ± 0.05%	0.42% ± 0.01%
Propane	%	0.33% ± 0.06%	0.09% ± 0.02%	0.03% ± 0.00%
Carbon dioxide	%	0.82% ± 0.09%	1.85% ± 0.39%	4.28% ± 0.18%
Nitrogen	%	1.83% ± 0.65%	2.64% ± 1.01%	1.77% ± 0.48%
Oxygen	%	0.42% ± 0.30%	0.42% ± 0.11%	0.18% ± 0.04%
Aromatic hydrocarbons	ppm	1.84 ± 0.24	1.73 ± 0.07	1.27 ± 0.12
Other hydrocarbons	ppm	7.04 ± 0.59	9.44 ± 2.23	5.11 ± 1.07
Sulfur-containing compounds	ppm	1.11 ± 0.18	1.95 ± 0.55	1.96 ± 0.36
Higher heating value	MJ·m <sup>-3</sup>	38.27 ± 0.34	36.31 ± 0.47	35.46 ± 0.22
Stoichiometric air/fuel Ratio	kg/kg	16.21 ± 0.15	15.67 ± 0.22	14.94 ± 0.10

### 3.2.2 Vehicle exhaust collection and chemical analysis

Motor vehicle exhaust tests were performed at the California Air Resource Board (CARB) Haagen-Smit Laboratory located in El Monte, CA. The lab is equipped with a 48-inch (1.2 m) single-roll electric chassis dynamometer for light-duty vehicles, a constant volume sampler (CVS, AVL CVS i60

Medium-Duty) operating at  $22.3 \text{ m}^3 \cdot \text{min}^{-1}$ , and an exhaust sampling system that meets certification requirements defined by 40 CFR 86. A 2015 Chevrolet Express 2500 cargo van designed to run on CNG was used for all emissions tests. This vehicle had a sequential fuel injection (SFI) system and a Heated Oxygen Sensor (HO<sub>2</sub>S) Three Way Catalytic Converter (TWC). No modifications were made to the vehicle when fueled with RNG. The standard California Unified Cycle (UC cycle) was selected as the driving schedule for all tests. The UC cycle consists of three phases, a “cold start” phase (Phase I: 300 seconds), a “stabilized phase” (Phase II: 1135 seconds), a “hot soak” period where the engine is off (600 seconds) and a final “hot start” phase (Phase III: 300 seconds, a repeat of phase I). A speed-time trace for the UC cycle is presented in Figure S.3- 1. The test vehicle was driven at a constant speed of  $80 \text{ km} \cdot \text{hr}^{-1}$  for 5 min, and then stored in a room at a controlled temperature of  $25^\circ\text{C}$  for 14 hours prior to each cold-start test. Two tests were conducted for each fuel over a total of six days in order of CNG, RNG1, and then RNG2.

The concentrations of regulated gaseous constituents (CO, CO<sub>2</sub>, NO<sub>x</sub>, N<sub>2</sub>O, CH<sub>4</sub>, THC) were measured with a HORIBA MEXA-ONE motor exhaust gas analyzer platform (HORIBA, Ltd.). Diluted exhaust from each phase of the driving cycle was drawn at constant flow rate from the CVS tunnel into a Tedlar bag. Each phase-averaged bag was analyzed separately at the end of the driving cycle. Fourier-Transform InfraRed spectroscopy (FTIR, AVL, SESAM 4) was used to measure a variety of gaseous species (CO<sub>2</sub>, CO, NO<sub>x</sub>, NH<sub>3</sub>, SO<sub>2</sub>, small HCs) from the undiluted tailpipe exhaust. The FTIR measured at 1 Hz with a flow rate of 13 LPM through a heated ( $191^\circ\text{C}$ ) sampling line to avoid interference from condensing water. A PTR-MS (Ionicon PTR-TOF 8000) measured a variety of volatile organic compounds ( $m/z$  1~500) from the CVS tunnel at a rate of 1 Hz. A further sample gas dilution of 1:4 was applied for all of the tests to optimize the linear signal response range for the current condition.

Limits of detection (LODs) were calculated as the average value of background (measured before or after each test) plus 3 times the standard deviation. The LODs, listed in Table S.3- 1 and Table S.3- 2 vary from 0.36 to 4.05 ppm for FTIR measurements and 0.5-38 ppb for PTR-MS measurements. An EEPS (TSI Model 3090) measured particles with diameters between 6.4 to 523 nm from the CVS tunnel at a rate of 1 Hz. Exhaust from CVS was also collected with XAD-2 sorbent tubes (8 x 110 mm 400 mg/200 mg, SKC, Inc.) at a flow rate of 1 L min<sup>-1</sup> throughout the UC cycle. The XAD-2 tubes were analyzed for semi-volatile organic compounds (SVOCs) using an Agilent 7890B Gas Chromatograph followed by a 7200B Quadrupole-Time-of-Flight Mass Spectrometer (GC-QTOF-MS). Details of sorbent tube analysis are provided in the supplementary material.

### 3.2.3 Vehicle exhaust toxicological analysis

**ROS assay.** The macrophage reactive oxygen species (ROS) assay measures the ROS generating capacity of exhaust PM samples collected on Teflon filters (47 mm, pore size 2 µm) and extracted in water. PM samples were collected at a flow rate of 61 LPM from the diluted CVS tunnel while the engine was running (1735 seconds total). Exhaust from two cold-start driving cycles with the same fuel were combined onto the same filter to collect sufficient material for analysis (a similar approach was used for all toxicity tests). Filters were sealed in cassettes and sent to Wisconsin State Laboratory of Hygiene for ROS analysis, following the method described in previous studies<sup>84-86</sup>. Results are reported as increase of fluorescence in treated samples relative to untreated controls. Further details are provided in the supplementary material and a summary of PM mass collected for different toxicity assays is presented in Table S.3- 6.

**Mutagenicity assay.** The micro-suspension modification of the Salmonella/microsome (Ames) assay described in previous studies<sup>48,49</sup> was used to measure the mutagenicity of exhaust PM. Samples were drawn at a flow rate of 225 LPM from the diluted CVS tunnel through 1-inch (2.54 cm) insulated stainless-steel tubing to a 90 mm pre-cleaned Teflon filter (Zefluor, Pall, Ann Arbor, MI. 2 um pore size) in a stainless-steel filter holder. Filters were stored at -20°C until shipment to the University of California, Davis, where they were extracted using pressurized dichloromethane (Burdick and Jackson GC grade) at 2000 psi and 100°C. The extracts were then dried and re-dissolved in dimethyl sulfoxide (DMSO) for testing. Further details are provided in the supplementary material.

**Biomarker assay.** The expression of in-vitro pro-inflammatory markers induced by exhaust PM was measured in human U937 macrophage cells (American Tissue Culture Collection, Manassas, VA) following the methods described in a previous study<sup>47</sup>. Extracts were in dimethyl sulfoxide (DMSO). Measured biomarkers included Cytochrome P450 monooxygenase (CYP1A1) which is a marker for PAHs, Interleukin 8 (IL-8) which is a marker for inflammation, and Cyclooxygenase (COX-2) which is a key enzyme for production of prostaglandins mediating pain and inflammation. Further details are provided in supplementary material.

**Elastic net regression.** Elastic net regression<sup>87</sup> was used to find relationships between the measured chemical features and toxicity responses. Toxicity data and chemical data (emission factors or mass spec peak area count) were  $\log_2$  transformed and chemical data was further Cyclic Loess normalized. The linear combination of chemical features that was most predictive of  $\log_2$  transformed toxicity response was then identified by the elastic net regression. Positive coefficients were returned for each toxicity end point, with the larger coefficients interpreted as a stronger association. A detailed description of the method is provided in SI.

**VEGA-QSAR mutagenicity model.** The VEGA-QSAR (Quantitative Structure Activity Relationship) model can be used to link chemical structure described by molecular descriptors to toxicity<sup>88</sup>. The mutagenicity (Ames test) of gas-phase species in the current study was predicted on a scale of 0-1 using the CONSENSUS model-v1.0.3. The concentrations of all gas-phase compounds quantified with PTR-MS were multiplied by their predicted mutagenicity score so that aggregate gas-phase mutagenicity totals could be calculated for each fuel (CNG, RNG1 or RNG2).

### 3.2.4 Photochemical aging of exhaust

Photochemical aging experiments were conducted in a 5.5 m<sup>3</sup> Teflon chamber (0.051 mm NORTON FEP fluoropolymer film) equipped with UV light panels (50 W·m<sup>-2</sup>). The Teflon reaction chamber was flushed three times before each test with air that was pre-cleaned using granulated activated carbon to remove background gases followed by a High Efficiency Particulate Air (HEPA) filter to remove PM. Dark aging tests started by filling the reaction chamber to 33% capacity with pre-cleaned air, followed by injecting freshly diluted exhaust from the CVS tunnel through a 0.5-inch (1.27 cm) insulated stainless steel transfer line at a constant flow rate of 60 LPM over the entire UC cycle while the engine was running (1735 seconds). The reaction chamber was then quickly filled to 100% capacity with pre-cleaned air, yielding a well-mixed system. The reaction chamber was aged for 3 h to represent a typical photochemical cycle, while concentration changes were recorded by the PTR-MS that sampled at a flow rate of 0.05 LPM. The light aging tests followed the same experimental protocol except that 100 liters of VOC surrogate gas (1.125±0.022 ppmv m-xylene and 3.29±0.07 ppmv n-hexane in air, Scott Marrin, Inc.) was injected into the chamber immediately after injecting the exhaust, creating a final VOC concentration of 90 ppbv. Hydroxyl radical concentrations during the light aging

tests were calculated to be  $5\text{-}6 \times 10^6$  molecules·cm<sup>-3</sup> based on the decay rate of the m-xylene. The final ozone concentrations at the end of the 3 h experiment were measured to be 110~125 ppb.

### 3.3 Results and discussion

#### 3.3.1 Fuel composition

Table 3-1 summarizes the concentrations of major and trace components in different fuels as well as basic fuel properties such as higher heating value (HHV) and stoichiometric air-fuel (A/F) ratio. Trace compound concentrations in each fuel are summarized in Tables S3-S5. CNG had the lowest CH<sub>4</sub> concentration but much higher ethane and propane concentration compared to the RNGs. RNG1 had more ethane and propane than RNG2 but similar CH<sub>4</sub> due to blending. Hence, the overall heating value and stoichiometric A/F ratio ranked CNG>RNG1>RNG2. CO<sub>2</sub> increased as more RNG was blended into the fuel (CNG<RNG1<RNG2) due to residual CO<sub>2</sub> in the RNG even after upgrading.

#### 3.3.2 Exhaust composition

##### *Gas-phase pollutant emissions*

**Regulated pollutants and fuel economy.** Emission factors for regulated pollutants and fuel economies measured during the cold-start UC cycle are displayed in Figure S.3- 2, while the pollutant concentrations measured as a function of time by FTIR during the cold start period (first 150 seconds) are presented in Figure S.3- 3. The fuel economy of the test vehicle was highest when using CNG (2.87 miles·m<sup>-3</sup>) with reduced fuel economy measured for RNG1 (-3.1%) and RNG2 (-4.9%). CO<sub>2</sub> emissions factors were inversely correlated with fuel economy, with the lowest values measured when using CNG (682 g mile<sup>-1</sup>) and slightly higher values measured for RNG1 (+1.2%) and RNG2 (+5.0%). Emissions

of CO and total hydrocarbons (HCs) were +59% and +72% higher when using RNG2 relative to CNG, while emissions of nitrogen compounds (NO<sub>x</sub>, N<sub>2</sub>O, NH<sub>3</sub>) were not strongly related to fuel composition. Further details of regulated pollutant emissions are provided in the supplementary material.

**Unregulated gaseous pollutants.** Figure 3-1 (a)-(u) presents the emission factors of various VOCs and SVOCs measured by PTR-MS. For CNG and RNG1, only one set of measurements was considered valid and reported. CVS tunnel background concentrations were monitored before each test and the averaged background values (“bkg”) were reported as part of the test measurements. Background (equivalent) emission factors account for the majority of the measured concentrations for many compounds, emphasizing the low emissions from both CNG and RNG combustion. The tunnel background concentrations observed in the current study are similar to those reported in previous studies<sup>79,89</sup>. More advanced measurement techniques, improved exhaust-sampling protocols, and new system designs will be required to measure low levels of tailpipe emissions in future vehicle tests involving clean fuels. In the present study, tailpipe emissions above background were detected by the PTRMS in at least one test phase for formaldehyde, methanol, ethanol, propanol, dimethyl sulfide, propene, butene, methyl ketene, and benzene.

Figure 3-1 panels (a - d) show the emission factors for one aldehyde (formaldehyde) and three alcohols (methanol, ethanol, and propanol) that were emitted above background concentrations. These compounds are formed from the oxidation reactions in the combustion chamber, in the exhaust system, and on the surface of the three-way catalytic converter (TWC)<sup>90-92</sup>. Studies have shown that the emission of these oxygenated compounds are primarily affected by the details of the combustion system with less impact from fuel composition especially for the smaller compounds (C<sub>1</sub>, C<sub>2</sub> – alcohols, aldehydes, ketones, acids), which can be formed through multiple reaction pathways. Important factors

include the equivalent A/F ratio, exhaust oxygen and HC levels, and exhaust temperature and residence time. Zervas et al.<sup>93,94</sup> reported that emissions of small alcohols peaked at  $\lambda=1$  (stoichiometric conditions), organic acid emissions increased when  $\lambda>1$  (lean burn conditions), and CO emissions increased when  $\lambda<1$  (rich burn conditions). Therefore, the observed different emissions rates for oxygenated HCs between CNG and RNGs as shown in Figure 3-1 (a-d) are likely affected by the different combustion conditions, indirectly linking to fuel H/C ratios.

Emission factors for benzene (the only aromatic compound above background in the PTR-MS data) are presented in Figure 3-1 (u). Benzene emissions from the different fuels were similar, with slightly higher emissions from vehicles fueled with CNG compared to RNG. Benzene emissions factors measured in the current study are also similar in magnitude to those measured from previous tests on CNG and RNG vehicles<sup>73,95</sup>. Figure 3-1 (k) shows that emissions of dimethyl sulfide (DMS) were higher in Phase 3 (hot catalyst) vs. Phase 1 (cold catalyst). Previous studies have shown that sulfides can form on the surface of the hot catalyst with excess unburned fuel<sup>96</sup>. Emissions of propene (Figure 3-1 m) and butene (Figure 3-1 n) were similar when using CNG and RNG. Butene was emitted across all phases of the UC cycle, while propene was emitted mainly during the cold start (phase 1).

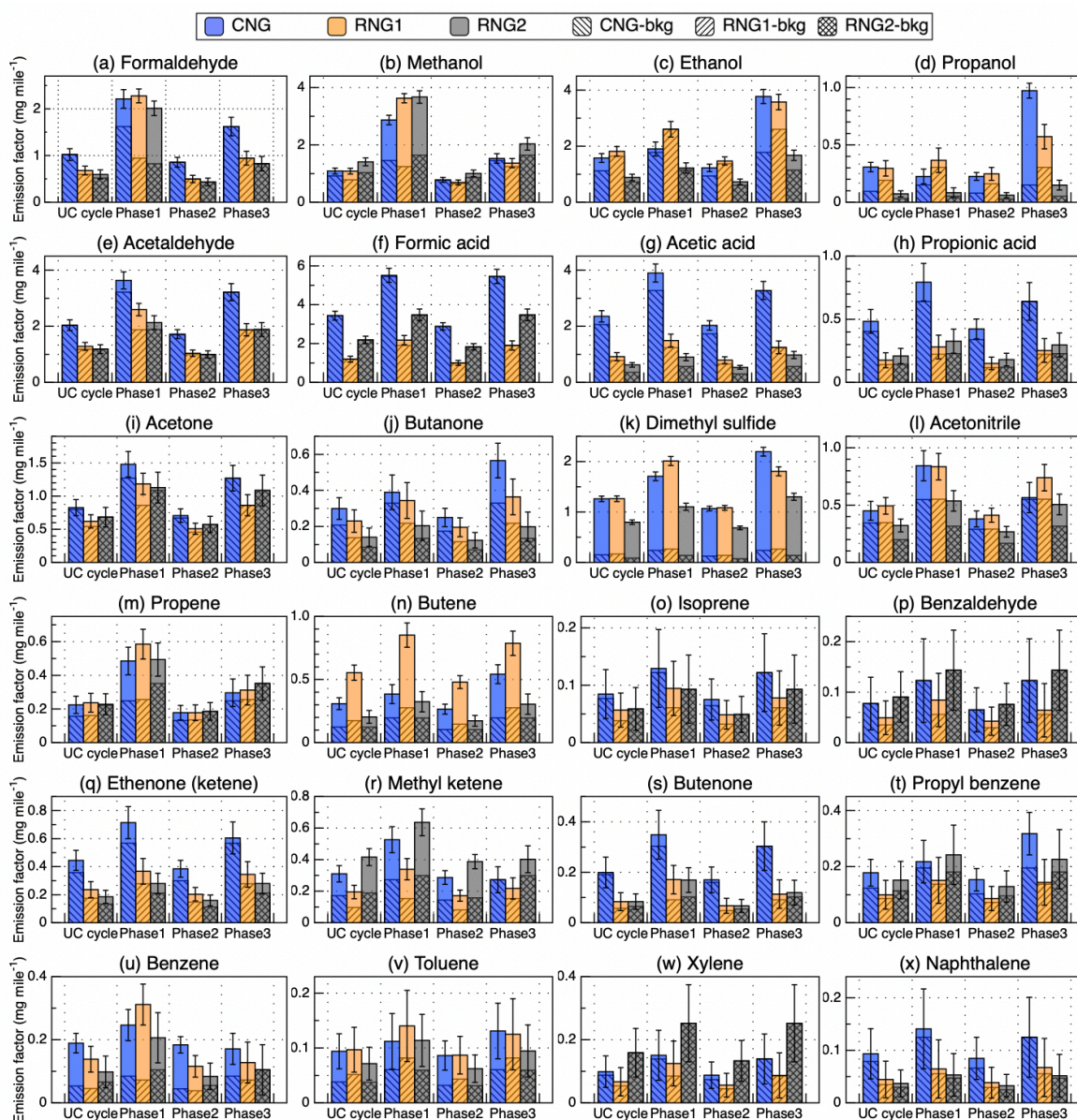


Figure 3-1 (a)-(x). Emission factors ( $\text{mg}\cdot\text{mile}^{-1}$ ) of different pollutants for the averaged cold-start UC cycle as well as different phases of the cycle.

Error bar represents standard deviation of tunnel background measurement.

Alignment of the nontarget GC-QTOF-MS data across different tests isolated 826 molecular features having similar retention indexes and primary mass spectral features. After applying filters to remove features with a maximum abundance in the samples less than five times the average tunnel blank and features with average signal to noise ratios below ten, a total of 74 features remained. Of these, 42 compounds were tentatively identified against the NIST17 mass spectral database, producing

combined spectral similarity and retention index match scores above 800. A full list of these 42 compound abundances in the tailpipe exhaust is available in Table S.3- 7. A subset of 17/42 compounds were on our target list and are considered to be confirmed identifications including a number of substituted benzenes, substituted phenols, and polycyclic aromatic hydrocarbons. The remaining compounds are a diverse set that includes cycloalkanes (e.g., cyclohexane, 1-ethyl-1-methyl-), aldehydes/ketones (e.g., 3-furaldehyde), and heterocyclic aromatics (e.g., 2-methylquinoline and 1,2-benzisothiazole).

### ***Particulate matter emissions***

Figure 3-2 presents ultrafine particle mass and number emission factors from the overall UC cycle. Tailpipe particulate matter number emissions were more than an order of magnitude higher than background concentrations. The CNG tests emitted lower particle count but higher particle mass than the RNG tests, possibly because the CNG contained higher concentrations of C2 and C3 alkanes (ethane, propane) enhancing PM precursor formation<sup>73,76</sup>. PM precursors nucleate to form nanoparticles that grow and ultimately serve as condensation sites for lubricating oil that enters the combustion chamber. Multiple studies have shown that engine lubricating oil is a significant source of vehicle PM emissions<sup>76,97-99</sup> and that the level of oil emission, although not directly related to fuel composition, is closely related to air-fuel ratio and combustion chamber temperature<sup>100</sup>. The higher heating value of the CNG may therefore influence the PM trends measured in the current study.

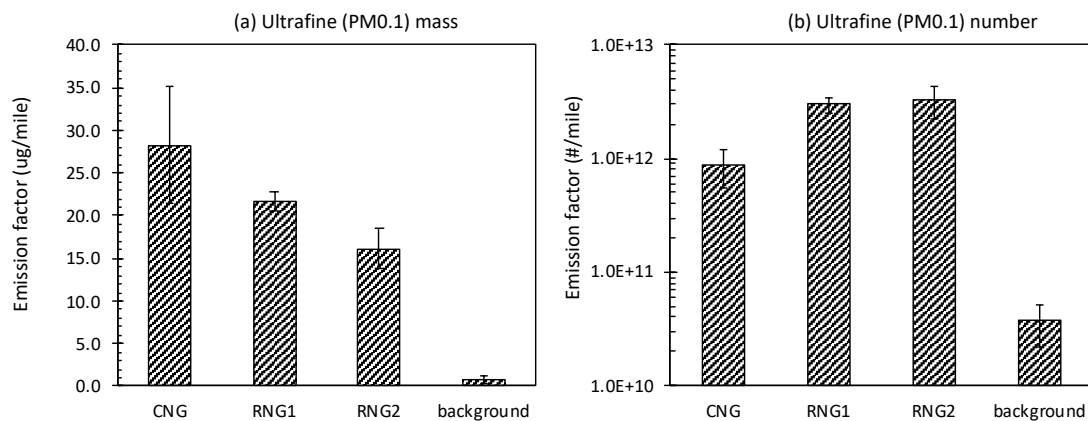


Figure 3-2 UC cycle-averaged emission factor of ultrafine particle (PM<sub>0.1</sub>) (a) mass ( $\mu\text{g}\cdot\text{mile}^{-1}$ ) and (b) number ( $\mu\text{g}\cdot\text{mile}^{-1}$ ) from the tested vehicle running on different fuels.

The height of the bars represents the average value of total PM mass or number emission factor calculated from EEPS measurement (only including 6.4nm -93.1nm) of the duplicate tests on the same fuel. Error bars represent the min and max values from the duplicate tests on the same fuel.

### 3.3.3 Atmospheric aging of exhaust

Dilution and photochemical reactions will change the properties of the exhaust over time in the atmosphere. Figure S.3- 6 shows the time evolution of xylene and ethenone concentrations measured after dilution in a photochemical aging chamber using PTR-MS. Concentrations for both of these compounds were stable in 3-hr dark aging tests (Figure S.3- 6 (a),(c)), but xylene injected at the beginning of the test was consumed while ethenone was formed during photochemical reactions in 3-hr light aging tests (Figure S.3- 6 (b),(d)). Figure 3-3 presents final concentrations of different chemical compounds measured at the end of 3-hr aging experiments across multiple fuels. Butene concentrations were only slightly lower in light aging tests relative to dark tests, likely because butene is an intermediate breakdown product from surrogate VOC (hexane and xylene) reactions. The rest of the compounds summarized in Figure 3-3 were all oxygenated and increased in light aging tests. Most

importantly in the context of the current study, engine exhaust from CNG and RNG behaved similarly during photochemical aging, suggesting similar atmospheric reaction pathways and products.

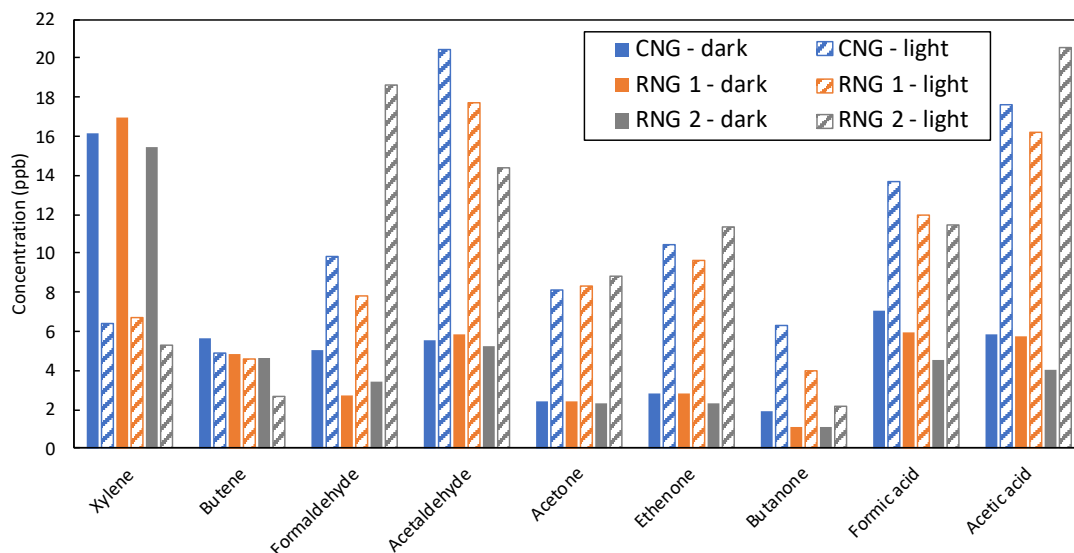


Figure 3-3 Concentration (ppb) of selected compounds measured from chamber after 3h of aging under either dark or light condition

### 3.3.4 Exhaust toxicity

Figure 3-4 (a-c) shows toxicity induced by engine exhaust PM measured using different bioassays. Figure 3-4 (a) shows that the reactive oxygen species (ROS) present in the water-soluble portion of the PM is significantly higher in CNG exhaust compared to the exhaust from RNGs even when accounting for the variability of the three replicate analyses. Figure 3-4 (b) shows the levels of biomarker expression (CYP1A1, IL-8 and COX-2, respectively) as fold increased emissions above blank levels in U937 human macrophages. PM from CNG exhaust induced the highest biomarker signal followed by RNG1 and RNG2. The significant enhancement of ROS as well as higher level of pro-inflammation biomarkers from CNG exhaust were consistent with the higher PM mass emissions factor from CNG exhaust. Lubricating oil emissions have been reported to be strongly associated with ROS activity<sup>101</sup>.

In contrast, the mutagenicity of CNG and RNG exhaust was similar (same order of magnitude) as shown in Figure 3-4 (c). The mutagenicity measured in the CVS tunnel background was several orders of magnitude lower than the samples.

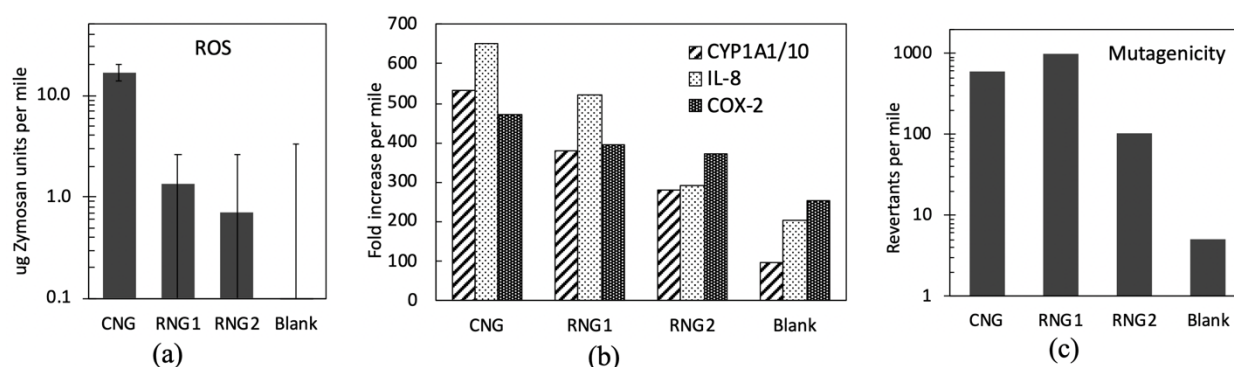


Figure 3-4 Toxicity of vehicle exhaust running on different fuels.

(a) reactive oxygen species (ROS) measured with macrophage assay (error bars represent the standard deviation resulting from 3 replicate analysis of the same sample), (b) pro-inflammatory biomarker expression measured in human U937 macrophage cells (panel (b)-CYP1A1 is divided by ten and plotted), (c) mutagenicity measured with a micro-suspension modification of the *Salmonella*/microsome (AMES) assay

PM toxicity may be influenced by semi-volatile chemical constituents that partition from the gas phase to the particle phase. The sorbent tubes used for the GC-QTOF-MS analysis in the current study capture gas-phase constituents and some fraction of the particle-phase constituents. These GC-QTOF-MS measurements complement the PTR-MS measurements discussed in the previous section. Elastic net regression was used to study the relationship between toxicity responses and chemical constituents measured by GC-QTOF-MS and PTR-MS (Figure 3-5). A total of 22 features with positive coefficients were selected by the regularized linear regression out of a list of 107 constituents. Chemical compounds that were strongly correlated with various toxicity responses include a subset of the small carbonyls (C1 C2 aldehydes, ketene) and many of the aromatic compounds. Naphthalene was measured with both PTR-MS and GC-QTOF-MS but in different units. Elastic net regression returned similar coefficients

for the parallel naphthalene measurements, building confidence in the robustness of the results. Note that some of the significant chemical components identified in the elastic net regression analysis (including naphthalene) are primarily derived from the test background conditions (see Figure 3-1).

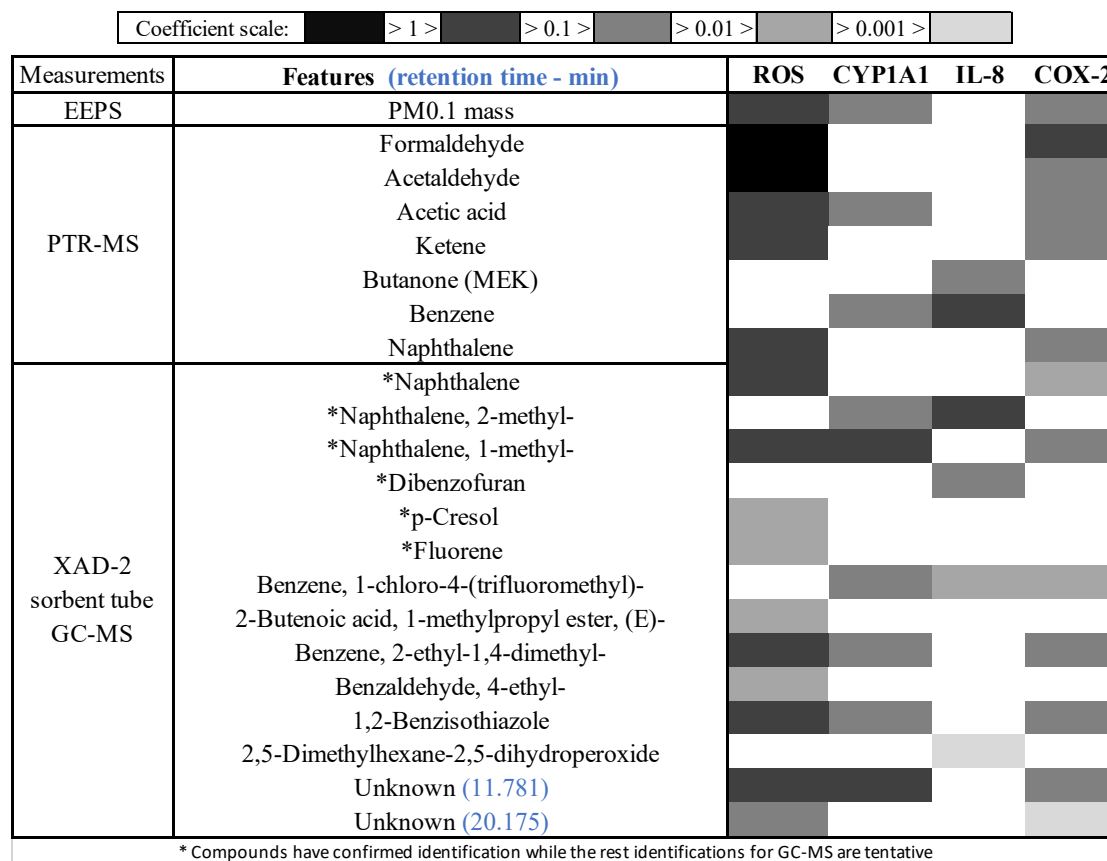


Figure 3-5 Summary of elastic net regression results on the linear coefficients between chemical features and toxicity responses.

Figure 3-6 summarizes all of the chemical components associated with toxicity in the current study using either emissions factor ( $\mu\text{g mile}^{-1}$ ) or emissions peak area depending on the measurement technique. Background concentrations (hatched patterns in Figure 3-6) account for the majority of the concentration for many of the species identified as toxicologically significant by elastic net regression. The background concentrations for the GC-QTOF-MS measurements were characterized with a single blank test and so the threshold for significant tailpipe emissions was interpreted conservatively as three times the background level for these constituents. Based on Figure 3-6, the primary tailpipe emissions

associated with toxicity in the vehicle exhaust include benzene, dibenzofuran, and dihydroperoxide dimethyl hexane (the last identification is considered tentative/uncertain). In all cases, RNG tailpipe emissions of these potentially toxic compounds are lower than CNG tailpipe emissions.

Elastic net regression was not able to detect associations between gas-phase chemical constituents and mutagenicity outcomes in the current study. The aggregated mutagenicity of the gas-phase exhaust was therefore calculated using the consensus Ames score from the VEGA-QSAR model for each tested fuel (Figure 3-7). The chemical constituents emitted above background levels in at least one phase of testing (see Figure 3-1) that made the greatest contribution to gas-phase mutagenicity included formaldehyde, dimethyl-sulfide, propene, and methyl ketene. Formaldehyde accounted for more than half of the aggregated exhaust mutagenic score for all of the fuels due to its abundance and toxicity. Gas-phase CNG exhaust had higher aggregate mutagenic score compared to gas-phase RNG exhaust.

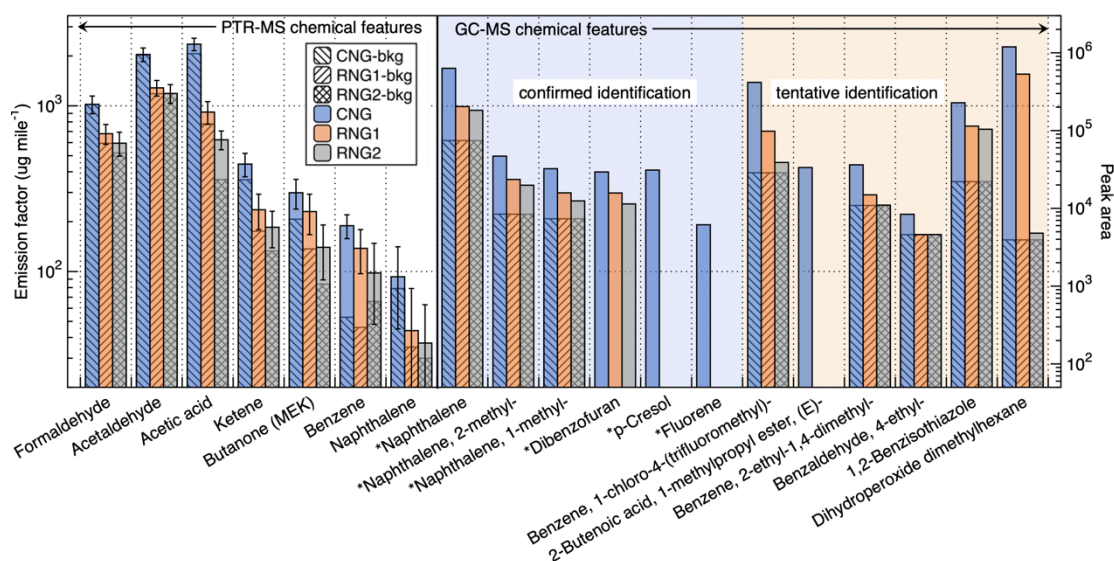


Figure 3-6 Abundance of selected chemical compounds that had non-zero coefficient associated with toxicity responses.

Units in  $\mu\text{g}\cdot\text{mile}^{-1}$  for PTR-MS measurements and peak area for XAD + GC-QTOF-MS measurements). Background signals shown for PTR-MS were measured before each test with error bars represented standard deviations of the background measurements. Background signals shown for GC-QTOF-MS were measured with a dedicated tunnel blank sorbent tube sample.

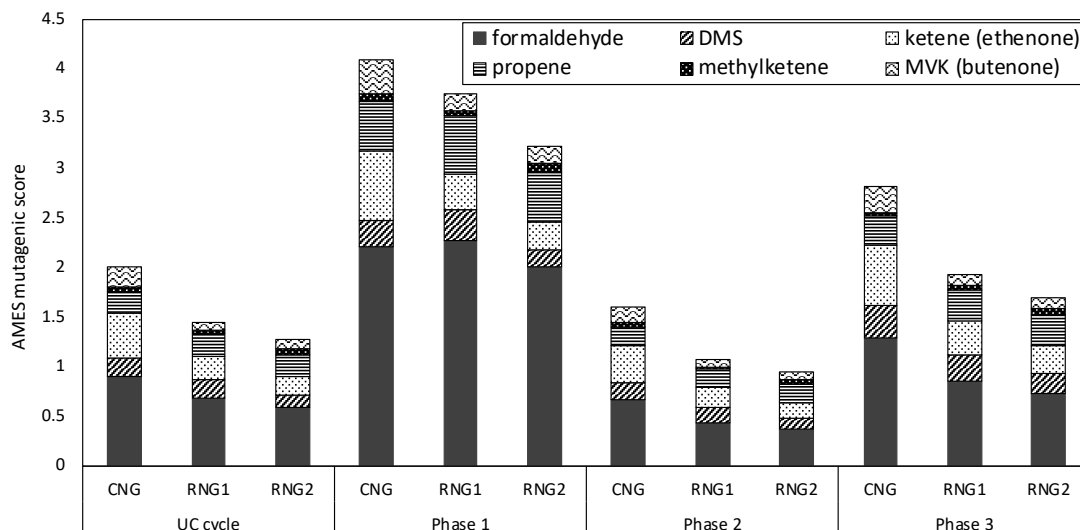


Figure 3-7 Mutagenic score calculated based on gas phase concentration measured by PTR-MS and AMES test consensus score given by the VEGA-QSAR model.

### 3.4 Implications

The results of the current study indicate that the toxicity of the exhaust from motor vehicles powered by RNG is less than or equal to the toxicity of the exhaust from vehicles powered by CNG. Photochemical aging of the exhaust had the same effect for CNG and RNG and therefore is not expected to alter this conclusion. Multiple studies show that modern CNG engines equipped with three-way catalysts (TWCs) operating under stoichiometric conditions emit far less pollution than older engines powered by CNG or diesel with lean burn and oxidation catalyst (or even no aftertreatment). The corresponding toxicity of exhaust from modern CNG engines is orders of magnitude lower than the toxicity of exhaust from older engines<sup>79,82,89,102</sup>. The widespread adoption of modern engines powered by RNG in the transportation sector to replace existing CNG or diesel engines should therefore yield reduced toxicity. Future studies should expand the testing to include a greater number of RNG fuels, more repetitions of the driving cycle, a broader range of medium-duty and heavy-duty vehicles, and an

expanded suite of toxicology tests to confirm that the results from this preliminary study can be extended to the entire motor vehicle fleet.

Multiple studies have explored the technological and economic aspects of biogas upgrading under different biomethane production and utilization scenarios. The results indicate that the economic uncertainties in biogas production are substantial. Most studies agree that the scale of the biogas production plant, the type of feedstock, and the availability of tax incentives/subsidies are the most important economic factors <sup>103–107</sup>. Despite this economic uncertainty, the adoption of RNG to replace fossil fuels in the transportation sector appears to be a worthy policy goal since this fuel switch has the potential to further decarbonize energy production, yielding long-term climate benefits that complement the potential immediate public health benefits associated with reduced toxicity.

## 3.5 Appendix

### **Biomethane composition analysis**

RNG cylinders were transported back to the lab for chemical composition analysis. A dual stage natural gas regulator with stainless steel diaphragm (The Fitting Source, Inc.) was connected to the compressed gas cylinder to reduce the pressure from 3600 psi to less than 0.3 psi. From the outlet of the regulator, RNG was sampled with an 8L Tedlar® bag (SKC-West, Inc.) for major components and sulfur-containing compounds analysis, and with adsorbent tubes (charcoal tube, DNPH coated silica tube and XAD tube, SKC, Inc.) for hydrocarbons, carbonyls, and a variety of different VOC and SVOCs analysis. The details of sampling and analysis methods as well as a comprehensive list of all the compounds analyzed can be found in previous studies<sup>65,83</sup>.

### **Engine exhaust toxicity analysis**

**ROS assay.** The macrophage reactive oxygen species (ROS) assay measures the ROS generating capacity of water extracts of particulate matter in exhaust samples. The reagent DCFH-DA (2',7'-Dichlorofluorescein diacetate) is a cell-permeable ROS indicator that is modified by the ubiquitous esterases in the cell cytoplasm and then by the ROS species to generate a fluorescent product DCF (Dichlorofluorescein), which is detected using a fluorometer. Rat alveolar macrophage cells (NR8383) were exposed to filter water extract at three different dilutions for a 2.5-hour incubation (37°C, 5% CO<sub>2</sub>), together with positive controls exposed to Zymosan as well as untreated controls. Linear regression of fluorescence units vs. Zymosan concentration was performed so that final ROS concentrations were expressed in units of equivalent µg-Zymosan.

**Mutagenicity assay.** The mutagenicity bioassay adopted a micro-suspension modification of the *Salmonella*/microsome Ames assay described in previous studies<sup>48,49</sup> that is ten times more sensitive than the standard plate incorporation method. Frame-shift mutations of *Salmonella typhimurium* tester strain TA98 were observed, with liver homogenate (S9) from male Sprague Dawley rats (Mol Tox, Boone, NC) added to provide metabolic activation of the sample. Filters were stored at -20°C until shipment to the University of California, Davis lab where they were extracted using pressurized solvent dichloromethane (Burdick and Jackson GC grade) at 2,000 psi, 100°C. The extracts obtained were dried and re-dissolved in dimethyl sulfoxide (DMSO) for testing.

**Biomarker assay.** The expression of in-vitro pro-inflammatory markers induced by particulate matter from vehicle exhaust was measured in human U937 macrophage cells (American Tissue Culture Collection, Manassas, VA). Macrophages U937 are the first line of defense in human lungs. Substances in exhaust may interact with the macrophage cells through the Toll-Like Receptors (TLR), Aryl hydrocarbon Receptor (AhR) and the NF-KappaB protein complex to induce inflammatory responses. After treating the U937 macrophage cells for 6 hours with water extract of exhaust PM collecting filter, mRNA was isolated from the cells and reverse-transcribed into cDNA for quantitative expression analysis using qPCR. Results were normalized to housekeeping gene  $\beta$ -Actin expression and expressed as fold increase of mRNA in treated cells relative to untreated cells.

## Engine exhaust non-target chemical analysis

Engine exhaust samples from the CVS dilution tunnel were drawn through an 8 x 110 mm 400 mg/200 mg XAD-2 sorbent tube (SKC, Inc.) during the entire UC cycle (1735 seconds) at a flow rate of 1 L min<sup>-1</sup>. Sorbent tubes were unsealed immediately prior to sampling, and flow rate was controlled with a calibrated 1-5 L min<sup>-1</sup> adjustable flow meter (Dwyer Instruments, Inc.). Negative pressure was created at the back end of the sampling apparatus using an explosion-proof Teflon diaphragm pump. At the conclusion of the sampling period, the sorbent tube was immediately capped, labeled, and placed into a cooler. Once transported back to the lab, samples were stored in a 0 °C freezer for up to 30 days until extraction. Sorbent tubes were extracted by breaking open each section and separately transferring the sorbent material to labeled glass vials. Ethyl acetate (1 ml) was added to each vial, which was then capped and sonicated for 30 minutes. The supernatant liquid was transferred to a labeled amber glass autosampler vial.

Analysis was carried out on an Agilent 7890B Gas Chromatograph and mass spectra were acquired using a 7200B Quadrupole-Time-of-Flight Mass Spectrometer (GC-QTOF-MS). Each sample run includes a system blank, two sample blanks (1 set of sorbent tube extracts), calibration standards, and the samples. A series of standard semivolatile organic compounds (Restek 31850 8270 Megamix) was used to produce a retention time-retention index calibration curve. Separation was accomplished using an Agilent J&W HP5-MS UI column (30 m x 0.25 mm x 0.25 µm) with an injection volume of 1.0 µl and a flow rate of 0.8 mL min<sup>-1</sup> in (He). The injector temperature was 250 °C and the temperature program was: 35 °C for 3 min, ramp to 325 °C at 4°C min<sup>-1</sup>, hold at 325°C for 3 minutes.

Raw data from the GC-QTOF-MS experiments were first converted from vendor format to analysis base file format for further processing (Reifycs Analysis Base File Converter v. 4.0.0). All

data were subsequently deconvoluted and aligned using MS-DIAL (v. 3.66). Compounds not on the target list were tentatively identified based on retention index and mass spectral similarity using the NIST17 database with a cutoff score of 800. When the aligned nontarget feature was present in the standard solution, the feature was considered to be confirmed. If the nontarget feature was not present in the standard, but was independently identified in each sample as the same compound its identification is considered tentative/confident. In some cases the feature alignment was good but the spectral quality did not allow a confident identification of the compound. These features are listed as tentative/uncertain if at least one sample had an annotation that met the RI and spectral similarity cutoff score (800). If that criterion was not met, the feature is listed as unknown.

### **Elastic net regression<sup>87</sup> on exhaust features and toxicity responses**

The Elastic Net Regression is a regularized regression method that linearly combines the L1 and L2 penalties of the lasso and ridge methods. It fits a least-squares regression model to the data, subject to a penalty on a weighted sum of the absolute value of the model coefficients (the L1-norm) and the sum of squares the model coefficients (the L2-norm):

i.e. solve for  $\beta$ 's in minimizing:

$$\sum_{i=1}^n (Y - \hat{Y})^2 + \lambda \sum_{j=1}^p \left[ \frac{1}{2} (1 - \alpha) \beta_j^2 + \alpha |\beta_j| \right]$$

where

$$\hat{Y} = \sum_{j=1}^p \beta_j X_j$$

The penalty was selected using an  $\alpha$  value of 0.5. Cross validation was not used due to a small sample size. In the fitted model, variables with a negligible association with the outcome have a

coefficient of 0 (a result of the penalty on the L1-norm) and are thus effectively not included in the model.

Chemical data (emission factors or peak area count of mass spec) were transformed prior to statistical analysis using the relationship  $\log_2(x + c)$ , where x is the original value and c was selected to minimize the absolute value of the regression slope of the analyte standard deviations on the analyte means. The log-transformed data were then normalized with the Cyclic Loess normalization function in Bioconductor limma package (version 3.46.0). The toxicity response data (i.e. ROS, CYP1A1, IL-8, COS-2, mutagenicity) were also  $\log_2$  transformed. Elastic net regression was then used to identify the linear combination of chemical features that was most predictive of  $\log_2$  transformed toxicity response. Positive coefficients were returned for each toxicity end point, with the larger coefficients interpreted as a stronger association.

### Fuel consumption calculation<sup>72</sup>:

$$\text{Fuel economy (mile} \cdot \text{m}^{-3}\text{)} = \frac{\text{Density of fuel at 15 }^\circ\text{C (g} \cdot \text{m}^{-3}\text{)}}{1.212 * cf * (\text{HC} \times \frac{m_C}{m_{\text{HC}}} + \text{CO} \times \frac{m_C}{m_{\text{CO}}} + \text{CO}_2 \times \frac{m_C}{m_{\text{CO}_2}})}$$

Where,

$cf = \text{correctinon factor} = 0.825 + 0.0693 \times (\text{fuel H:C ratio})$ , fuel H:C ratio is 3.88 for CNG, 3.96 for RNG1 and 3.99 for RNG2 calculated based on fuel composition measurements summarized in Table 1.

$\frac{m_C}{m_{\text{HC}}} = \frac{\text{mass of carbon from HCs in the fuel}}{\text{mass of HCs in the fuel}}$  calculated from fuel composition is 0.754 for CNG, 0.750 for RNG1 and 0.749 for RNG2

$\frac{m_C}{m_{\text{CO}}} = 0.429$ ,  $\frac{m_C}{m_{\text{CO}_2}} = 0.273$ , for all fuels

HC, CO and  $\text{CO}_2$  are mass emission factors measured from exhaust ( $\text{g} \cdot \text{mile}^{-1}$ ).

**Fuel economy and CO<sub>2</sub> emissions.** Figure S.3- 2 (a) and (b) present fuel economy and CO<sub>2</sub> emission factors averaged over the entire cold-start UC cycle and for each phase of the UC cycle. Each bar represents the average emissions from two tests of the indicated fuel type, while error bars represent the range (min and max values). The cold start effect and the amount of acceleration within the speed trace influence the fuel economy and CO<sub>2</sub> emission during different phases of the UC cycle. Phase 1 and 3 emission can be compared to quantify the effect of the cold start (Phase 1) vs. hot start (Phase 2) engine conditions over an identical 300 sec driving pattern. Phase 2 was based on a longer 1135 sec high-speed driving period designed to represent highway travel. The fuel economy was lowest in phase 1 and highest in phase 2, with an overall cycle-averaged value similar to phase 2. The fuel economy of the test vehicle was highest when using CNG (2.87 miles m<sup>-3</sup>) with reduced fuel economy measured for RNG1 (-3.1%) and RNG2 (-4.9%). This trend is consistent with the fact that CNG (38.27 MJ·m<sup>-3</sup>) had the highest fuel energy content with lower energy content for RNG1 (-5.1% vs. CNG) and RNG2 (-7.3% vs. CNG). The energy consumed for each mile traveled showed less variability between CNG (13.3 MJ·mile<sup>-1</sup>), RNG1 (13.1 MJ·mile<sup>-1</sup>; -1.5% vs. CNG), and RNG2 (12.9 MJ·mile<sup>-1</sup>; -3% vs. CNG). CO<sub>2</sub> emissions factors were inversely correlated with fuel economy, with the lowest values measured when using CNG (682 g mile<sup>-1</sup>) and slightly higher values measured for RNG1 (+1.2%) and RNG2 (+5.0%). CO<sub>2</sub> emissions were higher from RNG because the lower heating value of RNG required more fuel consumption per mile, and because RNG had higher fuel CO<sub>2</sub> content, as previously discussed. Karavalakis et al., 2012<sup>75</sup> used the UC driving cycle to test two passenger cars (2002 Ford Crown Victoria and 2006 Honda Civic GX) fueled with CNG yielding slightly higher fuel economy and lower pollutant emissions rates than the current study. This result is expected since the current study tested a light duty cargo van rather than a light duty passenger car.

**Carbon monoxide and unburned HCs emissions.** CO emissions reflect the combustion and oxidation conditions inside the vehicle engine and exhaust system. Figure S.3- 2(c) shows that phase 1 of the UC cycle had the highest CO emissions because the temperature of both engine and three-way catalyst (TWC) were initially low yielding reduced oxidation of CO to CO<sub>2</sub>. The cold-start effect is also visible from the time series plot of CO concentration in undiluted exhaust measured by FTIR as shown in Figure S.3- 3 (a). CO concentration quickly increased as the vehicle started moving and then decreased after ~100 seconds as the engine and TWC warmed up. Emissions are generally ranked in descending order of phase 1 > phase 2 > phase 3 because phase 1 contains the cold-start effect, while phase 2 consists of several fast-acceleration periods to reach a maximum speed of 107 km·hr<sup>-1</sup>. The demand for increased speed and power required the engine to operate at a rich air/fuel (A/F) ratio ( $\lambda < 1$  where  $\lambda = \text{actual A/F ratio} \div \text{stoichiometric A/F ratio}$ ), resulting in higher CO emission. Overall, CO emission factors were lowest when using CNG (0.94 g·mile<sup>-1</sup>), with increasing CO emissions when using RNG1 (+25% vs. CNG) and RNG2 (+59% vs. CNG). This trend may be caused by increasing fuel CO<sub>2</sub> concentrations in the RNG blends. CO<sub>2</sub> in the fuel displaces oxygen in the combustion chamber and can act as an inert diluent contributing to pockets of incomplete combustion. This trend was consistent and significant for the phase 2 and phase 3 CO emissions. CO emissions in phase 1 had higher variability with no clear trend by fuel type.

Figure S.3- 2 (d) and Figure 2-1 (e) show that emissions of unburned HCs largely follow the CO trend because both constituents result from incomplete fuel combustion and poor oxidation in the catalyst before it reaches operating temperatures<sup>6</sup>. The RNG1 and RNG2 emissions of total HCs exceed the CNG HC emissions by 63% and 72%, respectively. The elevated HC emissions from RNG result from higher emissions of unburned methane (Figure S.3- 2(d)). CNG emitted higher concentrations of

C2 and C3 HCs (ethane and propane) as shown in Figure S.3- 2(e) and Figure S.3- 3(b) and (c), but this increase was overwhelmed by the increased methane emission from RNGs.

**Oxides of Nitrogen (NO<sub>x</sub>), nitrous oxide, and ammonia emissions.** High temperature and long residence time favor the formation of thermal NO<sub>x</sub> created from the N<sub>2</sub> in the combustion air. Figure S.3- 2(f) shows that the NO<sub>x</sub> emissions vary significantly from phase to phase with no consistent trend among different fuels. Averaged across the UC cycle, RNG emitted more NO<sub>x</sub> than CNG in the current study, which is consistent with the results reported by Subramanian et al.<sup>72</sup>. Both nitrous oxide (N<sub>2</sub>O, a strong GHG) and ammonia (NH<sub>3</sub>, an important PM precursor) are formed during TWC reduction of NO in the exhaust<sup>108-110</sup>. N<sub>2</sub>O is formed on the cold surface of the TWC usually under a narrow equivalent  $\lambda$  window of lean A/F ratio, while NH<sub>3</sub> is formed on the hot TWC under a wider  $\lambda$  range<sup>108</sup>. The time-series relationship between NO<sub>x</sub>, N<sub>2</sub>O and NH<sub>3</sub> for the first 150 seconds of each test is shown in Figure S.3- 3(d)-(f). NO<sub>x</sub> (mostly NO) concentrations quickly increased as the vehicle started, while N<sub>2</sub>O concentrations increased later in the cycle. As the catalyst temperature increased, NO<sub>x</sub> and N<sub>2</sub>O concentrations decreased while NH<sub>3</sub> increased. Emissions factors for N<sub>2</sub>O from different phases of the UC cycle are presented in Figure S.3- 2(g). The cold-start phase 1 emissions were more than 5 times higher than phase 2 and 3 emissions. Fuel composition did not affect N<sub>2</sub>O emissions.

**Particulate matter emissions and size distributions.** Figure S.3- 4 presents the time series of PM mass ( $\mu\text{g}\cdot\text{m}^{-3}$ ) and PM number ( $\#\cdot\text{cm}^{-3}$ ) concentration measured from the CVS tunnel during RNG2 tests. Emissions from other fuels follow similar trends, with both PM number and mass concentrations increasing with vehicle speed and hard accelerations. The measured size distributions of particle number (Figure S.3- 5 b) show that the majority of the particles have diameter smaller than 20nm. This agrees well with previous studies<sup>76,98</sup>, although one study by Lim et al.<sup>73</sup> reported bimodal distribution

with nucleation mode <10 nm and accumulation mode ~ 30 nm. The calculated size distributions of ultrafine particle (PM<sub>0.1</sub>) mass (Figure S.3- 5 a) have a peak approaching 100 nm particle diameter. Particles with mobility diameter greater than 100nm were not included in the analysis due to the potential for electrometer noise in the higher channels of the EEPS instrument<sup>97</sup> and because previous studies found that CNG engines emit only minor concentrations of particles larger than 100nm<sup>73,76,97,111,112</sup>.

Table S.3- 1 Experimentally determined limit of detection (LOD) for different compounds measured by FTIR

Compound	LOD	unit
H <sub>2</sub> O	2.72	%
CO <sub>2</sub>	0.65	%
CO	3.59	ppm
NO	0.82	ppm
NO <sub>2</sub>	0.42	ppm
NO <sub>x</sub>	1.01	ppm
N <sub>2</sub> O	0.62	ppm
NH <sub>3</sub>	1.18	ppm
SO <sub>2</sub>	1.69	ppm
CH <sub>4</sub>	3.72	ppm
C <sub>2</sub> H <sub>6</sub>	1.78	ppm
C <sub>2</sub> H <sub>2</sub>	4.05	ppm
C <sub>2</sub> H <sub>4</sub>	0.39	ppm
C <sub>3</sub> H <sub>6</sub>	1.97	ppm
C <sub>4</sub> H <sub>6</sub>	0.81	ppm
HCHO	0.67	ppm
CH <sub>3</sub> OH	0.36	ppm

Table S.3- 2 Experimentally determined limit of detection (LOD) for different compounds measured by PTR-MS

Compound	LOD (ppb)	Compound	LOD (ppb)
methanol	25.4	ethenone(ketene)	4.2
ethanol	38.0	methyl ketene	2.1
propanol	7.4	propene	3.5
formaldehyde	17.7	butene	2.5
acetaldehyde	19.3	isoprene	1.0
acetone	6.9	butenone	1.5
formic acid	20.5	benzene	1.0
acetic acid	14.3	toluene	0.9
Propionic acid	2.6	ethylbenzene/xylene	0.9
dimethyl sulfide	2.9	propyl benzene	1.4
acetonitrile	5.6	naphthalene	0.5
		benzaldehyde	0.7

Table S.3- 3 Concentration (%) of major compounds measured in different fuels. Limit of quantifications (LOQs), average values as well as standard deviations from 3 measurements are reported. Note that values below LOQs are possible because RNG1 and RNG2 are blends from CNG and different biomethane sources which can each have measured values above or below LOQs.

Compound Name	LOQ (%)	CNG	RNG 1	RNG 2
Nitrogen/Carbon Monoxide	0.23	1.83% ± 0.65%	2.64% ± 1.01%	1.77% ± 0.48%
Oxygen/Argon	0.14	0.42% ± 0.30%	0.42% ± 0.11%	0.18% ± 0.04%
Methane	0.76	91.20% ± 0.82%	93.50% ± 1.26%	93.33% ± 0.59%
Carbon Dioxide	0.72	0.82% ± 0.09%	1.85% ± 0.39%	4.28% ± 0.18%
Ammonia	0.00001	ND*	ND	ND
Ethane	1.29	5.41% ± 0.18%	1.50% ± 0.05%	0.42% ± 0.01%
Ethene	1.08	ND	ND	ND
Ethyne	1.07	ND	ND	ND
Propane	0.23	0.33% ± 0.06%	0.09% ± 0.02%	0.03% ± 0.00%
Propene	1.07	ND	ND	ND
Propadiene	0.97	ND	ND	ND
Propyne	0.97	ND	ND	ND
i-Butane	0.98	ND	ND	ND
n-Butane	0.77	ND	ND	ND
1-Butene	0.86	ND	ND	ND
i-Butene	0.85	ND	ND	ND
trans-2-Butene	0.72	ND	ND	ND
cis-2-Butene	0.72	ND	ND	ND
1,3-Butadiene	0.71	ND	ND	ND
Isoprene	0.72	ND	ND	ND
i-Pentane	0.54	ND	ND	ND
n-Pentane	0.54	ND	ND	ND
neo-Pentane	0.54	ND	ND	ND
Pentenes	0.54	ND	ND	ND

\* ND = Not Detected.

Table S.3- 4 Concentration (ppbv) of different sulfur-containing compounds measured in different fuels. Limit of quantifications (LOQs), average values as well as standard deviations from 3 measurements are reported. Note that values below LOQs are possible because RNG1 and RNG2 are blends from CNG and different biomethane sources which can each have measured values above or below LOQs.

Compound name	LOQ (ppbv)	CNG	RNG 1	RNG 2
Hydrogen Sulfide	298.7	<LOQ ± -	<LOQ ± -	<LOQ ± -
Sulfur Dioxide	26.2	<LOQ ± -	<LOQ ± -	124.3 ± 30.1
Carbonyl sulfide	15.2	<LOQ ± -	5.1 ± 10.3	10.6 ± 5.2
Carbon disulfide	2.9	6.9 ± 4.6	53.7 ± 37.2	49.3 ± 17.9
Methyl mercaptan	52.5	<LOQ ± -	11.2 ± 22.4	135.2 ± 29.2
Ethyl mercaptan	7.8	171.8 ± 25.4	47.8 ± 7.1	27.5 ± 24.7
Isopropyl mercaptan	4.9	43.7 ± 16.6	110.6 ± 196.9	118.8 ± 111.5
n-Propyl mercaptan	4.3	12.0 ± 10.4	23.0 ± 39.4	31.5 ± 30.6
t-Butyl mercaptan	4.4	677.0 ± 173.1	188.2 ± 48.1	100.7 ± 66.4
sec-Butyl mercaptan	4.9	<LOQ ± -	192.3 ± -	106.9 ± -
Dimethyl sulfide	4.3	<LOQ ± -	756.1 ± 476.9	810.6 ± 315.2
Methyl Ethyl sulfide	3.5	5.2 ± 0.6	14.3 ± 9.3	26.8 ± 17.0
Diethyl sulfide	5.7	28.3 ± 0.2	7.9 ± 0.0	2.2 ± 0.0
Di-tert-butyl sulfide	3.0	<LOQ ± -	<LOQ ± -	<LOQ ± -
Dimethyl Disulfide	0.8	<LOQ ± -	35.0 ± 69.9	53.0 ± 34.8
Diethyl Disulfide	1.1	<LOQ ± -	2.3 ± 1.6	1.1 ± 0.8
Thiofuran	3.0	<LOQ ± -	<LOQ ± -	9.7 ± 5.0
Methyl Ethyl Disulfide	10.0	<LOQ ± -	24.3 ± 30.1	30.1 ± 16.7
Methyl i-Propyl Disulfide	10.0	12.2 ± 21.2	76.1 ± 117.0	70.1 ± 57.4
Methyl n-Propyl Disulfide	10.0	15.5 ± 0.0	34.7 ± 29.3	39.6 ± 16.5
Methyl t-Butyl Disulfide	10.0	51.3 ± 11.9	139.1 ± 44.5	63.4 ± 21.2
Ethyl i-Propyl Disulfide	10.0	<LOQ ± -	<LOQ ± -	0.0 ± 0.0
Ethyl n-Propyl Disulfide	10.0	<LOQ ± -	126.4 ± 93.9	60.2 ± 44.7
Ethyl t-Butyl Disulfide	10.0	13.6 ± -	3.8 ± 0.0	1.0 ± 0.0
Di-i-Propyl Disulfide	10.0	<LOQ ± -	0.0 ± 0.0	0.0 ± 0.0
i-Propyl n-Propyl Disulfide	10.0	28.9 ± 35.3	17.6 ± 21.6	6.8 ± 9.5
Di-n-Propyl Disulfide	10.0	10.7 ± -	3.0 ± 0.0	0.8 ± 0.0
i-Propyl t-Butyl Disulfide	10.0	<LOQ ± -	0.0 ± 0.0	0.0 ± 0.0
n-Propyl t-Butyl Disulfide	10.0	<LOQ ± -	0.0 ± 0.0	0.0 ± 0.0
Di-t-Butyl Disulfide	10.0	17.1 ± 5.1	31.5 ± 19.9	14.1 ± 9.4
Thiophene	10.0	13.0 ± 2.0	3.6 ± 0.6	14.0 ± 1.8
C1-Thiophenes	10.0	<LOQ ± -	42.5 ± 0.0	48.1 ± 8.5
Thiophane	10.0	<LOQ ± -	1.1 ± 0.9	0.5 ± 0.4
Thiophenol	10.0	<LOQ ± -	1.1 ± 0.9	0.5 ± 0.4

Table S.3- 5 Concentration (ppbv) of different hydrocarbons measured in different fuels. Limit of quantifications (LOQs), average values as well as standard deviations from 3 measurements are reported. Note that values below LOQs are possible because RNG1 and RNG2 are blends from CNG and different biomethane sources which can each have measured values above or below LOQs.

	LOQ (ppbv)	CNG		RNG1		RNG2	
		avg	std	avg	std	avg	std
Cyclopentane	1.9	< LOQ	± -	483.5	± 372.0	233.1	± 177.3
Methylcyclopentane	1.9	< LOQ	± -	1555.7	± 1123.8	764.0	± 535.5
Cyclohexane	1.9	< LOQ	± -	1356.4	± 963.4	664.7	± 459.1
Methylcyclohexane	1.9	2939.4	± 46.1	841.0	± 12.8	261.4	± 6.7
Hexanes	1.9	2828.7	± 587.9	2728.8	± 1384.3	1184.6	± 657.1
Heptanes	1.9	1043.9	± 48.9	1184.1	± 602.9	533.9	± 287.5
2,2,4-Trimethylpentane	1.9	36.2	± 3.5	200.2	± 1.0	877.6	± 118.9
Octanes	1.9	< LOQ	± -	1024.2	± 593.6	559.4	± 283.9
Nonanes	0.03	145.3	± 35.7	42.9	± 9.9	17.0	± 3.2
Decanes	0.003	37.2	± 5.8	11.6	± 1.6	5.3	± 0.6
Undecanes	0.012	8.3	± 3.2	3.4	± 0.9	2.3	± 0.3
Dodecanes	0.002	3.0	± 1.0	1.3	± 0.3	0.9	± 0.1
Tridecanes	0.002	0.6	± 0.3	0.3	± 0.1	0.2	± 0.0
Tetradecanes	0.009	< LOQ	± -	0.0	± 0.0	0.0	± 0.0
1,3-Butadiene	1.0	< LOQ	± -	5.3	± 0.0	10.1	± 0.1
Benzene	8.5	684.3	± 230.2	715.6	± 64.0	416.7	± 85.3
Toluene	4.1	768.1	± 64.4	352.6	± 17.9	328.7	± 17.8
Ethylbenzene	3.4	40.9	± 0.1	68.5	± 0.0	53.7	± 4.0
m,p-Xylene	3.1	244.9	± 6.4	311.4	± 1.8	204.6	± 32.2
o-Xylene	3.0	39.6	± 2.4	68.7	± 0.7	57.3	± 5.2
1,2,4-Trimethyl benzene	0.008	0.9	± 0.1	0.4	± 0.0	0.6	± 0.0
2-Ethyl toluene	0.003	0.3	± 0.1	0.1	± 0.0	0.1	± 0.0
Isopropyl Benzene	0.003	1.6	± 0.4	0.7	± 0.1	0.7	± 0.2
Styrene	2.8	< LOQ	± -	2.7	± 0.0	3.3	± 0.0
Isopropylbenzene	2.8	7.7	± 0.5	7.0	± 0.2	6.2	± 0.3
4-Ethyltoluene	1.9	22.7	± 0.6	12.5	± 0.2	13.7	± 0.0
n-Propylbenzene	2.5	14.3	± 4.7	9.9	± 1.3	7.1	± 1.1
1,3,5-trimethylbenzene	2.5	11.1	± 0.9	12.5	± 0.3	9.5	± 0.7
tert-butylbenzene	2.6	< LOQ	± -	3.3	± 0.0	2.5	± 0.6
1,2,4-Trimethylbenzene	6.1	< LOQ	± -	18.7	± 0.0	20.1	± 0.0
s-Butylbenzene	1.5	< LOQ	± -	5.3	± 0.0	6.2	± 0.5
p-Isopropyltoluene	472.8	< LOQ	± -	358.4	± 0.0	286.5	± 0.0
n-butylbenzene	10.8	< LOQ	± -	< LOQ	± -	< LOQ	± -
Naphthalene	6.1	< LOQ	± -	30.3	± 0.0	33.1	± 0.0

Table S.3- 6 PM mass ( $\mu\text{g}/\text{filter}$ ) collected for different toxicity assays.

Particle mass ( $\mu\text{g}$ ) per filter	CNG test	RNG1 test	RNG2 test	Blank
ROS assay	17.3	9.17	8.25	0.68
Mutagenicity	31.9	16.9	15.2	1.26
Molecular marker assays	31.9	16.9	15.2	1.26

Table S.3- 7 Abundance (in peak area) of compounds detected with XAD + GC/MS analysis from different exhaust samples.

Metabolite name	Retention time for unknowns (min)	CNG	RNG1	RNG2
2-Pentene, 2,4,4-trimethyl-		0.00E+00	2.46E+05	2.58E+05
3-Pentanol, 3-methyl-		1.05E+06	1.06E+06	0.00E+00
n-Propyl acrylate		0.00E+00	0.00E+00	6.81E+06
Cyclotrisiloxane, hexamethyl-		4.20E+05	7.32E+04	2.04E+07
3-Furaldehyde		8.40E+02	9.20E+02	6.13E+02
Benzene, 1-chloro-4-(trifluoromethyl)-		4.17E+05	9.82E+04	3.90E+04
2,4-Octadiyne		0.00E+00	0.00E+00	0.00E+00
Bicyclo[3.1.0]hex-2-ene, 2-methyl-5-(1-methylethyl)-		1.35E+05	7.04E+04	5.65E+04
2-Butenoic acid, 1-methylpropyl ester, (E)-		3.35E+04	0.00E+00	0.00E+00
Santolina triene		2.21E+04	1.38E+05	1.43E+04
Benzene, 1,3-dichloro-		3.74E+04	2.10E+04	1.34E+04
3-Carene		1.09E+05	5.77E+04	7.62E+04
7-Octen-4-one, 2,6-dimethyl-		1.22E+03	9.70E+03	1.28E+03
p-Cresol		3.11E+04	0.00E+00	0.00E+00
Benzene, 2-ethyl-1,4-dimethyl-		3.63E+04	1.49E+04	1.10E+04
Indan, 1-methyl-		0.00E+00	0.00E+00	0.00E+00
Benzene, 2-ethenyl-1,4-dimethyl-		3.00E+04	1.74E+04	1.02E+06
Benzaldehyde, 4-ethyl-		8.39E+03	0.00E+00	0.00E+00
Naphthalene		6.32E+05	2.04E+05	1.82E+05
1,3-Butadiene, 1,1,2,3,4,4-hexachloro-		5.46E+01	5.00E+01	5.84E+01
1,2-Benzisothiazole		2.28E+05	1.14E+05	1.04E+05
Naphthalene, 2-methyl-		4.70E+04	2.35E+04	1.98E+04
2-Propenoyl chloride, 3-phenyl-, (E)-		1.03E+04	9.63E+04	0.00E+00
1-Octanol, 2-butyl-		2.73E+04	1.00E+04	1.15E+04
Quinoline, 2-methyl-		9.79E+02	8.19E+02	0.00E+00
Naphthalene, 1-methyl-		3.24E+04	1.58E+04	1.25E+04
2,5-Dimethylhexane-2,5-dihydroperoxide		1.19E+06	5.32E+05	4.80E+03
4-(2-Methylcyclohex-1-enyl)-but-2-enal		3.82E+05	0.00E+00	4.49E+03
Acenaphthylene		4.16E+03	1.43E+03	2.36E+03
Dimethyl phthalate		1.92E+04	7.55E+03	1.03E+04
Dibenzofuran		2.94E+04	1.58E+04	1.14E+04
Fluorene		6.15E+03	0.00E+00	0.00E+00

1-Pentadecene, 2-methyl-		5.62E+04	2.30E+04	2.58E+04
Benzene, 1-bromo-4-phenoxy-		0.00E+00	0.00E+00	1.22E+02
Dibenzothiophene		3.94E+03	1.37E+02	2.93E+03
Anthracene		1.52E+04	7.85E+03	1.00E+04
Dodecane, 4-cyclohexyl-		2.83E+04	2.08E+04	1.81E+04
2-(Pentyloxycarbonyl)benzoic acid		3.15E+04	2.67E+04	1.50E+04
Phthalic acid, isobutyl undec-2-en-1-yl ester		0.00E+00	0.00E+00	0.00E+00
Unknown	4.961	3.65E+06	1.83E+07	1.63E+07
Unknown	5.299	0.00E+00	3.64E+06	3.56E+06
Unknown	5.335	0.00E+00	1.05E+05	0.00E+00
Unknown	5.448	0.00E+00	1.05E+06	0.00E+00
Unknown	5.746	5.61E+05	4.50E+04	2.89E+05
Unknown	6.593	1.33E+05	3.19E+04	3.77E+04
Unknown	6.69	0.00E+00	0.00E+00	0.00E+00
Unknown	6.934	0.00E+00	0.00E+00	1.10E+04
Unknown	7.107	0.00E+00	0.00E+00	1.87E+02
Unknown	7.674	0.00E+00	5.43E+04	5.69E+04
Unknown	10.244	4.71E+04	3.29E+04	3.18E+04
Unknown	10.539	0.00E+00	0.00E+00	9.96E+03
Unknown	10.796	0.00E+00	0.00E+00	3.08E+05
Unknown	11.781	2.21E+05	1.17E+05	1.03E+05
Unknown	12.696	0.00E+00	0.00E+00	1.29E+04
Unknown	12.918	4.66E+04	2.78E+04	2.75E+04
Unknown	14.249	0.00E+00	1.65E+04	1.60E+04
Unknown	14.254	5.21E+04	3.68E+04	2.26E+04
Unknown	14.369	6.43E+04	3.86E+04	1.50E+05
Unknown	15.277	1.90E+04	1.94E+04	1.21E+05
Unknown	17.738	9.42E+04	8.01E+04	7.24E+04
Unknown	18.741	1.06E+03	1.05E+03	1.40E+03
Unknown	18.743	7.65E+03	2.84E+04	2.19E+04
Unknown	20.175	2.62E+03	0.00E+00	0.00E+00
Unknown	33.34	3.87E+03	9.22E+03	0.00E+00
Unknown	33.44	2.39E+04	1.40E+04	9.05E+03
Unknown	43.883	9.23E+04	4.81E+04	9.43E+03
Unknown	76.454	1.98E+04	2.83E+04	1.04E+03
Unknown	76.623	0.00E+00	0.00E+00	0.00E+00

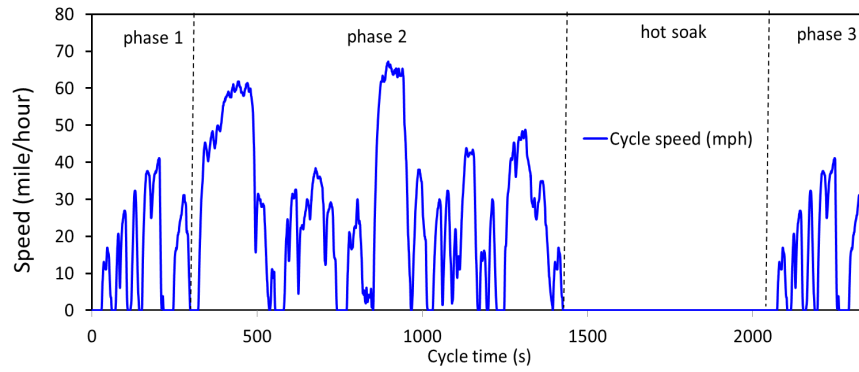


Figure S.3- 1 Speed trace from the California Unified Cycle<sup>111</sup>.

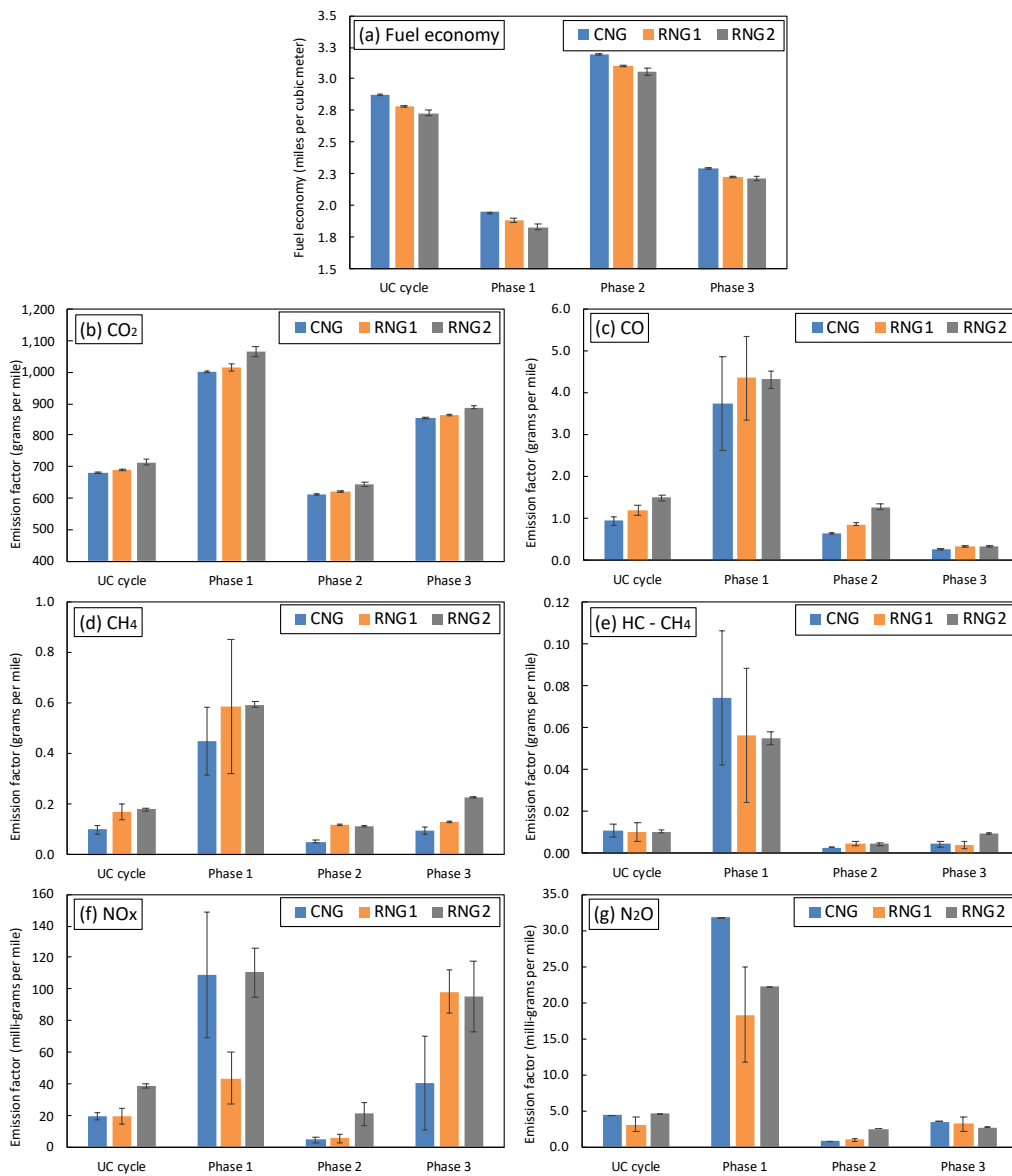


Figure S.3- 2 Fuel economy and emission factors of different pollutants for the averaged cold-start UC cycle as well as different phases of the cycle. Error bars define the range (min and max values) set by the duplicate tests.

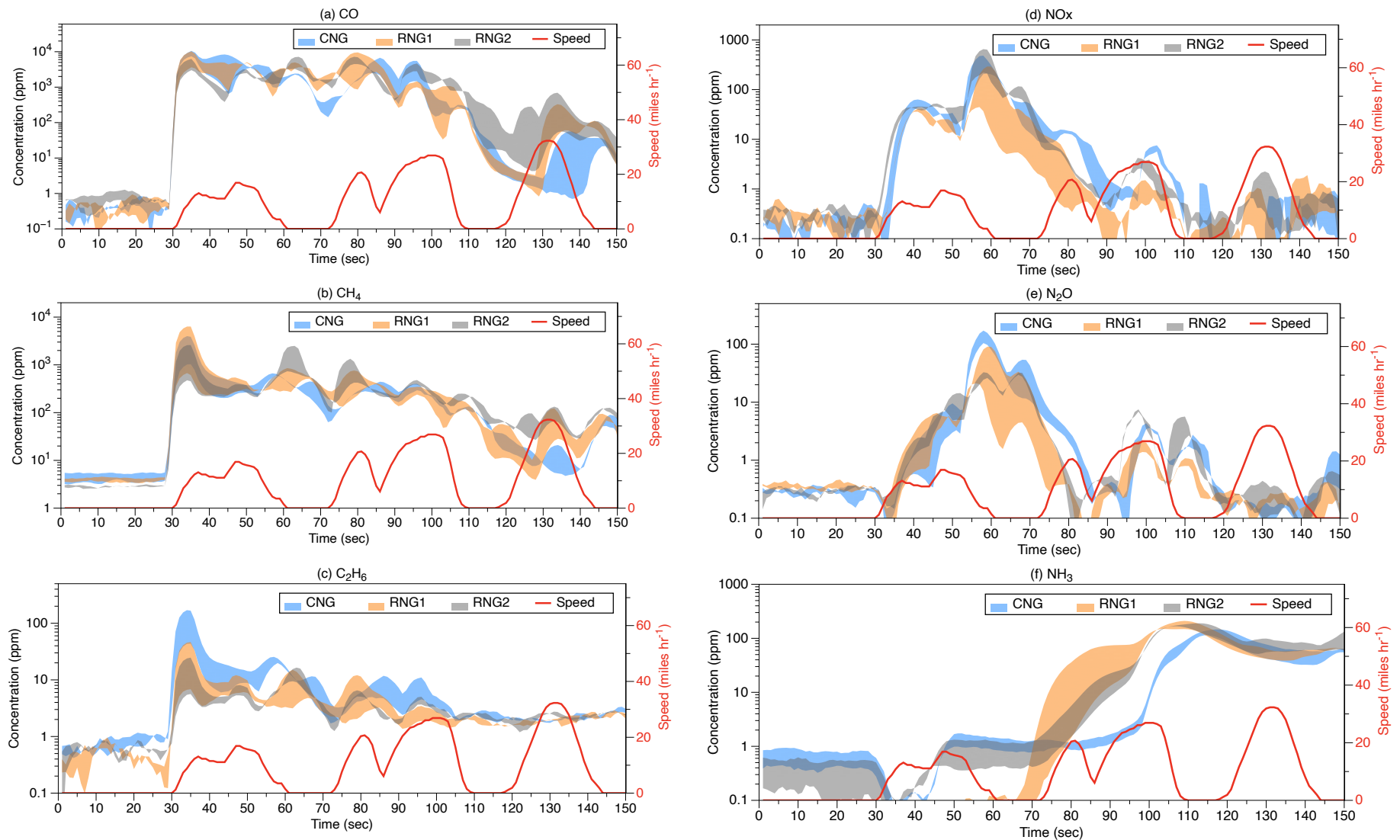


Figure S.3- 3 (a)-(f). Time series of concentration of different pollutants (ppm) measured by FTIR in the first 150 seconds of the cold-start UC cycle. The range for each fuel is outlined by the duplicate measurements from two cold-start UC cycle tests.

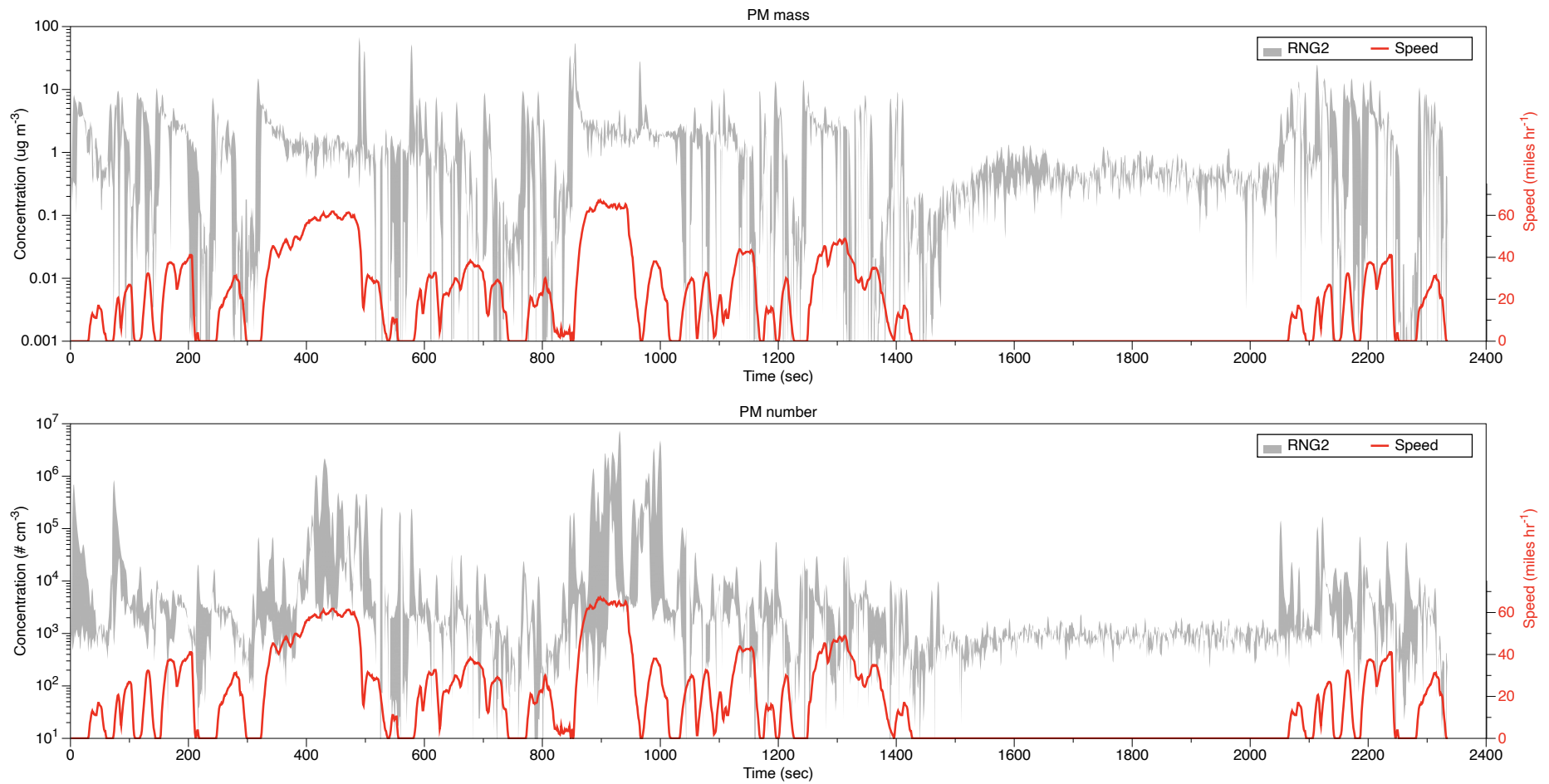


Figure S.3- 4 Time series of particle mass concentration ( $\mu\text{g}\cdot\text{m}^{-3}$ ) and number concentration ( $\#\cdot\text{cm}^{-3}$ ) measured from the CVS dilution tunnel. Showing the trace of RNG2 as an example

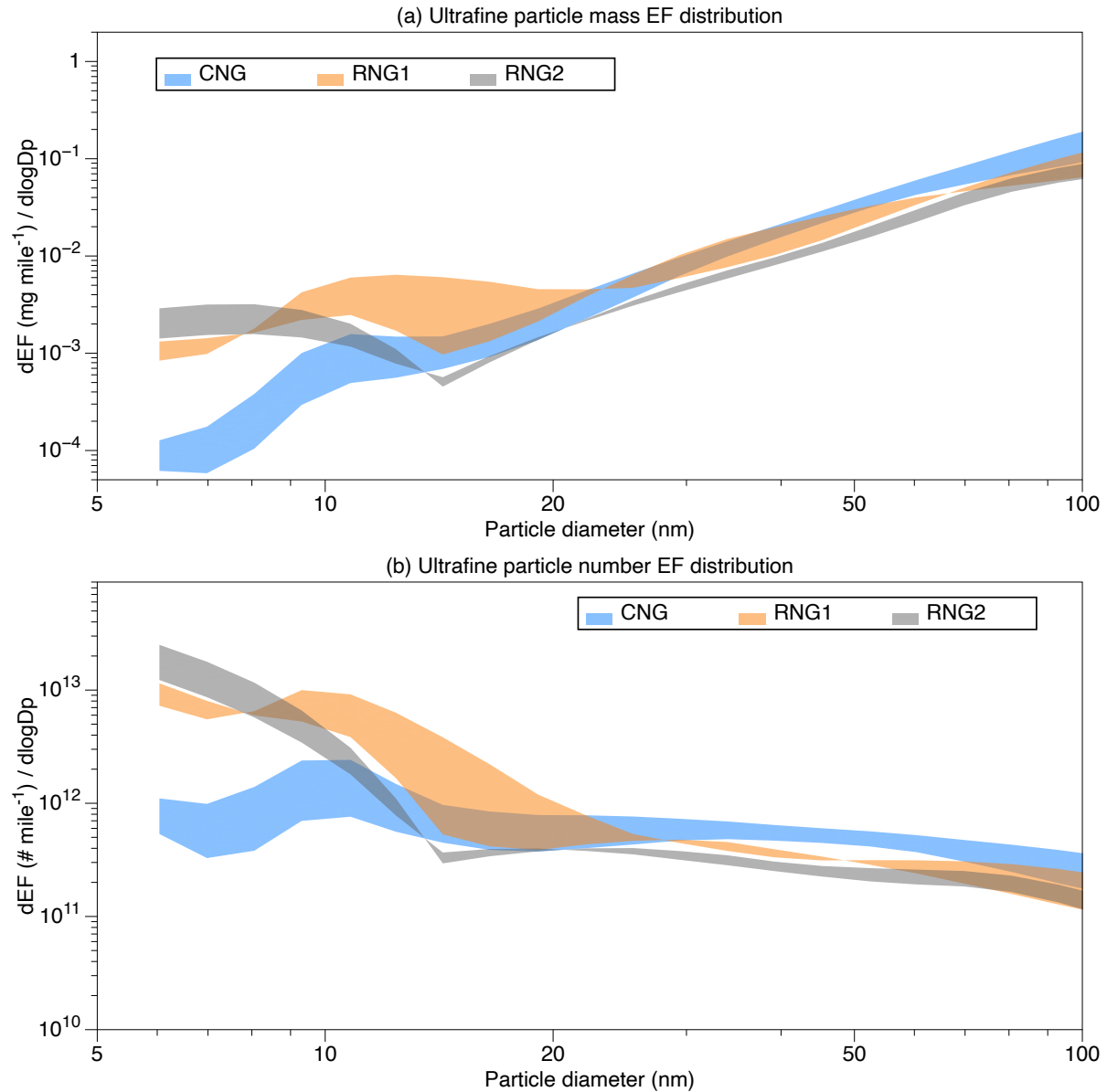


Figure S.3- 5 Distribution of (a) ultrafine particle mass emission factor ( $\text{mg}\cdot\text{mile}^{-1}$ ) and (b) ultrafine particle number emission factor ( $\#\cdot\text{mile}^{-1}$ ) from the tested vehicle running on different fuels. The range for each fuel (shaded area) is outlined by the duplicate measurements from two cold-start UC cycle tests.

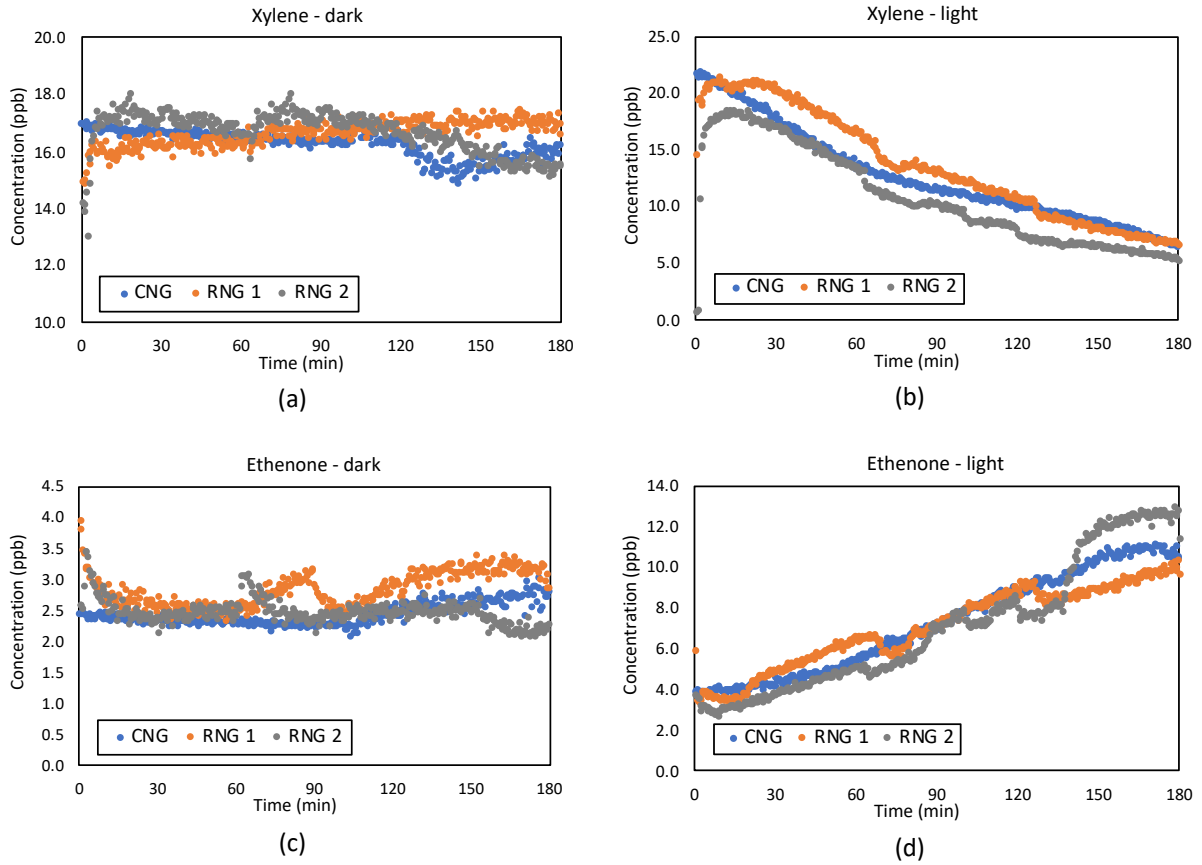


Figure S.3- 6 Typical concentration profiles (ppb) during atmospheric aging. (a) concentration of xylene during dark aging; (b) concentration of xylene during light aging; (c) concentration of ethenone during dark aging; (d) concentration of ethenone during light aging.

## **Chapter 4 – Future Emissions of Particles and Gases under Different Greenhouse Gas Mitigation Strategies**

### **4.1 Background**

Greenhouse gas (GHG) mitigation is a dynamic process that must recognize changes in population, attitudes towards policy enforcement, technology advancement, land-use and lifestyle<sup>1,2,113–119</sup>. GHG mitigation occurs within a framework of other environmental efforts with the potential for overlap in multiple areas, including air pollutant emissions and regional air quality impacts<sup>120</sup>. California is the most populous state and the second largest greenhouse gas emitter in the U.S. due to its high economic activity. California is also home to seven of the ten most polluted cities in the U.S.<sup>121</sup> primarily because of unfavorable topography and meteorology that keeps emissions trapped close to the surface. California is at the forefront of the leading economies across the world in the development of science-based policies to address climate change and air pollution issues. Since the passage of Assembly Bill 32<sup>122</sup> that calls for an 80% reduction in GHG emissions (relative to 1990 levels) by year 2050, researchers have been working on constructing and analyzing possible pathways to bring about the decarbonization of the energy system<sup>123–127</sup>. As part of this effort, a California-specific integrated multi-sector energy-economic-optimization model framework CA-TIMES<sup>123,127</sup> was developed to identify least-cost approaches to achieve target levels of GHG reduction subject to policy constraints. Zapata et al.<sup>117</sup> developed an emission inventory model CA-REMARQUE to map changes in energy, technology and activity from the CA-TIMES model to changes in air pollutant emissions. The resulting analysis determined that the transition to a low carbon energy future could avoid ~25% of the premature mortality associated with air pollution in California<sup>1</sup>. The public health savings associated with improved air quality are significant and must be considered in future planning exercises.

Although some of the technology advancements and fuel shifts needed to ensure a low-carbon sustainable future are well understood at this time (i.e. electric and fuel cell vehicles, wind and solar electricity generation), the optimal combination of other key technologies and their associated environmental impacts still require further analysis. For example, carbon capture and sequestration (CCS)

technology is being widely discussed due to its promising GHG reduction benefits, but some studies note the potential for environment and public health disbenefits<sup>2,128-131</sup>. Several studies report that CCS deployed in fossil fuel powerplants could increase emissions of GHGs, gas-phase oxides of nitrogen (NO<sub>x</sub>), and airborne particulate matter because of low carbon capture efficiency and the additional fuel consumption needed to power the CCS unit<sup>130,132,133</sup>. In contrast, CCS deployed in a biomass integrated gasification combined cycle (Bio-IGCC) is considered to be a promising negative carbon emission technology with competitive costs compared to other carbon mitigation strategies<sup>128,129,131,134</sup>. The air quality impacts of Bio-IGCC-CCS have not yet been evaluated, and this study provides information that will begin the process of addressing this gap. Natural gas is another energy resource that is being studied intensely in GHG mitigation plans due to its potential to provide a transition pathway from heavy petroleum fuel to renewable energy while simultaneously improving air quality. Natural gas powerplants and the associated infrastructure contribute to carbon “lock-in” where current structures would remain in place for decades before phasing out<sup>135</sup>, but natural gas pipeline infrastructure can also distribute renewable gaseous fuel (e.g. biomethane)<sup>136</sup> yielding climate benefits. The fast response time for natural gas powerplants also plays an important role in balancing electricity service load in grids that rely on intermittent renewable energy (i.e. wind and solar)<sup>137</sup>. Despite these potential climate benefits, natural gas combustion emits significant amounts of ultrafine particulate matter (PM<sub>0.1</sub>)<sup>64,138</sup>, potentially degrading some of the benefits provided by technologies with zero emissions (i.e. wind and solar). The optimal strategy for natural gas usage in a low carbon future that balances GHG emission and air quality remains to be explored.

In this chapter, we incorporate the latest energy system projections from the CA-TIMES model and update the accompanying emission inventory model CA-REMARQUE<sup>117</sup> to generate future air pollutant emission inventory under six different scenarios in California: (i) BAU - a business-as-usual future reference scenario, (ii) CAP30 - a loose GHG reduction scenario that meets current policy references but only achieves a 40% GHG reduction (relative to 1990 levels) by the year 2030, (iii) GHGAi - a climate-friendly 80% GHG reduction scenario featuring broad adoption of advanced technologies and renewable energies, (iv) CCS - a scenario that achieves 80% net GHG reductions but allows for more combustion to

generate electricity by focusing on adoption of carbon capture and sequestration technology, (v) NGT – a variation on the GHGAI scenario that allows for more natural gas combustion for residential and commercial buildings, and (vi) NGT – a variation of the GHGAI scenario that allows for more natural gas combustion for electricity generation. The combination of the latest versions of CA-TIMES and CA-REMARQUE produced a California-specific, detail-rich air pollutant emission inventory with 4km resolution. The two-model framework retains internally consistent new-technology and alternative-energy projections throughout the emission inventory while also considering the appropriate spatial allocation of the emissions. The present study updates the BAU and GHG scenarios created using previous versions of CA-TIMES and CA-REMARQUE<sup>1,117</sup> and compares them to alternative scenarios. These results will support calculations using chemical transport models to predict future air pollution concentration fields. The identification of potential benefits and disbenefits for future air quality can help policy makers minimize the undesirable outcomes of GHG mitigation efforts while simultaneously optimizing the energy-environment-economic relationship.

## **4.2 Methods**

### **4.2.1 The CA-TIMES model and future scenarios**

CA-TIMES is an integrated energy-engineering-environmental-economic systems model focusing on the transition of California's energy system<sup>127</sup>. Built upon the MARKAL-TIMES optimization framework, CA-TIMES is rich in technological detail across all of the supply and demand sectors of the energy economy, including fuel production and conversion, electricity production, and energy consumption in the residential, commercial, industrial, transportation, and agricultural end-use sectors. CA-TIMES selects the economically-optimal mix of energy supplies to satisfy demand subject to the specified resource limits, policies, and any exogeneous constraints. Numerous scenarios have been generated by the CA-TIMES model to understand the transition costs and technology / resource implication of long-term

strategies to decarbonize California's energy system<sup>123,127</sup>. Six scenarios in the year 2050 were chosen for detailed air pollution emissions analysis in the current study.

1) **“BAU”** - A “business-as-usual” scenario that serves as a future reference. This scenario incorporates current regulations to achieve the goal outlined in California AB32, which requires greenhouse gas emissions in 2020 to be below 1990 levels but otherwise does not constrain future emissions beyond that date. The BAU scenario assumes that population and economic growth through 2050 will require a baseline level of energy service similar to current conditions and it incorporates the most important current policies that drive this energy system development (see table Table S.4- 1). The BAU scenario provides an example for how California's energy system could potentially develop in the absence of any substantial effort to move toward a low-carbon society beyond 2020.

2) **“CAP30”** - A loose GHG mitigation scenario that reduces GHG emissions to 40% below 1990 levels by the year 2030 but does not constrain or invest further in future GHG reduction. This scenario represents an intermediate future decarbonization situation.

3) **“GHGAI”** - A “climate friendly” scenario that reduces 80% GHG emissions (relative to year 1990) by the year 2050. The deep decarbonization requires market mechanisms such as a cap-and-trade program or stringent carbon taxes to augment existing policy programs. The GHGAI scenario uses a “step” carbon cap, meaning GHG emissions are only limited at the 2020 level (=1990 level) between 2020 and 2049 but then dropped to 80% below 1990 emissions in the year 2050. This step-cap allows maximum flexibility to determine the optimum cost-effective trajectory to meet the GHG mitigation target by adjusting the timing for adoption of different types of efficient resources and technologies.

4) **“CCS”** - A scenario that focuses on the impact of deploying carbon capture and sequestration (CCS) technology. This scenario generates 24% of all electricity with Bio-IGCC-CCS, which results in over 80 M tons of CO<sub>2</sub>-eq negative carbon emissions. The negative emissions in the electrical sector allow for more fossil fuel consumption in other sectors (especially transportation), while still achieving a net GHG reduction of 80% relative to 1990 levels (similar to that in GHGAI).

5) “**NGB**” – A GHG mitigation variation scenario that focus on the impact of natural gas usage in residential and commercial buildings. The shift from natural gas appliances (furnaces, water heating, etc.) to electricity appliances is limited, resulting in 20% more natural gas usage in buildings compared to other deeply decarbonized scenarios such as GHGAI.

6) “**NGT**” – A GHG mitigation variation scenario that focus on the impact of natural gas usage to generate electricity. Electricity generation from natural gas is allowed to increase from 10% in the GHGAI scenario to 30% in the NGT scenario.

#### 4.2.2 The updated CA-REMARQUE model

The California Regional Multisector Air Quality Emissions (CA-REMARQUE\_v1.0) model<sup>117</sup> was developed to predict changes to criteria pollutant emission inventories in California in response to sophisticated emission control programs and energy scenario projections provided by the CA-TIMES model. CA-REMARQUE achieves this goal by combining detailed information from each economic sector with the latest outputs from multiple models to better represent activity patterns and emission locations in a series of tailored algorithms. For example, the EMFAC model<sup>139</sup> is used to project future on-road mobile emissions, the VISION<sup>140</sup> scenario planning model is used to project future off-road transportation activities, the SWITCH-WECC model<sup>141</sup> is used to project future electricity load in different subregions of California, the GREET<sup>142,143</sup> model is used to predict emissions from biomass and hydrogen facilities, and the H<sub>2</sub>-TIMES model<sup>125</sup> is used to project locations for new hydrogen production facilities. The CA-REMARQUE model also compiles the latest published values for pollutant emission factors from new energy and technologies. All of these features make the CA-REMARQUE model a high resolution, detail-rich emission inventory model catering specifically to California’s needs. The original version of the model CA-REMARQUE model (v1.0) has been documented in a previous study<sup>117</sup>. CA-REMARQUE was updated to version 2.0 in the current study to be compatible with the latest version of the CA-TIMES model and other related model outputs as summarized below.

In the on-road transportation sector, CA-REMARQUE\_v2.0 incorporated the updated Emission Factors (EMFAC) 2014 model results, which allowed direct emission projection to the year 2050. CA-REMARQUE\_v1.0 worked with the EMFAC 2007 model that only projected emissions to the year 2035 and required extrapolation from 2035 to 2050. The Emission Inventory Code (EIC) cross-reference table between EMFAC vehicle class and technology and CA-TIMES vehicle types was updated in CA-REMARQUE\_v2.0 (see Table S.4- 2).

CA-REMARQUE\_v2.0 was updated to require the adoption of diesel particle filter treatment technology for all of the off-road and agricultural equipment that run on diesel and biodiesel in the year 2050. This specific control technology was not fully implemented in CA-REMARQUE\_v1.0. Aircraft emissions in the Los Angeles region that were missing in CA-REMARQUE\_v1.0 were added in CA-REMARQUE\_v2.0. Additional emission scaling factors of 0.45 for SO<sub>x</sub> and 0.85 for NO<sub>x</sub> were applied to all of the Bio-IGCC-CCS powerplants in the CCS scenario in CA-REMARQUE\_v2.0 because NaOH scrubbers are typically used to control flue gas SO<sub>2</sub> concentrations to avoid contamination of the amine-based carbon capture solvent<sup>144,145</sup>. Exhaust stack information was updated and carefully matched to corresponding emissions records in the electricity generation, industrial, and commercial sectors in CA-REMARQUE\_v2.0 to ensure reasonable plume rise heights. The updates summarized above slightly alter the BAU and GHG-Step scenarios analyzed previously<sup>1,117</sup>. The current study presents updated versions of the BAU and GHGAi scenarios as internally-consistent reference points for comparison to the CAP30, CCS, NGB, and NGT scenarios.

#### 4.2.3 Air Quality Model

Future air pollution concentrations were predicted using the UCD/CIT air quality model<sup>146,147</sup> with a spatial resolution of 4 km over central California and Southern California that contains more than 90% of the total population in the state. Simulations were conducted over 32 individual weeks (each including three days of spin up time) randomly selected over a ten-year window from 2046 through 2055. The

resulting concentrations characterize the long-term average concentration in the presence of meteorological variability associated with the El Nino Southern Oscillation (ENSO). Large scale meteorological inputs were obtained from the Community Climate System Model (CCSM)<sup>148</sup> under the Representative Concentration Pathway 8.5 (RCP8.5)<sup>149</sup>. Fine scale meteorology was downscaled using the Weather Research and Forecasting (WRF) model v3.4. Biogenic emissions were predicted using the Model of Emissions of Gases and Aerosols from Nature (MEGAN) v2.1. Wildfire emissions were assumed to be independent of the energy scenarios and so were not considered in the current analysis since they would not change the relative difference between each scenario.

#### 4.2.4 Health Impact Model

The public health impacts of altered PM<sub>2.5</sub> concentrations were predicted using the BenMAP-CE v1.5 model maintained by the US EPA<sup>150</sup>. The PM<sub>2.5</sub> health impact function was taken to be an evenly-weighted average of four independent epidemiological studies<sup>151–154</sup>. Avoided mortality was translated to a monetary value using the standard value of a statistical life (VSL) recommended by US EPA yielding a VSL equivalent to USD 7.6 M. Avoided mortality per 1M residents was projected to total avoided mortality based on an expected population in California of 45M in the year 2050<sup>155</sup>. The spatial distribution of population assumed in health impact calculations was consistent with the distribution assumed in emissions projections.

## 4.3 Results and discussion

### 4.3.1 Energy system transition and GHG emission

California's energy system must change significantly in order to reduce GHG emissions by 80%. Figure 4-1 summarizes the primary energy portfolios used in 2010 and in the scenarios developed for the year 2050. Large differences are apparent between the energy mix used in current vs. future energy scenarios, and between future energy scenarios that meet the 80% reduction target vs. scenarios that have

lower levels of GHG reduction. Figure S.4- 1 presents the evolution of primary energy consumption (PJ) within each scenario from 2010 to 2050 with a 5-year time step. Renewable sources (solar, wind, biomass, and other renewables including hydraulic power) account for only 5% of total energy in the year 2010 but grow to ~30% of total energy in the 2050 BAU scenario and over 50% in the GHGAi, NGB and NGT scenarios.

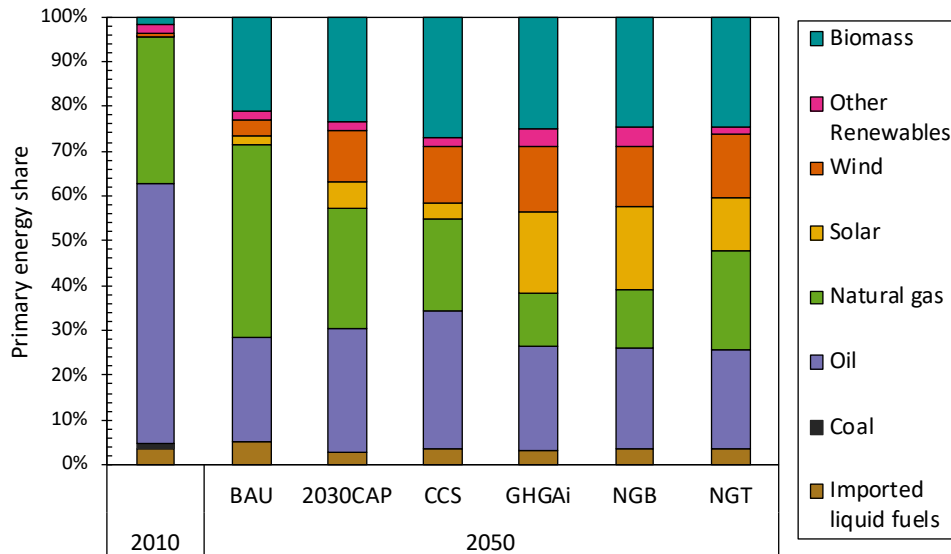


Figure 4-1. California energy system transition as represented by the percentage of different types of primary energy in 2010 and 2050 scenarios.

GHG emissions are closely related to the portfolio of energy sources used in each scenario. Figure 4-2 summarizes the CO<sub>2</sub>-equivalent GHG emission in 2010 and each of the 2050 scenarios while Figure S.4- 2 shows the evolution of GHG emissions between 2010 and 2050. The reference scenario BAU reduces GHG emissions by 39% relative to the base year 2010, mainly through decarbonizing the transportation sector (-24%) and the electricity generation sector (-9%). These predictions reflect the effectiveness of current policies that target mobile and powerplant emissions. GHG emissions from the residential and commercial sectors increase in the 2050 BAU scenario compared to the year 2010 due to population growth. The GHGAi scenario eliminates 61% of the electricity generation GHG emissions, 87% of the building sector GHG emissions, and almost 100% of the transportation sector GHG emissions relative to the BAU. The CAP30 scenario produces electricity with less carbon intensity than the BAU scenario but shows no

further decarbonization in either the building or the transportation sectors. The CCS scenario is able to generate negative GHG emissions due to the adoption of Bio-IGCC-CCS technology that captures carbon from the atmosphere during biomass accumulation and “eliminates” carbon from the atmosphere by storing it in underground reservoirs. The negative emissions are used to offset emissions from the transportation and residential sectors yielding a net reduction in total GHG emissions in the CCS scenario that are similar to the GHGAi scenario (87.5 M ton CO<sub>2</sub>-eq). As expected, GHG emissions are higher in the NGB scenario (buildings) and in the NGT scenario (electricity generation) compared to the GHGAi scenario. It is also noteworthy that the GHG emissions contributions from non-energy sectors (soil, livestock, waste treatment, etc.) increase from 11% in the BAU scenario to 37% in the GHGAi scenario as the major GHG emissions sources undergo deep decarbonization.

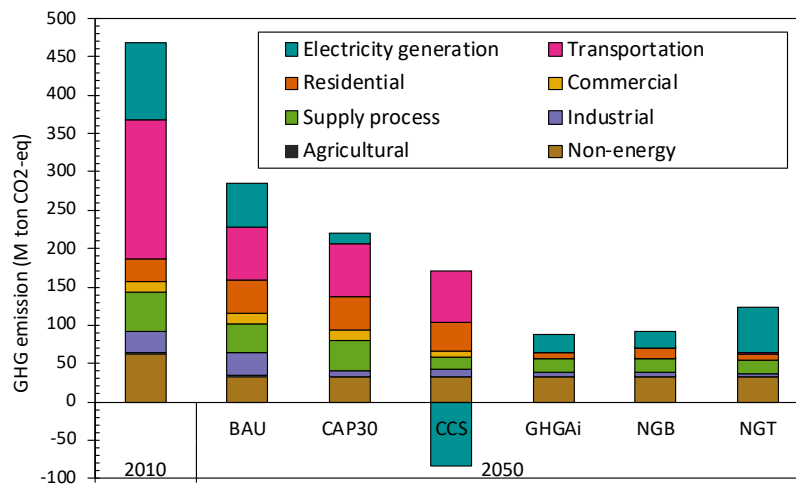


Figure 4-2. Total greenhouse gas emission (M ton CO<sub>2</sub>-eq) from different economic sectors modeled by CA-TIMES in 2010 and 2050 different scenarios

#### 4.3.2 Particulate and gaseous pollutant emissions from different future scenarios

Figure 4-3 summarizes the changes to criteria pollutant emissions under the CAP30, CCS, GHGAi, NGB, and NGT scenarios relative to their reference scenarios. For CAP30 (Figure 3a), CCS (3b) and GHGAi (3c) the reference scenario is BAU, and for NGB (3d) and NGT (3e), the reference scenario is GHGAi. The emissions changes contributed from sectors 1 to 7 are represented by the colored bars and the final value illustrates the net total change. For example, when looking at PM<sub>2.5</sub> change in the GHGAi

scenario (Figure 4-3c, 2<sup>nd</sup> column), sectors 1 to 7 contributed -1.1%, -0.8%, -3.0%, +5.3%, +5.3%, -2.6% and -0.2% respectively, resulting in a net total PM<sub>2.5</sub> change of -7.6% relative to the BAU scenario. NO<sub>x</sub> emissions decrease by 26% in the GHGAI scenario relative to the BAU scenario, mainly from sector 3 (off-road equipment -12%) and sector 5 (residential and commercial buildings -9%). The CAP30 scenario also achieves noticeable PM<sub>2.5</sub> reductions from sector 3 (-1.2%) and sector 6 (electricity generation -3.1%) but overall, as a partial mitigation scenario, it results in less PM<sub>2.5</sub> reduction compared to the GHGAI scenario (-4.6% vs. -7.6%). The CCS scenario has elevated PM<sub>2.5</sub> emission (+2.5%) because there is a major emission increase from sector 4 (marine and aviation +5.3%) and no major reduction from sector 5 or sector 6 (+0.44%). SO<sub>x</sub> emissions increase in the CCS scenario because the Bio-IGCC plants emit more SO<sub>x</sub> than other electricity generation processes even though the accoupling CCS section removes more than half of it. PM<sub>2.5</sub> emissions increase 1.8% and 2.3% in the NGB and NGT scenarios, respectively, due to increased natural utilization.

Emissions of ultrafine particles (D<sub>p</sub><0.1 μm) change much more than emissions of fine particles (D<sub>p</sub><2.5 μm) and coarse particles (D<sub>p</sub><10 μm) across all scenarios. This effect is illustrated in the first three columns of Figure 4-3 and in panels a-c of Figure S.4- 3. Figure 4-4a summarizes sector contributions to PM<sub>0.1</sub> emissions under different scenarios, while Figure 4-4b compares the sector contributions to PM<sub>0.1</sub>, PM<sub>2.5</sub> and PM<sub>10</sub> under the BAU scenario. PM<sub>2.5</sub> and PM<sub>10</sub> pie charts for the other scenarios are not shown because they show minimal difference (< 5%) as discussed with Figure 4-3. Sector 5 (residential and commercial buildings) and sector 6 (electricity generation) together account for approximately 50% of the ultrafine particles emissions. Sector 3 (off-road equipment and railroad) and sector 4 (marine and aviation) account for approximately 25% of the total ultrafine particle emissions. The remaining ~25% of the ultrafine particle emissions come from sector 8 (“other processes”) that does not vary between future scenarios. On-road mobile emissions (type 1 & 2) are projected to contribute only ~1% of the ultrafine emissions in the future.

By comparing the height of the colored bars for various pollutants (Figure 4-3), the top four contributors to emissions changes are identified: residential and commercial buildings, electricity

generation, marine and rail, and off-road equipment. The following sections discuss the fuel and technology changes leading to the observed emissions differences in each of these sectors.

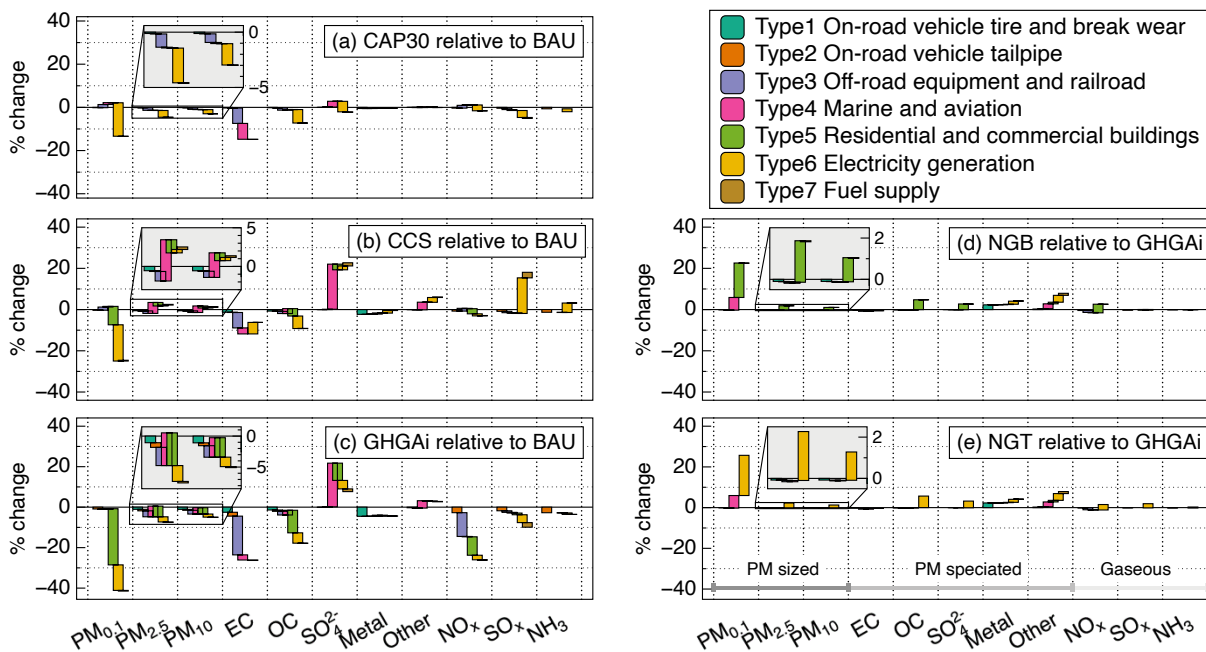


Figure 4-3. Pollutant emission change (%) in different scenarios relative to their reference scenario. Stacked colored bars represent contributions from different socio-economic sectors

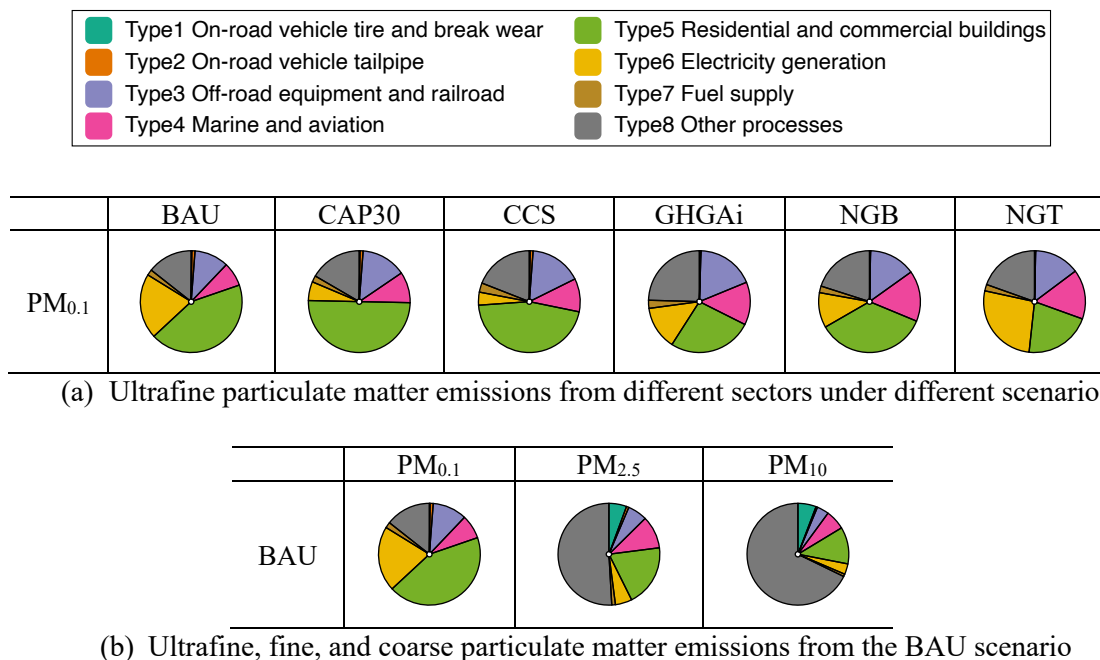


Figure 4-4. Particulate matter emissions from different sectors under different scenarios

#### 4.3.3 Particulate and gaseous pollutant emissions from different socio-economic sectors

**Residential and commercial buildings.** The residential and commercial building sector consumes large amounts of energy and therefore produces large amounts of emissions. This sector accounts for approximately 40% of end-use energy consumption in California and contributes to 13% of the GHG emissions from direct fossil fuel combustion in the year 2010, not including GHG emissions associated with electricity consumption in buildings<sup>127</sup>. In 2050, the CA-REMARQUE\_v2.0 model predicts that residential and commercial buildings will account for 20-50% of total PM<sub>0.1</sub> emissions and 15-20% of total PM<sub>2.5</sub> emissions. The majority (+70%) of the PM<sub>2.5</sub> emitted by commercial and residential buildings is composed of organic compounds.

Figure 4-5 (a-f) shows PM<sub>0.1</sub> emission rates (ug·m<sup>-2</sup>·min<sup>-1</sup>) from northern and southern California domains under the six scenarios analyzed in the present study. Figure 5 panel (a) presents the absolute PM<sub>0.1</sub> emissions rate from the reference BAU scenario, while panels (b)-(d) show the difference in the PM<sub>0.1</sub> emissions rate relative to the reference scenario. The GHGAI scenario generates the greatest amount of PM<sub>0.1</sub> emission reduction around the cities with large populations (San Francisco Bay Area, Greater Los Angeles). The spatial pattern of the PM<sub>0.1</sub> emissions are similar to the spatial pattern for the PM<sub>2.5</sub> and NO<sub>x</sub> emissions (Figure S.4- 14 and Figure S.4- 28).

Changes to ultrafine particle emissions in the building sector can be linked directly to changes in natural gas combustion in the built environment. Buildings in California are projected to use either natural gas or electricity in the year 2050, but emissions from the latter energy source are tabulated in the electricity generation sector. Figure S.4- 8 summarizes the demand for natural gas and electricity from residential and commercial buildings in 2050. The deep GHG reduction scenarios (GHGAI, NGB and NGT) are able to satisfy the same energy service demand with only 74% of the total energy needed in the BAU scenario due to the adoption of more efficient building appliances (efficiency gains of 1.7x for residential and 1.3x for commercial buildings appliances). Moreover, many natural gas appliances are replaced by electric appliances the GHGAI scenario, as reflected by the increasing share of electricity demand. These two factors combine to reduce natural gas consumption by 80% in residential buildings and 57% in commercial

buildings under the GHGAI scenario. Measurements have shown that natural gas combustion in appliances emits particles exclusively in the ultrafine size range<sup>111</sup>. The widespread use of natural gas as an energy source makes it a dominant contributor to ultrafine particle emissions but relatively low emissions rates dilute the contributions to PM<sub>2.5</sub> emissions<sup>147</sup>. Natural gas combustion in the building sector accounts for 28% of the PM<sub>0.1</sub> emission change but only 5.3% of the PM<sub>2.5</sub> emission change in the GHGAI vs BAU scenarios.

The share of natural gas increases from 21% to 39% of total building energy demand in the NGB scenario vs. the GHGAI scenario, resulting in more PM<sub>0.1</sub> emissions around major population centers (Figure 4-5 e). Although the building sector PM<sub>0.1</sub> emissions are still less in the NGB scenario than in the BAU scenario (see Figure S.4- 13), the increased use of natural gas in the NGB scenario offsets a third of the PM<sub>0.1</sub> reduction achieved through electrification and efficiency improvement in the GHGAI scenario (GHGAI PM<sub>0.1</sub> -41.5%, NGB PM<sub>0.1</sub> -28.4% relative to BAU). These results emphasize the importance of limiting natural gas in the building sector if reducing PM<sub>0.1</sub> emissions is a priority.

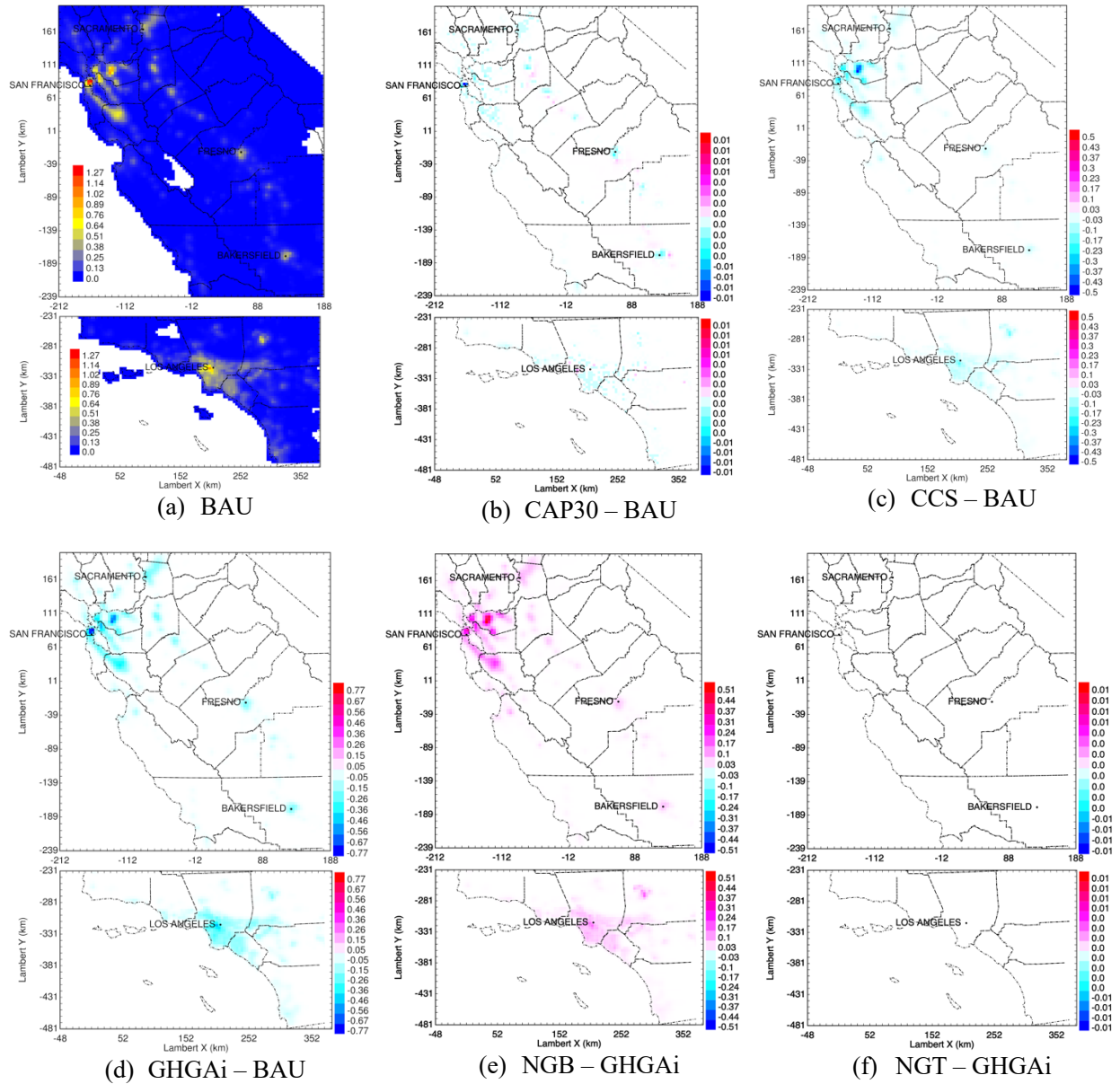
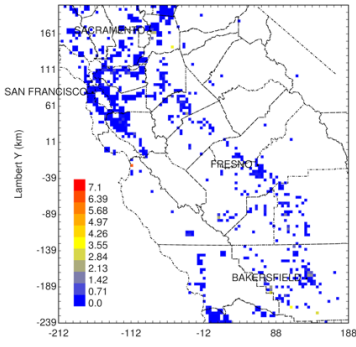


Figure 4-5. PM<sub>0.1</sub> emission ( $\mu\text{g m}^{-2} \text{min}^{-1}$ ) from residential and commercial sector.  
 (a) PM<sub>0.1</sub> emission ( $\mu\text{g m}^{-2} \text{min}^{-1}$ ) from residential and commercial sector in the BAU scenario, and (b-f) changes in PM<sub>0.1</sub> emissions ( $\mu\text{g m}^{-2} \text{min}^{-1}$ ) relative to the indicated reference scenario.

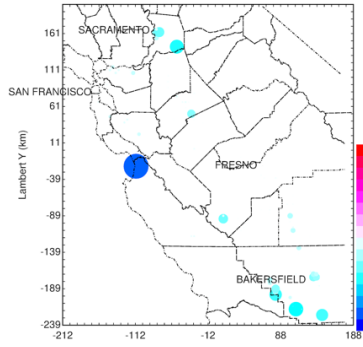
**Electricity generation.** Figure 4-6 (a) shows the statewide PM<sub>0.1</sub> emissions from electricity generation under the BAU scenario and Figure 4-6 (b-f) show the change in emissions associated with

other scenarios. Powerplants are point sources but the BAU scenario assigns these emissions to the 4 km model grid, with a small number of major emissions cells and a much larger number of low-level emissions cells around the populated regions (see Figure 4-6a). Changes to point source emissions in Figure 4-6(b)-(f) are illustrated as circles with radius proportional to the emission values to show the results more clearly. The CAP30, CCS and GHGAi scenarios all have major PM<sub>0.1</sub> emissions reductions compared to the BAU scenario due to reductions in natural gas combustion to generate electricity. The BAU scenario generates 676 PJ of electricity from natural gas powerplants, with significant reductions for CAP30 (-80%), CCS (-96%) and GHGAi (-64%) scenarios. The GHGAi, NGB and NGT scenarios electrify across many economic sectors and therefore require much more total electricity generation than other scenarios. This extra electricity is mainly generated from renewable resources including wind, solar, geothermal, biomass and hydro. Natural gas accounts for only 9% of the electricity generation in the GHGAi and NGB scenarios. However, the share of natural gas electricity increases to 26% in the NGT scenario, resulting in a significant PM<sub>0.1</sub> emission increase centered at the natural gas powerplants (Figure 4-6f). Total PM<sub>0.1</sub> emissions still decrease by 22.4% under the NGT scenario relative to the BAU scenario but a significant portion of the 41.5% PM<sub>0.1</sub> emissions reduction in GHGAi scenario is eroded in the NGT scenario.

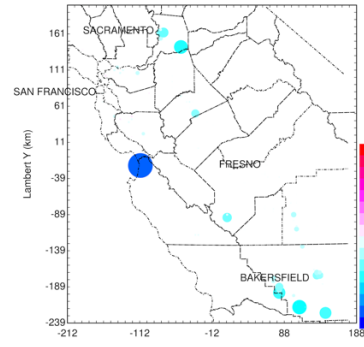
Despite the decrease of natural gas electricity and the increase of wind and solar power, the CCS scenario is drastically different from the other scenarios in the way that 24% of the electricity (379 PJ, see Figure S.4- 9) comes from Bio-IGCC-CCS. Therefore, in the CCS scenario PM<sub>2.5</sub> and NO<sub>x</sub> emission increase from the northern California biomass and solid waste powerplants as shown in Figure 4-7 and Figure S.4- 29 It is noteworthy that the changes of PM<sub>0.1</sub> and PM<sub>2.5</sub> in the CCS scenario relative to BAU can go in different directions (Figure 4-6c vs Figure 4-7) because powerplants with different technologies have different PM emission profiles that center in the ultrafine (natural gas electricity) or fine (biomass electricity) portion of the airborne particle size distribution.



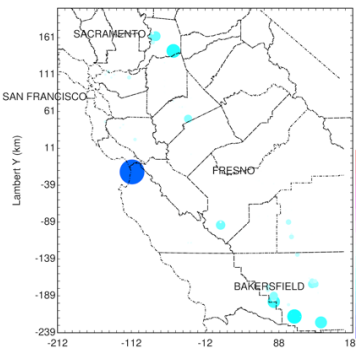
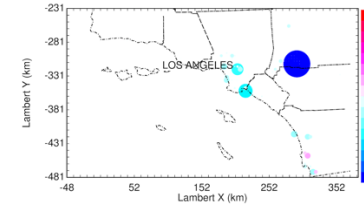
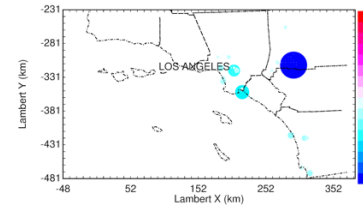
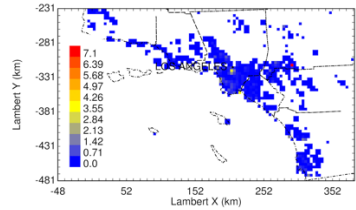
(a)BAU



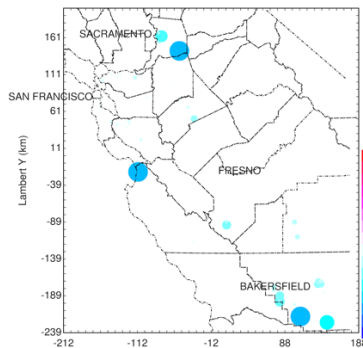
(b)CAP30 – BAU



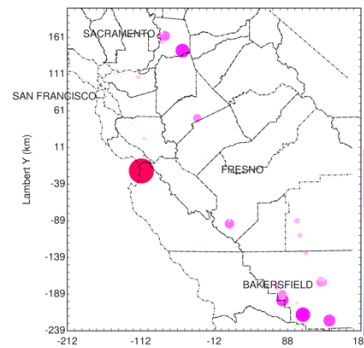
(c)CCS – BAU



(d)GHGai – BAU



(e)NGB – GHGai



(f)NGT – GHGai

Figure 4-6. PM<sub>0.1</sub> emission ( $\mu\text{g m}^{-2} \text{min}^{-1}$ ) from electricity generation.  
 (a) PM<sub>0.1</sub> emissions ( $\mu\text{g m}^{-2} \text{min}^{-1}$ ) from electricity generation in the BAU scenario, and (b-f) changes in PM<sub>0.1</sub> emissions ( $\mu\text{g m}^{-2} \text{min}^{-1}$ ) relative to the indicated reference scenario

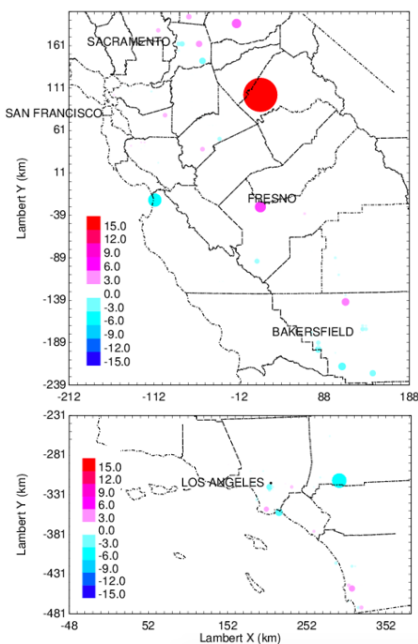


Figure 4-7. PM<sub>2.5</sub> emission (ug m<sup>-2</sup> min<sup>-1</sup>) from electricity generation, CCS-BAU

**Marine vessels and aircrafts.** Sector 4 emissions are dominated by marine vessels including ocean-going vessels, shipping on inland waterways, and recreational boating. PM<sub>2.5</sub> emissions from sector 4 account for 10% of total PM<sub>2.5</sub> emissions in the BAU scenario, but this contribution increases to 17% in the deep GHG reduction scenarios (GHGAI, NGB and NGT). Figure S.4- 16 illustrates the spatial pattern of the increasing emissions from sector 4. PM<sub>2.5</sub> emissions increase from shipping lanes far offshore in all scenarios (CAP30, CCS and GHGAI) relative to BAU, with significantly larger increases apparent in the CCS and GHGAI scenarios. Shipping activities far offshore currently use residual fuel oil (RFO), which is a heavy petroleum fuel. All of the RFO is replaced with biomass-based residual fuel oil (BRFO) in the BAU scenario to lower pollutant emissions (see Figure S.4- 7). Supplies of BRFO are limited by available feedstocks, and the increased demand for biofuels in the CCS, GHGAI, NGB and NGT scenarios redirects most of those feedstocks to the production of transportation fuels or electricity generation. The CCS, GHGAI, NGB, and NGT scenarios therefore use RFO for most offshore shipping needs. A slight PM<sub>2.5</sub> emissions decrease from near-shore shipping activities and inland waterway activities shown in the CAP30 scenario is the result of switching from diesel to biodiesel. The GHGAI, NGB and NGT shipping emissions are very similar.

**Off road equipment and railroads.** Figure S.4- 17, Figure S.4- 23 and Figure S.4- 31 show the statewide PM<sub>2.5</sub>, PM<sub>0.1</sub> and NO<sub>x</sub> emissions rates from off road equipment and railroads respectively. PM<sub>2.5</sub> emissions rates uniformly decrease in the CAP30, CCS, and GHG scenarios relative to the BAU scenario in and around large cities and along the rail lines. This decrease results from replacing diesel with biodiesel in railroads and off-road equipment, electrifying railroads, and replacing gasoline with ethanol in off-road equipment. The fuel usage changes are presented in Figure S.4- 5 as total energy demand from different scenarios. PM<sub>0.1</sub> and NO<sub>x</sub> emissions do not decrease uniformly, but rather emissions for these pollutants increase in some locations and decrease in other locations (Figure S.4- 23 and Figure S.4- 31) For example, PM<sub>0.1</sub> emissions in the GHGAI scenario decrease along the rail lines but increase at and around major cities (Figure S.4- 23 d) because all railroads are electrified to eliminate PM<sub>0.1</sub> emissions while replacing gasoline with ethanol in the off-road equipment increases PM<sub>0.1</sub> emissions<sup>117,156</sup>. NO<sub>x</sub> emissions decrease at most locations across California in the GHGAI, NGB and NGT scenarios (Figure S.4- 30), but the CAP30 and CCS scenarios produce increased NO<sub>x</sub> emissions along the rail lines and at the Port of Los Angeles. This is because replacing biodiesel with diesel increases NO<sub>x</sub> emissions in railroads (+13%) and off-road equipment (+8%), while replacing gasoline with ethanol reduces NO<sub>x</sub> emissions in off-road equipment (-45%)<sup>117</sup>. These results illustrate the complexity in predicting the effects of fuel switching on criteria pollutant emissions. Multiple factors acting in opposite directions dictate the net effect on overall emissions.

**On-road vehicles.** PM<sub>2.5</sub> emissions from vehicle tailpipes account for only 0.8% of total PM<sub>2.5</sub> emissions in the 2050 BAU scenario due to the implementation of existing standards. These tailpipe emissions further decreases to less than 0.1% of total PM<sub>2.5</sub> emissions in the deep GHG mitigation scenarios (GHGAI, NGB and NGT) as a result of large-scale electric vehicle adoption. Figure S.4- 4 shows that the share of electric and fuel cell vehicles is only 5.5% in the BAU scenario but increases to over 70% in the GHGAI, NGB and NGT scenarios. The CCS scenario allows more gasoline and diesel in vehicles compared to the GHGAI scenario (but still less than BAU) because of the negative GHG emissions from electricity generation. The NGB scenario further increases the share of electric and fuel cell vehicles to over 88% to compensate for the increased GHG emissions from residential and commercial buildings. Therefore, all

scenarios reduce PM<sub>2.5</sub>, PM<sub>0.1</sub> and NO<sub>x</sub> emissions from tailpipes relative to the BAU scenario, with the GHGAI, NGB, and NGT scenarios getting close to zero tailpipe emissions in 2050 (Figure S.4- 18, Figure S.4- 24 and Figure S.4- 32). PM<sub>2.5</sub> emissions from vehicle tire and brake wear accounts for 5-6% of the overall PM<sub>2.5</sub> emissions in the year 2050 BAU scenario, exceeding emissions from tailpipes. CA-TIMES predicts the same vehicle miles traveled in all scenarios and so the differences in predicted tire and brake wear emissions are related to the adoption of various amounts of regenerative braking and vehicle weight in electric, hybrid electric and fuel cell vehicles (Figure S.4- 19). Regenerative braking systems are estimated to reduce tire and brake wear PM emissions by 59%<sup>157</sup>.

#### 4.3.4 Airborne Particulate Matter Concentrations

The long-term (~10 year average) ground-level PM<sub>2.5</sub> concentrations predicted under each of the emissions scenarios considered in the current study are summarized in Figure 4-8. PM<sub>2.5</sub> concentrations under the BAU scenario peak over urban areas such as Los Angeles and the San Francisco Bay Area, but concentrations are also high downwind of major electrical generating stations near Monterey Bay (south of San Francisco) and around intensive agricultural sources in the San Joaquin Valley between Fresno and Bakersfield (Figure 4-8a). PM<sub>2.5</sub> concentrations decrease under all scenarios that reduce GHG emissions, but the extent of the reductions and the spatial pattern depend on the details of the emissions changes (Figure 4-8 b-f). The CAP30 scenario and the CCS scenario produce similar levels of PM<sub>2.5</sub> reduction in major urban centers but increasing PM<sub>2.5</sub> concentrations are predicted at locations outside of urban centers under the CCS scenario due to the increased use of fossil fuel combustion under this scenario. Much stronger PM<sub>2.5</sub> reductions are predicted across the entire study region under the GHGAI scenario, with more than 1 µg m<sup>-3</sup> of reductions across most populated regions in the study domain (Figure 4-8d). PM<sub>2.5</sub> concentrations under the NGB and NGT scenarios are slightly higher than the GHGAI scenario (Figure 4-8 e-f) due to the increased use of natural gas combustion but still significantly lower than concentrations under the CAP30 and CCS scenarios.

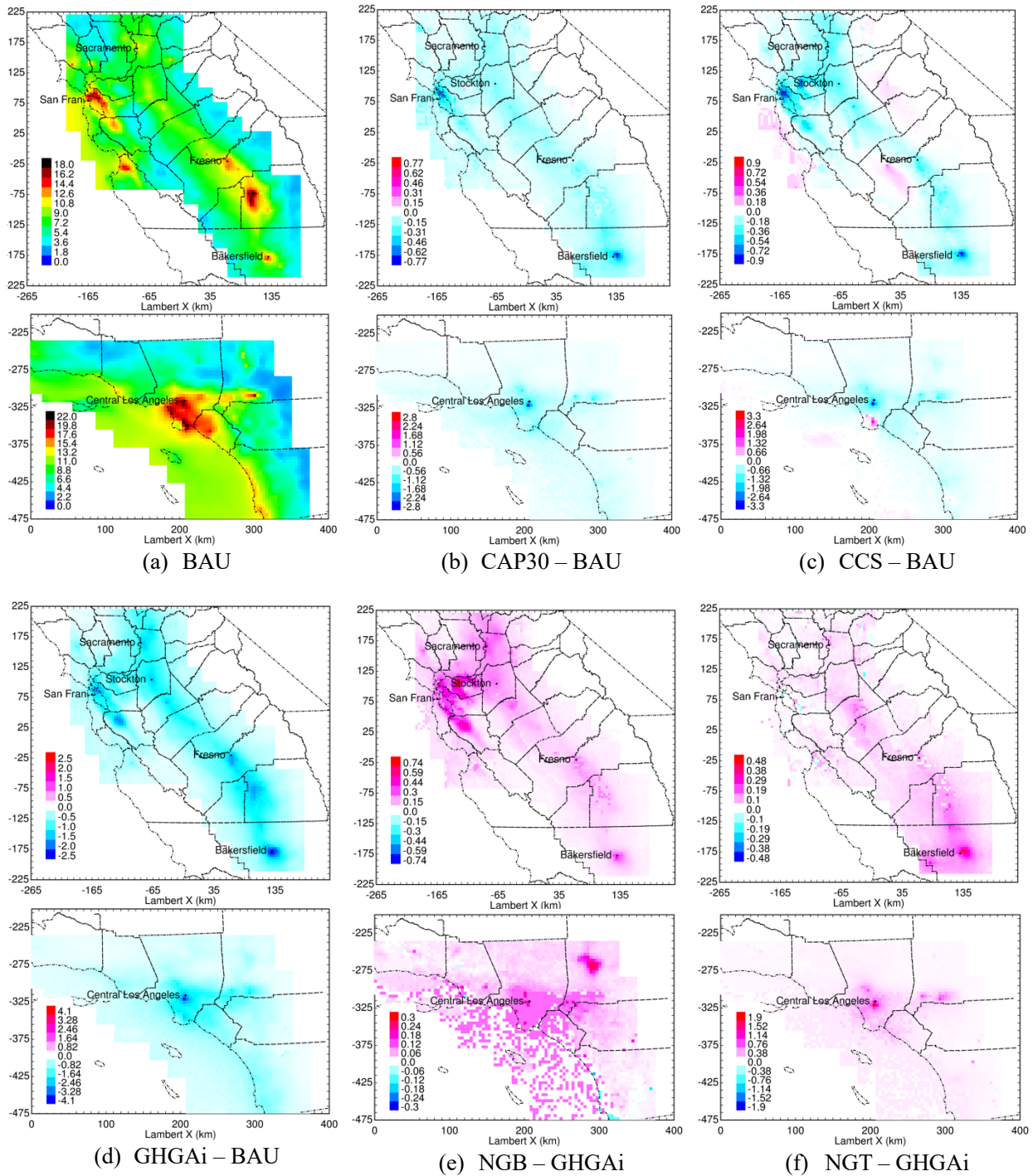


Figure 4-8. Projection of  $PM_{2.5}$  concentration in 2050.

(a) Long-term  $PM_{2.5}$  concentrations predicted under the BAU emissions inventory, and (b-f) change in long-term  $PM_{2.5}$  concentrations associated with changing energy portfolios relative to the indicated reference scenario in the panel title. All units  $\mu g m^{-3}$ .

### 4.3.5 Public Health Benefits

Figure 4-9 illustrates the public health benefits associated with reduced PM<sub>2.5</sub> concentrations under the emissions scenarios considered in the current study. All GHG mitigation scenarios produce net health savings relative to the BAU across the study region, including the CCS scenario that produced some zones of increasing PM<sub>2.5</sub> concentrations. Air pollution mortality associated with PM<sub>2.5</sub> exposure was estimated at 23,875 deaths year<sup>-1</sup> in the 2050 BAU scenario. The GHGAi scenario produced the greatest overall health benefits equivalent to approximately 3500 avoided deaths per year, and an annual public health benefit greater than USD 20B yr<sup>-1</sup>. The less aggressive CAP30 and CCS scenarios produced only one third of these public health benefits due to more modest PM<sub>2.5</sub> reductions in these scenarios. The NGB and NGT scenarios are similar to the GHGAi scenario with approximately 90% of the public health benefits (3300 avoided deaths yr<sup>-1</sup>).

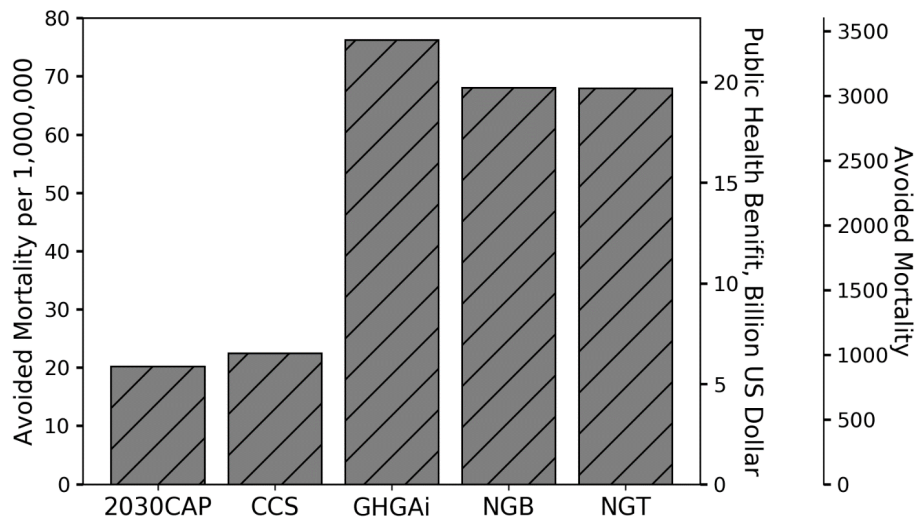


Figure 4-9. Avoided mortality due to improved air quality associated with changing energy portfolios relative to the BAU scenario. Size of population in 2050 is estimated to be 45million. Public health benefits estimation assumes a present-day value of a statistical life equivalent to USD7.6M. All calculations performed with BenMAP-CE

## 4.4 Implications

Six different future energy scenarios in California were analyzed for their emissions of particulate matter and gaseous pollutants related to regional air quality using the CA-TIMES and CA-REMARQUE model framework. These scenarios are informative examples of possible carbon emissions reduction strategies, not literal predictions of future energy consumption. The scenarios provide valuable information to understand the key resources, technologies and policies while trying to simultaneously reduce GHG emissions and improve air quality.

The GHGAi scenario represents the most cost-effective pathway to reduce GHG emissions by 80% (relative to 1990 level) without the deployment of negative carbon emission technology. Strategies in the GHGAi scenario include aggressive decarbonization of electricity generation, adoption of electricity for most end-use applications, efficiency improvements for appliances, and deployment of low-carbon transportation fuels and technologies. Major air quality and public health benefits are generated under the GHGAi scenario due to the significant emissions reductions for PM<sub>0.1</sub> (41%), PM<sub>2.5</sub> (8%), and NO<sub>x</sub> (26%) relative to the reference future BAU scenario. Long-term air quality simulations predict that ground-level PM<sub>2.5</sub> concentrations will decrease by more than 1 µg m<sup>-3</sup> across most of California's major population centers under the GHGAi scenario, reducing air pollution mortality by approximately 3500 deaths yr<sup>-1</sup> with a public health benefit greater than USD 20B yr<sup>-1</sup>.

The CCS scenario achieves the same GHG reductions as the GHGAi scenario, but the negative GHG emissions from Bio-IGCC-CCS technology allow more fossil energy consumption in transportation and built environment. PM<sub>0.1</sub> emissions in the CCS scenario decrease (-25%) relative to the BAU scenario as a result of less natural gas usage in buildings and electricity generation, but PM<sub>2.5</sub> emission increase (+2.5%) suggesting potential air quality disbenefit associated with the CCS future especially around the Bio-IGCC-CCS powerplant locations. The air quality benefits associated with the CCS scenario are a factor of three lower than the air quality benefits associated with the GHGAi scenario. The strong difference in public health benefits should be considered in future planning exercises for GHG mitigation strategies.

The NGB and NGT scenarios tested the impact of loosening natural gas usage limitations in the built environment and power generation compared to the strict GHGAI scenario. Increasing the share of natural gas by 18% in buildings increased PM<sub>0.1</sub> emissions (22%), PM<sub>2.5</sub> emissions (1.8%) and NO<sub>x</sub> emissions (2.5%) in the NGB scenario relative to the GHGAI scenario. Increasing the share of natural gas in electricity generation by 15% increased PM<sub>0.1</sub> emissions (26%), PM<sub>2.5</sub> emissions (2.3%) and NO<sub>x</sub> emissions (1.5%) in the NGT scenario relative to the GHGAI scenario. The PM<sub>2.5</sub> concentrations and associated public health benefits were only slightly degraded in the NGB and NGT scenarios relative to the GHGAI scenario, but these projections do not account for the potential independent health effects of ultrafine particles (PM<sub>0.1</sub>) that are beginning to come into focus <sup>158</sup>. The precautionary principle suggests that natural gas utilization in the built environment and electricity generation should be kept at a low level in order to maximize the air quality benefits gained from adoption of low carbon energy sources in California.

## 4.5 Appendix

Table S.4-1. Policies represented in the BAU scenario.

Table S.4-2. Emission Inventory Code (EIC) cross-reference table between EMFAC vehicle class and technology and CA-TIMES vehicle types

Figure S.4-1. Primary energy consumption (PJ) from 2010 to 2050 in different CA-TIMES scenarios

Figure S.4-2. GHG emission from different economic sectors over the years in different CA-TIMES scenarios

Figure S.4-3. Ultrafine (PM0.1), fine (PM2.5) and coarse (PM10) particulate matter emission rates from different scenarios

Figure S.4-4. Energy demand (PJ) from on-road vehicles in year 2050

Figure S.4-5. Energy demand (PJ) from off-road equipment and railroads in year 2050

Figure S.4-6. Energy demand (PJ) from aircrafts in year 2050

Figure S.4-7. Energy demand (PJ) from marine vessels in year 2050

Figure S.4-8. Energy demand (PJ) from residential and commercial buildings in year 2050

Figure S.4-9. Electricity generation (PJ) from different resources in year 2050

Figure S.4-10. Energy demand from petroleum refining processes (PJ) in year 2050

Figure S.4-11. Energy output from biorefineries (PJ) in year 2050

Figure S.4-12. Hydrogen production (PJ) from different processes in year 2050

Figure S.4-13. Pollutant emission change (%) in different scenarios NGB and NGT relative to the BAU scenario

Figure S.4-14. PM2.5 emissions ( $\text{ug}\cdot\text{m}^{-2}\cdot\text{min}^{-1}$ ) from residential and commercial buildings

Figure S.4-13. PM2.5 emissions ( $\text{ug}\cdot\text{m}^{-2}\cdot\text{min}^{-1}$ ) from electricity generation

Figure S.4-14. PM2.5 emissions ( $\text{ug}\cdot\text{m}^{-2}\cdot\text{min}^{-1}$ ) from on-road vehicle tailpipe

Figure S.4-15. PM2.5 emissions ( $\text{ug}\cdot\text{m}^{-2}\cdot\text{min}^{-1}$ ) from on-road vehicle tire and break wear

Figure S.4-16. PM2.5 emissions ( $\text{ug}\cdot\text{m}^{-2}\cdot\text{min}^{-1}$ ) from marine vessels and aircrafts

Figure S.4-17. PM<sub>2.5</sub> emissions ( $\mu\text{g}\cdot\text{m}^{-2}\cdot\text{min}^{-1}$ ) from off-road equipment and railroad

Figure S.4-18. PM<sub>2.5</sub> emissions ( $\mu\text{g}\cdot\text{m}^{-2}\cdot\text{min}^{-1}$ ) from on-road vehicle tailpipe

Figure S.4-19. PM<sub>2.5</sub> emissions ( $\mu\text{g}\cdot\text{m}^{-2}\cdot\text{min}^{-1}$ ) from on-road vehicle tire and break wear

Figure S.4-20. PM<sub>2.5</sub> emissions ( $\mu\text{g}\cdot\text{m}^{-2}\cdot\text{min}^{-1}$ ) from fuel supply processes

Figure S.4-21. PM<sub>2.5</sub> emissions ( $\mu\text{g}\cdot\text{m}^{-2}\cdot\text{min}^{-1}$ ) from other processes

Figure S.4-22. PM<sub>0.1</sub> emissions ( $\mu\text{g}\cdot\text{m}^{-2}\cdot\text{min}^{-1}$ ) from marine vessels and aircrafts

Figure S.4-23. PM<sub>0.1</sub> emissions ( $\mu\text{g}\cdot\text{m}^{-2}\cdot\text{min}^{-1}$ ) from off-road equipment and railroad

Figure S.4-24. PM<sub>0.1</sub> emissions ( $\mu\text{g}\cdot\text{m}^{-2}\cdot\text{min}^{-1}$ ) from on-road vehicle tailpipe

Figure S.4-25. PM<sub>0.1</sub> emissions ( $\mu\text{g}\cdot\text{m}^{-2}\cdot\text{min}^{-1}$ ) from on-road vehicle tire and break wear

Figure S.4-26. PM<sub>0.1</sub> emissions ( $\mu\text{g}\cdot\text{m}^{-2}\cdot\text{min}^{-1}$ ) from fuel supply processes

Figure S.4-27. PM<sub>0.1</sub> emissions ( $\mu\text{g}\cdot\text{m}^{-2}\cdot\text{min}^{-1}$ ) from other processes

Figure S.4-28. NO<sub>x</sub> emissions ( $\text{ppb}\cdot\text{m}\cdot\text{min}^{-1}$ ) from residential and commercial buildings

Figure S.4-29. NO<sub>x</sub> emissions ( $\text{ppb}\cdot\text{m}\cdot\text{min}^{-1}$ ) from electricity generation

Figure S.4-30. NO<sub>x</sub> emissions ( $\text{ppb}\cdot\text{m}\cdot\text{min}^{-1}$ ) from marine vessels and aircrafts

Figure S.4-31. NO<sub>x</sub> emissions ( $\text{ppb}\cdot\text{m}\cdot\text{min}^{-1}$ ) from off-road equipment and railroad

Figure S.4-32. NO<sub>x</sub> emissions ( $\text{ppb}\cdot\text{m}\cdot\text{min}^{-1}$ ) from on-road vehicle tailpipe

Figure S.4-33. NO<sub>x</sub> emissions ( $\text{ppb}\cdot\text{m}\cdot\text{min}^{-1}$ ) from fuel supply processes

Table S.4- 1 Policies represented in the BAU scenario. A more detailed description of the assumptions associated with each of the policies are presented in Appendix D. of Yang et al., 2014<sup>127</sup>

- Current biofuel tax credits
- Current biofuel import tariffs
- Current transportation fuel taxes
- CAFÉ standards to 2016 (39.5 mpg and 29.8 mpg for cars and trucks, respectively)
- CAFÉ standards to 2025 (59.8 mpg and 45.1 mpg for cars and trucks, respectively)
- Federal and California electric vehicle subsidies
- Low carbon fuel standard (LCFS) biofuel volume scenario to 2022 (retired after 2022)
- Power plant electricity GHG standard (base load must meet NGCC emissions)
- Renewable portfolio standard (33% by 2020 and remains at 33% until 2050)
- Renewable electricity production tax credit, solar investment tax credit
- Zero Emission Vehicle (ZEV) mandate policy constraint to 2025 (retired after 2025)
- No new nuclear powerplants (and retirement of SONGS by 2030)

Table S.4- 2 Emission Inventory Code (EIC) cross-reference table between EMFAC vehicle class and technology and CA-TIMES vehicle types.

Vehicle class	Process	CAT	NCAT	DSL
BUS	-all-	15	16	17
-all-	STREX	02	04	-
	RUNEX	03	05	08
	IDLEX	18	19	20
	HOTSOAK		06	-
	DIURN		07	-
	RUNLOSS		09	-

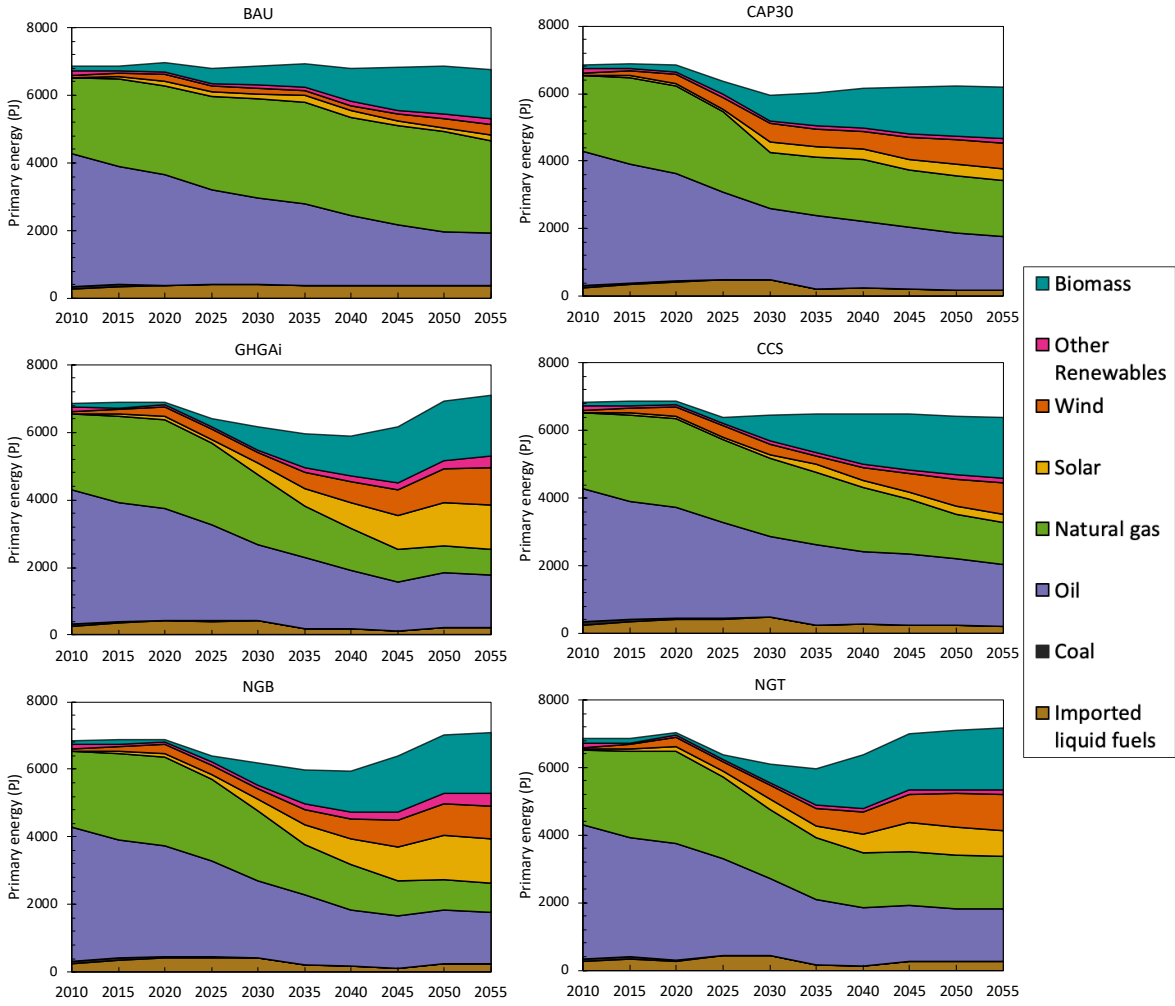


Figure S.4- 1 Primary energy consumption (PJ) from 2010 to 2050 in different CA-TIMES scenarios.

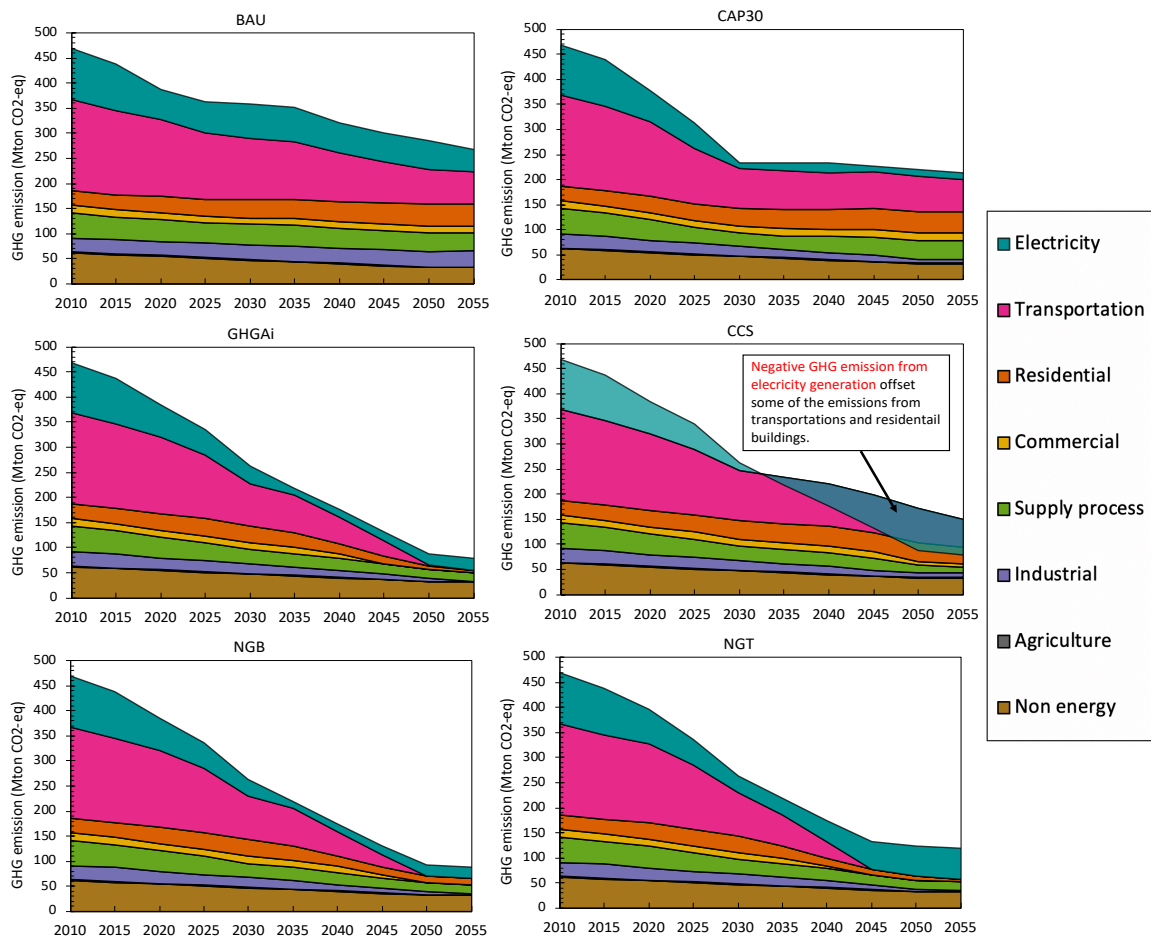


Figure S.4- 2 GHG emission (M ton CO<sub>2</sub>-eq) from different economic sectors over the years in different CA-TIMES scenarios.

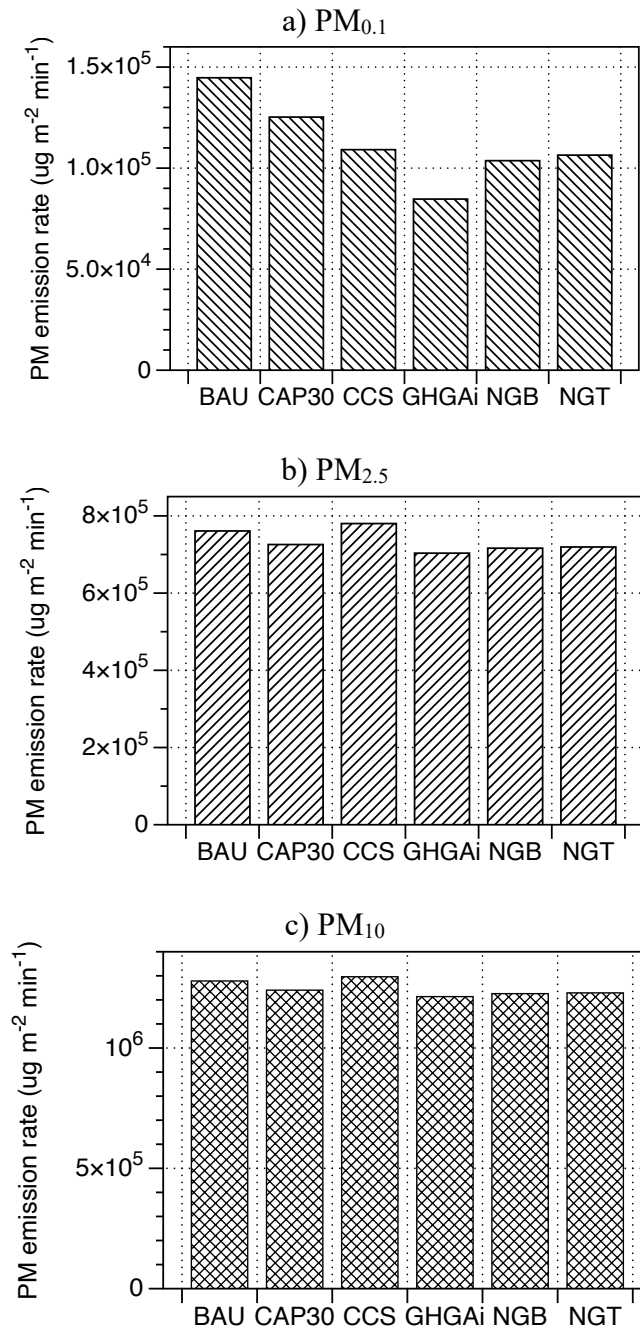


Figure S.4- 3 (a-c). Ultrafine (PM<sub>0.1</sub>), fine (PM<sub>2.5</sub>) and coarse (PM<sub>10</sub>) particulate matter emission rates from different scenarios.

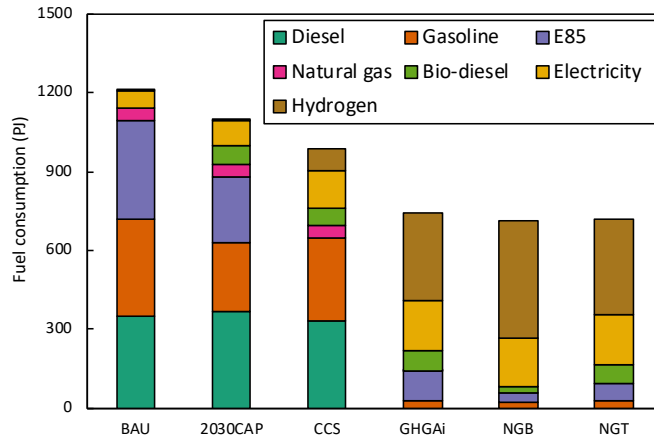


Figure S.4- 4 Energy demand (PJ) from on-road vehicles in year 2050.

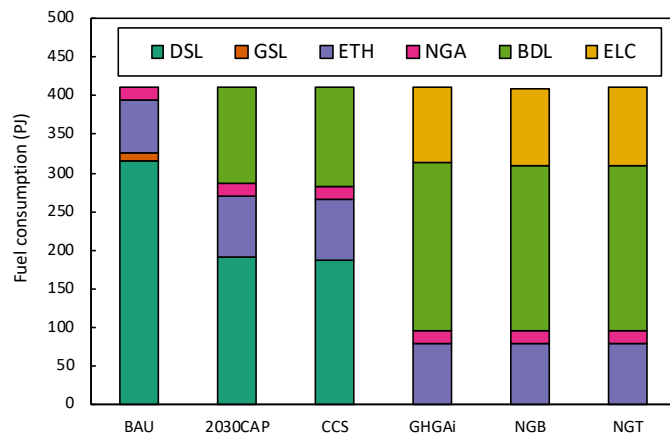


Figure S.4- 5 Energy demand (PJ) from off-road equipment and railroads in year 2050. (DSL=diesel, GSL=gasoline, ETH=ethanol, NGA=natural gas, BDL=biodiesel, ELC=electricity)

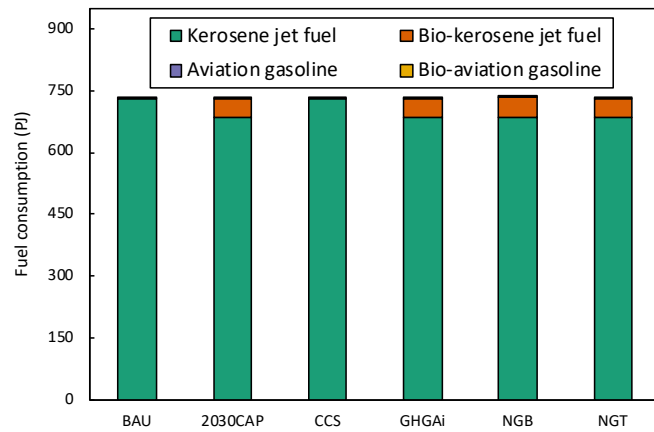


Figure S.4- 6 Energy demand (PJ) from aircrafts in year 2050.

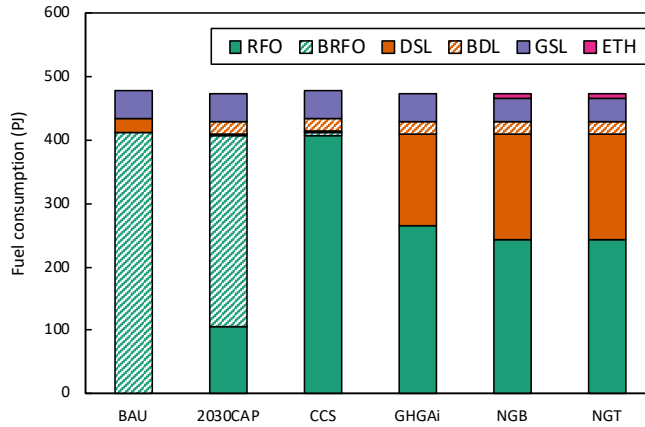


Figure S.4- 7 Energy demand (PJ) from marine vessels in year 2050. (RFO=residual fuel oil, BRFO=bio-derived residual fuel oil, DSL=diesel, BDL=biodiesel, GSL=gasoline, ETH=ethanol)

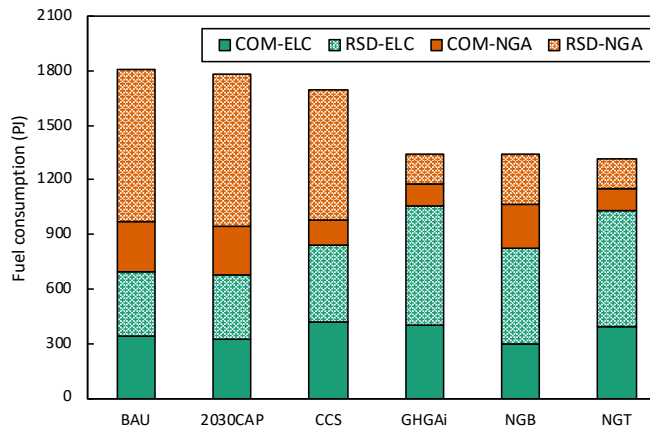


Figure S.4- 8 Energy demand (PJ) from residential (RSD) and commercial (COM) buildings in year 2050. (ELC=electricity, NGA=natural gas)

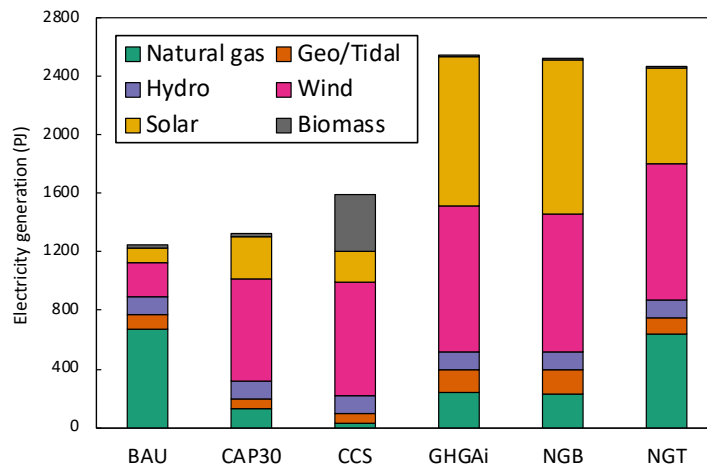


Figure S.4- 9 Electricity generation (PJ) from different resources in year 2050.

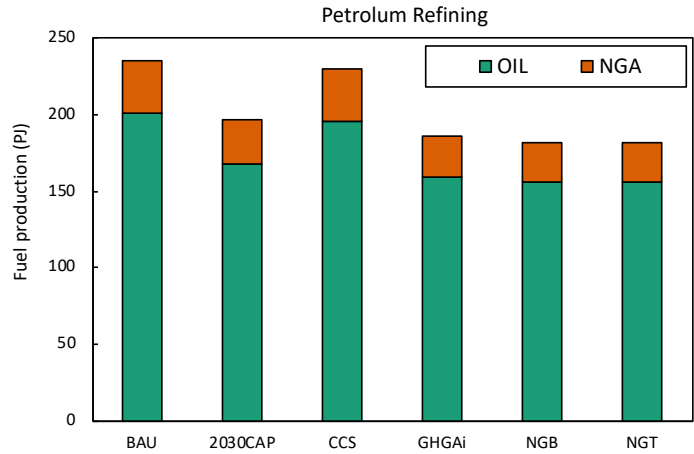


Figure S.4- 10 Energy demand from petroleum refining processes (PJ) in year 2050. (OIL=crude oil, NGA=natural gas)

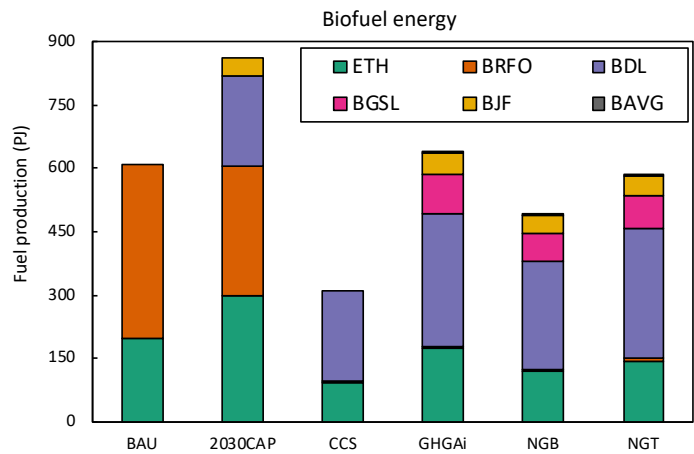


Figure S.4- 11 Energy output from biorefineries (PJ) in year 2050. (ETH=ethanol, BRFO=bio-derived residual fuel oil, BDL=biodiesel, BGSL=bio-gasoline, BJJ=bio-derived jet fuel, BAVG=bio-derived aviation gasoline)

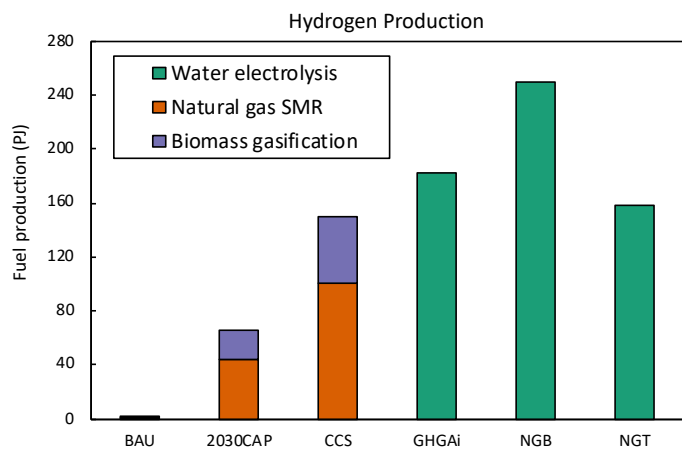


Figure S.4- 12 Hydrogen production (PJ) from different processes in year 2050.

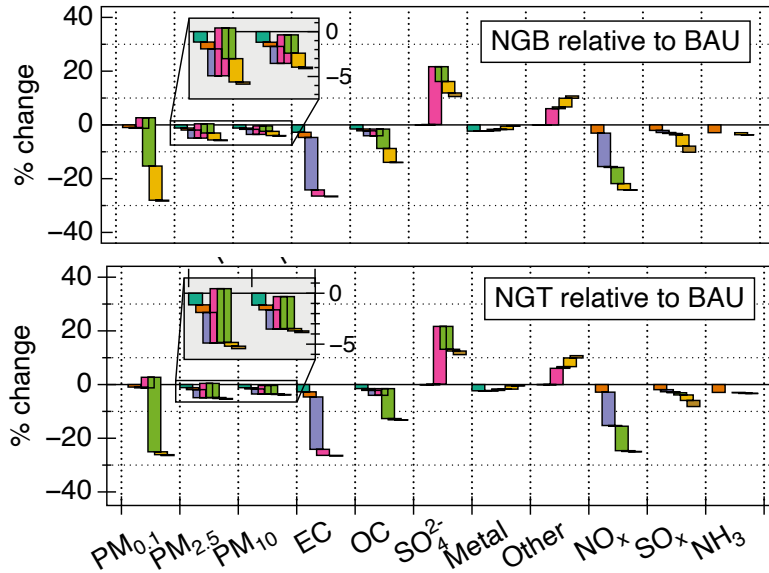
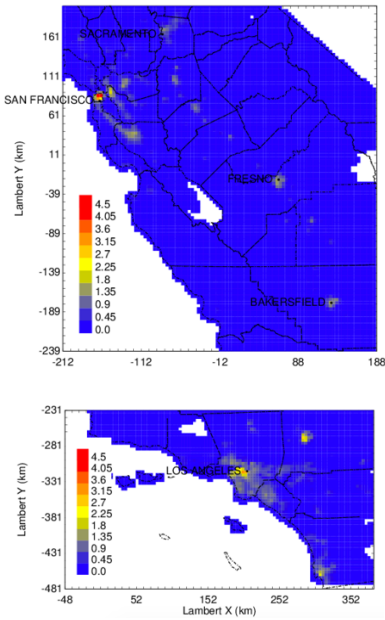
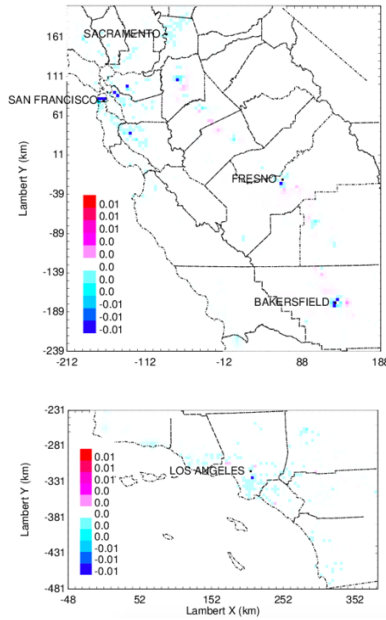


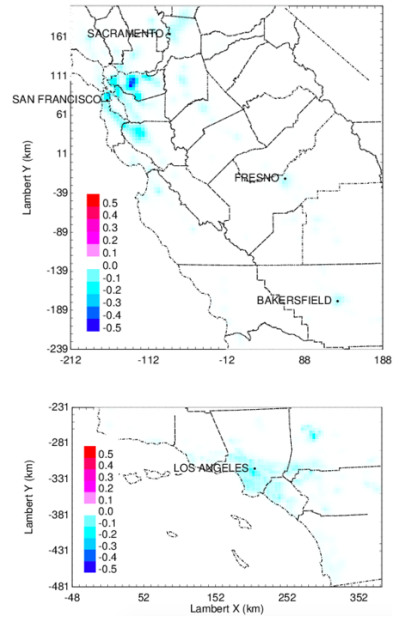
Figure S.4- 13 Pollutant emission change (%) in different scenarios NGB and NGT relative to the BAU scenario. Stacked colored bars represent contributions from different socio-economic sectors



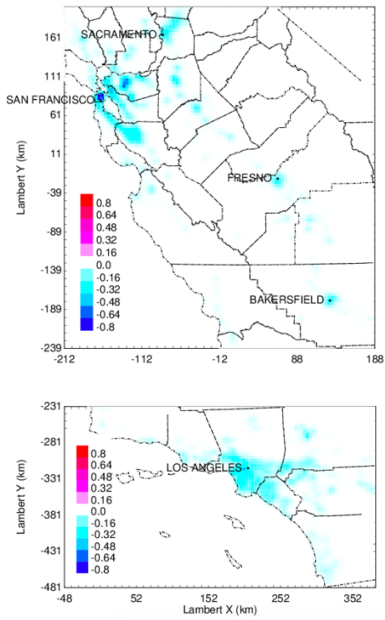
(a) BAU



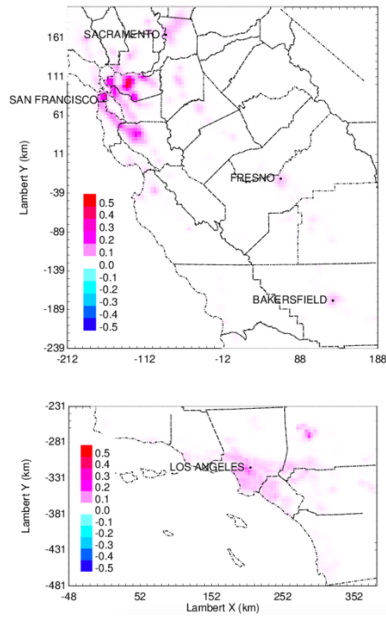
(b) CAP30 - BAU



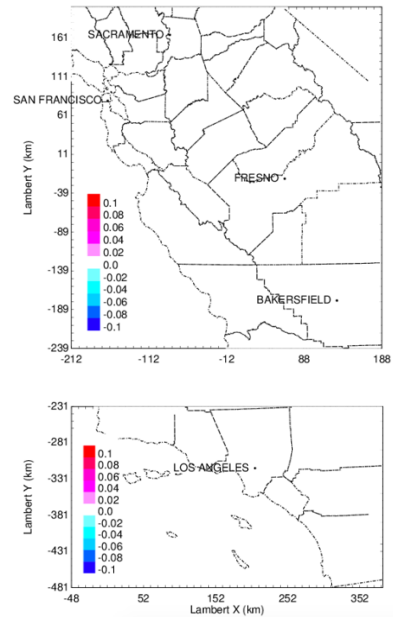
(c) CCS - BAU



(d) GHGai - BAU

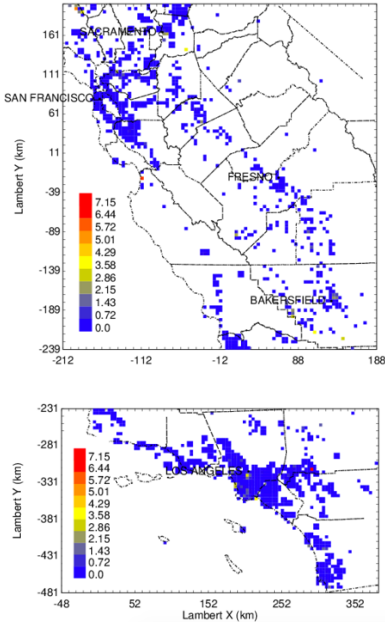


(e) NGB - GHGai

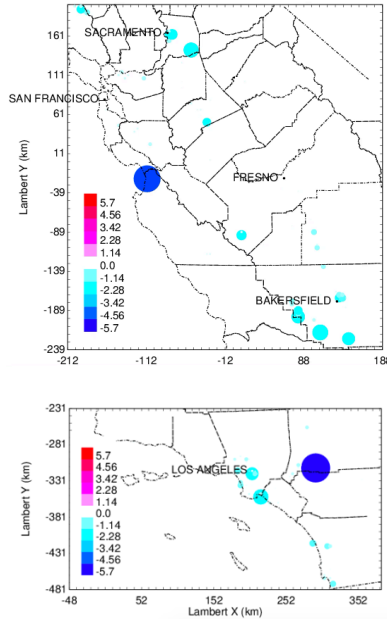


(f) NGT - GHGai

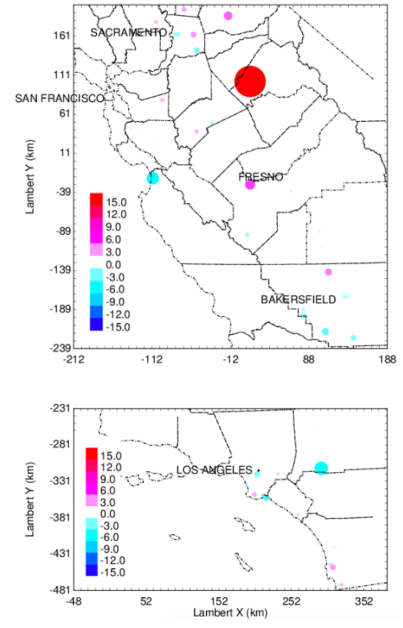
Figure S.4- 14 PM<sub>2.5</sub> emissions (ug-m<sup>-2</sup>·min<sup>-1</sup>) from residential and commercial sector.



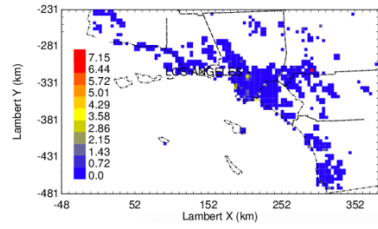
(a) BAU



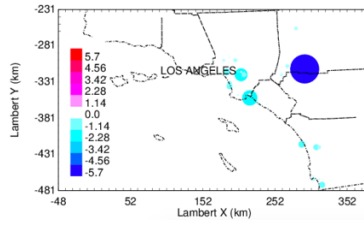
(b) CAP30 – BAU



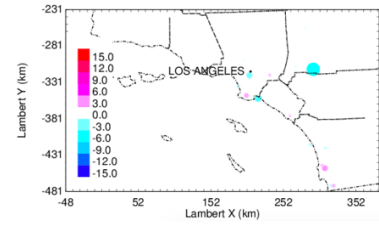
(c) CCS – BAU



(d) GHGai – BAU

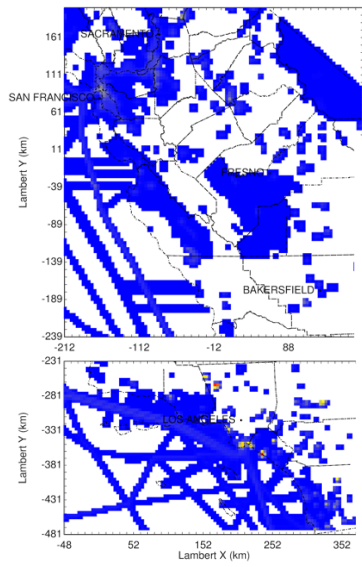


(e) NGB – GHGai

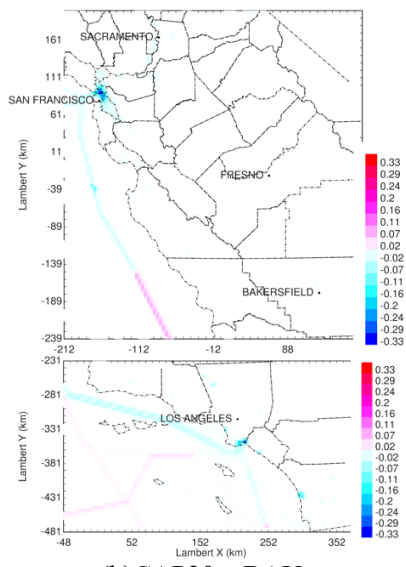


(f) NGT – GHGai

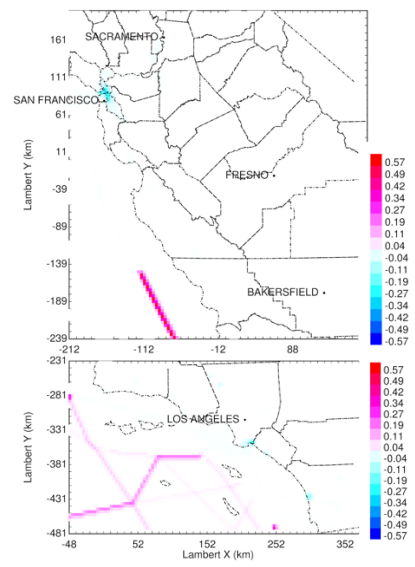
Figure S.4- 15  $PM_{2.5}$  emissions ( $ug \cdot m^{-2} \cdot min^{-1}$ ) from electricity generation.



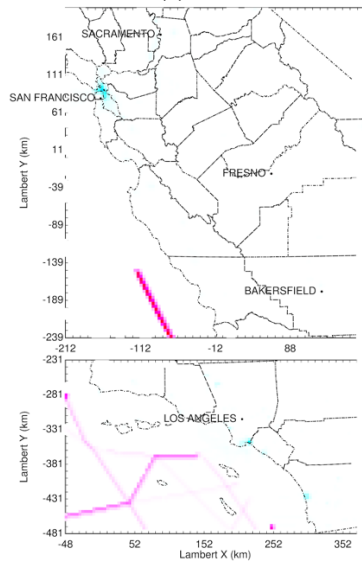
(a)BAU



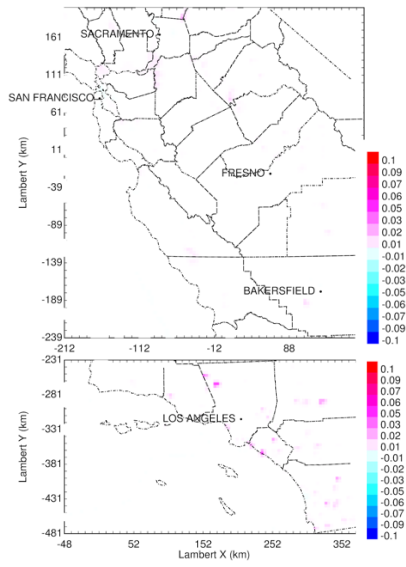
(b)CAP30 – BAU



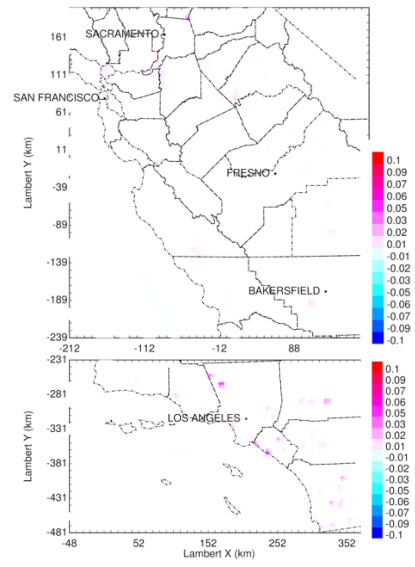
(c)CCS – BAU



(d)GHGAi – BAU

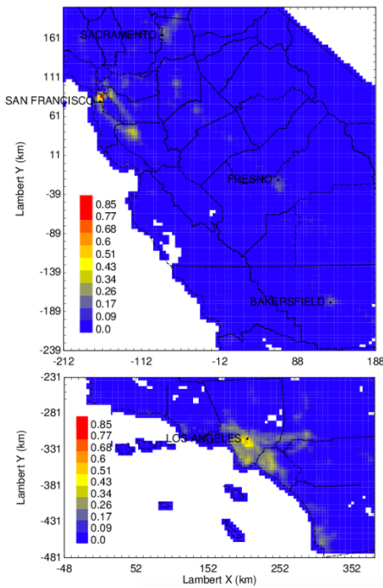


(e)NGB – GHGAi

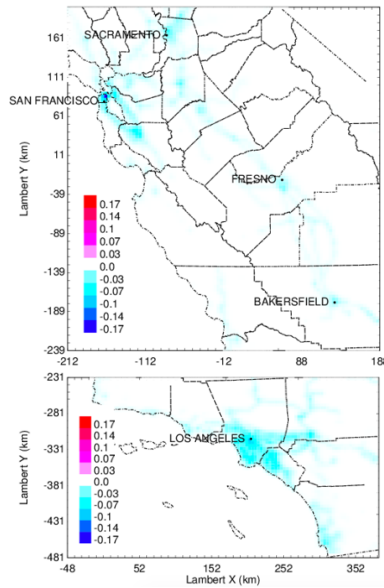


(f)NGT – GHGAi

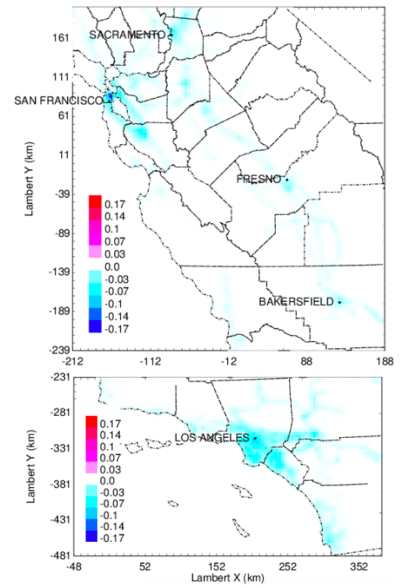
Figure S.4- 16 PM<sub>2.5</sub> emissions (ug·m<sup>-2</sup>·min<sup>-1</sup>) from marine vessels and aircraft.



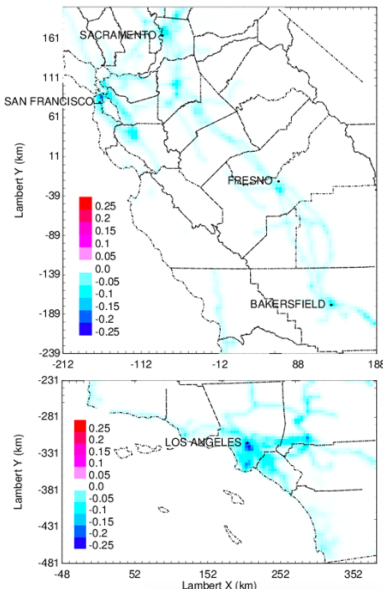
(a) BAU



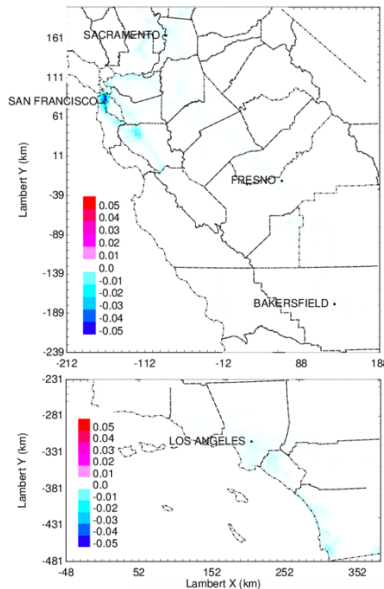
(b) CAP30 - BAU



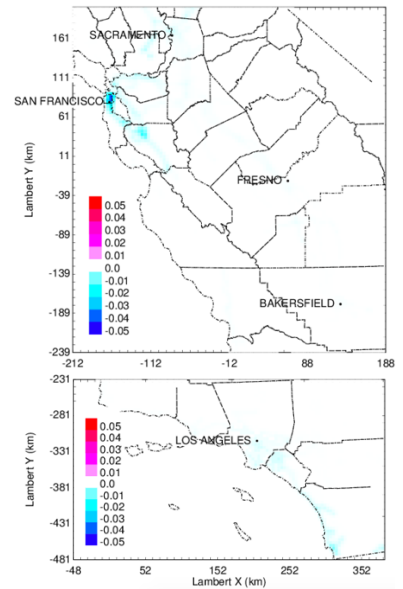
(c) CCS - BAU



(d) GHG - BAU

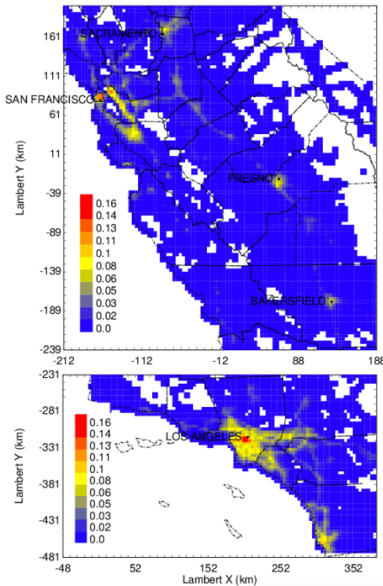


(e) NGB - GHG

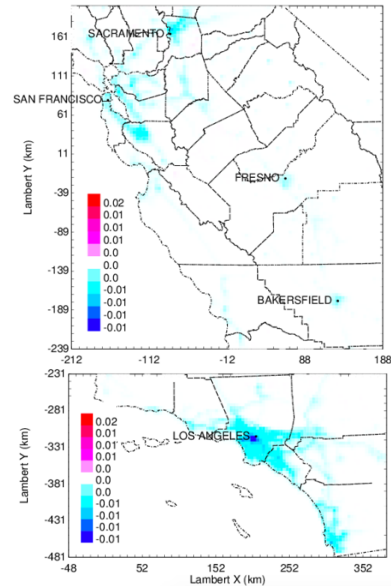


(f) NGT - GHG

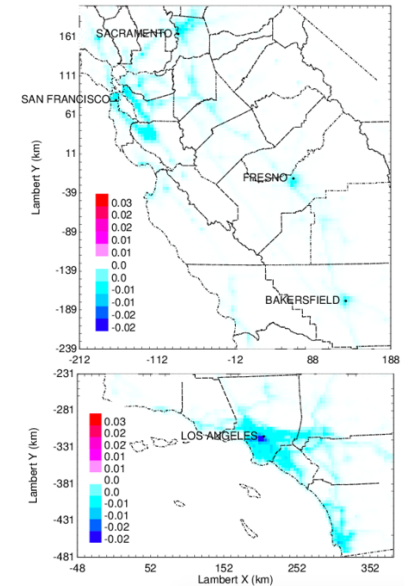
Figure S.4- 17 PM<sub>2.5</sub> emissions ( $\mu\text{g}\cdot\text{m}^{-2}\cdot\text{min}^{-1}$ ) from off-road equipment and railroad.



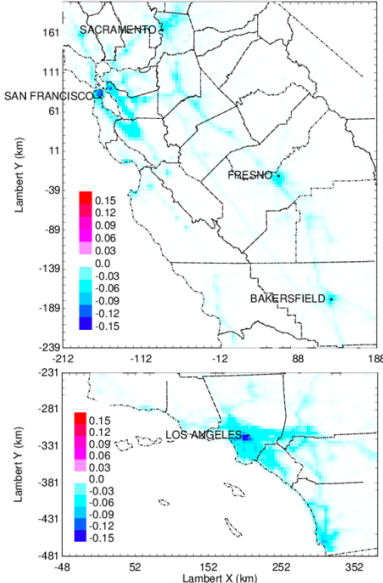
(a) BAU



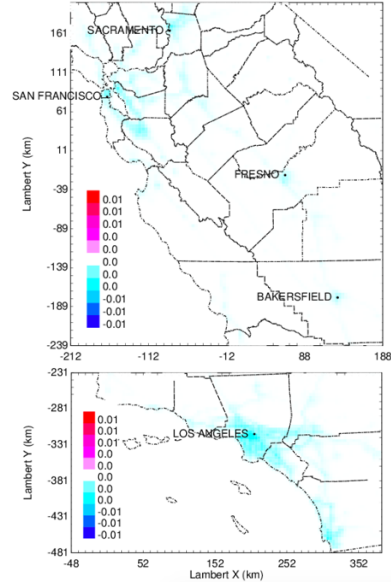
(b) CAP30 – BAU



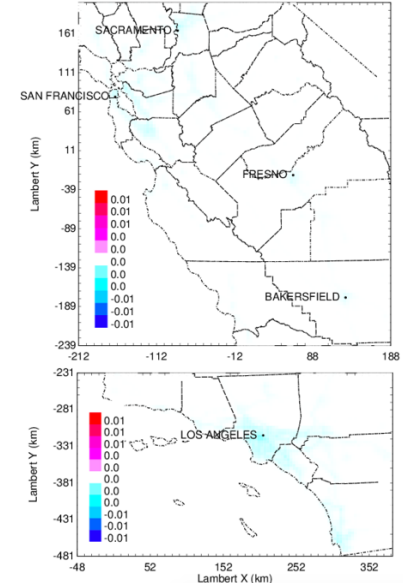
(c) CCS – BAU



(d) GHGai – BAU

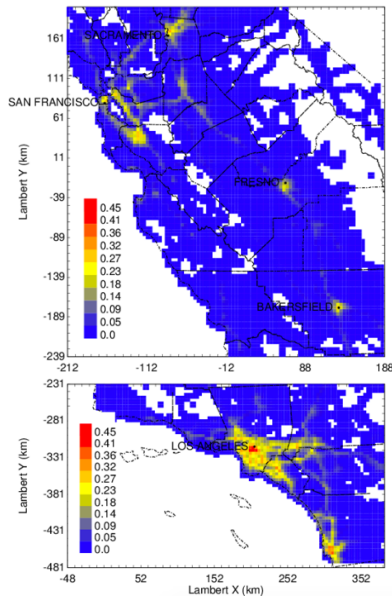


(e) NGB – GHGai

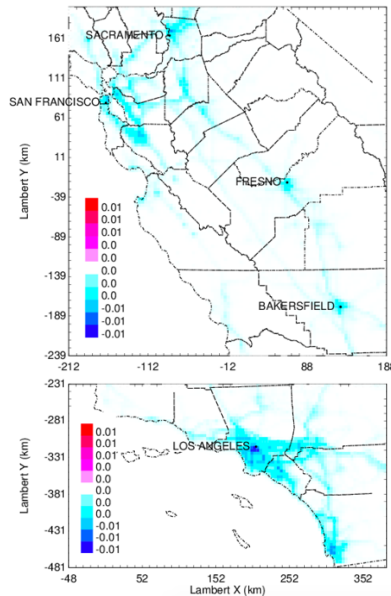


(f) NGT – GHGai

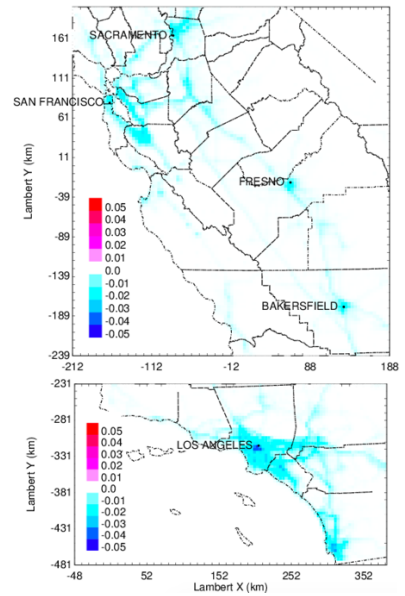
Figure S.4- 18 PM<sub>2.5</sub> emissions (ug-m<sup>-2</sup>.min<sup>-1</sup>) from on-road vehicle tailpipe.



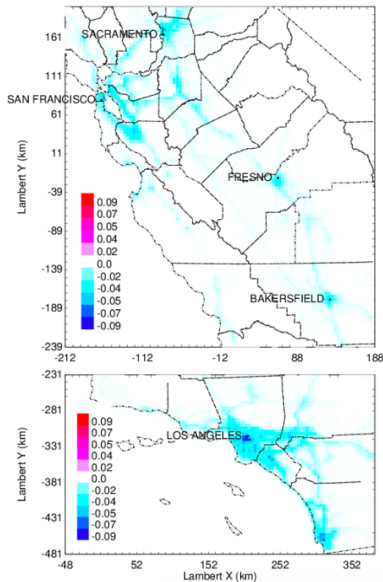
(a) BAU



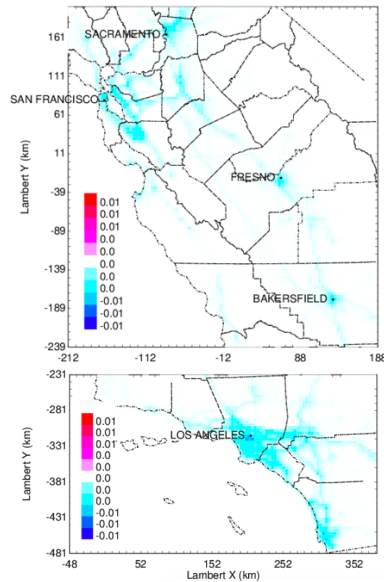
(b) CAP30 – BAU



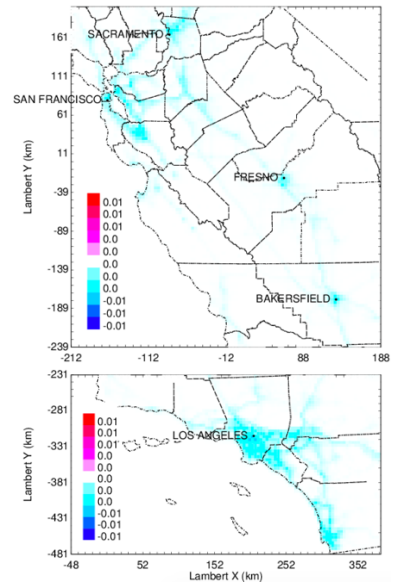
(c) CCS – BAU



(d) GHGai – BAU



(e) NGB – GHGai



(f) NGT – GHGai

Figure S.4- 19  $PM_{2.5}$  emissions ( $ug\cdot m^{-2}\cdot min^{-1}$ ) from on-road vehicle tire and break wear.

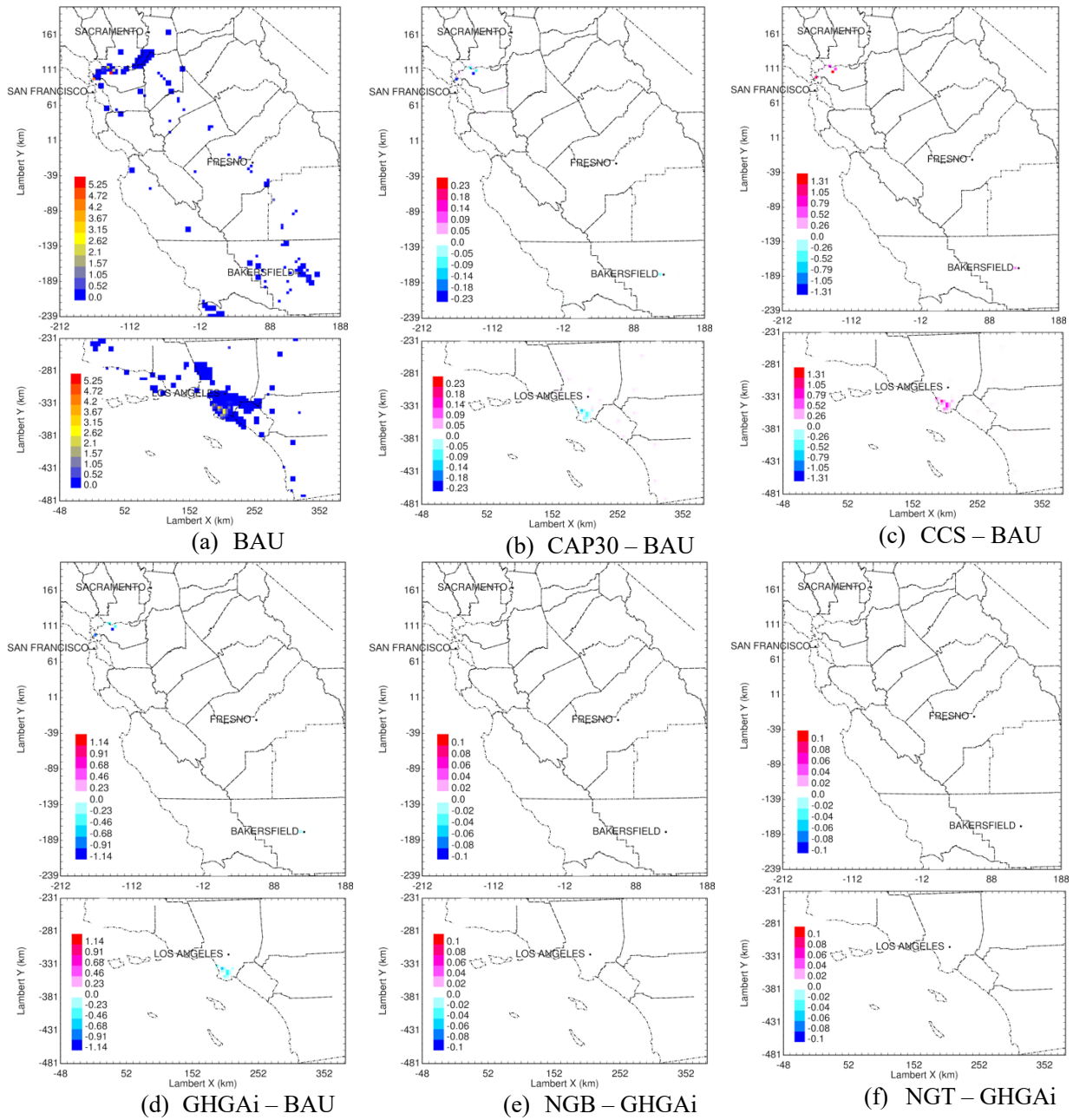
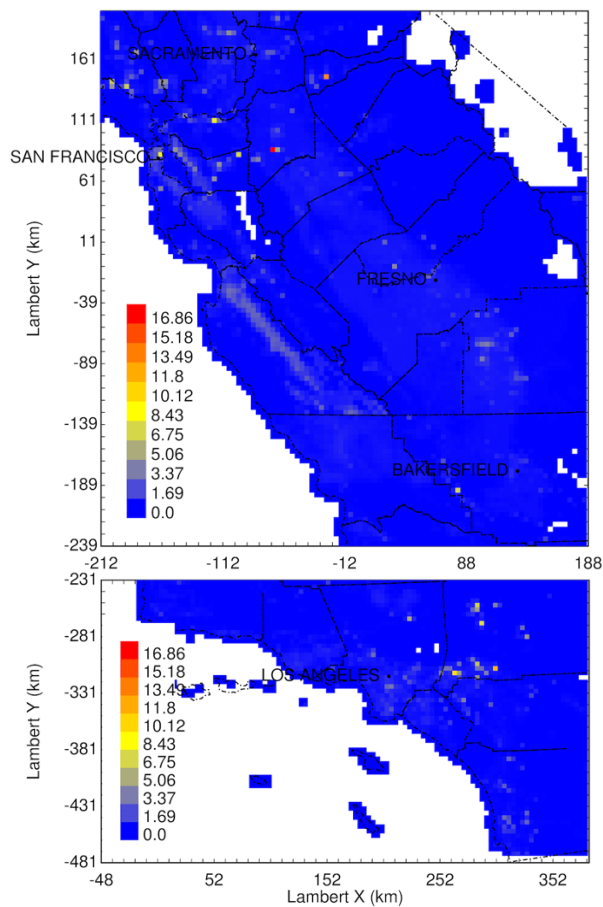
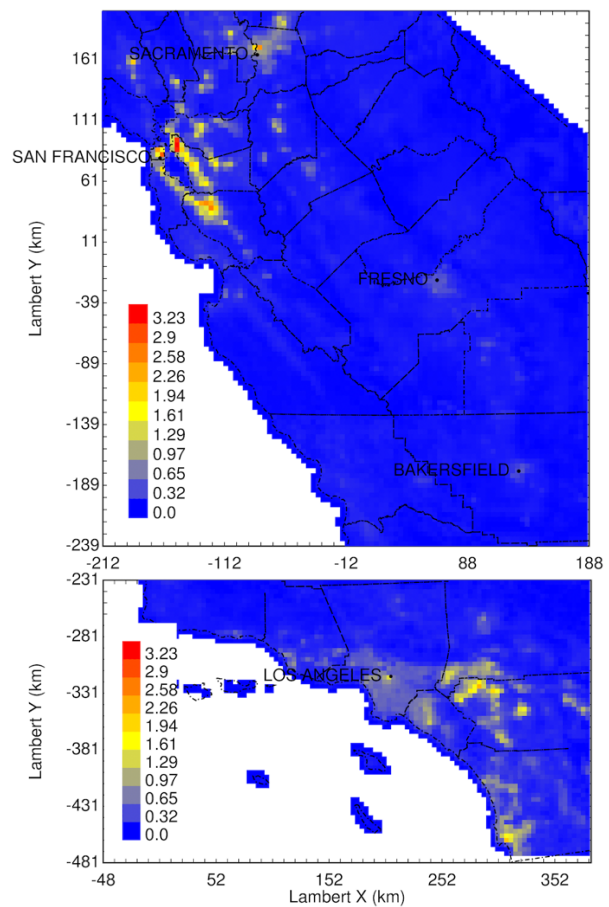


Figure S.4- 20 PM<sub>2.5</sub> emissions (ug·m<sup>-2</sup>·min<sup>-1</sup>) from fuel supply processes.



(a) industrial and agricultural emissions



(b) dust emissions

Figure S.4- 21  $PM_{2.5}$  emissions ( $\mu g \cdot m^{-2} \cdot min^{-1}$ ) from other processes. (including (a) industrial and agricultural emissions, and (b) dust emissions) that are not varying with scenarios.

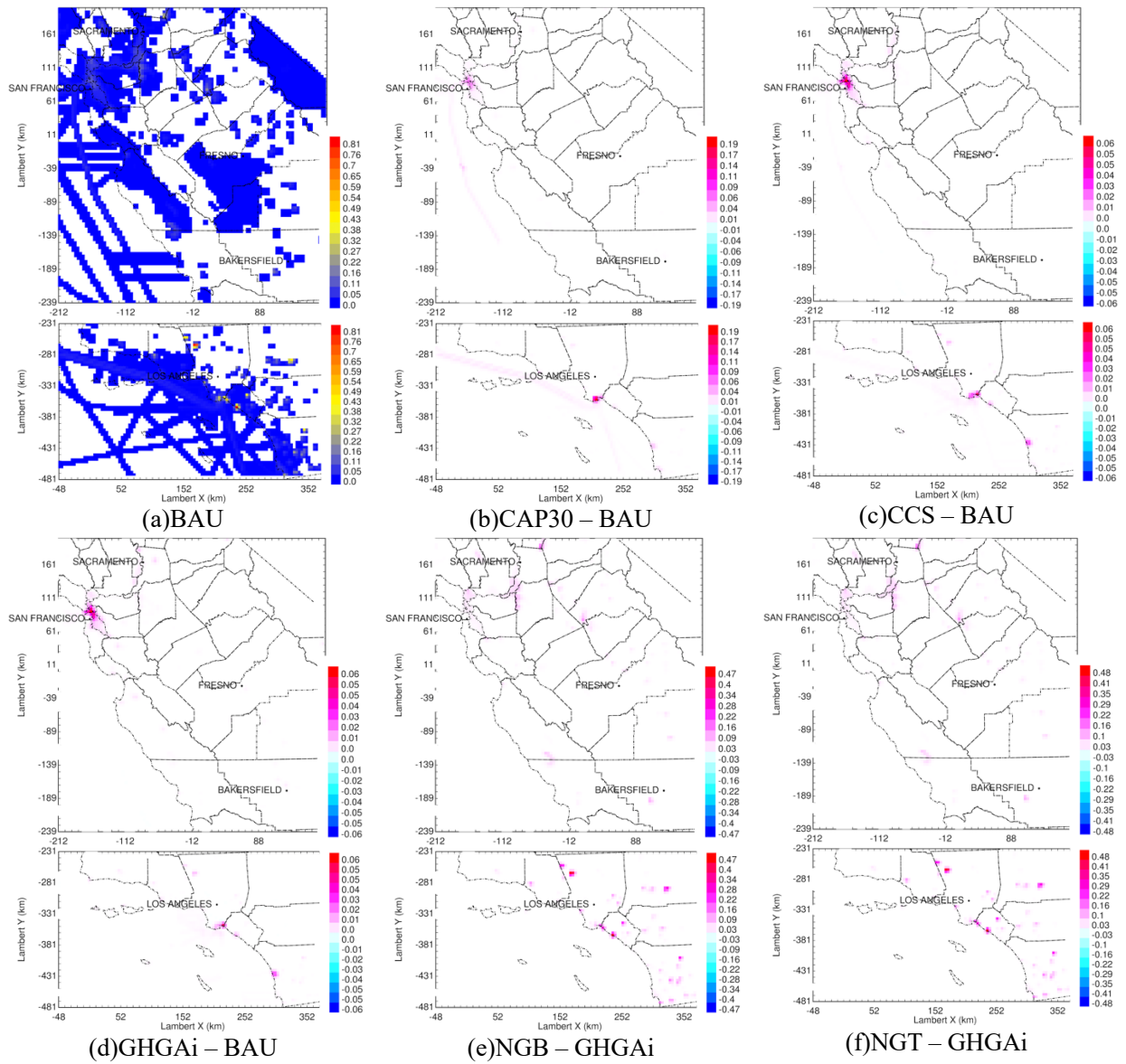


Figure S.4- 22 PM<sub>0.1</sub> emissions ( $\mu\text{g}\cdot\text{m}^{-2}\cdot\text{min}^{-1}$ ) from marine vessels and aircraft.

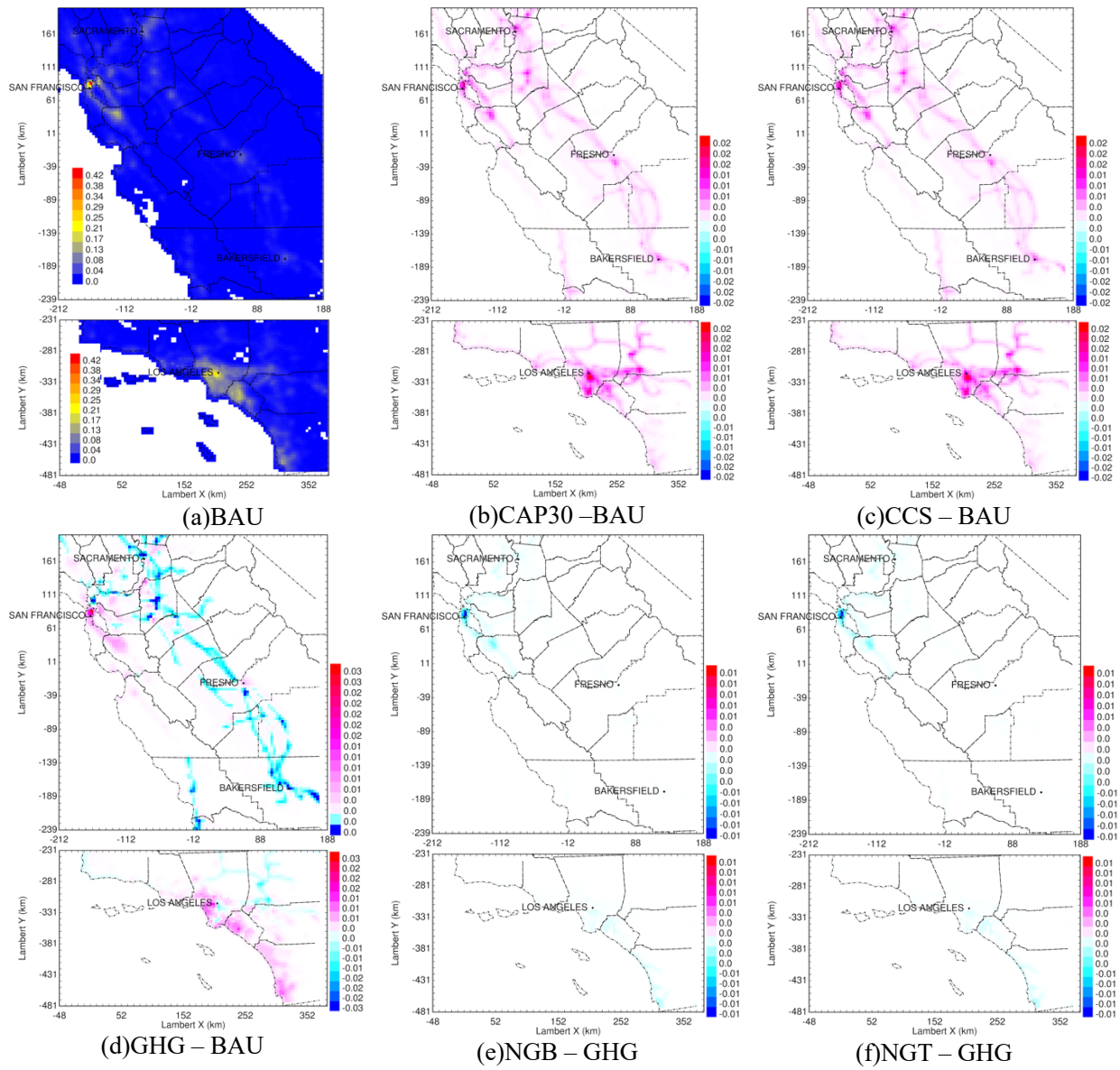


Figure S.4- 23 PM<sub>0.1</sub> emissions ( $\mu\text{g}\cdot\text{m}^{-2}\cdot\text{min}^{-1}$ ) from off-road equipment and railroad.

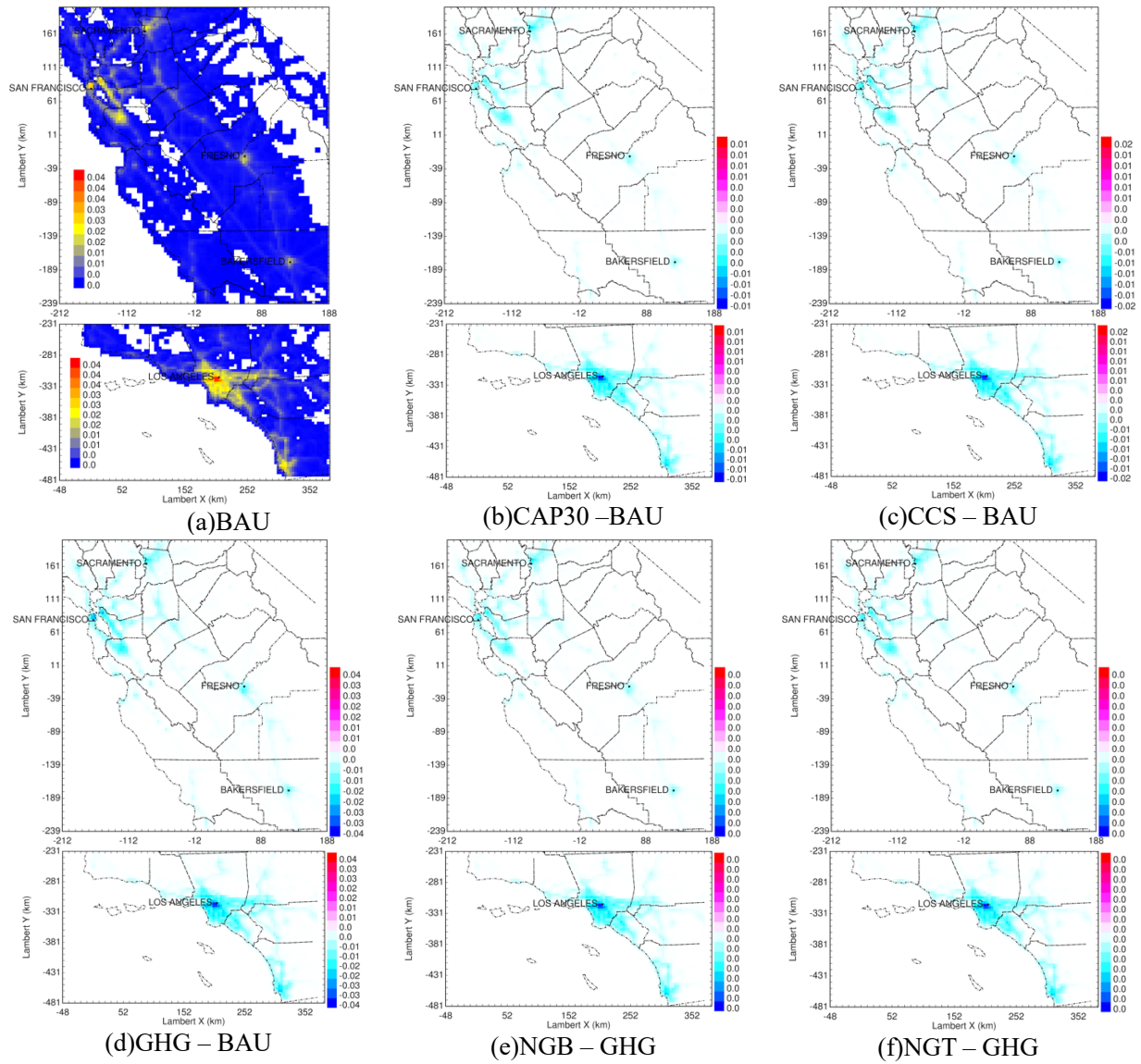
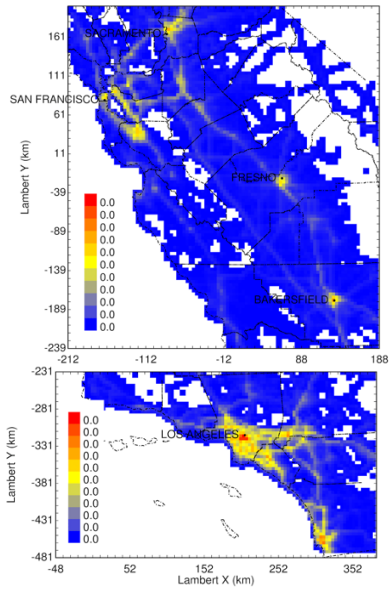
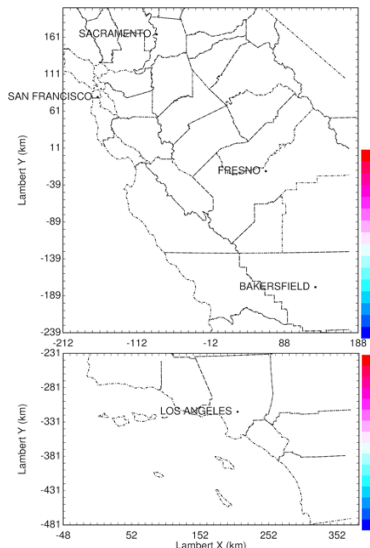


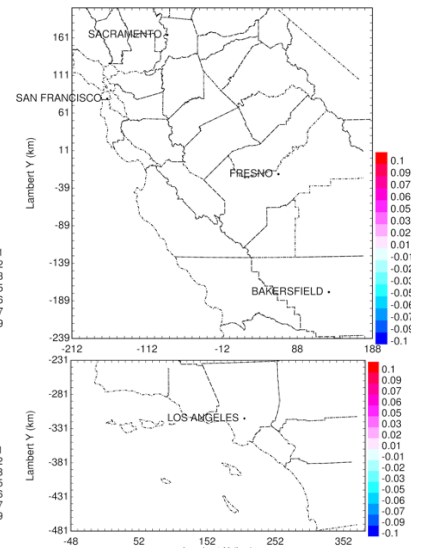
Figure S.4- 24 PM<sub>0.1</sub> emissions ( $\mu\text{g}\cdot\text{m}^{-2}\cdot\text{min}^{-1}$ ) from on-road vehicle tailpipe.



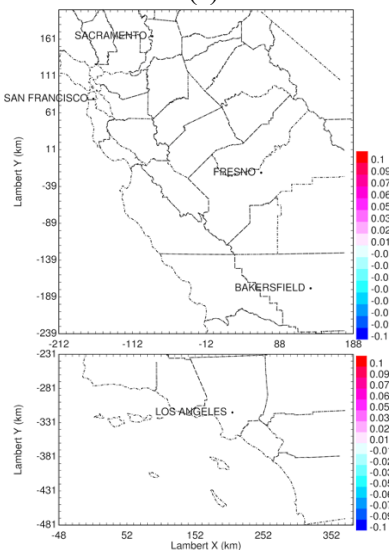
(a)BAU



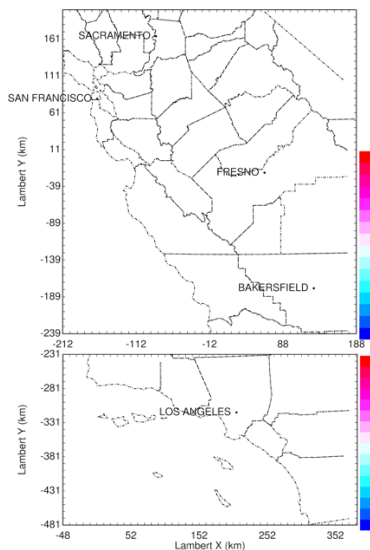
(b)CAP30 –BAU



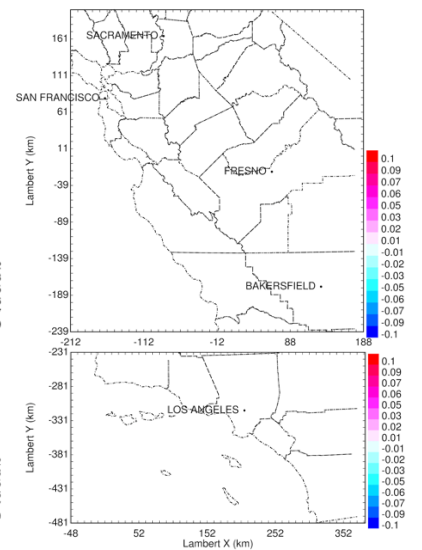
(c)CCS – BAU



(d)GHG – BAU



(e)NGB – GHG



(f)NGT – GHG

Figure S.4- 25  $PM_{0.1}$  emissions ( $\mu g \cdot m^{-2} \cdot min^{-1}$ ) from on-road vehicle tire and break wear.

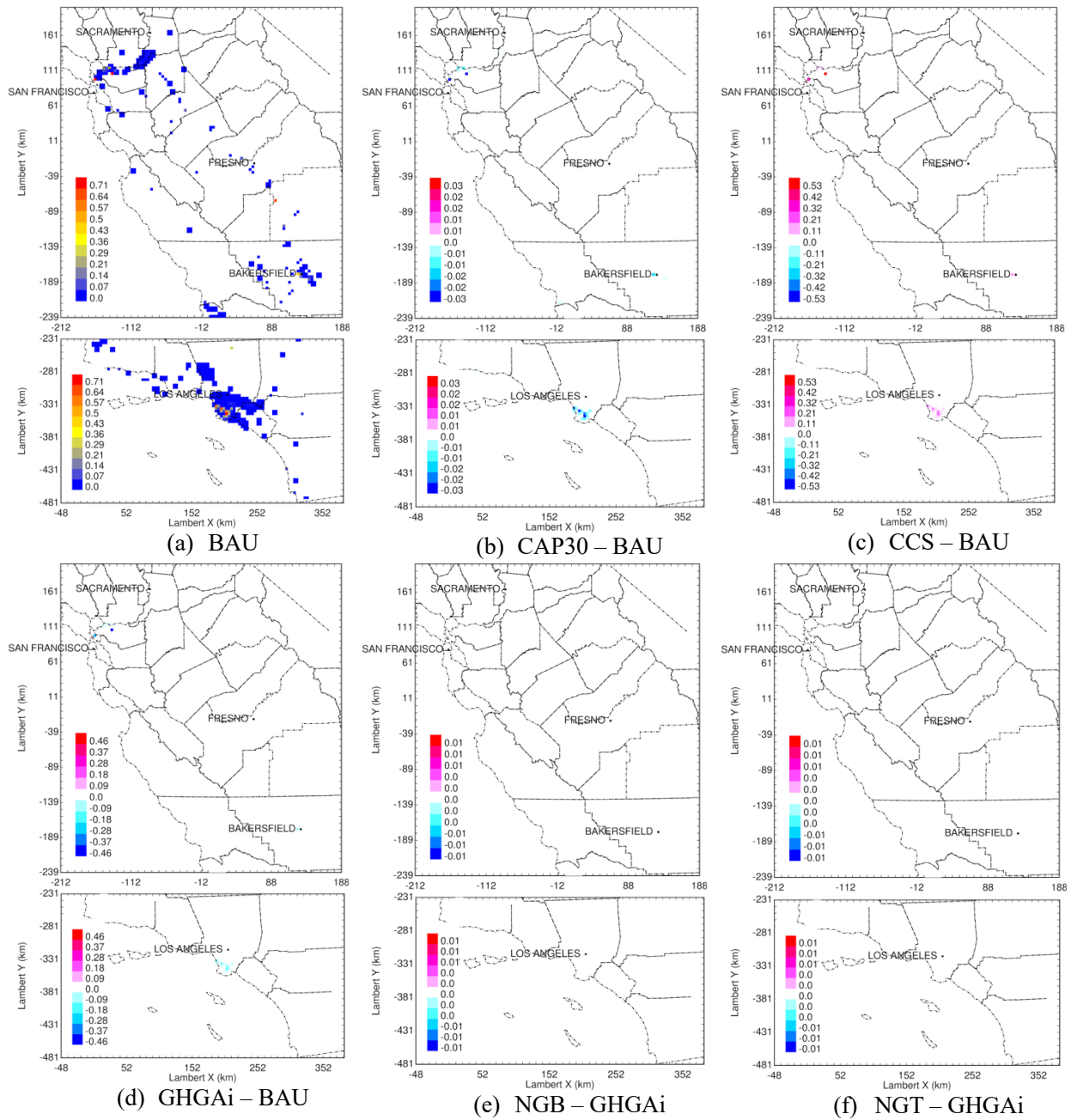


Figure S.4- 26  $PM_{0.1}$  emissions ( $ug \cdot m^{-2} \cdot min^{-1}$ ) from fuel supply processes.

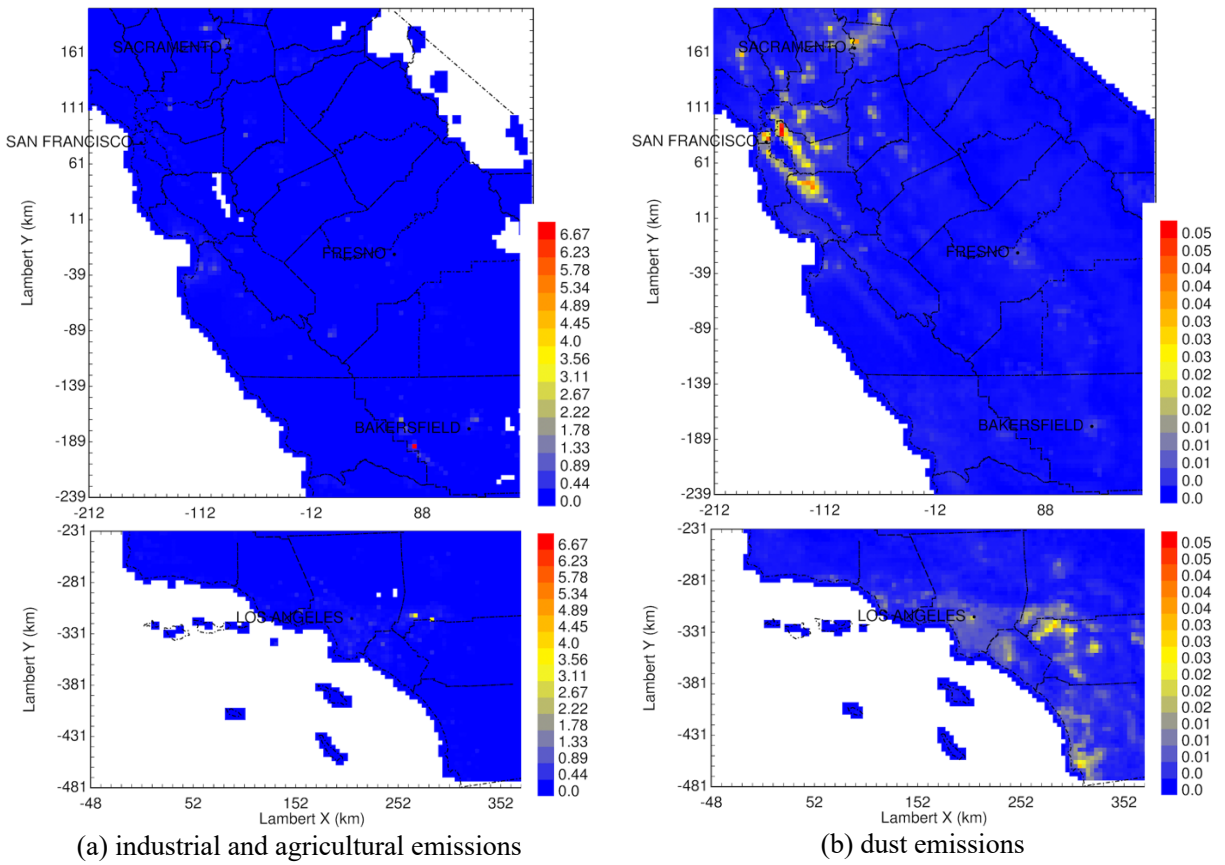


Figure S.4- 27  $PM_{0.1}$  emissions ( $\mu g \cdot m^{-2} \cdot min^{-1}$ ) from other processes. (including (a) industrial and agricultural emissions, and (b) dust emissions) that are not varying with scenarios.

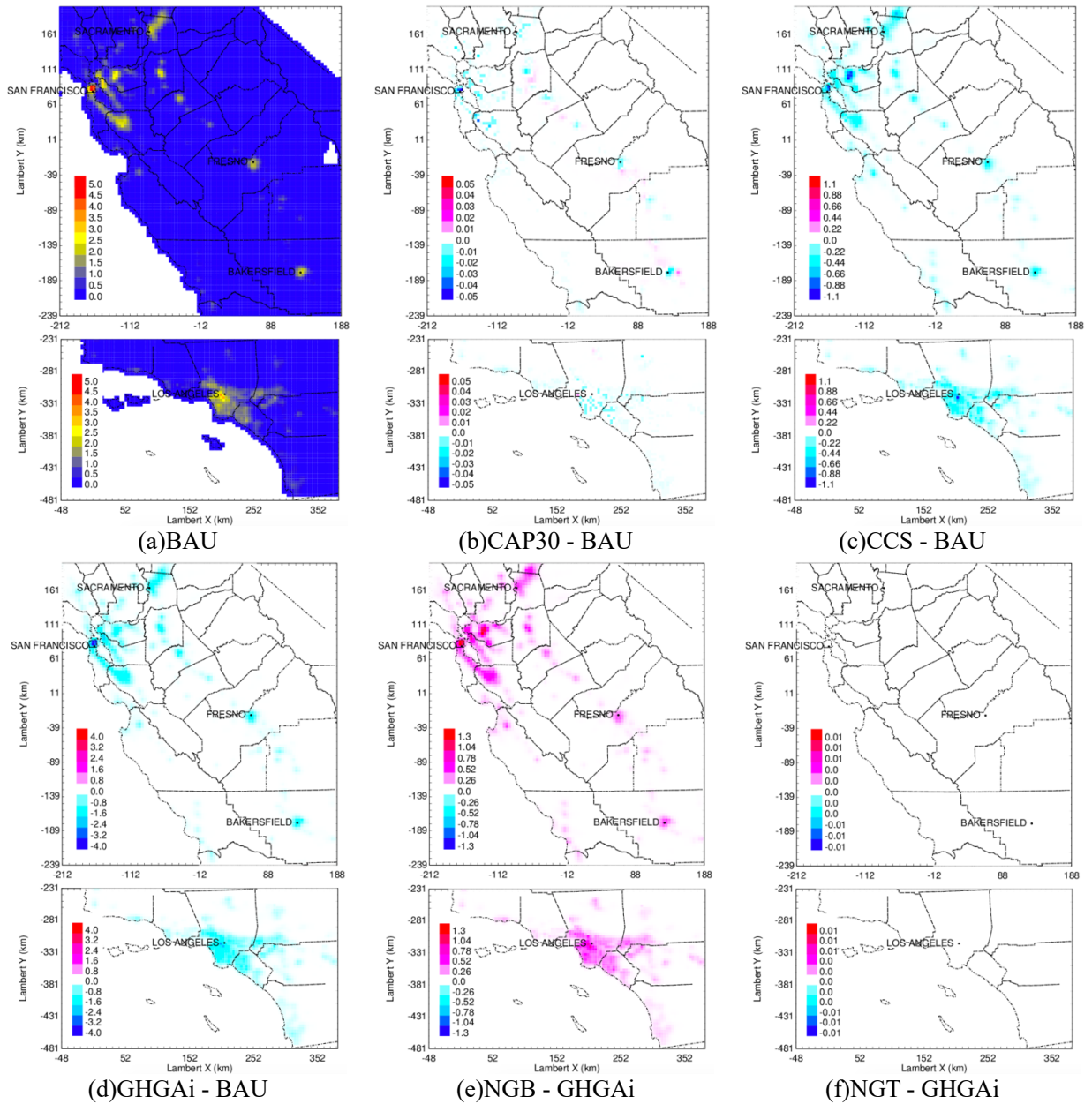


Figure S.4- 28 NO<sub>x</sub> emissions (ppb·m·min<sup>-1</sup>) from residential and commercial buildings.

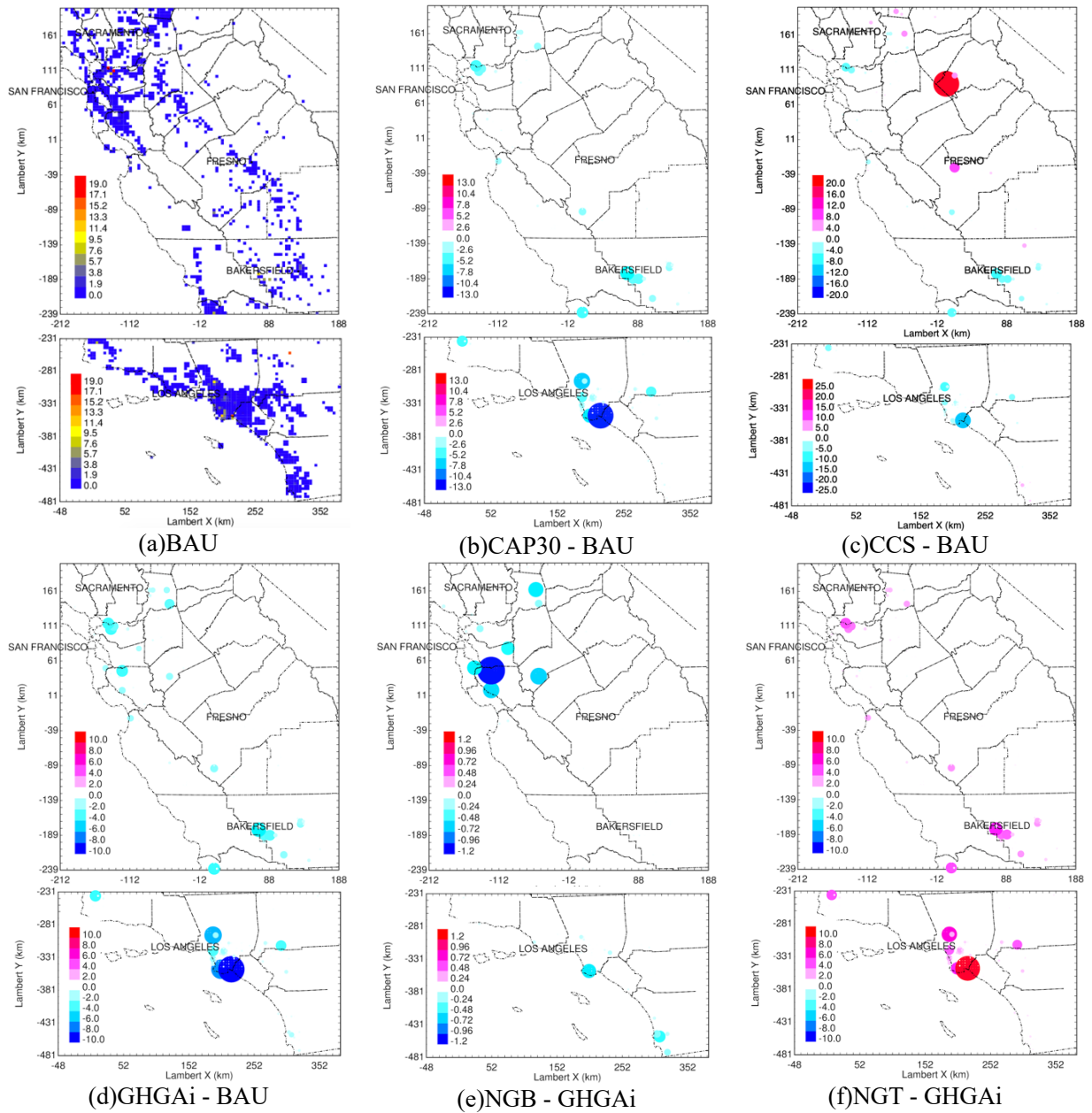


Figure S.4- 29 NO<sub>x</sub> emissions (ppb·m·min<sup>-1</sup>) from electricity generation.

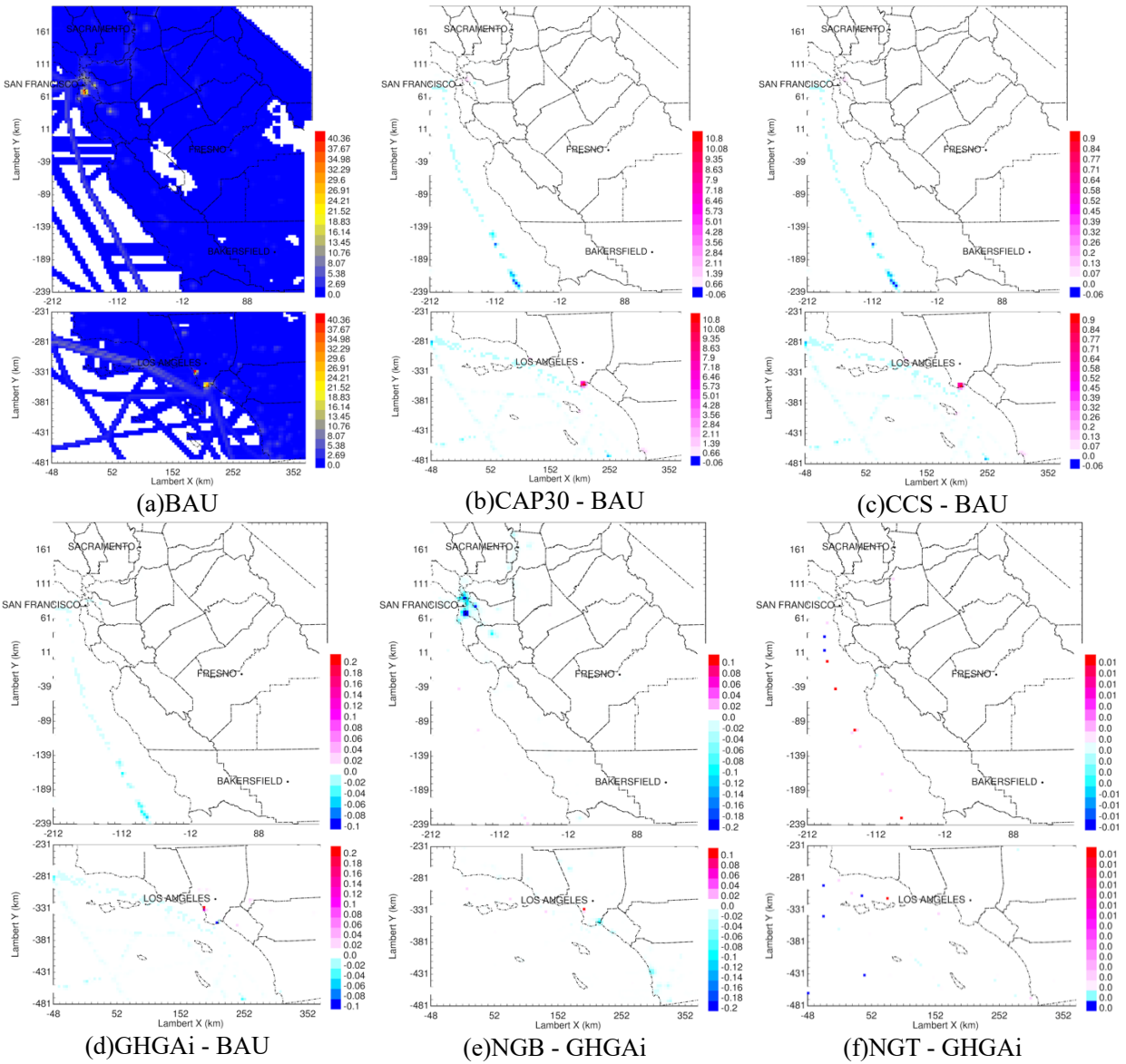
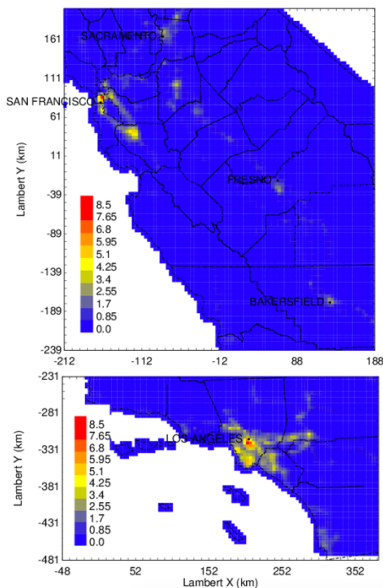
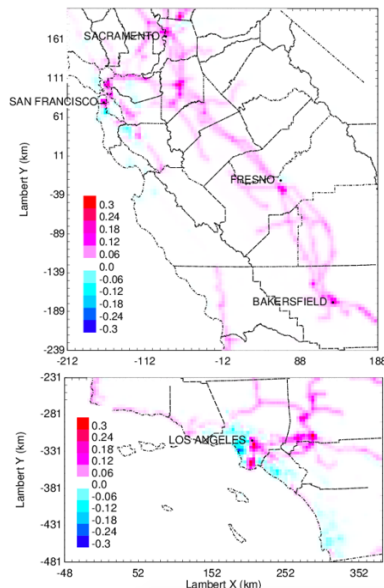


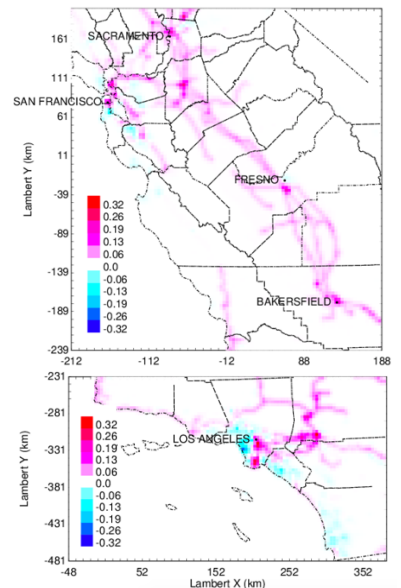
Figure S.4- 30 NO<sub>x</sub> emissions (ppb-m-min<sup>-1</sup>) from marine vessels and aircrafts.



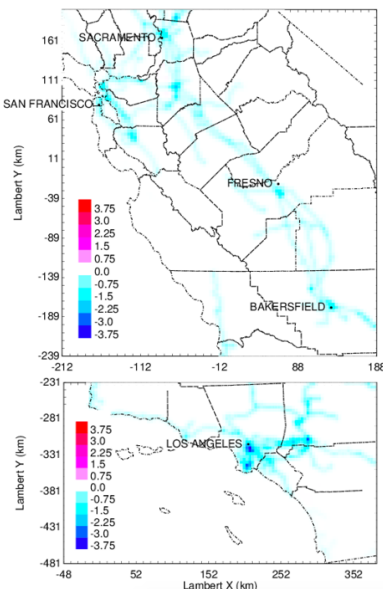
(a)BAU



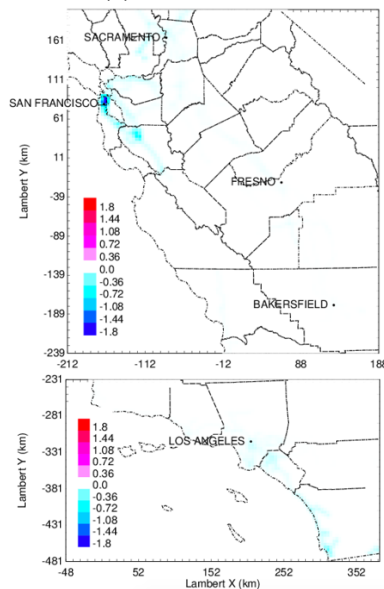
(b)CAP30 - BAU



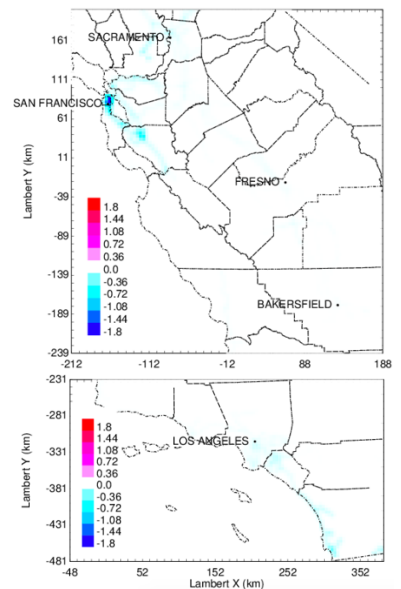
(c)CCS - BAU



(d)GHGai - BAU



(e)NGB - GHGai



(f)NGT - GHGai

Figure S.4- 31 NO<sub>x</sub> emissions (ppb-m-min<sup>-1</sup>) from off-road equipment and railroad.

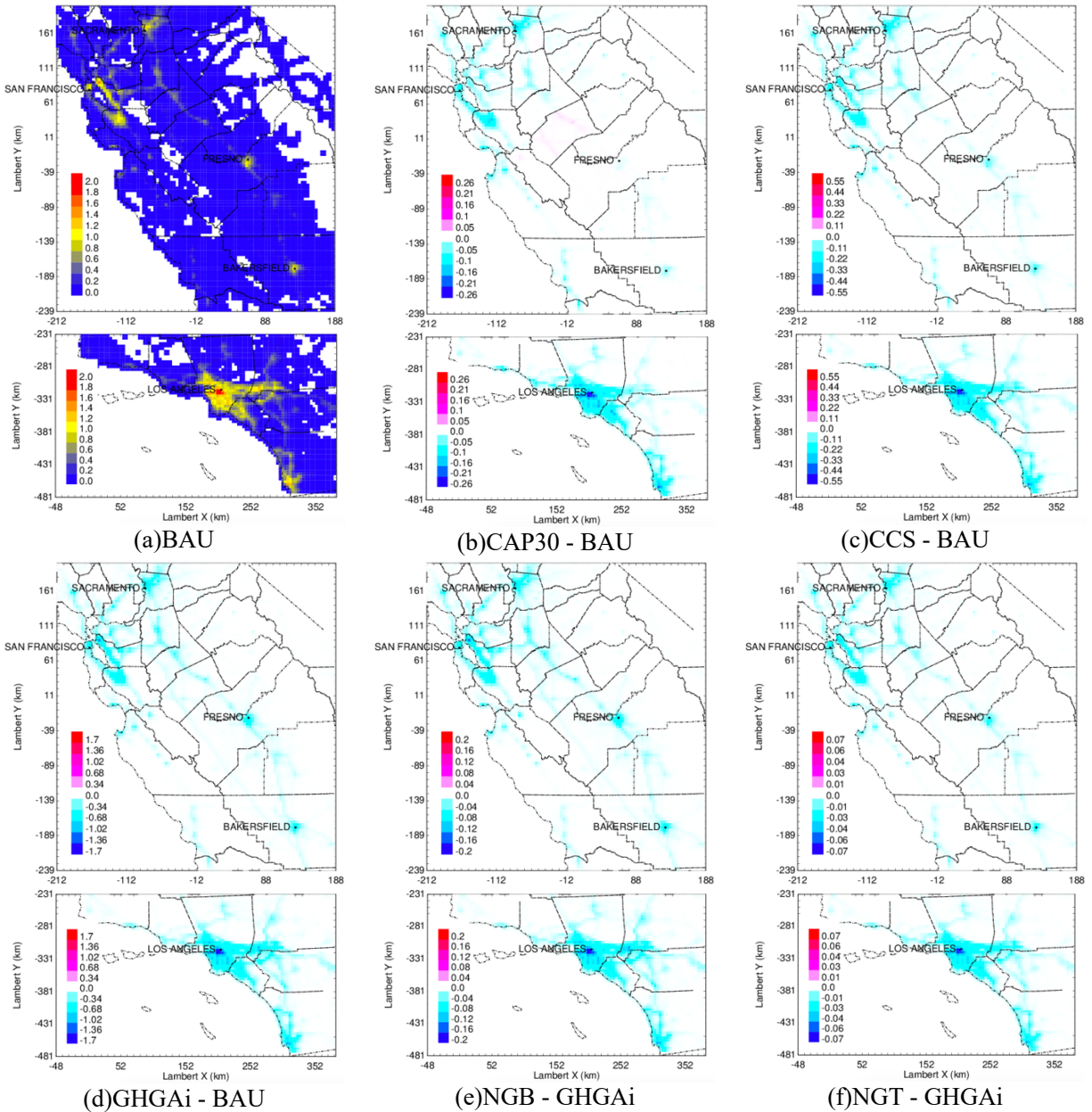


Figure S.4- 32 NO<sub>x</sub> emissions (ppb·m·min<sup>-1</sup>) from on-road vehicle tailpipe.

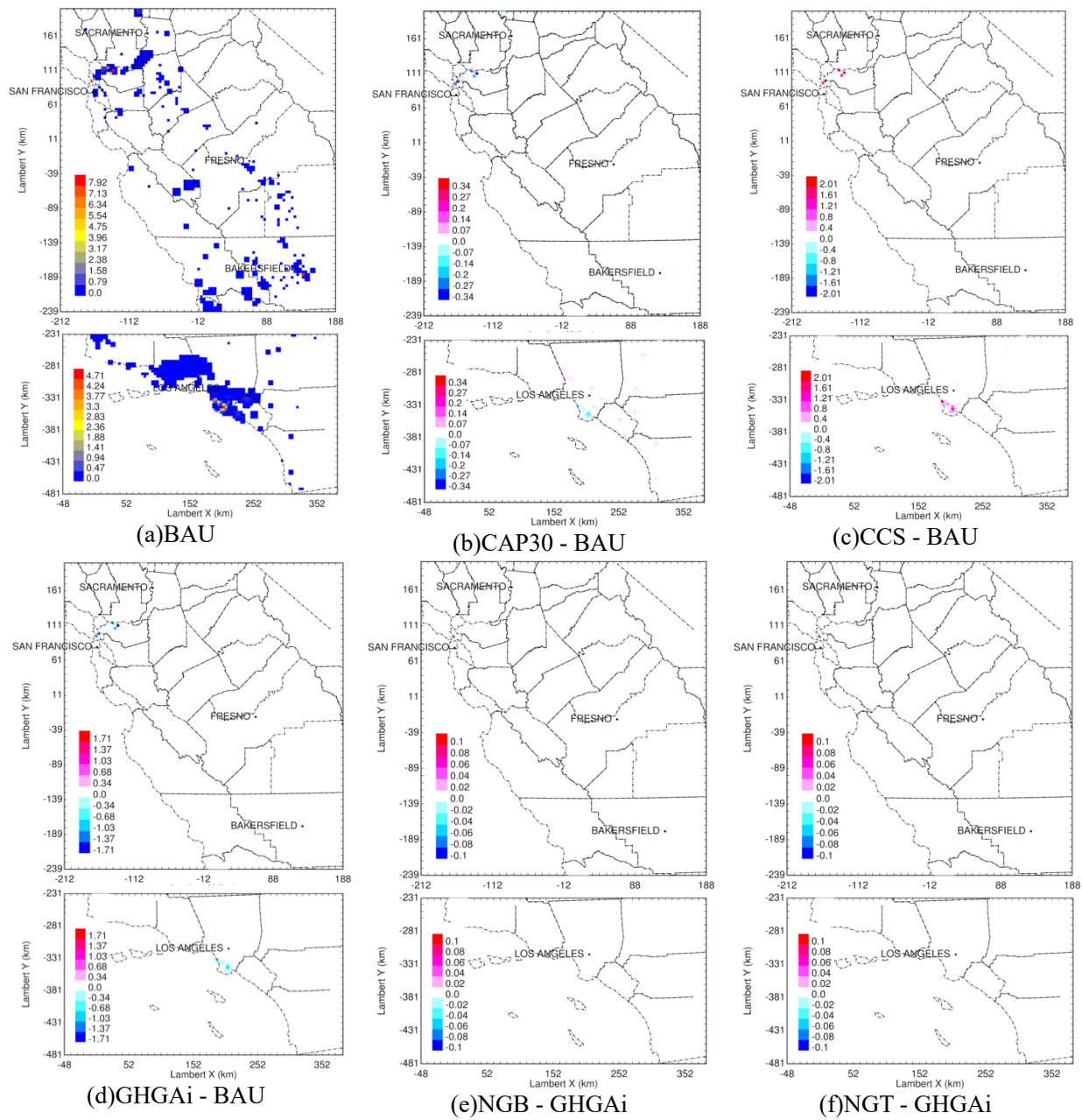


Figure S.4- 33 NO<sub>x</sub> emissions (ppb-m-min<sup>-1</sup>) from fuel supply processes.

## Chapter 5 – Conclusions

Biogas is a renewable energy source composed of methane, carbon dioxide, and other trace compounds produced from anaerobic digestion of organic matter. A variety of feedstocks can be combined with different digestion techniques that each yield biogas with different trace composition. California is expanding biogas production systems to help meet greenhouse gas reduction goals. The second chapter reports the composition of six California biogas streams from three different feedstocks (dairy manure, food waste and municipal solid waste). The chemical and biological composition of raw biogas is reported and the toxicity of combusted biogas is tested under fresh and photo-chemically aged conditions. Results show that municipal waste biogas contained elevated levels of chemicals associated with volatile consumer products (VCPs) such as aromatic hydrocarbons, siloxanes, and certain halogenated hydrocarbons. Food waste biogas contained elevated levels of sulfur-containing compounds including hydrogen sulfide, mercaptans, and sulfur dioxide. Biogas produced from dairy manure generally had lower concentrations of trace chemicals, but the combustion products had slightly higher toxicity response compared to the other feedstocks. Atmospheric aging performed in a photochemical smog chamber did not strongly change the toxicity (oxidative capacity or mutagenicity) of biogas combustion exhaust.

Biogas can be upgraded to a transportation fuel referred to as renewable natural gas (RNG) by removing CO<sub>2</sub> and other impurities. RNG has energy content comparable to compressed fossil natural gas (CNG) but with lower life-cycle greenhouse gas (GHG) emissions. In the third chapter, a light-duty cargo van was tested with CNG and two RNG blends on a chassis dynamometer in order to compare the toxicity of the resulting exhaust. Tests for reactive oxygen species (ROS), biomarker expressions (CYP1A1, IL8, COX-2), and mutagenicity (Ames) show that RNG exhaust has toxicity that is comparable or lower than CNG exhaust. Statistical analysis reveals associations between toxicity and tailpipe emissions of benzene, dibenzofuran, and dihydroperoxide dimethyl hexane (the last identification is considered tentative/uncertain). Further gas-phase toxicity may be associated with tailpipe emissions of formaldehyde, dimethyl-sulfide, propene, and methyl ketene. CNG exhaust contained higher concentrations of these

potentially toxic chemical constituents than RNG exhaust in all of the current tests. Photochemical aging of the vehicle exhaust did not alter these trends. These preliminary results suggest that RNG adoption may be a useful strategy to reduce the carbon intensity of transportation fuels without increasing the toxicity of the vehicle exhaust.

Mitigating future climate change and managing future air quality are inter-related fields that have the potential to benefit from coordinated strategies that leverage the efforts in one area to achieve positive outcomes in the other area. California plans to reduce greenhouse gas (GHG) emission by 80% (relative to year 1990) by the year 2050. The changes required to meet this target also have the potential to improve air quality. Previous work developed an energy-economic model CA-TIMES and an emission inventory model CA-REMARQUE to study the possible pathways of meeting the GHG mitigation target and the air pollutant emissions associated with those pathways. Here we update the CA-TIMES and CA-REMARQUE model framework and analyze six different scenarios: (i) BAU - a business-as-usual future reference scenario, (ii) CAP30 - a loose GHG reduction scenario that meets current policy references but only achieves a 40% GHG reduction (relative to 1990 levels) by the year 2030, (iii) GHGAI - a climate-friendly 80% GHG reduction scenario featuring broad adoption of advanced technologies and renewable energies, (iv) CCS - a scenario that achieves 80% net GHG reductions but allows for more fossil energy combustion by focusing on adoption of carbon capture and sequestration technology, (v) NGB— a variation on the GHGAI scenario that allows for more natural gas combustion for residential and commercial buildings, and (vi) NGT – a variation of the GHGAI scenario that allows for more natural gas combustion for electricity generation. Results show that the GHGAI deep GHG mitigation scenario significantly reduces emissions (-41%  $PM_{0.1}$ , -8%  $PM_{2.5}$ , and -26%  $NO_x$ ) and improves air quality ( $-1 \mu g m^{-3} PM_{2.5}$ ) yielding public health benefits (+USD 20B  $yr^{-1}$ ) relative to the BAU scenario. The CCS scenario achieves the same GHG reductions but increases emissions in some areas (+2.5%  $PM_{2.5}$ ) yielding only one third of the public health benefits compared to the GHGAI scenario. The NGB and NGT scenarios show that an 18% increase in natural gas utilization in buildings or a 15% increase in natural gas power generation offsets 32% and 46% of the ultrafine particle emission reduction achieved in the GHGAI scenario but has little impact on  $PM_{2.5}$

concentrations, yielding approximately 90% of the public health benefits of the GHGAi scenario. These public health benefits should be considered when making decisions about future GHG mitigation strategies.

## References

1. Zapata CB, Yang C, Yeh S, Ogden J, Kleeman MJ. Low-carbon energy generates public health savings in California. *Atmos Chem Phys*. 2018;18(7):4817-4830. doi:10.5194/acp-18-4817-2018
2. Shindell D, Faluvegi G, Seltzer K, Shindell C. Quantified, localized health benefits of accelerated carbon dioxide emissions reductions. *Nat Clim Chang*. 2018;8(April):1-5. doi:10.1038/s41558-018-0108-y
3. Milbrandt A. Biogas Potential in the United States (Fact Sheet), Energy Analysis, NREL (National Renewable Energy Laboratory). :1-4. <http://www.nrel.gov/docs/fy14osti/60178.pdf>
4. Williams RB, Kaffka SR, Oglesby R. DRAFT INTERIM PROJECT REPORT DRAFT Comparative Assessment of Technology Options for Biogas Clean - up. Published online 2014.
5. Wellinger A, Murphy J, Baxter D. *The Biogas Handbook: Science, Production and Applications.*; 2013. doi:10.1533/9780857097415
6. Poeschl M, Ward S, Owende P. Environmental impacts of biogas deployment - Part II: Life Cycle Assessment of multiple production and utilization pathways. *J Clean Prod*. 2012;24:184-201. doi:10.1016/j.jclepro.2011.10.030
7. Hijazi O, Munro S, Zerhusen B, Effenberger M. Review of life cycle assessment for biogas production in Europe. *Renew Sustain Energy Rev*. 2016;54:1291-1300. doi:10.1016/j.rser.2015.10.013
8. Poeschl M, Ward S, Owende P. Environmental impacts of biogas deployment - Part I: Life Cycle Inventory for evaluation of production process emissions to air. *J Clean Prod*. 2012;24:168-183. doi:10.1016/j.jclepro.2011.10.039
9. CalEPA. California Environmental Protection Agency; Recommendations to the California Public Utilities Commission Regarding Health Protective Standards for the Injection of Biomethane into the Common Carrier Pipeline. Available [https://www.arb.ca.gov/energy/biogas/documents/FINAL\\_AB\\_1900\\_Staff\\_Report\\_&\\_Appendices\\_%20051513.pdf](https://www.arb.ca.gov/energy/biogas/documents/FINAL_AB_1900_Staff_Report_&_Appendices_%20051513.pdf) Last access August 2017. Published online 2013. doi:10.1007/s11104-007-9437-8
10. Parker N, Williams R, Dominguez-Faus R, Scheitrum D. Renewable natural gas in California: An assessment of the technical and economic potential. *Energy Policy*. 2017;111:235-245. doi:10.1016/j.enpol.2017.09.034
11. Williams RB, Jenkins BM, Kaffka S (California BC. An Assessment of Biomass Resources in California, 2013 - DRAFT. *Contract Rep to CEC PIER Contract 500-11-020*. 2015;(March):1-155. doi:500-11-020
12. American Lung Association. Most Polluted Cities. Published 2019. <https://www.lung.org/our-initiatives/healthy-air/sota/city-rankings/most-polluted-cities.html>
13. Brosseau JE, Heitz LE. Trace Gas Compound Emissions from Municipal Landfill Sanitary Sites. 1994;28(2):285-293.
14. Allen MR, Braithwaite A, Hills CC. Trace organic compounds in landfill gas at seven U.K. waste disposal sites. *Environ Sci Technol*. 1997;31(4):1054-1061. doi:10.1021/es9605634
15. Eklund B, Anderson EP, Walker BL, Burrows DB. Characterization of landfill gas composition at the Fresh Kills municipal solid-waste landfill. *Environ Sci Technol*. 1998;32(15):2233-2237. doi:10.1021/es980004s
16. Powell J, Jain P, Kim H, Townsend T, Reinhart D. Changes in landfill gas quality as a result of controlled air injection. *Environ Sci Technol*. 2006;40(3):1029-1034. doi:10.1021/es051114j
17. Rasi S, Veijanen A, Rintala J. Trace compounds of biogas from different biogas production plants. *Energy*. 2007;32(8):1375-1380. doi:10.1016/j.energy.2006.10.018
18. Schweigkofler M, Niessner R. Determination of siloxanes and VOC in landfill gas and sewage gas by canister sampling and GC-MS/AES analysis. *Environ Sci Technol*. 1999;33(20):3680-3685. doi:10.1021/es9902569
19. Shin HC, Park JW, Park K, Song HC. Removal characteristics of trace compounds of landfill gas by activated carbon adsorption. *Environ Pollut*. 2002;119(2):227-236. doi:10.1016/S0269-7491(01)00331-1
20. Saber DL, Takach SF. Task 1 Final Report: Technology Investigation, Assessment, and Analysis. 2009;(20614).
21. Bothi KL. Characterization of Biogas From Anaerobically Digested Dairy Waste for Energy Use. *Master's Thesis*. Published online 2007. doi:10.1017/CBO9781107415324.004
22. Zhang, R. Zhang, M. Aramreang, N. Rapport J. *Energy Research and Development Division Final Project Report UC Davis Renewable Energy Anaerobic Digestion Project Feedstock Analysis and Performance Assessment. CEC-500-2017-021.*; 2017. <http://www.energy.ca.gov/2017publications/CEC-500-2017-021/CEC-500-2017-021.pdf>

23. Tomich M, Marianne M. *Waste-to-Fuel: A Case Study of Converting Food Waste to Renewable Natural Gas as a Transportation Fuel.*; 2017. [https://afdc.energy.gov/files/u/publication/waste\\_to\\_fuel.pdf](https://afdc.energy.gov/files/u/publication/waste_to_fuel.pdf)
24. Huang J, Crookes RJ. Assessment of simulated biogas as a fuel for the spark ignition engine. *Fuel*. 1998;77(15):1793-1801. doi:10.1016/S0016-2361(98)00114-8
25. Pandya CB, Shah PDR, Patel TM, Rathod GP. Performance Analysis of Enriched Biogas Fuelled Stationary Single Cylinder SI Engine. 2016;13(2):21-27. doi:10.9790/1684-1302042127
26. Kim Y, Kawahara N, Tsuboi K, Tomita E. Combustion characteristics and NOX emissions of biogas fuels with various CO2 contents in a micro co-generation spark-ignition engine. *Appl Energy*. 2016;182(X):539-547. doi:10.1016/j.apenergy.2016.08.152
27. Chandra R, Vijay VK, Subbarao PMV, Khura TK. Performance evaluation of a constant speed IC engine on CNG, methane enriched biogas and biogas. *Appl Energy*. 2011;88(11):3969-3977. doi:10.1016/j.apenergy.2011.04.032
28. Verma S, Das LM, Kaushik SC. Effects of varying composition of biogas on performance and emission characteristics of compression ignition engine using exergy analysis. *Energy Convers Manag*. 2017;138:346-359. doi:10.1016/j.enconman.2017.01.066
29. Kang DW, Kim TS, Hur KB, Park JK. The effect of firing biogas on the performance and operating characteristics of simple and recuperative cycle gas turbine combined heat and power systems. *Appl Energy*. 2012;93:215-228. doi:10.1016/j.apenergy.2011.12.038
30. Piechota G, Igliński B, Buczkowski R. Development of measurement techniques for determination main and hazardous components in biogas utilised for energy purposes. *Energy Convers Manag*. 2013;68:219-226. doi:10.1016/j.enconman.2013.01.011
31. Mariné S, Pedrouzo M, Maria Marcé R, Fonseca I, Borrull F. Comparison between sampling and analytical methods in characterization of pollutants in biogas. *Talanta*. 2012;100:145-152. doi:10.1016/j.talanta.2012.07.074
32. U.S. Environmental Protection Agency (EPA). Compendium of methods for the determination of toxic organic compounds in ambient air compendium method TO-15. *Epa*. 1999;(January):1-32. [https://www.epa.gov/sites/production/files/2015-07/documents/epa-to-15\\_0.pdf](https://www.epa.gov/sites/production/files/2015-07/documents/epa-to-15_0.pdf)
33. U.S. Environmental Protection Agency (EPA). EPA method 8081B for analysis of Organochlorine Pesticides (OCPs) in extracts from solid, tissue and liquid matrices. 2007;(February). <https://www.epa.gov/sites/production/files/2015-12/documents/8081b.pdf>
34. U.S. Environmental Protection Agency (EPA). EPA method 8270d for analysis of semivolatile organic compounds by gas chromatography/mass spectrometry. Published online 1998:1-62. <https://www.epa.gov/sites/production/files/2015-07/documents/epa-8270d.pdf>
35. U.S. Environmental Protection Agency (EPA). EPA method 8082a for analysis of polychlorinated biphenyls (PCBs) by gas chromatography. Published online 2007:1-56.
36. EPA. "Method 29-Determination of metals emission from stationary sources", <https://www.epa.gov/emc/method-29-metals-emissions-stationary-sources>. Published online 2017:1-37. [https://www.epa.gov/sites/production/files/2017-08/documents/method\\_29.pdf](https://www.epa.gov/sites/production/files/2017-08/documents/method_29.pdf)
37. ASTM International. D1945-14 Standard Test Method for Analysis of Natural Gas by Gas Chromatography. 2001;96(Reapproved):1-17. doi:10.1520/D1945-14.2
38. ASTM International. Standard Test Method for Determination of Sulfur Compounds in Natural Gas and Gaseous Fuels by Gas Chromatography and Flame. 1998;05(Reapproved):6. doi:10.1520/D6228-10.2
39. NASA. Handbook for the microbial examination of space hardware. *NASA Tech Handb*. Published online 2010:1-52. doi:NASA-HDBK-6022b
40. Saber D. *Pipeline Quality Biogas: Guidance Document for Dairy Waste, Wastewater Treatment Sludge, and Landfill Conversion.*; 2009.
41. Nadkarni MA, Martin FE, Jacques NA, Hunter N. Determination of bacterial load by real-time PCR using a broad-range (universal) probe and primer set. 2002;148(1):257-266. doi:10.1099/00221287-148-1-257
42. Suzuki MT, Taylor LT. Quantitative Analysis of Small-Subunit rRNA Genes in Mixed Microbial Populations via 5 J -Nuclease Assays Downloaded from <http://aem.asm.org/> on November 26 , 2014 by SERIALS CONTROL Lane Medical Library. 2000;66(11):4605-4614. doi:10.1128/AEM.66.11.4605-4614.2000.Updated
43. Vital M, Penton CR, Wang Q, et al. A gene-targeted approach to investigate the intestinal butyrate-producing bacterial community. *Microbiome*. 2013;1(1):1-14. doi:10.1186/2049-2618-1-8
44. Li D, Li Z, Yu J, Cao N, Liu R, Yang M. Characterization of bacterial community structure in a drinking water distribution system during an occurrence of red water. *Appl Environ Microbiol*. 2010;76(21):7171-

7180. doi:10.1128/AEM.00832-10
45. Johnson KW, Carmichael MJ, McDonald W, et al. Increased Abundance of Gallionella spp., Leptothrix spp. and Total Bacteria in Response to Enhanced Mn and Fe Concentrations in a Disturbed Southern Appalachian High Elevation Wetland. *Geomicrobiol J.* 2012;29(2):124-138. doi:10.1080/01490451.2011.558557
  46. Foti M, Sorokin DY, Lomans B, et al. Diversity, activity, and abundance of sulfate-reducing bacteria in saline and hypersaline soda lakes. *Appl Environ Microbiol.* 2007;73(7):2093-2100. doi:10.1128/AEM.02622-06
  47. A Vogel CF, Garcia J, Wu D, et al. Activation of inflammatory responses in human U937 macrophages by particulate matter collected from dairy farms: An in vitro expression analysis of pro-inflammatory markers. *Environ Heal A Glob Access Sci Source.* 2012;11(1):1-9. doi:10.1186/1476-069X-11-17
  48. Kado NY, Langley D, Eisenstadt E. A simple modification of the Salmonella liquid-incubation assay Increased sensitivity for detecting mutagens in human urine. *Mutat Res Lett.* 1983;121(1):25-32. doi:10.1016/0165-7992(83)90082-9
  49. Kado NY, Guirguis GN, Flessel CP, Chan RC, Chang K -I, Wesolowski JJ. Mutagenicity of fine airborne particles: Diurnal variation in community air determined by a salmonella micro preincubation (microsuspension) procedure. *Environ Mutagen.* 1986;8(1):53-66. doi:10.1002/em.2860080106
  50. Saber DL. Task 2 Final Report: Laboratory Testing and Analysis. 2009;(GTI Project #20614).
  51. Chen Y, Cheng JJ, Creamer KS. Inhibition of anaerobic digestion process: A review. *Bioresour Technol.* 2008;99(10):4044-4064. doi:10.1016/j.biortech.2007.01.057
  52. Wang Y, Mei K. Ammonia and Greenhouse Gas Emissions from Biogas Digester Effluent Stored at Different Depths. *Trans ASABE.* 2014;57(5):1483-1491. doi:10.13031/trans.57.10630
  53. Amon B, Kryvoruchko V, Amon T, Zechmeister-Boltenstern S. Methane, nitrous oxide and ammonia emissions during storage and after application of dairy cattle slurry and influence of slurry treatment. *Agric Ecosyst Environ.* 2006;112(2-3):153-162. doi:10.1016/j.agee.2005.08.030
  54. Clarens M, Bernet N, Delgene J. Effects of nitrogen oxides and denitrification by Pseudomonas stutzeri on acetotrophic methanogenesis by Methanosarcina mazei. 1998;25:271-276.
  55. Wheeler P, Holm-Nielsen JB, Jaatinen T, Wellinger A, Lindberg A, Pettigrew A. Biogas Upgrading and Utilisation. *IEA Bioenergy.* Published online 1999:3-20. [http://www.energiotech.info/pdfs/Biogas\\_upgrading.pdf](http://www.energiotech.info/pdfs/Biogas_upgrading.pdf)
  56. Botheju D. Oxygen Effects in Anaerobic Digestion – A Review. *Open Waste Manag J.* 2011;4(1):1-19. doi:10.2174/1876400201104010001
  57. Chiavarini C, Cremisini C, Morabito R, Caricchia AM, De Poli F. GC/MS Characterisation of Main and Trace Organic Constituents of Gaseous Emissions from a MSW Landfill. *Fourth Int Landfill Symp Sardinia, Italy.* 1993;(October):617-621. <http://www.scopus.com/inward/record.url?eid=2-s2.0-12944266772&partnerID=tZOtx3y1>
  58. Durmusoglu E, Taspinar F, Karademir A. Health risk assessment of BTEX emissions in the landfill environment. *J Hazard Mater.* 2010;176(1-3):870-877. doi:10.1016/j.jhazmat.2009.11.117
  59. Rasi S. Biogas Composition and Upgrading to Biomethane. *Univ Jyväskylä.* Published online 2009. <https://pdfs.semanticscholar.org/80e1/1a47714afdbab936372669aaafa8c172c003.pdf>
  60. Wheelless E, Pierce J. Siloxanes in landfill and digester gas update. *SCS Eng Environ Consult Contract.* 2004;March:1-10. [http://mercmail.scsengineers.com/Papers/Pierce\\_2004Siloxanes\\_Update\\_Paper.pdf](http://mercmail.scsengineers.com/Papers/Pierce_2004Siloxanes_Update_Paper.pdf)
  61. Jaganathan H, Godin B. Biocompatibility assessment of Si-based nano- and micro-particles. *Adv Drug Deliv Rev.* 2012;64(15):1800-1819. doi:10.1016/j.addr.2012.05.008
  62. Saber DL, Manager SP, Cruz KMH, Scientist P. Pipeline quality biomethane: North American guidance document for introduction of dairy waste derived biomethane into existing natural gas networks: Task 2. 2009;(20614). [http://www.gastechnology.org/market\\_results/Pages/Dairy-Waste-Biomethane-Interchangeability-Oct2009.aspx](http://www.gastechnology.org/market_results/Pages/Dairy-Waste-Biomethane-Interchangeability-Oct2009.aspx)
  63. Vinnerås B, Schönning C, Nordin A. Identification of the microbiological community in biogas systems and evaluation of microbial risks from gas usage. *Sci Total Environ.* 2006;367(2-3):606-615. doi:10.1016/j.scitotenv.2006.02.008
  64. Xue J, Li Y, Peppers J, et al. Ultrafine Particle Emissions from Natural Gas, Biogas, and Biomethane Combustion. *Environ Sci Technol.* 2018;52(22):13619-13628. doi:10.1021/acs.est.8b04170
  65. Peppers J, Li Y, Xue J, et al. Performance analysis of membrane separation for upgrading biogas to biomethane at small scale production sites. *Biomass and Bioenergy.* 2019;128:105314. doi:10.1016/J.BIOMBIOE.2019.105314

66. EPA. *AP 42, Fifth Edition, Volume I Chapter 3: Stationary Internal Combustion Sources 3.2 Natural Gas-Fired Reciprocating Engines.*; 2000. <https://www3.epa.gov/ttn/chief/ap42/ch03/final/c03s02.pdf>
67. Cal/OSHA. California division of occupational safety and health administration (Cal/OSHA) permissible exposure limits (PELs) OSHA Annotated Table Z-1. Published 2018. <https://www.osha.gov/dsg/annotated-pels/tablez-1.html>
68. Cal/OSHA. California division of occupational safety and health administration (Cal/OSHA) permissible exposure limits (PELs) for chemical contaminants Table AC-1. <https://www.dir.ca.gov/title8/ac1.pdf>
69. Urban W, Lohmann H, Gómez JIS. Catalytically upgraded landfill gas as a cost-effective alternative for fuel cells. *J Power Sources*. 2009;193(1):359-366. doi:10.1016/j.jpowsour.2008.12.029
70. Schweigkofler M, Niessner R. Removal of siloxanes in biogases. *J Hazard Mater*. 2001;83(3):183-196. doi:10.1016/S0304-3894(00)00318-6
71. Lyng KA, Brekke A. Environmental life cycle assessment of biogas as a fuel for transport compared with alternative fuels. *Energies*. 2019;12(3). doi:10.3390/en12030532
72. Subramanian KA, Mathad VC, Vijay VK, Subbarao PMV. Comparative evaluation of emission and fuel economy of an automotive spark ignition vehicle fuelled with methane enriched biogas and CNG using chassis dynamometer. *Appl Energy*. 2013;105(x):17-29. doi:10.1016/j.apenergy.2012.12.011
73. Lim C, Kim D, Song C, Kim J, Han J, Cha JS. Performance and emission characteristics of a vehicle fueled with enriched biogas and natural gases. *Appl Energy*. 2015;139(2015):17-29. doi:10.1016/j.apenergy.2014.10.084
74. Matthews R, Chiu J, Hilden D. CNG compositions in Texas and the effects of composition on emissions, fuel economy, and driveability of NGVs. *SAE Tech Pap*. 1996;105(May):2170-2185. doi:10.4271/962097
75. Karavalakis G, Durbin TD, Villela M, Miller JW. Air pollutant emissions of light-duty vehicles operating on various natural gas compositions. *J Nat Gas Sci Eng*. 2012;4:8-16. doi:10.1016/j.jngse.2011.08.005
76. Hajbabaie M, Karavalakis G, Johnson KC, Lee L, Durbin TD. Impact of natural gas fuel composition on criteria, toxic, and particle emissions from transit buses equipped with lean burn and stoichiometric engines. *Energy*. 2013;62:425-434. doi:10.1016/j.energy.2013.09.040
77. Kakaee AH, Paykani A, Ghajar M. The influence of fuel composition on the combustion and emission characteristics of natural gas fueled engines. *Renew Sustain Energy Rev*. 2014;38:64-78. doi:10.1016/j.rser.2014.05.080
78. Park C, Kim C, Lee S, Lee S, Lee J. Comparative evaluation of performance and emissions of CNG engine for heavy-duty vehicles fueled with various calorific natural gases. *Energy*. Published online 2019. doi:10.1016/j.energy.2019.02.120
79. Kado NY, Okamoto RA, Kuzmicky PA, et al. Emissions of toxic pollutants from compressed natural gas and low sulfur diesel-fueled heavy-duty transit buses tested over multiple driving cycles. *Environ Sci Technol*. 2005;39(19):7638-7649. doi:10.1021/es0491127
80. Seagrave JC, Gigliotti A, McDonald JD, et al. Composition, toxicity, and mutagenicity of particulate and semivolatile emissions from heavy-duty compressed natural gas-powered vehicles. *Toxicol Sci*. 2005;87(1):232-241. doi:10.1093/toxsci/kfi230
81. Turrio-Baldassarri L, Battistelli CL, Conti L, et al. Evaluation of emission toxicity of urban bus engines: Compressed natural gas and comparison with liquid fuels. *Sci Total Environ*. 2006;355(1-3):64-77. doi:10.1016/j.scitotenv.2005.02.037
82. Yoon S, Hu S, Kado NY, et al. Chemical and toxicological properties of emissions from CNG transit buses equipped with three-way catalysts compared to lean-burn engines and oxidation catalyst technologies. *Atmos Environ*. 2014;83(X):220-228. doi:10.1016/j.atmosenv.2013.11.003
83. Li Y, Alaimo CP, Kim M, et al. Composition and Toxicity of Biogas Produced from Different Feedstocks in California. *Environ Sci Technol*. Published online 2019. doi:10.1021/acs.est.9b03003
84. Landreman AP, Shafer MM, Hemming JC, Hannigan MP, Schauer JJ. A macrophage-based method for the assessment of the reactive oxygen species (ROS) activity of atmospheric particulate matter (PM) and application to routine (daily-24 h) aerosol monitoring studies. *Aerosol Sci Technol*. 2008;42(11):946-957. doi:10.1080/02786820802363819
85. Shafer MM, Perkins DA, Antkiewicz DS, Stone EA, Quraishi TA, Schauer JJ. Reactive oxygen species activity and chemical speciation of size-fractionated atmospheric particulate matter from Lahore, Pakistan: An important role for transition metals. *J Environ Monit*. 2010;12(3):704-715. doi:10.1039/b915008k
86. Wang D, Pakbin P, Shafer MM, Antkiewicz D, Schauer JJ, Sioutas C. Macrophage reactive oxygen species activity of water-soluble and water-insoluble fractions of ambient coarse, PM<sub>2.5</sub> and ultrafine particulate matter (PM) in Los Angeles. *Atmos Environ*. 2013;77:301-310. doi:10.1016/j.atmosenv.2013.05.031

87. Zou H, Hastie T. Regularization and variable selection via the elastic net. *J R Stat Soc Ser B Stat Methodol.* 2005;67(5):768. doi:10.1111/j.1467-9868.2005.00527.x
88. Benfenati E, Manganaro A, Gini G. VEGA-QSAR: AI inside a platform for predictive toxicology. *CEUR Workshop Proc.* 2013;1107:21-28.
89. Okamoto RA, Kado NY, Kuzmicky PA, Ayala A, Kobayashi R. Unregulated emissions from compressed natural gas (CNG) transit buses configured with and without oxidation catalyst. *Environ Sci Technol.* 2006;40(1):332-341. doi:10.1021/es0479742
90. Wagner T, Ing D, Wyszyhki ML. Aldehydes and ketones in engine exhaust emissions -a review reactions also take place in the combustion of other. 210.
91. Nichols RJ, Clinton EL, King ET, Smith CS, Wineland RJ. A view of flexible fuel vehicle aldehyde emissions. *SAE Tech Pap.* 1988;97(May):422-429. doi:10.4271/881200
92. Nakamura H, Motoyama H, Kiyota Y. Passenger Car Engines for the 21st Century. Published online 1991. doi:10.4271/911908
93. Zervas E, Montagne X, Lahaye J. C1 - C5 organic acid emissions from an SI engine: Influence of fuel and air/fuel equivalence ratio. *Environ Sci Technol.* 2001;35(13):2746-2751. doi:10.1021/es000237v
94. Zervas E, Montagne X, Lahaye J. Emission of alcohols and carbonyl compounds from a spark ignition engine. Influence of fuel and air/fuel equivalence ratio. *Environ Sci Technol.* 2002;36(11):2414-2421. doi:10.1021/es010265t
95. Shah A, Yun-shan G. A Comparative Study on VOCs and Aldehyde-Ketone Emissions from a Spark Ignition Vehicle Fuelled on Compressed Natural Gas and Gasoline. *Pak J Engg Appl Sci ....* 2012;10:29-35. <http://www.uet.edu.pk/research/researchinfo/10-RJ-January-2012/Art-4-17.pdf>
96. Cadle SH, Mulawa PA. Sulfide emissions from catalyst-equipped cars. *SAE Tech Pap.* Published online 1978. doi:10.4271/780200
97. Thiruvengadam A, Besch MC, Yoon S, et al. Characterization of particulate matter emissions from a current technology natural gas engine. *Environ Sci Technol.* 2014;48(14):8235-8242. doi:10.1021/es5005973
98. Jayaratne ER, He C, Ristovski ZD, Morawska L, Johnson GR. A comparative investigation of ultrafine particle number and mass emissions from a fleet of on-road diesel and CNG buses. *Environ Sci Technol.* 2008;42(17):6736-6742. doi:10.1021/es800394x
99. Kuwayama T, Collier S, Forestieri S, et al. Volatility of primary organic aerosol emitted from light duty gasoline vehicles. *Environ Sci Technol.* 2015;49(3):1569-1577. doi:10.1021/es504009w
100. Gautam M, Thiruvengadam A, Carder D, et al. *Characterization of Toxicity as a Function of Volatility of Ultrafine PM Emissions from Compressed Natural Gas Vehicles.*; 2011.
101. Cheung KL, Ntziachristos L, Tzankiozis T, et al. Emissions of particulate trace elements, metals and organic species from gasoline, diesel, and biodiesel passenger vehicles and their relation to oxidative potential. *Aerosol Sci Technol.* 2010;44(7):500-513. doi:10.1080/02786821003758294
102. Yoon S, Collins J, Thiruvengadam A, Gautam M, Herner J, Ayala A. Criteria pollutant and greenhouse gas emissions from CNG transit buses equipped with three-way catalysts compared to lean-burn engines and oxidation catalyst technologies. *J Air Waste Manag Assoc.* 2013;63(8):926-933. doi:10.1080/10962247.2013.800170
103. Von Wald G, Brandt A, Rajagopal D, et al. *Biomethane in California Common Carrier Pipelines: Assessing Heating Value and Maximum Siloxane Specifications.*; 2018.
104. Pääkkönen A, Aro K, Aalto P, Kontinen J, Kojo M. The potential of biomethane in replacing fossil fuels in heavy transport-a case study on Finland. *Sustain.* 2019;11(17):1-19. doi:10.3390/su11174750
105. Rotunno P, Lanzini A, Leone P. Energy and economic analysis of a water scrubbing based biogas upgrading process for biomethane injection into the gas grid or use as transportation fuel. *Renew Energy.* 2017;102:417-432. doi:10.1016/j.renene.2016.10.062
106. Cucchiella F, D'Adamo I. Technical and economic analysis of biomethane: A focus on the role of subsidies. *Energy Convers Manag.* 2016;119:338-351. doi:10.1016/j.enconman.2016.04.058
107. Cucchiella F, D'Adamo I, Gastaldi M. Biomethane: A renewable resource as vehicle fuel. *Resources.* 2017;6(4). doi:10.3390/resources6040058
108. Nevalainen P, Kinnunen NM, Kirveslahti A, et al. Formation of NH<sub>3</sub> and N<sub>2</sub>O in a modern natural gas three-way catalyst designed for heavy-duty vehicles: the effects of simulated exhaust gas composition and ageing. *Appl Catal A Gen.* 2018;552(September 2017):30-37. doi:10.1016/j.apcata.2017.12.017
109. Behrentz E, Ling R, Rieger P, Winer AM. Measurements of nitrous oxide emissions from light-duty motor vehicles: A pilot study. *Atmos Environ.* 2004;38(26):4291-4303. doi:10.1016/j.atmosenv.2004.04.027
110. Livingston C, Rieger P, Winer A. Ammonia emissions from a representative in-use fleet of light and

- medium-duty vehicles in the California South Coast Air Basin. *Atmos Environ.* 2009;43(21):3326-3333. doi:10.1016/j.atmosenv.2009.04.009
111. Xue J, Li Y, Peppers J, et al. Ultrafine Particle Emissions from Natural Gas, Biogas, and Biomethane Combustion. *Environ Sci Technol.* 2018;52(22):13619-13628. doi:10.1021/acs.est.8b04170
  112. Amirante R, Distaso E, Tamburrano P, Reitz RD. Measured and predicted soot particle emissions from natural gas engines. *SAE Tech Pap.* 2015;2015. doi:10.4271/2015-24-2518
  113. Penrod A, Zhang Y, Wang K, Wu SY, Leung LR. Impacts of future climate and emission changes on U.S. air quality. *Atmos Environ.* 2014;89:533-547. doi:10.1016/j.atmosenv.2014.01.001
  114. Rudokas J, Miller PJ, Trail MA, Russell AG. Regional air quality management aspects of climate change: Impact of climate mitigation options on regional air emissions. *Environ Sci Technol.* 2015;49(8):5170-5177. doi:10.1021/es505159z
  115. Shi W, Ou Y, Smith SJ, Ledna CM, Nolte CG, Loughlin DH. Projecting state-level air pollutant emissions using an integrated assessment model: GCAM-USA. *Appl Energy.* 2017;208(October):511-521. doi:10.1016/j.apenergy.2017.09.122
  116. Brown KE, Hottle TA, Bandyopadhyay R, et al. Evolution of the United States Energy System and Related Emissions under Varying Social and Technological Development Paradigms: Plausible Scenarios for Use in Robust Decision Making. *Environ Sci Technol.* 2018;52(14):8027-8038. doi:10.1021/acs.est.8b00575
  117. Zapata CB, Yang C, Yeh S, Ogden J, Kleeman MJ. Estimating criteria pollutant emissions using the California Regional Multisector Air Quality Emissions (CA-REMARQUE) model v1. 0. *Geosci Model Dev.* 2018;11(4):1293.
  118. Keshavarzmohammadian A, Henze DK, Milford JB. Emission Impacts of Electric Vehicles in the US Transportation Sector Following Optimistic Cost and Efficiency Projections. *Environ Sci Technol.* 2017;51(12):6665-6673. doi:10.1021/acs.est.6b04801
  119. Trail MA, Tsimpidi AP, Liu P, et al. Impacts of potential CO<sub>2</sub>-reduction policies on air quality in the United States. *Environ Sci Technol.* 2015;49(8):5133-5141. doi:10.1021/acs.est.5b00473
  120. Ellis TJ, Wolf G. Air quality influences of post-combustion carbon capture. *Energy Procedia.* 2011;4(x):488-495. doi:10.1016/j.egypro.2011.01.079
  121. American Lung Association. Most polluted cities in the U.S. Published 2021. <https://www.lung.org/research/sota/city-rankings/most-polluted-cities>
  122. CARB. Assembly Bill 32 Overview. <https://ww3.arb.ca.gov/cc/ab32/ab32.htm>
  123. Yang C, Yeh S, Zakerinia S, Ramea K, McCollum D. Achieving California's 80% greenhouse gas reduction target in 2050: Technology, policy and scenario analysis using CA-TIMES energy economic systems model. *Energy Policy.* Published online 2015. doi:10.1016/j.enpol.2014.12.006
  124. McCollum D, Yang C, Yeh S, Ogden J. Deep greenhouse gas reduction scenarios for California - Strategic implications from the CA-TIMES energy-economic systems model. *Energy Strateg Rev.* 2012;1(1):19-32. doi:10.1016/j.esr.2011.12.003
  125. Yang C, Ogden JM. Renewable and low carbon hydrogen for California-Modeling the long term evolution of fuel infrastructure using a quasi-spatial TIMES model. *Int J Hydrogen Energy.* 2013;38(11):4250-4265. doi:10.1016/j.ijhydene.2013.01.195
  126. Yang C, Yeh S, Ramea K, Zakerinia S, Jenn A, Bunch DS. Modeling of Greenhouse Gas Reductions Options and Policies for California to 2050 : Analysis and Model Development Using the CA-TIMES Model. 2016;(530). <https://steps.ucdavis.edu/wp-content/uploads/2017/05/2016-UCD-ITS-RR-16-09.pdf>
  127. Yang C, Yeh S, Ramea K, et al. *Modeling Optimal Transition Pathways to a Low Carbon Economy in California: Appendices and Supplemental Material for California TIMES (CA-TIMES) Model.*; 2014. <https://ww3.arb.ca.gov/research/apr/past/09-346.pdf>
  128. Rhodes JS, Keith DW. Engineering economic analysis of biomass IGCC with carbon capture and storage. *Biomass and Bioenergy.* 2005;29(6):440-450. doi:10.1016/j.biombioe.2005.06.007
  129. Klein D, Bauer N, Bodirsky B, Dietrich JP, Popp A. Bio-IGCC with CCS as a long-term mitigation option in a coupled energy-system and land-use model. *Energy Procedia.* 2011;4:2933-2940. doi:10.1016/j.egypro.2011.02.201
  130. Sanchez DL, Kammen DM. A commercialization strategy for carbon-negative energy. *Nat Energy.* 2016;1(1):1-4. doi:10.1038/nenergy.2015.2
  131. Muratori M, Kheshgi H, Mignone B, Clarke L, McJeon H, Edmonds J. Carbon capture and storage across fuels and sectors in energy system transformation pathways. *Int J Greenh Gas Control.* 2017;57:34-41. doi:10.1016/j.ijggc.2016.11.026
  132. Jacobson MZ. The health and climate impacts of carbon capture and direct air capture. *Energy Environ Sci.*

- 2019;12(12):3567-3574. doi:10.1039/c9ee02709b
133. European Environment Agency. *Air Pollution Impacts from Carbon Capture and Storage (CCS)*.; 2011.
  134. Zang G, Zhang J, Jia J, Lora ES, Ratner A. Life cycle assessment of power-generation systems based on biomass integrated gasification combined cycles. *Renew Energy*. 2020;149:336-346. doi:10.1016/j.renene.2019.12.013
  135. Sproul E, Barlow J, Quinn JC. Time-Resolved Cost Analysis of Natural Gas Power Plant Conversion to Bioenergy with Carbon Capture and Storage to Support Net-Zero Emissions. *Environ Sci Technol*. Published online 2020. doi:10.1021/acs.est.0c04041
  136. Mac Kinnon MA, Brouwer J, Samuelsen S. The role of natural gas and its infrastructure in mitigating greenhouse gas emissions, improving regional air quality, and renewable resource integration. *Prog Energy Combust Sci*. 2018;64:62-92. doi:10.1016/j.peecs.2017.10.002
  137. Demirhan CD, Tso WW, Powell JB, Pistikopoulos EN. A multi-scale energy systems engineering approach towards integrated multi-product network optimization. *Appl Energy*. 2021;281:116020. doi:10.1016/j.apenergy.2020.116020
  138. Venecek MA, Yu X, Kleeman MJ. Predicted ultrafine particulate matter source contribution across the continental United States during summertime air pollution events. *Atmos Chem Phys*. 2019;19(14):9399-9412. doi:10.5194/acp-19-9399-2019
  139. CARB. EMFAC model. California Air Resources Board. <https://arb.ca.gov/emfac/%0D%0A>
  140. CARB. VISION model. California Air Resources Board. <https://ww2.arb.ca.gov/resources/documents/vision-scenario-planning%0D%0A>
  141. RAEL. SWITCH model. Renewable & Appropriate Energy Laboratory. [http://rael.berkeley.edu/old\\_drupal/switch/](http://rael.berkeley.edu/old_drupal/switch/)
  142. ANL. GREET model. Argonne National Laboratory. <https://greet.es.anl.gov>
  143. CARB. CA-GREET model. California Air Resources Board. <https://ww2.arb.ca.gov/resources/documents/lcfs-life-cycle-analysis-models-and-documentation>
  144. Koornneef J, Ramirez A, van Harmelen T, van Horssen A, Turkenburg W, Faaij A. The impact of CO<sub>2</sub> capture in the power and heat sector on the emission of SO<sub>2</sub>, NO<sub>x</sub>, particulate matter, volatile organic compounds and NH<sub>3</sub> in the European Union. *Atmos Environ*. 2010;44(11):1369-1385. doi:10.1016/j.atmosenv.2010.01.022
  145. Young B, Krynock M, Carlson D, et al. Comparative environmental life cycle assessment of carbon capture for petroleum refining, ammonia production, and thermoelectric power generation in the United States. *Int J Greenh Gas Control*. 2019;91. doi:10.1016/j.ijggc.2019.102821
  146. Kleeman MJ, Cass GR. A 3D Eulerian source-oriented model for an externally mixed aerosol. *Environ Sci Technol*. 2001;35(24):4834-4848. doi:10.1021/es010886m
  147. Yu X, Venecek M, Kumar A, et al. Regional sources of airborne ultrafine particle number and mass concentrations in California. *Atmos Chem Phys*. 2019;19(23):14677-14702. doi:10.5194/acp-19-14677-2019
  148. NCAR. NCAR Community Earth System Model, EaSM Project Dataset. Research Data Archive at the National Center for Atmospheric Research, Computational and Information Systems Laboratory. Published online 2011. doi:<https://doi.org/10.5065/D6TH8JP5>. Accessed† 10 01 2018
  149. IPCC. *Climate Change 2014: Synthesis Report. Contribution of Working Groups I, II and III to the Fifth Assessment Report of the Intergovernmental Panel on Climate Change.*; 2014.
  150. Sacks JD, Lloyd JM, Zhu Y, et al. The Environmental Benefits Mapping and Analysis Program - Community Edition (BenMAP-CE): A tool to estimate the health and economic benefits of reducing air pollution. *Environ Model Softw with Environ data news*. 2018;104:118-129.
  151. Krewski D, Jerrett M, Burnett RT, et al. *Extended Follow-Up and Spatial Analysis of the American Cancer Society Study Linking Particulate Air Pollution and Mortality*. Health Effects Institute (HEI); 2009.
  152. Laden F, Schwartz J, Speizer FE, Dockery DW. Reduction in fine particulate air pollution and mortality: Extended follow-up of the Harvard Six Cities study. *Am J Respir Crit Care Med*. 2006;173(6):667-672. doi:10.1164/rccm.200503-443OC
  153. Pope CA 3rd, Burnett RT, Thun MJ, et al. Lung cancer, cardiopulmonary mortality, and long-term exposure to fine particulate air pollution. *JAMA*. 2002;287(9):1132-1141. doi:10.1001/jama.287.9.1132
  154. Lepeule J, Laden F, Dockery D, Schwartz J. Chronic exposure to fine particles and mortality: an extended follow-up of the Harvard Six Cities study from 1974 to 2009. *Env Heal Perspect*. 2012;120(7):965-970. doi:10.1289/ehp.1104660
  155. *Report P-1A: Total Population Projections, California, 2010-2060 (Baseline 2019 Population Projections; Vintage 2020 Release)*.; 2021.

156. Surawski NC, Miljevic B, Roberts BA, et al. Particle emissions, volatility, and toxicity from an ethanol fumigated compression ignition engine. *Environ Sci Technol.* 2010;44(1):229-235. doi:10.1021/es9021377
157. Antanaitis DB. Effect of regenerative braking on foundation brake performance. In: *SAE Technical Papers.* ; 2010. doi:10.4271/2010-01-1681
158. Ostro B, Hu JL, Goldberg D, et al. Associations of Mortality with Long-Term Exposures to Fine and Ultrafine Particles, Species and Sources: Results from the California Teachers Study Cohort. *Environ Health Perspect.* 2015;123(6):549-556. doi:10.1289/ehp.1408565